

7-1-2014

GEOCHRONOLOGY, GEOCHEMISTRY,
AND TECTONIC CHARACTERIZATION OF
QUATERNARY LARGE-VOLUME
TRAVERTINE DEPOSITS IN THE
SOUTHWESTERN UNITED STATES AND
THEIR IMPLICATIONS FOR CO₂
SEQUESTRATION

Alexandra Priewisch

Follow this and additional works at: https://digitalrepository.unm.edu/eps_etds

Recommended Citation

Priewisch, Alexandra. "GEOCHRONOLOGY, GEOCHEMISTRY, AND TECTONIC CHARACTERIZATION OF QUATERNARY LARGE-VOLUME TRAVERTINE DEPOSITS IN THE SOUTHWESTERN UNITED STATES AND THEIR IMPLICATIONS FOR CO₂ SEQUESTRATION." (2014). https://digitalrepository.unm.edu/eps_etds/65

This Dissertation is brought to you for free and open access by the Electronic Theses and Dissertations at UNM Digital Repository. It has been accepted for inclusion in Earth and Planetary Sciences ETDs by an authorized administrator of UNM Digital Repository. For more information, please contact disc@unm.edu.

Alexandra Priewisch

Candidate

Earth and Planetary Sciences

Department

This dissertation is approved, and it is acceptable in quality and form for publication:

Approved by the Dissertation Committee:

Dr. Laura Crossey, Chairperson

Dr. Karl Karlstrom

Dr. Yemane Asmerom

Dr. Peter Mozley

**GEOCHRONOLOGY, GEOCHEMISTRY, AND TECTONIC
CHARACTERIZATION OF QUATERNARY LARGE-
VOLUME TRAVERTINE DEPOSITS IN THE
SOUTHWESTERN UNITED STATES AND THEIR
IMPLICATIONS FOR CO₂ SEQUESTRATION**

by

ALEXANDRA PRIEWISCH

B.S., Geology, University of Mainz, Germany, 1994
M.S., Geology, University of Mainz, Germany, 1998

DISSERTATION

Submitted in Partial Fulfillment of the
Requirements for the Degree of

**Doctor of Philosophy
Earth and Planetary Sciences**

The University of New Mexico
Albuquerque, New Mexico

July 2014

ACKNOWLEDGEMENTS

I would like to take this opportunity to first thank my advisor, Laura Crossey, for inspiring me to work on this project and for guiding me through the last five years with her encouragement and support. I also thank Karl Karlstrom for his patience and assistance with so many different projects and for not only being on my committee but also a second advisor. I extend my gratitude to my other committee members, Yemane Asmerom and Peter Mozley who contributed ideas, knowledge, and support to my research. Besides my committee many others have assisted with field work, valuable discussions, laboratory analyses, and general encouragement and support. I thank Victor Polyak for patiently helping me to prepare samples in the radiogenic isotope laboratory and explaining U-series and model ages to me on more than one occasion. Viorel Atudorei helped me greatly with stable isotope analyses and Mehdi Ali was a great help in the geochemistry laboratory; I thank both of them for their support and kindness. I extend my thanks to Aurora Pun who taught me everything I know about teaching and who was always kind and encouraging. I would like to thank Alexander Nereson for his friendship and support and his assistance in the field. I could not have finished my work without the help of Rebecca Wacker who diligently drilled hundreds of travertine samples for me and who became a dear friend to me. A number of people assisted me in the field and I am grateful for their support: Patrick Naranjo, Tom Kipling, Corentin Le Guillou, Jason Ricketts, and Nadine Warneke. I thank Becky Frus and Chris McGibbon for discussing water samples with me and sharing many good conversations and laughs. I am very thankful for the new friendships that I have made during my time here at the University of New Mexico. I would also like to thank several people outside the university for their support: the staff of the New Mexico Bureau of Geology and Mineral Resources for making travertine cores from Mesa del Oro, Riley North Mesa and Riley South Mesa available; Jim Lardner of New Mexico Travertine Inc. for access to the travertine quarries at Mesa Aparejo; Bob Worsley, owner of NZ Legacy LLC, for access to his property and travertine quarries at Mesa del Oro; Jim Harrison, manager of NZ Legacy LLC, for valuable information about the travertine deposit; the rancher Mark Chavez for access to his land. Last but not least, I want to thank my parents, Dieter and Marianne Priewisch, for their endless support across the Atlantic.

Financial support that made this work possible came from a variety of sources including National Science Foundation (NSF) EAR-0838575 (to Crossey), New Mexico Geological

Society grants-in-aid, American Association of Petroleum Geologists Grants-In-Aid, Graduate and Professional Student Association of the University of New Mexico, Department of Earth and Planetary Science Scholarships, Geological Society of America Travel Grants, an American Geophysical Union Travel Grant, and the University of New Mexico Research, Provision and Travel Grant.

Geochronology, Geochemistry, and Tectonic Characterization of Quaternary Large-Volume Travertine Deposits in the Southwestern United States and Their Implications for CO₂ Sequestration

by

Alexandra Priewisch

B.S. Geology, University of Mainz, Germany, 1994

M.S. Geology, University of Mainz, Germany, 1998

Ph.D. Earth and Planetary Sciences, University of New Mexico, 2014

Abstract

Travertines are freshwater carbonates that precipitate from carbonic groundwater due to the degassing of CO₂. Travertine deposits are often situated along faults that serve as conduits for CO₂-charged groundwater and their geochemistry often records mixing of deeply-derived fluids and volatiles with shallow meteoric water. Travertines are surface expressions of dynamic mantle processes related to the tectonic setting. This dissertation includes four chapters that focus on different aspects of travertine formation and their scientific value. They are excellent, although underestimated, diagnostic tools for climatology, hydrology, tectonics, geochemistry, geomicrobiology, and they can inform carbon sequestration models.

Quaternary Large-volume travertine deposits in New Mexico and Arizona occur in an extensional tectonic stress regime on the southeastern Colorado Plateau and along the Rio Grande rift. They accumulated above fault systems during episodes of high hydraulic head in confined aquifers, increased regional volcanic activity, and high input of mantle-derived volatiles

such as CO₂ and He. Stable isotope and trace element geochemistry of travertines is controlled by groundwater geochemistry as well as the degassing of CO₂. The geochemical composition allows for distinguishing different travertine facies and evaluating past groundwater flow. The travertine deposits in New Mexico are interpreted to be extinct CO₂ fields due to the large volumes that accumulated and in analogy to the travertine deposits in Arizona that are associated with an active CO₂-gas field. Travertines are natural analogues for CO₂ leakage along fault systems that bypassed regional cap rocks and they provide important insight into the migration of CO₂ from a reservoir to the surface. The volume of travertine can be used to infer the integrated CO₂ leakage along a fault system over geologic time. This leakage is estimated as: (1) CO₂ that becomes fixed in CaCO₃/travertine (tons of carbon converted into tons of carbonate), (2) the amount of CO₂ that degassed into the atmosphere (twice the amount of (1), based on reaction stoichiometry), (3) dissolved CO₂ that is carried away with the water discharging from a spring (based on modern spring discharge and dissolved carbon content), and (4) CO₂ that escapes through the soil (based on modern soil flux measurements). Better understanding of integrated CO₂ leakage and fault-related seal bypass is needed to design CO₂ sequestration sites to effectively store anthropogenic CO₂ in the subsurface.

PREFACE

The four chapters included in this dissertation are all independent works related to the common theme of large-volume travertine deposits in New Mexico and Arizona. Each chapter is written as a stand-alone entity for publication, and thus repetition of some material is necessary. Each chapter has its own abstract, introduction, methods, results, discussion, and references sections. The collaborating coauthors are listed for each chapter and their specific contributions are detailed below. For each chapter, I conducted the majority of the field work, sample analysis, interpretation and writing, and I am the lead author on each manuscript.

Chapter 1 presents geochronological data on travertine deposits across New Mexico and Arizona which allowed me to evaluate times of travertine deposition and tectonic and paleohydrological controls on travertine formation. U-series ages show that the formation of large volumes of travertine in New Mexico and Arizona occurred episodically at 700-500 ka, 350-200 ka, and 100-40 ka. These episodes are interpreted to reflect the combination of times of high hydraulic head in confined aquifers and regional volcanic activity with associated high CO₂ flux. Because of the large volumes that accumulated and by analogy to the currently active CO₂-gas field in the study area in Arizona, it is inferred that the other travertine deposits in New Mexico represent past degassing of CO₂ reservoirs. This study highlights the locations and volumes of huge travertine systems in the Southwest, provides, for the first time, estimates of their age and duration, and proposes a mechanism to explain them. Coauthors who contributed significant ideas, analytical facilities and assistance on the chapter included Laura Crossey, Karl Karlstrom, Victor Polyak, Yemane Asmerom, Alexander Nereson, and Jason Ricketts. Laura Crossey, Karl Karlstrom, and Eileen Embid had done extensive research at travertine deposits in Arizona which laid the groundwork for the studies I conducted in New Mexico on similar

travertine deposits. I extensively used Yemane Asmerom's radiogenic isotope laboratory at the University of New Mexico and Victor Polyak helped with sample preparation and analysis. Alex and Jason provided valuable field support and discussions. This chapter was published in *Geosphere* in April 2014.

Chapter 2 is a more detailed study of just one of the large-volume travertine deposit, at Mesa del Oro in New Mexico, to evaluate paleohydrologic and paleoclimate relationships, constrained by U-series ages. New U-series ages show that large-volume travertine formation occurred here in two intervals at 360-250 ka, and at 760-560 ka, coinciding with local volcanism which led to high influx of CO₂ and with high head in a confined aquifer leading to artesian springs and travertine precipitation. Travertine formation at Mesa del Oro is interpreted to represent extended wet times that coincide with times of extensive CO₂ degassing.

This chapter presents extensive mapping of the large travertine platforms as well as a detailed analysis of travertine morphology and facies. Laura Crossey and Karl Karlstrom supervised initial field work and provided valuable assistance in interpreting travertine field relationships and the structural setting. The manuscript that was published in the NMGS Guidebook for the 64th field conference in 2013 provided a case study for the audience of the NMGS field conference and added more detailed stratigraphic and facies data to the geochronology for this important occurrence along the field trip route.

Chapter 3 is a contribution to research related to CO₂ sequestration. Travertines are natural analogues for CO₂ leakage along fault systems over geologic time and the volume of travertines can be used to infer integrated CO₂ leakage. This leakage is estimated as the sum of: CO₂ that becomes fixed in CaCO₃/travertine, the amount of CO₂ that degassed into the atmosphere, dissolved CO₂ that is carried away with the water discharging from a spring, and

CO₂ that escapes through the soil. The main conclusion of this paper is that the accumulations of large-volume travertine deposits on the Colorado Plateau and along the Rio Grande rift provide a quantifiable record of extensive CO₂ leakage from past CO₂ reservoirs. The mechanism for leakage involved fluid flux along fault systems which bypassed regional seals and served as conduits for groundwater flow and upward migration of deeply-derived CO₂. A potentially globally significant contribution of this case study is that better understanding of integrated CO₂ leakage along fault systems may be able to better constrain global estimates of natural CO₂ fluxes, and to help in risk assessment of CO₂ sequestration sites designed to effectively store anthropogenic CO₂ in the subsurface. Coauthors who contributed significant ideas and assistance on the chapter include Laura Crossey, Karl Karlstrom, and Peter Mozley. This chapter was submitted to the International Journal of Greenhouse Gas Control in April 2014 and is currently in review.

Chapter 4 presents stable isotope and trace element composition of travertine in a stratigraphic and facies context. I discovered that geochemistry of travertine varies according to individual facies. Thus, geochemistry can be used to evaluate past flow paths of groundwater, to elucidate processes of travertine deposition, and to distinguish facies associations during travertine formation. Depositional environments of travertine, e.g. spring mound and marsh, produce distinctive travertine facies such as step-pool, paludal (marsh), and vein facies. The goal of this chapter is to better why travertines show the widest stable isotope variations of all carbonates. Stable oxygen and carbon isotope values of the different travertine deposits vary widely with $\delta^{18}\text{O}$ and $\delta^{13}\text{C}$ ranging from -14‰ to -3.8‰ and -4.9‰ to 9.8‰, respectively. I interpret this variation of reflect complex groundwater mixing, variable CO₂ degassing, and other processes within the depositional system, such as evaporation. Within individual travertine

deposits, geochemical results overlap substantially: trace element analyses show similar trends throughout the region, with high (> 1000 mg/kg) concentrations of Fe, Mg, Mn, Na, and Sr, but different results for individual facies. $\delta^{13}\text{C}$ values of the paludal facies vary between -1‰ and -5‰ as opposed to the step-pool facies where most $\delta^{13}\text{C}$ values range from 2‰ to 7‰. I interpret this difference in stable isotope composition with the influence of vegetation in marshy areas and the effect of CO_2 degassing along step-pools. The vein facies shows higher concentrations of certain trace elements (e.g., Fe, Ni, and Sr) than the other facies. I interpret this difference to result from the input of deeply-derived fluids which are enriched in certain elements. In addition, veins precipitate in the subsurface and thus in a relatively closed environment in contrast to the surficial depositional environments which are influenced by meteoric water. Potential coauthors include Laura Crossey, Karl Karlstrom, Peter Mozley, Mehdi Ali, Viorel Atudorei, and Alexander Nereson. This chapter will be turned into a manuscript for submission to *Chemical Geology*.

Table of Contents

CHAPTER1 U-SERIES GEOCHRONOLOGY OF LARGE-VOLUME QUATERNARY TRAVERTIN DEPOSITS OF THE SOUTHEASTERN COLORADO PLATEAU: EVALUATING EPISODICITY AND TECTONIC AND PALEOHYDROLOGIC CONTROLS .1	
CHAPTER ABSTRACT	1
INTRODUCTION	2
BACKGROUND ON TRAVERTINE FORMATION.....	4
GEOLOGIC SETTING OF THE STUDY AREAS	8
TRAVERTINE FACIES.....	10
Morphology and facies of the large-volume travertine deposits	10
METHODS	12
RESULTS	17
Summary of travertine ages	22
DISCUSSION AND IMPLICATIONS	24
CONCLUSIONS.....	34
ACKNOWLEDGEMENTS	35
REFERENCES	36

Table of Contents

CHAPTER1 U-SERIES GEOCHRONOLOGY OF LARGE-VOLUME QUATERNARY TRAVERTIN DEPOSITS OF THE SOUTHEASTERN COLORADO PLATEAU: EVALUATING EPISODICITY AND TECTONIC AND PALEOHYDROLOGIC CONTROLS .1	
CHAPTER ABSTRACT	1
INTRODUCTION	2
BACKGROUND ON TRAVERTINE FORMATION.....	4
GEOLOGIC SETTING OF THE STUDY AREAS	8
TRAVERTINE FACIES.....	10
Morphology and Facies of the Large-Volume Travertine Deposits	10
METHODS	12
RESULTS	18
Summary of Travertine Ages.....	23
DISCUSSION AND IMPLICATIONS	25
CONCLUSIONS.....	36
ACKNOWLEDGEMENTS	37
REFERENCES	38

CHAPTER2 U-SERIES AGES AND MORPHOLOGY OF A QUATERNARY LARGE-VOLUME TRAVERTIN DEPOSIT AT MESA DEL ORO, NM: IMPLICATIONS FOR PALEOHYDROLOGY, PALEOCLIMATE, AND NEOTECTONIC PROCESSES	49
CHAPTER ABSTRACT	49
INTRODUCTION	50
BACKGROUND ON TRAVERTINE FORMATION.....	52
METHODS	54
TRAVERTINE MORPHOLOGIES AND FACIES.....	55
TRAVERTINE VOLUMES AND AGES	62
DISCUSSION.....	63
CONCLUSIONS.....	65
ACKNOWLEDGEMENTS	65
REFERENCES	66
CHAPTER3 CO ₂ LEAKAGE FORM EXTINCT AND MODERN CO ₂ RESERVOIRS IN NEW MEXICO AND ARIZONA: EVALUATING THE ROLE OF SEAL BYPASSAND LARGE-VOLUME TRAVERTINE DEPOSITION WITH IMPLICATIONS FOR CO ₂ SEQUESTRATION	70
CHAPTER ABSTRACT	70
INTRODUCTION	71
BACKGROUND ON TRAVERTINE FORMATION.....	73

GEOLOGIC SETTING OF THE STUDY AREAS	75
METHODS	75
Calculation of Travertine Volume	75
Calculation of the Total Amount of CO ₂	77
Calculation of Spring CO ₂ Flux	78
Calculation of Diffuse CO ₂ Flux	79
Calculation of the Integrated Amount of CO ₂ Leakage	81
RESULTS	82
Discussion of Assumptions for CO ₂ Leakage Calculations	82
Calculated Amounts of CO ₂ Leakage	83
DISCUSSION	83
Importance of Seal Bypass	83
Wider Significance of Integrated CO ₂ Leakage and Implications for CO ₂ Sequestration	90
CONCLUSIONS	95
ACKNOWLEDGEMENTS	96
REFERENCES	96

CHAPTER4 GEOCHEMICAL ANALYSIS OF QUATERNARY TRAVERTINE DEPOSITS ON THE SOUTHEASTERN COLORADO PLATEAU: EVLAUATION OF TRAVERTINE FACIES FOR PALEOHYDROLGY AND PALEOENVIRONMENT STUDIES	103
CHAPTER ABSTRACT	103
INTRODUCTION	104
TRAVERTINE AND TRAVERTINE FORMATION.....	105
GEOLOGIC SETTING OF THE STUDY AREAS	106
METHODS	106
Facies Analysis	106
Stable Isotope Analysis.....	108
Trace Element Analysis	108
RESULTS	109
Travertine Facies and their Depositional Environment	109
Stable Isotope Analysis.....	115
Major, Minor and Trace Elements of Travertine Samples	117
DISCUSSION	121
Interpretation of the Stable Isotopic Composition of Travertines According to Facies	122
Oxygen Isotopes Travertines	122

Carbon Isotope Travertines.....	123
Geochemical Analysis of Minor and Trace Elements According to Facies (excluding Rare Earth Elements).....	125
Rare Earth Element Concentrations According To Facies	130
Modeling Past Water Temperatures and Water Compositions.....	131
CONCLUSIONS.....	138
ACKNOWLEDGEMENTS.....	139
REFERENCES	140

CHAPTER 1

U-Series Geochronology of large-volume Quaternary Travertine Deposits of the southeastern Colorado Plateau: Evaluating Episodicity and tectonic and paleohydrologic Controls

Priewisch, A.¹, Crossey, L.J.¹, Karlstrom, K.E.¹, Polyak, V.J.¹, Asmerom, Y.¹, Nereson, A.² and Ricketts, J.W.¹

¹ Dept. of Earth and Planetary Sciences, University of New Mexico, Albuquerque, NM 87131

² Dept. of Earth and Planetary Sciences, University of California Santa Cruz, Santa Cruz, CA 95064

(Published in Geosphere, April 2014, Vol. 10, No. 2, p. 401-423)

CHAPTER ABSTRACT

Large-volume travertine deposits in the southeastern Colorado Plateau of New Mexico and Arizona, USA, occur along the Jemez lineament and Rio Grande rift. These groundwater discharge deposits reflect vent locations for mantle-derived CO₂, which was conveyed by deeply-sourced hydrothermal fluid input into springs. U-series dating of stratigraphic sections shows that major aggradation and large-volume (2.5 km³) deposition took place across the region episodically at 700-500 ka, 350-200 ka, and 100-40 ka. These pulses of travertine formation coincide with the occurrence of regional basaltic volcanism, which implies an association of travertine deposits with underlying low-velocity mantle that could supply the excess CO₂. The calculation of landscape denudation rates based on basalt paleosurfaces shows that travertine platforms developed on local topographic highs which required artesian head and fault conduits. In conclusion, episodic travertine accumulation which led to the formation of the observed travertine platforms represents conditions when fault conduits, high hydraulic head, and high CO₂ flux within confined aquifer systems were all favorable for facilitating large-volume

travertine formation and was thus controlled by tectonic activity and paleohydrology. By analogy to the active Springerville-St. Johns CO₂-gas field, the large volumes and similar platform geometries of travertine occurrences in this study are interpreted to represent extinct CO₂-gas reservoirs that were vents for degassing of mantle volatiles into the near-surface system.

INTRODUCTION

The southeastern Colorado Plateau in New Mexico and Arizona (Barker et al., 1996; Embid, 2009) and the Colorado Plateau- Rocky Mountain region in general (Crossey et al., 2009; Karlstrom et al., 2013) host numerous well-preserved travertine deposits (Fig. 1.1). This paper focuses on a set of remarkable large-volume (0.2-0.9 km³) travertine deposits with surface areas of 10 - 40 km² and thicknesses ranging from 5 to more than 60 m. These deposits are of particular interest because they provide a stratigraphic record of degassing of significant amounts of carbon dioxide (CO₂) during discharge of groundwater from carbonic springs.

The large-volume travertine deposits of this study occur in the same general regions as Cenozoic basaltic volcanism, suggesting an over-pressuring of the CO₂/groundwater system with magmatic gases (e.g. Ballentine and Sherwood Lollar, 2002; Gilfillan et al., 2008 and 2009). They are preferentially located along faults of the eastern edge of the Rio Grande rift and along the Jemez lineament, a NE-trending zone of late Cenozoic volcanic fields that transects the southeastern Colorado Plateau (Fig. 1.1). Two of the large-volume travertine deposits in New Mexico, Mesa Aparejo and the Riley Travertine (Fig. 1.2), are in the proximity of an active magmatic system, both located near the margins of the Socorro magma body system, a sill-like intrusion at about 19 km depth (Rinehart and Sanford, 1981; Ake and Sanford, 1988; Balch et al., 1997) that causes active uplift in the area (Fialko and Simons, 2001; Pearse and Fialko, 2010; Reiter et al., 2010) and long-lived high heat flow (Reiter et al., 2010). The travertine deposit at

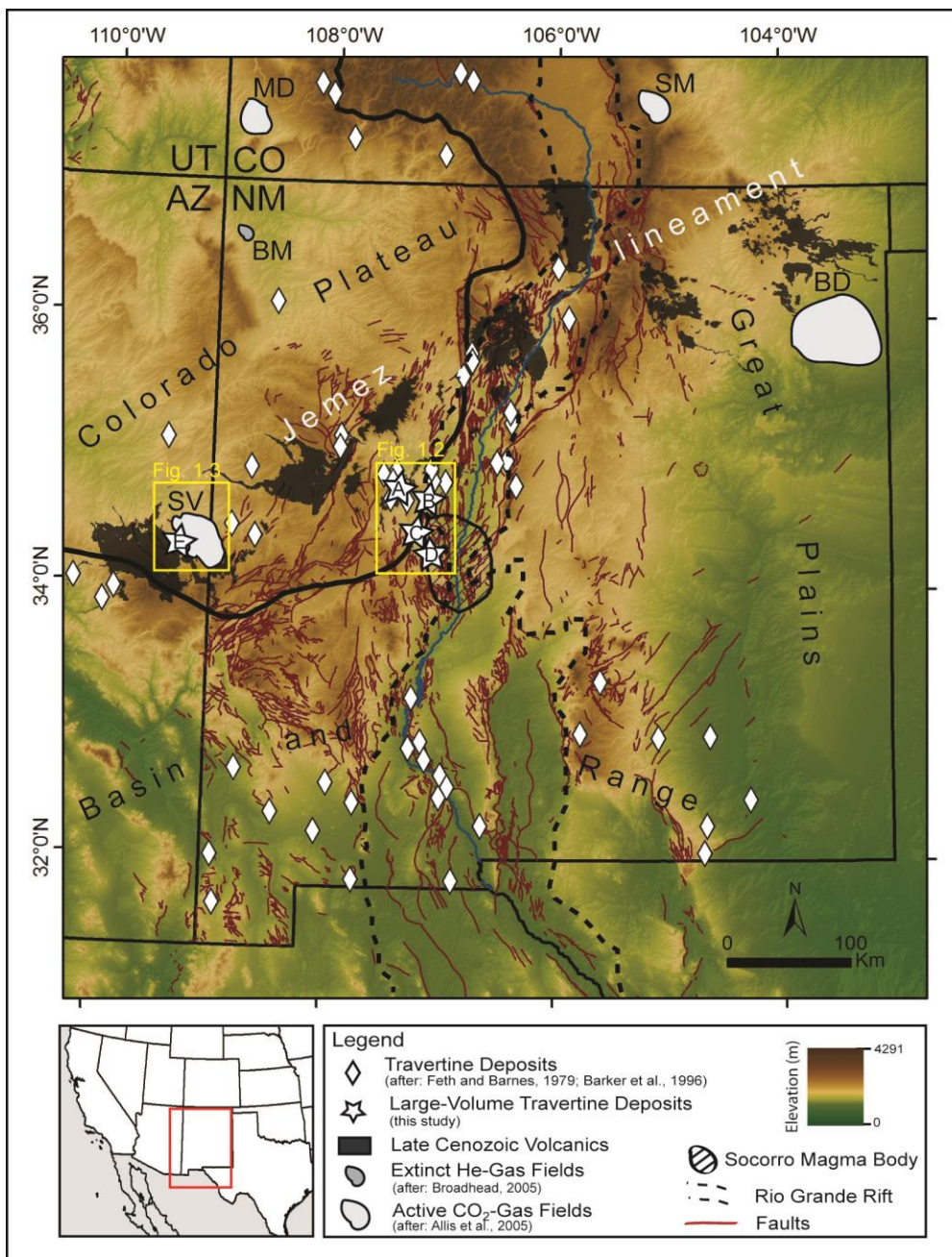


Figure 1.1. Digital elevation model (70 m) showing locations of travertine accumulations (Feth and Barnes, 1979; Barker et al., 1996), large-volume travertine deposits (this study) and associated tectonic features such as the Rio Grande rift and Jemez lineament. Also shown are Colorado Plateau, Great Plains, and Basin and Range physiographic provinces. Active CO₂ gas fields are Bravo Dome (BD) in New Mexico, Sheep Mountain (SM) and McElmo Dome (MD) in Colorado, and the Springerville-St. Johns Field (SV) in Arizona (Allis et al., 2005). Extinct He gas fields in northwestern New Mexico (BM) are Beautiful Mountain-Big Gap Organ Rock, Tocito Dome North, Table Mesa, and Rattlesnake (Broadhead, 2005). Large-volume travertine deposits in New Mexico are Mesa del Oro (A), Mesa Aparejo (B), Riley North Mesa (C), Riley South Mesa (D), and Springerville (E). Yellow boxes indicate locations of Figures 1.2 and 1.3.

Mesa Del Oro is associated with Cenozoic basaltic volcanism (Fig. 1.2). The travertine deposits at Springerville, AZ, are associated with an active modern CO₂-gas field and a Late Cenozoic volcanic field (Figs. 1.1 and 1.3).

Travertines of the Colorado Plateau have been the focus of recent attention in terms of models for diffuse mantle degassing through continents and degradation of groundwater quality due to input of endogenic fluids (Newell et al., 2005; Crossey et al., 2009; Karlstrom et al., 2013). The travertine record has also been linked to CO₂ degassing during seismic events (Uysal et al., 2009), and used as a natural laboratory for studying CO₂ sequestration and leakage (Shipton et al., 2005; Dockrill and Shipton, 2010; Kampman et al., 2012). Some authors conclude that travertines may provide a potential terrestrial record of paleoclimate and paleohydrologic cycles (Szabo, 1990), and more specifically, that episodes of travertine deposition may take place in response to climatic warming (Kampman et al., 2012), and may provide a tool to date important climate transitions (Faccenna et al., 2008).

The goal of this paper is to evaluate both the history and processes of formation of large-volume travertine deposits of the southeastern Colorado Plateau. U-series dating is employed to determine when they formed, and their spatial and temporal distribution is used to discuss several potential influences on travertine deposition including: 1) tectonic forcings such as faulting, basaltic magmatism, and mantle degassing along the Rio Grande rift and Jemez lineament, 2) rates and patterns of long-term landscape denudation in this region, and 3) possible temporal associations with regional paleoclimate and paleohydrology records.

BACKGROUND ON TRAVERTINE FORMATION

The term “travertine” is used here for continental limestones formed from discharge in springs and along streams (Ford and Pedley, 1996; Pentecost, 2005). A key to the formation of

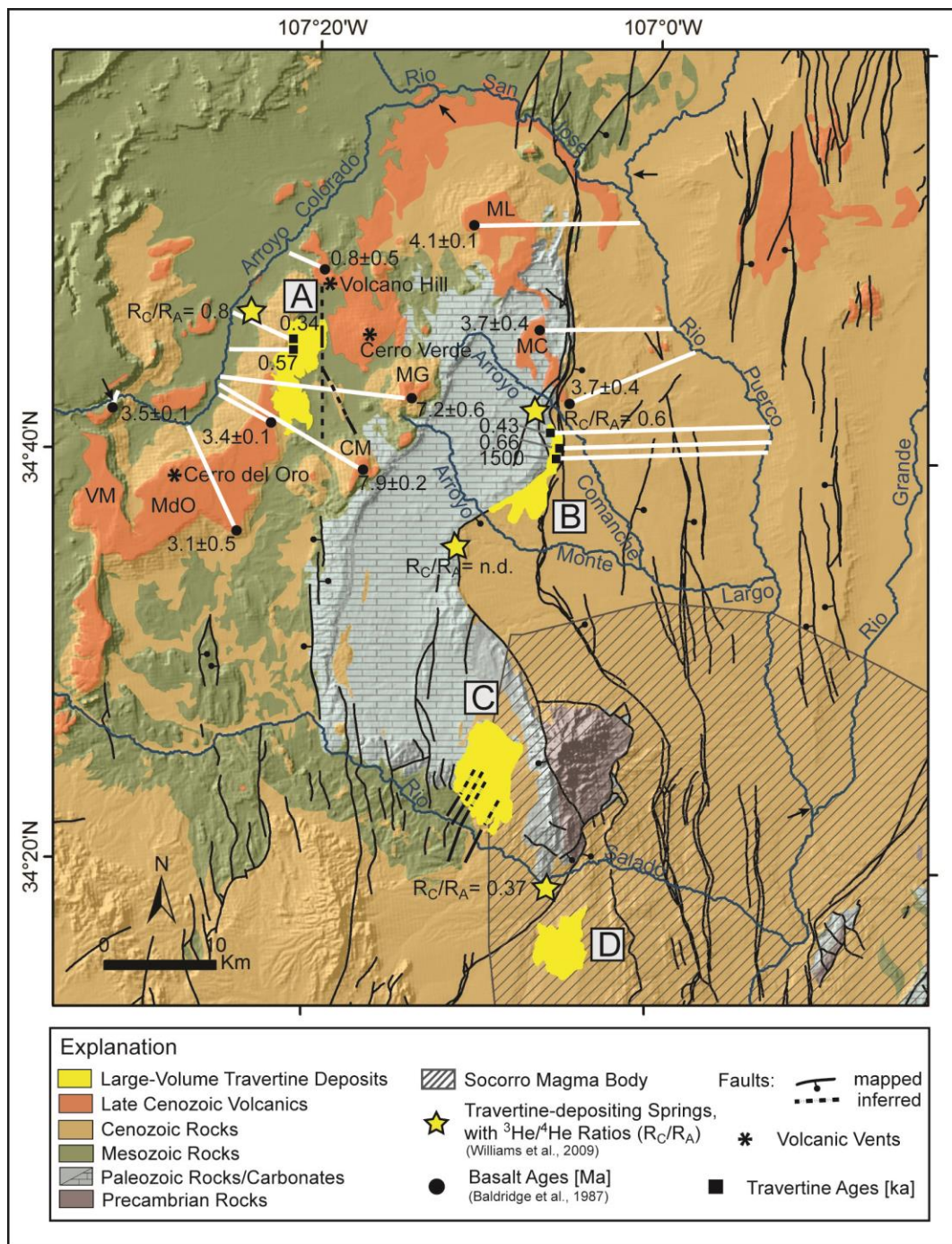


Figure 1.2. Geologic map of study areas in New Mexico showing large-volume travertine deposits, associated volcanics, basalt ages (Baldrige et al., 1987) travertine ages (this study), and travertine-depositing springs with $^3\text{He}/^4\text{He}$ ratios (Williams et al., 2009). White lines indicate topographic profiles for denudation rate calculations and are drawn to the local base levels. Black arrows indicate the range of base level elevation. Large-volume travertine deposits are: Mesa del Oro (A), Mesa Aparejo (B), Riley North Mesa (C), Riley South Mesa (D). Basalt Mesas are: Victorino Mesa (VM), Mesa del Oro (MdO), Mesa Lucero (ML), and Mesa Carrizo (MC). R_C = air-corrected $^3\text{He}/^4\text{He}$, R_A = $^3\text{He}/^4\text{He}$ of air (1.4×10^{-6}).

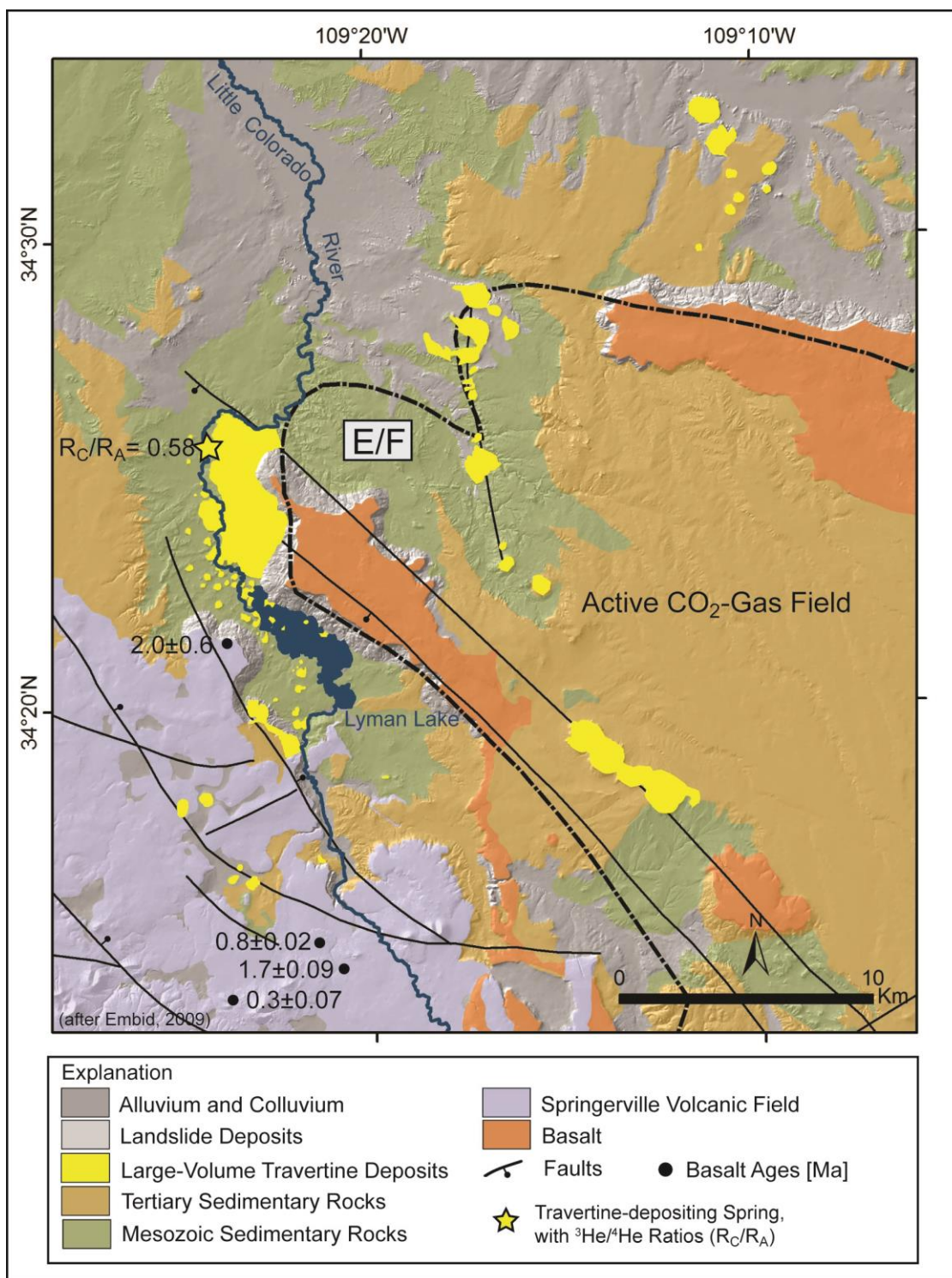


Figure 1.3. Geologic map of large-volume travertine deposits at Springerville, Arizona, showing travertine platforms and mounds located at the active Springerville-St. Johns Field (dot-dash line), basalt ages, and a modern travertine-depositing spring with ³He/⁴He ratios (Embaid, 2009). E/F indicate location of major travertine deposit and refer to Figure 4. R_C = air-corrected ³He/⁴He, R_A = ³He/⁴He of air (1.4 × 10⁻⁶).

these fresh water carbonate deposits is the degassing of carbon dioxide (CO₂) from groundwater that is supersaturated with respect to calcium carbonate according to the following reactions (Pentecost, 2005; Crossey et al., 2006 and 2009):



It is the external CO₂ that makes groundwater aggressive enough to dissolve the limestone. In modern travertine-depositing springs of the region a significant component of the external CO₂ has been shown to be derived from deep geological sources (Crossey et al., 2009; Karlstrom et al., 2013; Williams et al., 2013). Of the other volatiles carried with the CO₂, helium isotopes provide a tracer of potential mantle contributions (Ballentine and Sherwood Lollar, 2002). In particular, ³He/⁴He ratios of > 0.1 R_A (R_A = ³He/⁴He ratio in air = 1.4 x 10⁻⁶) show that the active travertine-depositing springs near the large-volume travertine deposits contain unequivocal evidence for the presence of mantle-derived volatiles (Newell et al., 2005). The sources of the deeply derived CO₂ are varied and the water chemistry of modern travertine-depositing springs shows complex mixing of meteoric recharge, groundwater with long residence times, and the deeply-derived fluids (Minissale et al., 2002; Newell et al., 2005; Crossey et al., 2006 and 2009; Embid, 2009; Williams et al., 2013)

The morphology of travertine deposits is controlled by topography and the tectonic setting of the springs (Hancock et al., 1999; Pentecost, 2005). Fault-related fissure ridges, analogous to magmatic dikes, form on tensional fissures where travertine precipitates from spring orifices along a central fracture (Hancock et al., 1999; Chafetz and Folk, 1984; Pentecost, 2005; Brogi and Capezzuoli, 2009), and sometimes a fissure ridge is associated with spring mounds, circular domes of travertine that surround a central spring orifice (Pentecost, 2005).

Spring mounds and terraced mounds as described by Chafetz and Folk (1984) and Pentecost (2005) require a hydraulic head and water under artesian pressure (Pentecost, 2005; Linares et al., 2010). If they self-seal due to rapid deposition or a drop in hydraulic head the spring will migrate to a lower level, which leads to coalescing spring mounds and complex deposits (Pentecost, 2005; Linares et al., 2010). Coalescing spring mounds also form when the travertine-precipitating springs are aligned along a fault line (Pentecost, 2005). The travertine morphologies of the study areas in this paper comprise a fissure ridge, terraced mounds, spring mounds, and coalescing spring mounds. The latter form extensive planar travertine surfaces raised above the ground, referred to as travertine platforms in this paper.

GEOLOGIC SETTING OF THE STUDY AREAS

Travertine deposits in New Mexico and Arizona occur along two major tectonic features, the Rio Grande rift and the Jemez lineament. The north-south trending Rio Grande rift extends over more than 1,000 km from Colorado to Mexico (Fig. 1.1; e.g. Keller and Baldrige, 1999; Reiter and Chamberlin, 2011). Structurally, it consists of a series of asymmetric Miocene, *en-echelon* half-grabens that widen and become more diffuse to the south, until they interfinger with the Basin and Range province in south-central New Mexico (Keller and Baldrige, 1999; Reiter and Chamberlin, 2011). Extensional faults related to the extension of the Rio Grande rift were active from about 35 Ma to present, with the highest magnitude of extension of ~10-30% in the Miocene (Russell and Snelson, 1994). Normal faulting locally overprinted and reactivated compressional faults that formed Rocky Mountain uplifts during the Laramide orogeny (75-43 Ma) and thus, rift-bounding faults often record complex poly-stage movements (Keller and Baldrige, 1999; Cather, 2004; Seager, 2004; Minor et al., 2013). Ongoing extension in the Rio Grande rift is taking place at relatively slow rates of ~0.1 mm/yr (Berglund et al., 2012).

A distinct crustal feature in the central Rio Grande rift is the Socorro magma body (Fig. 1.1), a sill-like intrusion at about 19 km depth (Rinehart and Sanford, 1981; Ake and Sanford, 1988; Balch et al., 1997) that causes active uplift of the region it underlies (Fialko and Simons, 2001; Pearse and Fialko, 2010; Reiter et al., 2010). Observed heat flow data suggests that the Socorro magma body is only the most recent manifestation of a much longer-lived magmatic plumbing system within the rift (Reiter et al., 2010). The Socorro magma body is associated with the Socorro seismic anomaly which causes numerous small magnitude events per year. The microseismicity and associated magmatism in various parts of the Rio Grande rift are thought to provide a source for mantle-derived CO₂ and ³He (Newell et al., 2005; Williams et al., 2013).

In northern New Mexico, the Rio Grande rift intersects the Jemez lineament that cuts across the Colorado Plateau, Rio Grande rift, and southern Great Plains (Aldrich, 1986; Chamberlin, 2007). The Jemez lineament is defined as a prominent belt of late Cenozoic basaltic volcanic fields (Fig. 1.1; Dunbar, 2005) whose distribution has been attributed to the presence of a long-lived, NE-trending, intercontinental tectonic and magmatic zone that may have initially formed as a Proterozoic accretionary boundary (Aldrich and Laughlin, 1984; Karlstrom and Humphreys, 1998; Magnani et al., 2004; Karlstrom et al., 2005). This zone is directly underlain by a low-velocity sub-lithospheric mantle domain (Schmandt and Humphreys, 2010) which likely provided a source for the basaltic magmatism and appears to be tectonically active due to on-going mantle-driven uplift as suggested by bowed fluvial terraces, tilted basalt paleo-surfaces, and river channels with high normalized steepness indices along the lineament where it extends out into the Great Plains (Wisniewski et al., 2002; Nereson et al., 2013).

TRAVERTINE FACIES

A detailed facies analysis of the travertine deposits in the study areas is discussed more fully elsewhere (Priewisch et al., 2013) but also deserves to be briefly mentioned here. The two important travertine facies from the study areas in New Mexico are: a step-pool facies and a paludal facies. The step-pool facies forms along fissure ridges, on terraced mounds and spring mounds, and along streams. Several travertine lithologies and textures form in step-pool environments depending on location within these pools; these include: 1) peloidal travertine, 2) horizontally laminated travertine, 2) drapes, 3) microterraces, and 4) travertine breccia. The paludal facies represents marsh and lake margin environments, with a fluctuating water table, ponds, vegetated areas, and varying dry and wet conditions (Glover and Robertson, 2003; Pentecost, 2005; Crossey et al., 2011). Travertine lithologies in these environments include: 1) carbonate mud or silt, 2) peloidal travertine, 3) peloidal travertine with plant remains, 4) horizontally laminated travertine, and 5) travertine breccia. Embid (2009) used facies classifications based on Fouke et al. (2000), Chafetz and Guidry (2003), Chafetz and Folk (1984), and Fouke et al. (2003) for the large-volume travertine deposits at Springerville in which both of these broad facies associations may have overlapped to produce vents, ponds, waterfalls, proximal- and distal-slopes, channels, and vegetated marshes.

Morphology and facies of the large-volume travertine deposits

The study areas in New Mexico are Mesa del Oro, Mesa Aparejo, and the Riley Travertine (North Mesa and South Mesa). Mesa del Oro is a Cenozoic basalt-capped mesa located near the southeastern boundary of the Colorado Plateau and associated with the Jemez lineament (Fig. 1.1). Large-volume travertine deposits formed in an area between two lava flows (Fig. 1.2) and field relationships in the northwestern part of the travertine deposit show that

travertine overlies basalt. Travertine accumulation at Mesa del Oro led to the formation of a northern and a southern travertine platform (Fig. 1.2). A fissure ridge is part of the northern travertine platform that formed along an approximately NNW-SSE trending fault (Figs. 1.2 and 1.4 A; Priewisch et al., 2013). The travertine-precipitating groundwater discharged from spring orifices along a central fracture (Chafetz and Folk, 1984; Hancock et al., 1999; Pentecost, 2005; Brogi and Capezzuoli, 2009) and flowed down the slopes of the fissure ridge which led to the formation of terraced mounds and the step-pool facies (Priewisch, et al., 2013). The paludal facies can be found at the western edge of the travertine platform, representing the flow of the travertine-precipitating groundwater away from the fissure ridge in streams and channels, eventually forming of a marsh in the distal part of the deposit (Priewisch et al., 2013).

The large-volume travertine deposit at Mesa Aparejo is located on the eastern side of the Lucero uplift along a reactivated reverse fault called Comanche fault that, along with the Cenozoic Santa Fe normal fault, separates Precambrian and older Paleozoic carbonates from younger Cenozoic rocks (Figs. 1.2 and 1.4 B; Barker et al., 1996). Travertine-precipitating springs discharged along the Comanche fault leading to the formation of coalescing spring mounds. The northeastern part of the deposit is actively quarried by New Mexico Travertine, Inc. (Austin and Barker, 1990) and the quarried travertines have, for example, supplied facing stone for the University of New Mexico in Albuquerque and the New Mexico State Capitol in Santa Fe.

Other large-volume travertine deposits, called the Riley Travertine, are located south of Mesa Aparejo. The Riley Travertine consists of two travertine platforms separated by the Rio Salado (Figs. 1.1 and 1.2). Riley North Mesa overlies Paleozoic, Mesozoic, and Cenozoic rocks, while Riley South Mesa rests on Cenozoic strata (Fig. 1.2; Barker, 1983). Both travertine

platforms are situated directly above the west margin of the Socorro magma body system (Figs. 1.1 and 1.2). Riley North Mesa formed when travertine-precipitating groundwater discharged along faults leading to the formation of spring mounds which eventually coalesced (Fig. 1.4 C). The travertine step-pool facies can be found throughout most of the travertine platform, while the paludal facies formed in the southern part of the deposit. Riley South Mesa is located to the southeast of Riley North Mesa (Figs. 1.2 and 1.4 D) and this travertine platform consists entirely of the paludal facies that formed in a wetland or marsh area.

The study area in Arizona is Springerville where large-volume travertine deposits are located along the southwestern edge of the Colorado Plateau and the southwestern part of the Jemez lineament (Fig. 1.1). They consist of travertine platforms and travertine mounds that rest on Mesozoic and Cenozoic sedimentary rocks. Travertine-precipitating groundwater discharged in springs along normal faults, in particular the Coyote Wash Fault (Figs. 1.3 and 1.4 E/F) leading to the formation of spring mounds which, in some areas, coalesced and formed large travertine platforms (Figs. 1.3 and 1.4 E/F; Embid, 2009). At the spring mounds, the step-pool facies developed while the paludal facies formed in more distal areas. The large-volume travertine deposits at Springerville are associated with an active CO₂-gas field (Fig. 1.3; Embid, 2009).

METHODS

Mapping and GIS volume analysis of the travertine extent was conducted on USGS 7.5' topographic maps and RGIS digital orthophotos (1 m) in the field and digitally with ArcMap GIS, using additional information of geologic maps compiled by Jicha (1958), Cather and Read (2003), Chamberlin (2004), and the New Mexico Bureau of Geology and Mineral Resources

(NMBGMR; 2003). In order to assess the volume of travertine for each deposit ArcMap was used to digitize the travertine extent on the digital orthophotos. The area was multiplied by the

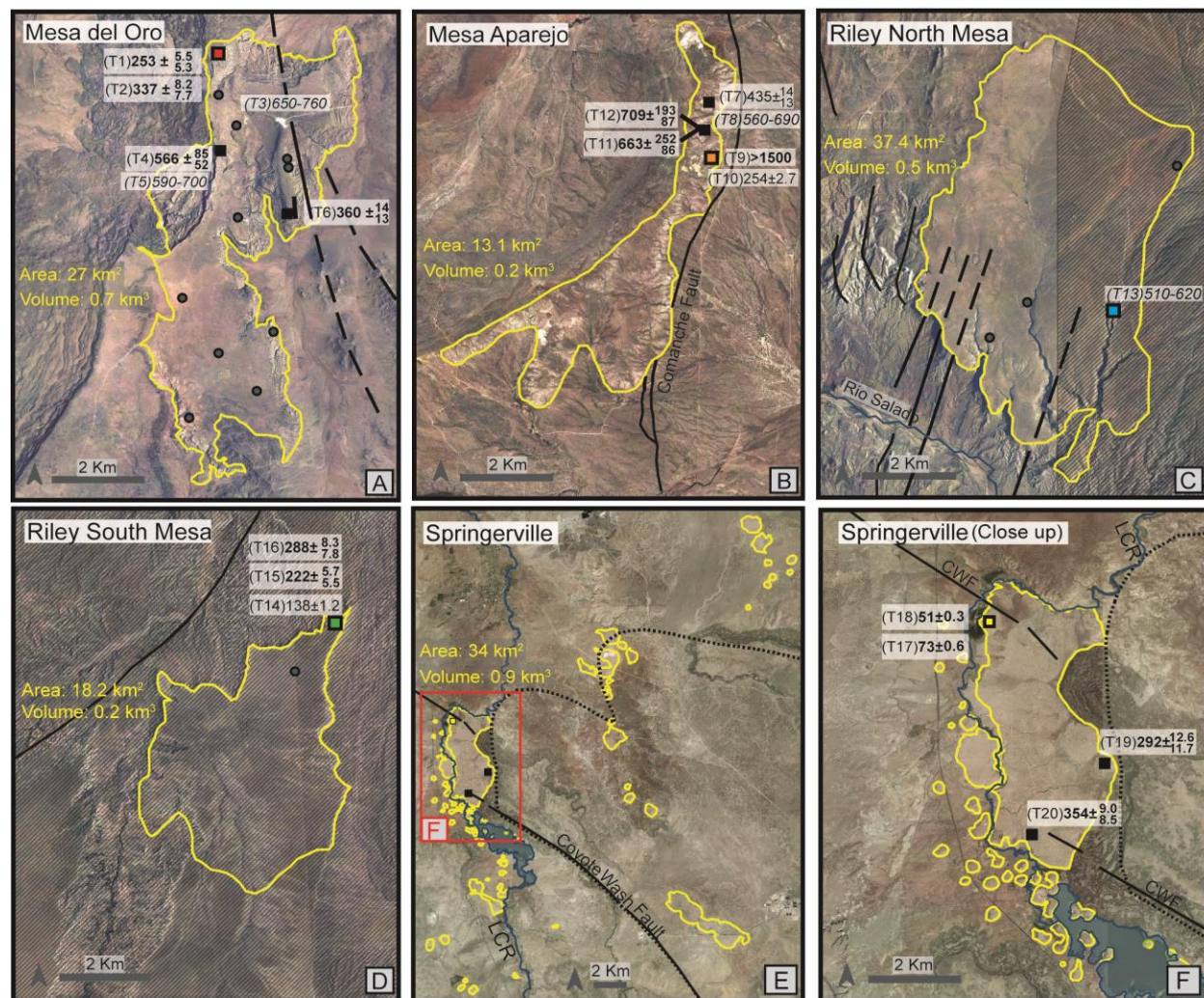


Figure 1.4. Aerial photos of large-volume travertine deposits in New Mexico and Arizona. The travertine extent is outlined in yellow; locations of measured sections are indicated by black and colored boxes (colored boxes correspond to colored boxes in Fig. 1.6). Ages in bold print are stratigraphic ages, ages in italics are model ages, and ages in regular font are infilling ages (all in ka). Also shown are borehole locations (grey circles), mapped faults (solid black lines), inferred faults (dashed black lines), Socorro magma body (hachured pattern in C, D), and active CO₂ gas field (black dashed line in E, F). (A) Mesa del Oro, (B) Mesa Aparejo, (C) Riley North Mesa, (D) Riley South Mesa. (E) Overview of deposits at Springerville. (F) Closeup view of the largest travertine platform (Salado Platform) and associated travertine mounds. LCR—Little Colorado River, CWF—Coyote Wash Fault.

average thickness of each deposit to determine the volume. Travertine thicknesses were obtained through mapping, from borehole reports provided by the NMBGMR, and published data (Moore et al., 2005; Embid, 2009).

Measured sections (Figs. 1.5 and 1.6; Table DR1) from the travertine platforms in New Mexico and Arizona (Table DR1) were sampled to try to assess the duration of accumulations as well as individual ages. The travertine samples were cut into slabs and dense layers of micrite or sparry calcite (Fig. 1.5) were micro-drilled to provide powder for strontium isotope and U-series analysis. Except for Springerville, where Embid (2009) collected and dated several samples, only top and bottom samples of the measured sections were dated in order to constrain the depositional interval.

Travertine samples were dated with the U-series method at the Radiogenic Isotope Laboratory at the University of New Mexico using the methods described in Asmerom et al. (2010). This is a reliable dating method for measuring geologic age back to about 500-600 ka (Edwards et al., 1987) due to the fact that the system $^{234}\text{U} - ^{230}\text{Th}$ returns to secular equilibrium within analytical resolution after $\sim 6-8$ half-lives of the daughter isotope, ^{230}Th , which has a half-life of 75,700 years (Cheng et al., 2000). All of the samples are plotted on a uranium evolution diagram in order to visualize samples that have robust ages, samples that underwent uranium loss (evidence for alteration), and samples that were beyond U-series range, but still within the age range ($\sim 1.5-2$ Ma) amenable for ^{234}U model ages (Figure DR1 and Table DR2). For samples outside of U-series range, model ages were calculated (Table 1.1) by using a range of assumed $\delta^{234}\text{U}$ values corresponding to values from dated samples that had robust U-series dates within the same location (Tables DR4 and DR5). This assumes that spring chemistry was similar through time in each area. If the minimum $\delta^{234}\text{U}$ values of the area generated model ages within

Table 1.1: U-Series Data and Strontium Isotope Ratios of all Travertine Samples

Sample No.	^{238}U (ppm)	2σ error	^{232}Th (pg/g)	\pm error	$(^{230}\text{Th}/^{232}\text{Th})$ activity	\pm error	$^{232}\text{Th}/^{238}\text{U}$ ratio	error	$(^{230}\text{Th}/^{238}\text{U})$ activity	2σ error	$\delta^{234}\text{U}_m$ measured	\pm error
T1	0.536	0.001	4,783.82	51.79	343.55	4.071	0.009	0.000	1.011	0.005	95.2	1.6
T2	0.205	0.000	41,548.61	125.35	17.29	0.075	0.210	0.000	1.156	0.004	156.3	0.6
T3	0.949	0.002	941.50	42.70	3292.90	149.610	0.001	0.000	1.077	0.005	47.8	1.2
T4	0.927	0.002	370,314.27	894.04	8.40	0.033	0.413	0.001	1.105	0.004	78.6	1.1
T5	0.660	0.003	57,891.70	519.31	37.99	0.370	0.091	0.000	1.098	0.006	57.4	2.3
T6	0.165	0.000	2,635.22	68.65	208.59	5.486	0.017	0.000	1.100	0.005	105.5	2.3
T7	0.550	0.000	1,222.47	48.19	269.59	1.213	0.012	0.000	1.039	0.002	42.6	1.0
T8	0.884	0.000	10,395.72	41.83	269.59	1.213	0.012	0.000	1.045	0.002	21.4	1.0
T9	0.613	0.000	26,837.64	48.94	69.84	0.190	0.045	0.000	1.009	0.002	0.9	1.0
T10	0.525	0.000	23,470.63	43.83	63.66	0.175	0.046	0.000	0.937	0.002	28.2	1.0
T11	0.445	0.000	3,784.95	52.39	359.05	5.024	0.009	0.000	1.007	0.002	6.3	1.0
T12	0.495	0.000	4,279.88	38.33	407.88	3.744	0.009	0.000	1.162	0.002	114.6	1.1
T13	0.701	0.002	439,489.50	1081.52	5.33	0.021	0.648	0.002	1.102	0.004	71.2	0.7
T14	0.459	0.001	33,870.13	91.72	41.36	0.170	0.076	0.000	1.007	0.004	335.4	0.5
T15	2.682	0.006	27,214.03	217.42	351.33	4.061	0.010	0.000	1.175	0.010	280.1	1.1
T16	2.345	0.005	2,127,046.00	65.10	4.90	0.019	0.937	0.003	1.466	0.006	429.2	0.6
T17	0.215	0.001	18,133.41	71.48	46.53	0.250	0.087	0.000	1.291	0.006	1486.0	3.3
T18	0.299	0.001	565.04	44.70	1440.28	114.069	0.002	0.000	0.897	0.005	1296.1	4.7
T19	0.026	0.000	1,936.65	47.09	55.32	1.425	0.087	0.002	1.384	0.012	370.2	5.4
T20	0.504	0.001	20,035.59	77.62	146.19	0.719	0.041	0.000	1.916	0.008	738.9	3.7
T21	0.460	0.002	17,068.20	74.30	437.43	2.490	0.038	0.000	0.990	0.007	35.3	4.8
T22	0.461	0.001	17,068.20	74.30	437.43	2.358	0.038	0.000	0.988	0.007	36.5	2.9
T23	0.874	0.000	24,986.13	43.31	110.38	0.293	0.030	0.000	1.040	0.002	2.7	1.0
T24	0.122	0.000	4,792.80	47.38	100.93	1.065	0.040	0.000	1.304	0.006	132.5	1.0
T25	0.542	0.001	6,427.96	65.11	307.54	3.256	0.012	0.000	1.203	0.005	52.0	0.6

(continued)

$\delta^{234}\text{U}_i$	+ error	- error	uncorr age	+ error	- error	corr age	+ error	- error	model age	$^{87}\text{Sr}/^{86}\text{Sr}$	2σ error
initial			ka	ka	ka	ka	ka	ka	ka		
194.5	4.5	4.4	252,969	5,510	5,285	252,750	5,500	5,275		0.709335	0.00001
405.4	9.7	8.9	341,470	8,242	7,731	337,163	8,241	7,728		0.709239	0.00001
									650-760		
388.8	105.6	53.5	574,440	93,882	55,313	565,700	84,917	52,105			
									590-700		
292.3	13.2	12.1	360,944	13,844	12,666	360,581	13,800	12,628		0.710445	0.00001
145.1	7.0	6.3	434,743	14,380	13,095	434,629	14,365	13,082		0.717823	0.00001
									560-690		
secular equilibrium (>1,500,000 ka)											
57.7	2.1	2.1	256,093	2,500	2,455	253,589	2,746	2,691		0.720272	0.00001
40.7	42.7	11.0	663,204	255,563	86,630	662,723	252,124	86,343			
847.8	613.9	185.0	709,683	193,842	87,294	709,408	193,042	87,145			
									510-620		
495.8	1.9	1.8	139,696	1,016	1,007	138,240	1,238	1,226		0.710328	0.00001
524.5	8.8	8.3	222,127	5,747	5,493	221,932	5,738	5,485		0.709553	0.00001
967.7	23.0	21.1	301,962	4,954	4,775	287,690	8,285	7,787		0.709127	0.00001
1825.0	5.2	5.2	73,586	457	456	72,710	630	627			
1499.0	5.7	5.7	51,487	354	353	51,465	354	353			
845.5	33.1	30.0	293,456	12,737	11,765	292,244	12,625	11,669			
2008.1	52.7	49.0	354,146	9,026	8,578	353,758	9,001	8,555			
86.7	12.1	12.0	318,897	18,242	16,200	318,891	11,775	10,436			
88.0	7.2	7.1	312,531	14,098	12,786	311,529	6,488	6,057			
uranium loss											
uranium loss											
uranium loss											

For sample locations and stratigraphic positions of samples see Table DR1.

U-series range, they were rejected and the area $\delta^{234}\text{U}$ mean and maximum values represent our preferred age brackets for these samples (Tables DR4 and DR5).

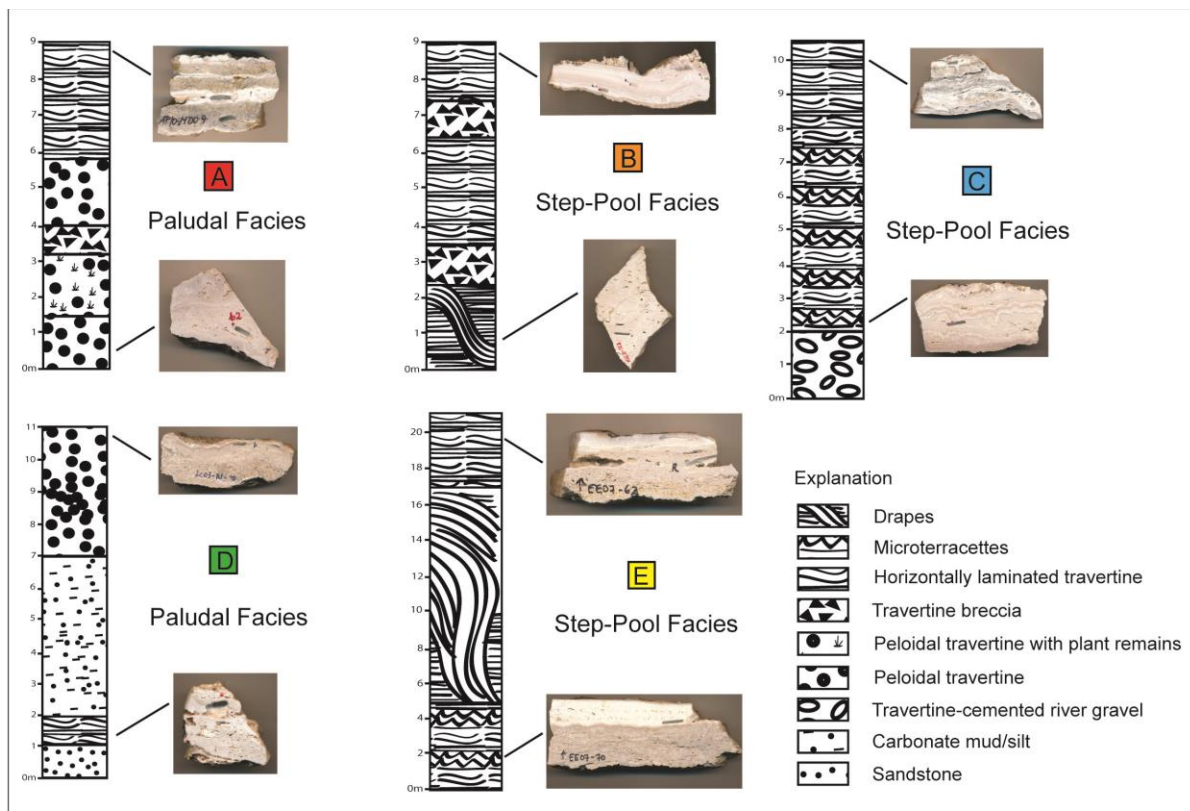


Figure 1.5. Schematic stratigraphic columns showing travertine lithologies: (A) Mesa del Oro, (B) Mesa Aparejo, (C) Riley North Mesa, (D) Riley South Mesa, and (E) Springerville. Also shown are photos of travertine samples that were used for U-series dating and strontium analysis and the position of these samples within the stratigraphic column. Colored boxes (A-E) correspond to Figure 1.6.

Strontium isotopes of eight travertine samples were analyzed to help understand mixing relationships of different groundwater components (Clark and Fritz, 1997; Crossey, 2006). For this analysis, 10-50 mg of powdered travertine sample was dissolved in 0.5 ml of 7 N HNO_3 and spiked with 1 ml ^{84}Sr spike. The sample solution was then fluxed for 1 hour. 0.2 ml of Sr-speciation resin was placed into 2-ml columns and conditioned with 3 N HNO_3 . Sr was dropped with

0.75ml H₂O, then Sr separates were dried down and re-dissolved in 1 ml of 3% HNO₃ for analysis on the Thermo Neptune MC-ICPMS.



Figure 1.6. Field photos of measured sections. (A) Mesa del Oro, (B) Mesa Aparejo, (C) Riley North Mesa, (D) Riley South Mesa, (E) Springerville. Color-coded boxes (A-E) correspond to Figure 1.4. Ages in bold print are stratigraphic ages, ages in italics are model ages, and ages in regular font are infilling ages (all in ka). A thickness of 8.30 m at the measured section at Mesa del Oro (A) was used to calculate a deposition rate over 84 k.y. which results in 10 cm/k.y. (see text). Height of travertine sections in (A) and (E) are approximately 8.30 m and 22.30 m, respectively.

RESULTS

Travertine platform geometries and travertine ages that are shown in Figure 1.4 are described and discussed below regarding their extent, thickness, association with faults and active springs in the area, and new U-series ages.

The travertine deposits at Mesa Del Oro cover an area of 27 km² and have an estimated travertine volume of 0.7 km³ (Fig. 1.4 A). The travertine is thickest at the fissure ridge, up to 65 m based on drill cores provided by the NMBGMR. The fissure ridge is part of a complex fault system which is mapped to the southeast of Mesa del Oro (Fig. 1.2; Jicha, 1958; Grauch and Connell, 2013). Well-preserved travertine vents were not found but they were probably located in the area where the travertine is thickest. There are no active springs associated with the travertine platforms; however, dissolution caves may attest to past spring locations and groundwater activity within the northern travertine platform (Forbes and Stephens, 1994). The nearest travertine-precipitating CO₂- and ³He-rich spring (Eddleman Spring) is approximately 6 km to the northwest of the northern travertine platform (Fig. 1.2; Williams et al., 2013). The travertine deposits at Mesa del Oro locally overlie Cenozoic basalts which erupted from volcanic vents located at the northern edge (Cerro del Oro) and in the western part of the basalt mesa (Fig. 1.2; Jicha, 1958; Baldrige et al., 1987). Basalt flows have K-Ar ages of 3.5 ± 0.1 Ma, 3.4 ± 0.1 Ma, and 3.1 ± 0.5 Ma, and 0.8 ± 0.5 Ma (Baldrige et al., 1987). These basalts flowed to the northeast and southeast along an arcuate paleodrainage subparallel to the modern Arroyo Colorado between 3.4 Ma and 0.8 Ma (Fig. 1.2).

U-series ages from Mesa del Oro are 566 ± 68.5 ka, 360 ± 13.5 ka, 337 ± 8.0 ka, and 253 ± 5.4 ka (Fig. 1.4 A; Table 1.1). Calculated model ages for two samples are slightly older, 590-700 ka and 650-760 ka. These results imply that travertine formation at Mesa del Oro occurred in

two intervals, from 360 ka to 250 ka and from ~560 ka to 760 ka. Samples T4 and T5 from the western edge of the deposit have similar ages (566 ka and 590-700 ka, respectively) that overlap within error (Fig. 1.4 A; Table 1.1). Two samples, T1 and T2, from the northwestern edge of the travertine platform gave stratigraphically constrained ages of 337 ka (bottom) and 253 ka (top), which suggests travertine deposition over 84 ka (Figs. 1.4 A and 1.6 A; Table 1.1). Strontium isotope values ($^{87}\text{Sr}/^{86}\text{Sr}$) of three travertine samples at Mesa del Oro are relatively non-radiogenic (Table 1.1) and compatible with hydrologic models where the majority of the water volume originates from surface recharge in the Lucero uplift (Goff et al., 1983). The $\delta^{234}\text{U}_{\text{initial}}$ values are also consistent with this interpretation (Table 1.1).

At Mesa Aparejo, the travertine platform extends over an area of 13.1 km² and has an estimated travertine volume of 0.2 km³ (Fig. 1.4 B). Coalescing mounds indicate that spring vents were aligned along the N-S trending Comanche fault, one of the major rift-bounding fault systems that is interpreted to have acted as a conduit for spring water. A significant fraction of the CO₂ may have originated from the Socorro magma body system and moved up a basement-penetrating Laramide fault system (Ricketts et al., 2012). Modern CO₂- and ³He-rich springs associated with modern travertine deposits, e. g. Salado Arroyo Spring, are located nearby in modern washes along the same fault system to the north and south of the travertine deposit (Fig. 1.2; Newell et al., 2005; Barker et al., 1996). Volcanic vents located to the north of Mesa Aparejo erupted 4.1 ± 0.1 Ma and 3.7 ± 0.4 Ma (Bachman and Mehnert, 1978; Baldrige et al., 1987) and produced basalt flows that followed paleo-drainages to the south (Fig. 1.2).

Travertine samples from the quarries Temple Cream, Sheherazade, and Vista Grande, located in the northeastern part of Mesa Aparejo (Fig. 1.4 B), were dated. At Temple Cream, sample T10 has a robust U-series age of 254 ± 2.7 ka while sample T9 is in secular equilibrium

and older than 1.5-2 Ma (Figs. 1.4 B and 1.6 B; Table 1.1). Two samples at Sheherazade, T11 and T12, gave U-series ages of 663 ± 169 ka and 709 ± 140 ka which overlap within error and which are considered to be usable, though imprecise, ages (Fig. 1.4 B; Table 1.1). A robust U-series age of 435 ± 13.5 ka was obtained from sample T7 at Vista Grande while a model age was calculated for sample T8 at the same location (Fig. 1.4 B; Table 1.1) that ranges from 560-690 ka. For both quarry locations the younger travertine samples are inferred to be infillings that formed when groundwater was injected into the existing section due to a high hydraulic head. Embid (2009) also described these types of infillings in a travertine mound at Springerville where secondary infillings occurred in a pulse late in the lifespan of the mound. Two travertine samples from Mesa Aparejo, T7 and T10, have strontium isotope values ($^{87}\text{Sr}/^{86}\text{Sr}$) of 0.717823 and 0.720272 (Table 1.1). These highly radiogenic values indicate circulation of waters through granitic Precambrian basement, compatible with hydrologic models for mixing of meteoric recharge with deep fluids along faults of the western Rio Grande rift (Goff et al., 1983; Williams et al., 2013) and supported by the $\delta^{234}\text{U}_{\text{initial}}$ values for these samples (Table 1.1).

Riley North Mesa covers an area of 37.4 km^2 and has an estimated travertine volume of 0.5 km^3 (Fig. 1.4 C). The travertine platform lacks well-preserved travertine vents. Rift-margin faults and the basement-Paleozoic unconformity probably served as conduits for the CO_2 -rich waters and springs discharged where faults intersected progressively down-cutting drainages. These faults are now concealed by the travertine but have been mapped to the south of Riley North Mesa (Figs. 1.2 and 1.4 C; Lewis and Baldrige, 1994). Based on borehole data provided by the NMBGMR, the travertine is thickest (up to 22 m) in the southwestern part of the travertine platform. A model age ranging from 510-620 ka for the dated sample was calculated by using the mean and maximum value of $\delta^{234}\text{U}$ of successful U-series ages from Mesa del Oro

(Table DR4), assuming that the travertine-precipitating groundwater that formed the deposits came from the same aquifer.

Riley South Mesa extends over an area of 18.2 km², and has an estimated travertine volume of 0.2 km³ (Fig. 1.4 D). The travertine platform consists of carbonate-cemented sandstone and cm- to m-scale travertine layers intercalated at the top with pedogenic carbonate. Barker (1983) describes travertine thicknesses of typically 4-6 m and as much as 15 m. Riley South Mesa is slightly tilted to the west (Barker, 1983) and lacks well-preserved travertine vents. This section has complex age-height relations but deposition took place from 288-138 ka. Individual ages of dated samples are shown in Figures 1.4 D and 1.6 D and Table 1.1. A modern example of a CO₂-/³He-rich travertine-depositing spring is the Rio Salado Spring located in the drainage between the two travertine platforms (Fig. 1.2; Newell et al., 2005) which discharges from the Pennsylvanian Madera limestone (Rawling, 2005). Three samples from Riley South Mesa, T14, T15, and T16 have strontium isotope values (⁸⁷Sr/⁸⁶Sr) of 0.710328, 0.709553, and 0.709127, respectively (Table 1.1). These values suggest mixing of dominantly meteoric waters with some input of deeply circulated waters which is supported by the $\delta^{234}\text{U}_{\text{initial}}$ values (Table 1.1).

The travertine deposits at Springerville occur over an area of 34 km² and have an estimated travertine volume of 0.9 km³ (Fig. 1.4 E/F; Embid, 2009). Travertine vents on the Salado Platform have pronounced shield geometries (Fig. 1.7 A) and central orifices (Fig. 1.7 B) and are located at the distal end of the Coyote Wash basalt flow that was dated between 2.94 ± 0.14 and 3.67 ± 0.12 Ma (Embid, 2009). The Springerville volcanic field was active from 8.97 ± 0.19 Ma until 0.31 ± 0.07 Ma (Condit and Connor, 1996) and volcanic activity overlaps with travertine deposition at 0.35 ± 0.01 Ma (Embid, 2009). Travertine deposition is still occurring

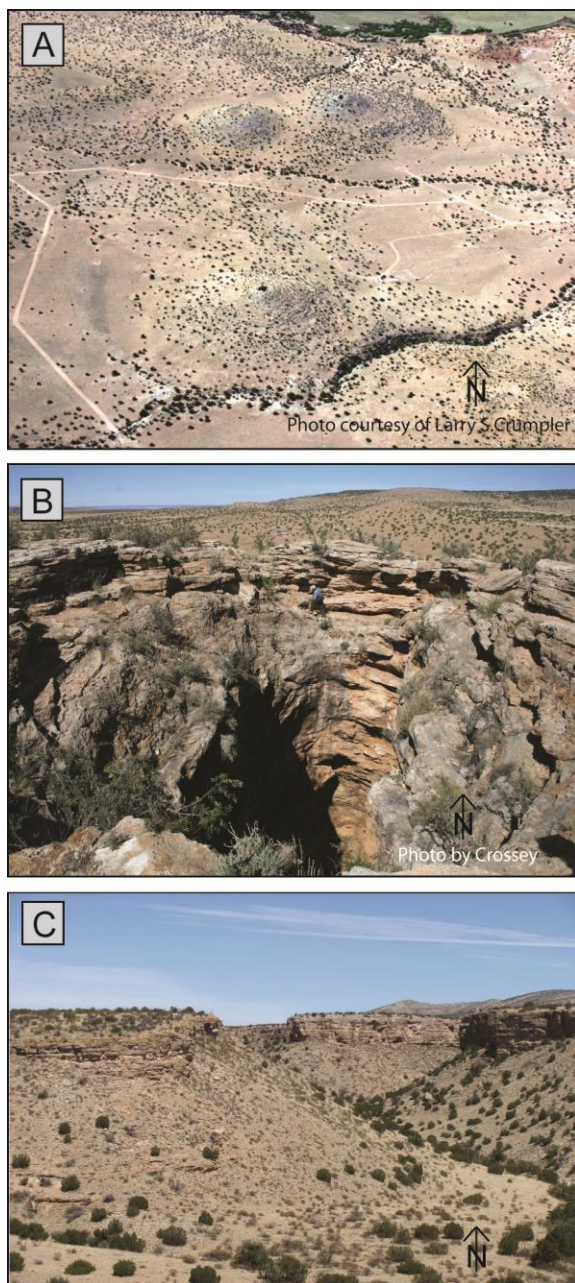


Figure 1.7. Travertine mounds and inverted topography of travertine platforms. (A) Coalesced travertine mounds at Springerville, Arizona. (B) Partly collapsed central orifice of a travertine mound at Springerville, Arizona. (C) Incised travertine platform capping underlying strata at Riley North Mesa, New Mexico, creating inverted topography.

today around Salado Springs, where the spring

water contains both CO_2 and mantle-derived ^3He

(Fig. 1.3; Gilfillan et al., 2008; Embid, 2009). The

travertine deposits at Springerville are located

above and along the western boundary of a

commercially important CO_2 -gas reservoir, the

Springerville-St. Johns Field (Figs. 1.3 and 1.4

E/F; Moore et al., 2005; Embid, 2009).

At Springerville, Embid (2009) obtained travertine

ages ranging from 51 ka to 354 ka (Fig. 1.4 F;

Table 1.1). The dated top and bottom samples of a

measured section at the largest travertine platform

are 51 ± 0.4 ka (T18) and 73 ± 0.6 ka (T17) old,

respectively, and represent semi-continuous travertine deposition spanning 22 ka (Figs. 1.4 F and

1.6 E; Table 1.1; Embid, 2009). Two other samples (T19, T20) from vents on the same travertine

platform have ages of 292 ± 12.1 ka and 354 ± 8.8 ka (Fig. 1.4 F; Table 1.1).

Summary of travertine ages

In this study, mainly tops and bottoms of travertine sections were dated in order to constrain time intervals of travertine formation. Other researchers who dated travertine (e. g. Sturchio et al., 1994; Faccenna et al., 2008; Sierralta et al., 2010) obtained individual ages throughout the Quaternary while this study shows that large volumes of travertine in New Mexico and Arizona formed episodically at 700-500 ka, 350-200 ka, and 100-40 ka (Fig. 1.8; Table 1.1). One sample which is older than 1.5 Ma indicates travertine formation at an earlier interval (Table 1.1), and travertine deposition is still taking place today around some spring vents. Nevertheless, the grouping of U-series dates is viewed as a record of episodes of large-volume travertine deposition in the region. As noted above, U-series ages show several general types of relationships relative to travertine stratigraphy. In some sections, e. g. at Mesa del Oro and Springerville, U-series ages are in agreement with stratigraphic position, and indicate that the vents or mounds were active for several 10 ka, with deposition rates of about 10 cm/k.y. (Fig. 1.6 A) to 1 m/k.y (Embid, 2009), respectively. In other cases, e. g. at Mesa Aparejo and Springerville, U-series infilling ages of travertine veins are younger than adjacent stratigraphic layers which indicates times when head was high enough to inject groundwater into fractures within existing travertine mounds or travertine platforms. This suggests that the same spring vents could be active at multiple times and that hydraulic head was high enough at a later time than during the initial mound accumulation to allow deposition at about the same elevation. Model ages are less precise in terms of durations and timing of episodes, but they demonstrate that many of the major travertine platforms were active in the interval of 500-700 ka.

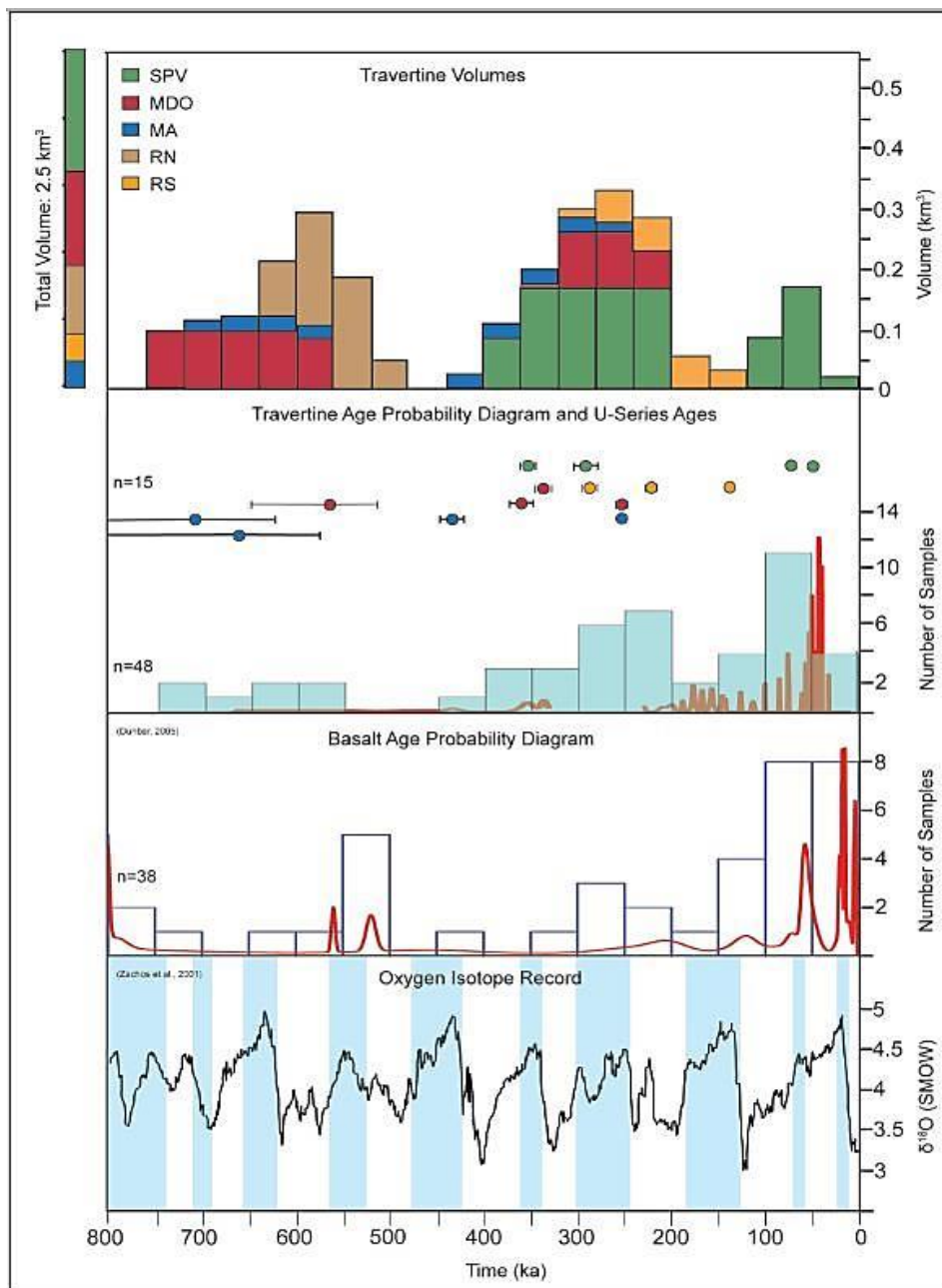


Figure 1.8. Travertine volumes and age probability diagram of dated travertine (this study) and basalt samples (Dunbar, 2005). Also shown is a deep sea oxygen isotope record (Zachos et al., 2001), where the blue-shaded areas represent glacial periods and the white areas interglacial periods. Color coding for travertine volumes: SPV (green) — Springerville, AZ; MDO (red) — Mesa del Oro, NM; MA (blue) — Mesa Aparejo, NM; RN (brown) — Riley North Mesa, NM; RS (orange) — Riley South Mesa, NM. Travertine volume histograms illustrate episodes of travertine formation and the amount of travertine for each episode, assuming steady-state deposition, based on the calculated volume for each deposit (Table DR6) and represented by the scale bar: individual volumes sum up to 2.5 km^3 . The travertine volume for Springerville was calculated based on travertine ages obtained by (Embaid, 2009). Travertine volumes for the study

areas in New Mexico are based on successful U-series ages reported in this study and shown as colored circles including four ages of representative top and bottom samples from Springerville (same color coding as for travertine volumes). The age probability diagram of travertine is based on 33 samples from Springerville dated by (Embid, 2009) and 15 dated samples of this study (Table DR7). The age probability diagram of basalt is based on 38 samples reported by Dunbar (2005). Both probability diagrams include a sample frequency histogram and the 2σ error curve; pronounced peaks of the curve represent smaller errors of travertine and basalt ages, whereas a flat curve represents large errors. The age probability diagrams were produced with Isoplot 4.15, an add-in program for Microsoft Excel used for the interpretation of radiogenic isotope data (Ludwig, 2003). SMOW — standard mean ocean water.

DISCUSSION AND IMPLICATIONS

This study attempts to evaluate possible drivers for episodic late Quaternary travertine deposition by examining potential tectonic drivers (faulting, magmatism, mantle degassing), as well as paleohydrologic drivers.

Tectonic influences on episodic travertine formation are documented at a local scale by the nearly ubiquitous association of travertine locations and major fault networks (Figs. 1.1-1.4). Movement along the Comanche fault allowed for travertine accumulation at Mesa Aparejo (Figs. 1.2 and 1.4 B; Callender and Zilinski, Jr, 1976; Austin and Barker, 1990; Barker et al., 1996). Ricketts et al. (2012) report a dominance of N-S subvertical calcite-filled extensional fractures in the travertine quarries at Mesa Aparejo that are compatible with the ~E-W trending extension of the rift. These fractures were active from ~250 ka to ~ 2 Ma suggesting upward flux of hydrothermal fluids over long periods of time despite potential clogging due to calcite precipitation (Curewitz and Karson, 1997; Ricketts et al., 2012). Travertine at Mesa del Oro precipitated from a fissure that is part of a complex extensional fault system to the southeast of the travertine platform (Figs. 1.2 and 1.4 A; Jicha, 1958; Priewisch et al., 2013) and associated with the E-W extension of the Rio Grande rift. The travertine platform at Riley North conceals a number of faults (Figs. 1.2 and 1.4 C) mapped by Lewis and Baldrige (1994) which might have

acted as potential pathways for CO₂-charged groundwater. At Springerville, the biggest travertine platform formed along the Coyote Wash fault (Figs. 1.3 and 1.4 E/F; Embid, 2009).

At much longer temporal and spatial scales, the association of travertine depositing springs and travertine platforms with regions of low mantle velocity (Fig. 1.9) suggests that diffuse mantle CO₂ degassing may be an important source for the external CO₂ necessary to deposit large volumes of travertine (Newell et al., 2005; Crossey et al., 2009). Episodes of travertine formation are associated with regional volcanism (Fig. 1.8) and underlying low-velocity mantle (Fig. 1.9) suggesting that magmatic degassing of CO₂ in addition to diffuse mantle degassing (e. g. Karlstrom et al., 2013) contributes to large-volume travertine deposition. This supports the interpretation that CO₂ in many Colorado Plateau travertines and gas fields is in large part of magmatic origin and ultimately mantle-derived. For example, the large-volume travertine deposits at Springerville are associated with the actively mined Springerville-St. Johns gas field that contains both CO₂ and helium. CO₂ is often considered to be a carrier gas for helium (Sherwood Lollar et al., 1997; Ballentine et al., 2001) which is reinforced by a mean ³He/⁴He value of 0.43 R_A (Gilfillan et al., 2008; Embid, 2009). This value indicates that about 20% of the helium is mantle-derived and suggests that a significant proportion of the CO₂ also likely originates from the mantle. Similarly, other large-volume travertine deposits in New Mexico and Arizona are associated with nearby springs that also contain mantle-derived helium and, by inference, mantle-derived CO₂ (Figs. 1.2 and 1.3; Embid, 2009; Williams et al., 2013). The association of mantle-derived helium and magmatically derived CO₂ is also present in some CO₂ gas fields in Colorado and Texas (Ballentine et al., 2001; Ballentine and Sherwood Lollar, 2002; Gilfillan et al., 2008 and 2009). These fields as well as most of the travertine-depositing

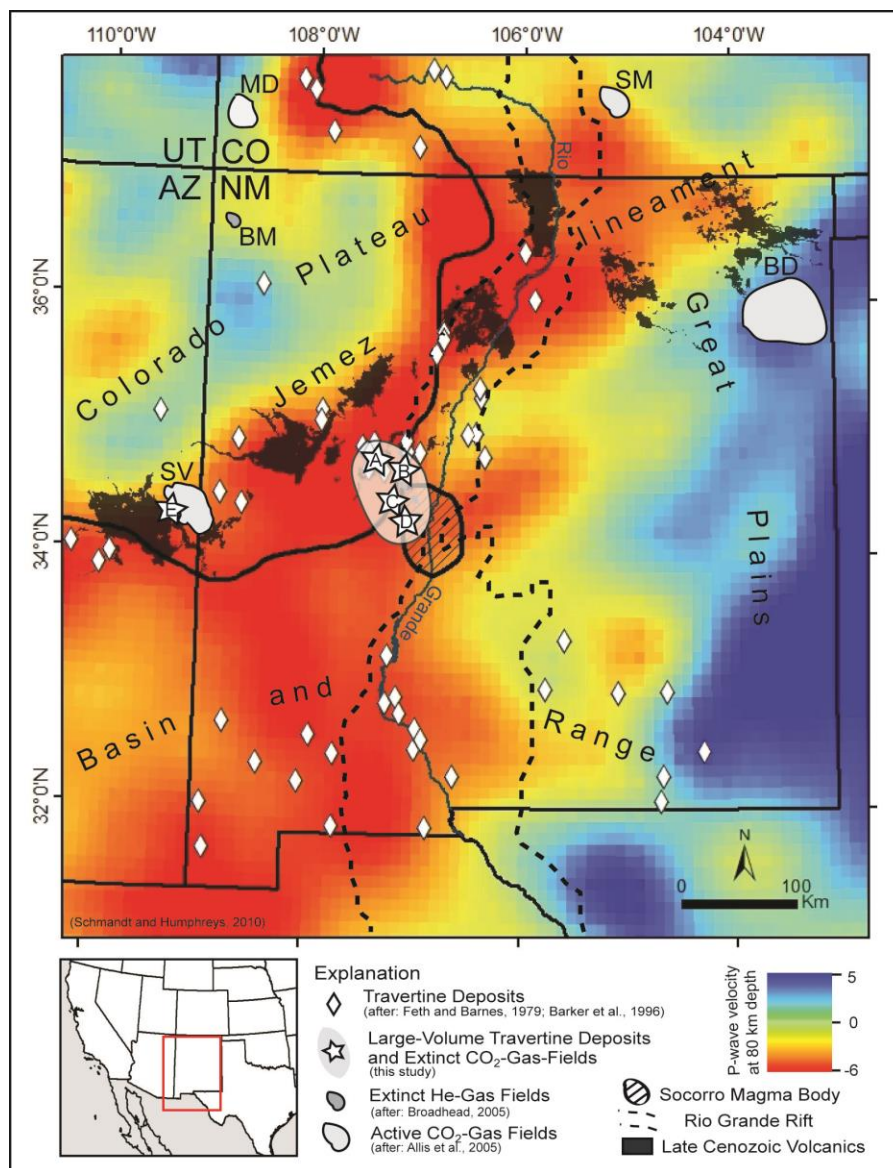


Figure 1.9. Mantle tomography image compiled by Schmandt and Humphreys (2010) showing p-wave velocities at 80 km depth. Based on slower p-wave velocities, areas in red are inferred to be warmer and less dense, and to contain partial melts. Areas in blue show higher p-wave velocities and are inferred to be cooler and denser. Also shown are: locations of travertine accumulations (Feth and Barnes, 1979; Barker et al., 1996), large-volume travertine deposits (this study) and associated tectonic features such as the Rio Grande rift and Jemez lineament, and Colorado Plateau, Great Plains, and Basin and Range physiographic provinces. Active CO₂ gas fields are Bravo Dome (BD) in New Mexico, Sheep Mountain (SM) and McElmo Dome (MD) in Colorado, and the Springerville-St. Johns Field (SV) in Arizona (Allis et al., 2005). Extinct He gas fields in northwestern New Mexico (BM) are Beautiful Mountain/Big Gap Organ Rock, Toco Dome North, Table Mesa, and Rattlesnake (Broadhead, 2005). Large-volume travertine deposits in New Mexico are Mesa del Oro (A), Mesa Aparejo (B), Riley North Mesa (C), Riley South Mesa (D), and Springerville (E).

springs are low in methane (Newell et al., 2005; Gilfillan et al., 2008) such that upward transport of CO₂ and helium in travertine-depositing springs is often independent of petroleum migration and instead reflects upward movement of carbonic fluids through the crust and along faults (Ballentine et al., 2001).

Neither of these tectonic associations, faults and mantle degassing, completely explains the episodes of travertine formation at 700-500 ka, 350-200 ka, and 100-40 ka. However, these intervals overlap with times of Quaternary basaltic volcanism (Fig. 1.8; Dunbar, 2005; Embid, 2009). This is compatible with models showing that magmatism and melt flux through the lithosphere is accompanied by high regional CO₂ flux (Fig. 1.10).

The landscape position of travertine deposition relative to local base level provides clues on the paleohydrology at the time of deposition. Travertine depositing springs are expected to discharge into drainage bottoms except in confined systems where artesian pressure may push waters above the local base level. Rates of landscape denudation from inverted topography were determined from dated basalt flows as well as travertine platforms which are now high in the landscape (Fig. 1.7 C). In order to calculate denudation rates, topographic profiles created in ArcMap GIS were used to measure the difference in elevation from the base of the basalt flow or travertine platform to the nearest stream base level which gives the denudation magnitude, and the denudation magnitude was then divided by the age of the basalt or travertine sample (Fig. 1.2; Table 1.2).

Denudation rates at Mesa del Oro show steady denudation of ~70 m/Ma over the last 8 Ma with variation of denudation rates over the last 4.5 Ma between 44 and 75 m/Ma (Fig. 1.11; Table 1.2). The basalt flows just southeast of the Arroyo Colorado valley have the same arcuate shape as the modern arroyo and are inferred to mark the paleo-channel of an ancestral Arroyo

Table 1.2: Denudation Rates for Study Areas in New Mexico

Sample No.	Location	Longitude (W)	Latitude (N)	Age (ka)	2 σ error (ka)	+ error (ka)	- error (ka)	Elevation at Base (m)
B1	Chicken Mountain	-107.280	34.663	7900	200			2341
B2	Mesa Gallina	-107.240	34.725	7200	600			2286
B3	VictorinoMesa	-107.539	34.677	3500	100			2168
B4	MesaOro (North)	-107.376	34.694	3400	100			2042
B5	MesaOro (South)	-107.407	34.608	3100	500			2018
B6	Volcano Hill	-107.322	34.818	800	500			1849
B7	MesaLucero	-107.191	34.858	4100	100			1908
B8	Mesa Carrizo (North)	-107.118	34.773	3700	400			1890
B9	Mesa Carrizo (South)	-107.105	34.703	3700	400			1780
T2	White Cliff	-107.359	34.768	337		8,241	7,728	2022
T4	Travertine Escarpment	-107.358	34.751	566		84,917	52,105	2000
T7	MA/Vista Grande	-107.098	34.691	430		14,365	13,082	1765
T9	MA_Temple Cream	-107.096	34.667	>1500				1731
T11	MA_Sheherazade	-107.098	34.672	660		252,124	86,343	1737

(continued)

Local Base Level (m)	Denudation Magnitude (m)	Age (Ma)	Denudation Rate (m/Ma)	Type of Unit	Base Level	Reference
1780	561	7.90	71	Basalt	Arroyo Colorado	Baldrige et al., 1987
1770	516	7.20	72	Basalt	Arroyo Colorado	Long/Lat: ArcMap
2015	153	3.50	44	Basalt	Arroyo Colorado	Baldrige et al., 1987
1786	256	3.40	75	Basalt	Arroyo Colorado	Long/Lat: ArcMap
1811	207	3.10	67	Basalt	Arroyo Colorado	Long/Lat: ArcMap
1748	101	0.80	126	Basalt	Arroyo Colorado	Baldrige et al., 1987
1545	363	4.10	89	Basalt	Rio Puerco	Baldrige et al., 1987
1528	361	3.70	98	Basalt	Rio Puerco	Long/Lat: ArcMap
1502	278	3.70	75	Basalt	Rio Puerco	Long/Lat: ArcMap
1758	263	0.34	774	Travertine	Arroyo Colorado	Long/Lat: ArcMap
1772	227	0.57	399	Travertine	Arroyo Colorado	Long/Lat: ArcMap
1502	263	0.43	611	Travertine	Rio Puerco	Long/Lat: ArcMap
1499	232	1.50	155	Travertine	Rio Puerco	Long/Lat: ArcMap
1498	239	0.66	362	Travertine	Rio Puerco	Long/Lat: ArcMap

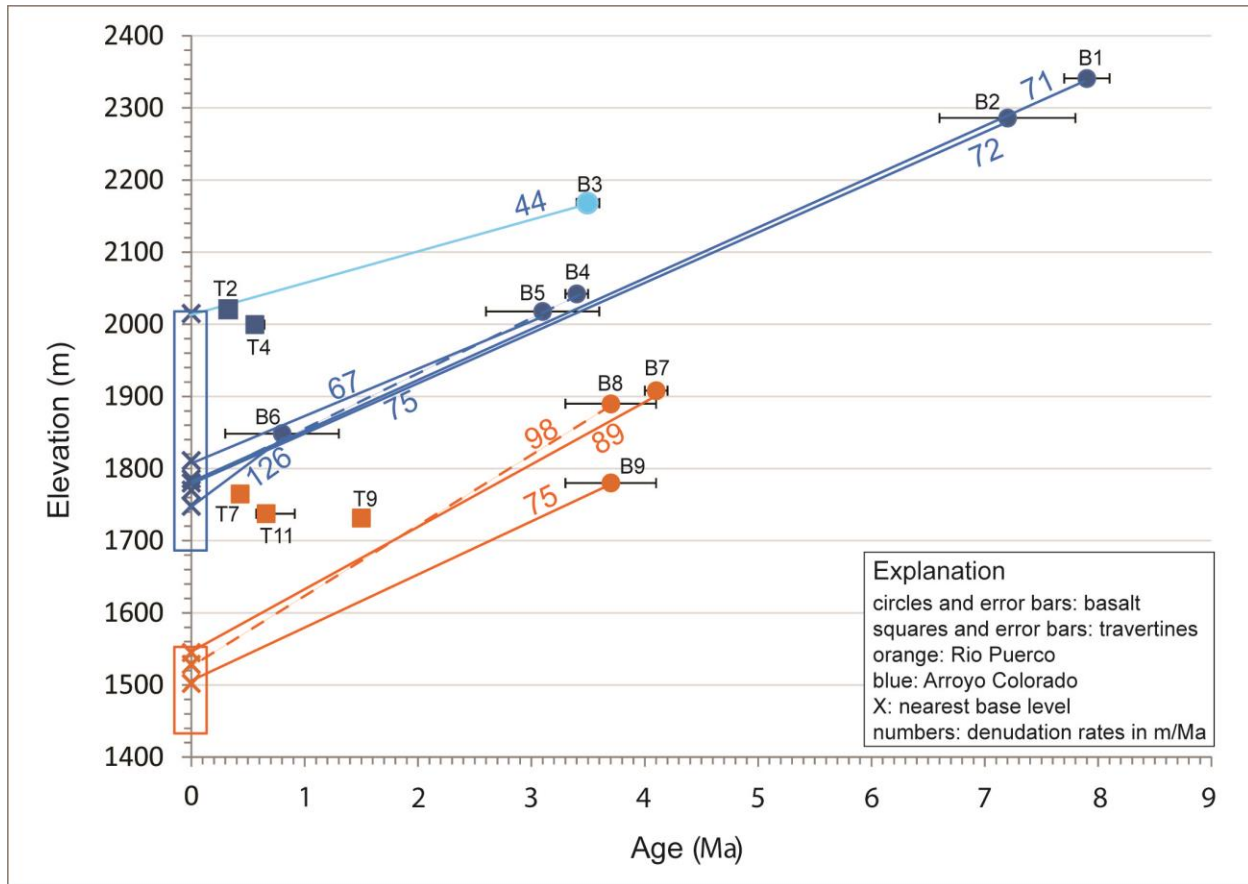


Figure 1.11. Diagram showing denudation rates (in m/m.y.) for the Rio Puerco valley and Arroyo Colorado valley in New Mexico based on dated basalt samples. Travertines are shown; they plot above paleosurfaces represented by basalt flows. Each basalt flow is projected to its nearest base level (colored crosses on the y-axis). Travertine samples T2 and T4 correspond to the paleosurface represented by basalt samples B4 and B5. The low denudation rate of 44 m/m.y. (light blue line) is generated by a sample from a basalt flow (Victorino Mesa) immediately above the local base level (Fig. 1.2). Sample B6 apparently stems from a vent at a high elevation and, therefore generates a high denudation rate (126 m/m.y.). Dashed lines are drawn to distinguish the different paleosurfaces from each other. Sample numbers of basalt and travertine samples are given in Table 1.2.

Colorado (Fig. 1.2). Similarly, the basalt flows of the Rio Puerco valley followed paleo-channels draining into an ancestral Rio Puerco (Fig. 1.2) that was located more to the west than the modern Rio Puerco (Love and Connell, 2005). Denudation rates based on the height of dated basalt samples near Mesa Aparejo relative to the modern Rio Puerco range from 75 to 98m/Ma over the last 4.1 Ma and are similar to rates at Mesa del Oro (Fig. 1.11; Table 1.2). In both

locations, dated travertine samples (T2, T4, T7, T9, and T11) are much higher in the landscape than corresponding basalt paleosurfaces of comparable age and give unreasonably high apparent denudation rates which indicates that they formed on elevated travertine platforms well above local base level (Fig. 1.11; Table 1.2). Similar hydrologic settings are known in the modern landscape where active travertine is depositing 100-200 m above local base level on elevated travertine platforms because of high head in confined aquifer and fault systems (VanHart, 2001; Cron, 2011; Crossey et al., 2011). These analogies imply that episodes of travertine deposition represent times of high artesian head in more than one location and likely across the region. This concept is also well displayed near Springerville, AZ, where Embid (2009) used travertines associated with gravel terraces to calculate incision rates for the Little Colorado River, which averaged 40-50 m/Ma from 7 Ma to 100 ka and increased to 320 m/Ma over the last 100 ka (Fig. 1.12). Travertine formation well above the local river-defined base level occurred at 350 ka, 200 ka, and 100 ka (Embid, 2009), showing that the hydraulic head was high during those times, and overlaps with regional episodes of high head and travertine accumulation in New Mexico.

Paleoclimate and paleohydrology influences provide another possible control on episodic travertine formation. The travertines of this study represent groundwater discharge deposits from regional confined aquifers; hence they provide information on the timing and magnitude of changes in the hydrologic budget related to recharge and discharge, i.e. paleoclimate. Previous workers have proposed correlations between travertine accumulation and climate cycles but different papers come to different conclusions. Pigati et al. (2011) found that groundwater-fed wetland deposits including carbonates formed during wet glacial periods in the Mojave Desert in California, USA, due to fluctuating groundwater levels during the Pleistocene driven by synoptic-scale climate changes. Faccenna et al. (2008) dated travertines from central Italy and

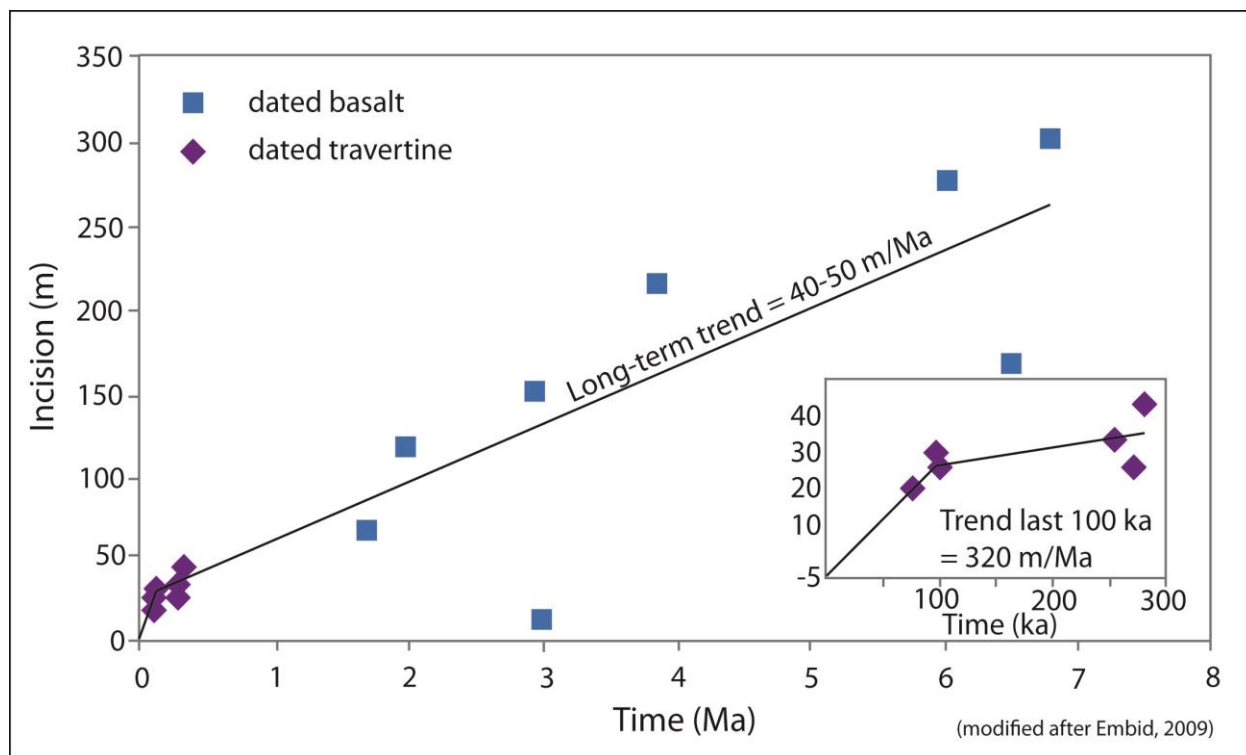


Figure 1.12. Calculated incision rates for the Little Colorado River at Springerville, Arizona. Incision rates through time are based on dated basalt and travertine samples; inset shows an increased incision rate over the last 300 k.y. (Embid, 2009).

suggested that they may provide a tool to date important climate transitions over the last 140 ka, but that fault activity also played a role in travertine formation. Similarly, Kampman et al. (2012) dated travertine mounds in Utah, USA, correlated the times of travertine formation to existing climate records, and stated that travertine formation occurred within 2000 years of the glacial to interglacial transitions over the last 140 ka, suggesting that CO₂ leakage increased at those times as a result of fracture openings potentially caused by “changes in groundwater hydrology” with resulting increased leakage from intermittent CO₂ gas caps. Contrasting views regarding paleoclimate conditions were expressed by Brogi et al. (2010) who reported travertine deposition mainly during dry glacial periods and they emphasized the importance of tectonic activity to facilitate travertine precipitation. Similarly, De Filippis et al. (2013) compared travertine deposits

at Tivoli, Central Italy, and at Pamukkale, Turkey, and concluded that travertine formation occurred during warm and humid periods and was modulated by interactions between paleoclimate, fluid discharge and fluid-driven tectonics. Özkul et al. (2013) studied travertine deposits in the Denizli Basin, Turkey, which formed both during warm and wet as well as dry and cold periods and concluded that travertine precipitation is more a function of tectonic activity and not related to climate. The present study is not a high enough resolution to resolve the issue. However, we note that the travertine record of this study shows some possible associations of wet (glacial) times as recorded by the marine oxygen isotope record (Fig. 1.8), and we also note that travertine deposition took place at times of high hydrologic head, implying wet times.

In our view, the best explanation for travertine episodicity involves an interplay between tectonic controls on the CO₂ flux and paleohydrologic controls on groundwater head. The large-volume travertine deposits in the study areas are interpreted mainly to represent a surface manifestation of mantle degassing focused through fault conduits. The travertines and associated springs with mantle volatiles (Newell et al., 2005; Williams et al., 2013) are located along the Rio Grande rift and Jemez lineament, both regions which are underlain by low-velocity (less dense and more buoyant) mantle (Fig. 1.9; Schmandt and Humphreys, 2010). They are related to basaltic volcanism, most notably at Mesa del Oro, Mesa Aparejo, and Springerville (Figs. 1.2 and 1.3), carrying mantle volatiles such as CO₂ which is critical for travertine formation. Dynamic mantle processes have been linked to lithospheric extension, faulting, basaltic volcanism, and migration of mantle gases to the surface (Newell et al., 2005; McMillan et al., 2006; Karlstrom et al., 2008; Crossey et al., 2009; Jayko, 2009; Karlstrom et al., 2012). The Socorro magma body system, also located above low-velocity mantle, is the inferred CO₂ source

for the Riley Travertine and the travertine deposits at Mesa Aparejo (Figs. 1.1 and 1.2). By analogy to the active Springerville-St. Johns gas field and its associated large-volume travertine deposits it is inferred that all of the ancient large-volume travertine deposits in New Mexico are extinct CO₂-gas fields (Fig. 1.9). A conceptual model of the tectonic setting in the Rio Grande rift, on the Colorado Plateau/Jemez lineament and associated travertine deposition is shown in Figure 1.10: rift-related normal faults serve as conduits that convey deeply-derived magmatic/hydrothermal fluids and CO₂ to the surface where they emerge as travertine-depositing springs. Magmatic systems originating in the upper mantle lead to the formation of the Socorro magma body and volcanic activity, e. g. along the Jemez lineament.

Paleohydrology controls are considered to be equally important as tectonic controls but they are not simply related to glacial-interglacial oscillations. Instead, evidence from this study focuses on high groundwater head during travertine formation which implies that groundwater originating from a confined aquifer system had significant artesian head to ascend along faults and discharge at fault-controlled locations. Hence interpretations at individual sites need to examine groundwater flow paths and fault conduits. Regional aquifers in the study areas in New Mexico and Arizona are the Permian San Andres-Glorieta (SAG) aquifer and Pennsylvanian Madera limestone. Recharge areas are the Lucero uplift and the Colorado Plateau (Goff et al., 1983; Baldwin and Anderholm, 1992; Rauzi, 1999; Rawling, 2005) and it is inferred that the groundwater that formed the large-volume deposits in the study areas discharged from these aquifers. Hydrologic studies show groundwater mixing and complex flow paths at Mesa Aparejo and Mesa del Oro because recharge areas are in the Lucero uplift to the east and the Zuni Mountains to the west. Mixing of different types of groundwater along the Lucero uplift was also found by Goff et al. (1983) and is in accordance with $\delta^{234}\text{U}_{\text{initial}}$ values and strontium isotope

values of the samples from Mesa Aparejo, Mesa del Oro, and Riley South Mesa (Table 1.1). The radiogenic strontium isotope values at Mesa Aparejo and low $\delta^{234}\text{U}_{\text{initial}}$ values reflect input of old, deeply circulating groundwater that interacted with Precambrian basement while non-radiogenic strontium isotope values and higher $\delta^{234}\text{U}_{\text{initial}}$ values at Mesa del Oro and Riley South Mesa represent input dominantly of shallow groundwater that reacted with Madera limestone (Forbes and Stephens, 1994; Barker et al., 1996; Rawling, 2005; Crossey et al., 2006; Hogan et al., 2007; Burnside, 2010). The recharge area for the SAG aquifer in Arizona is the Mogollon Rim, and groundwater flow is from the southwest to the northeast (Akers, 1964; Rauzi, 1999). Shallow and deeply circulating groundwater mixes in the study area at Springerville, rises along faults, and discharges as travertine-precipitating springs (Embid, 2009). More local thermally induced contributions to the groundwater system reflect local volcanic activity and hydrothermal circulation (Ingebritsen et al., 2008). Overall, hydraulic head is a response to 1) increased precipitation in the recharge area, 2) a rise of the water table within the aquifer, 3) a several thousand year response of distant springs to head change (Zhu et al., 1998; Sanford, 2002), and 4) local fault-related hydrothermal pressure (Ingebritsen et al., 2008; Uysal et al., 2009). There is clearly a connection between climate and recharge (Zhu et al., 1998; Sanford, 2002; Pigati et al., 2011) which leads to the conclusion that large volumes of travertine formed when recharge was high. Thus, artesian springs and travertine episodicity are likely to be a more complex function of wet and dry intervals.

CONCLUSIONS

U-series ages show that the formation of large volumes of travertine in New Mexico and Arizona occurred episodically at 700-500 ka, 350-200 ka, and 100-40 ka. Episodes of travertine deposition require both high flux of CO_2 and large amounts of groundwater discharge as well as

the availability of faults which serve as conduits for the CO₂-charged groundwater towards the surface. These episodes of travertine formation overlap with episodes of magmatic activity offering the permissive explanation that high CO₂ flux takes place during basaltic magmatism and associated high seismicity such as exemplified by the modern Socorro magma body system. Denudation rates show steady lowering of the land surface over 8 Ma in the study areas in New Mexico, varying from 44-98 m/Ma, while incision rates at Springerville average 40-50 m/Ma over the last 7 Ma with an increase over the last 100 ka. Travertine platforms that stand high in the landscape today do not track base level lowering which indicates that the travertine-precipitating springs discharged during episodes of high hydraulic head even as erosion lowered the landscape. Thus, it can be inferred that episodes of high head resulted from an interplay of wet climate and high hydrothermal pressures, as filtered through complex artesian aquifer systems. A simple correspondence of travertine accumulation episodes to glacial- and interglacial cycles is not observed in the dataset of this study. The accumulated travertine volume of the study areas is 2.5 km³ (minimum) and by analogy to the active CO₂-gas field at Springerville, AZ, it is inferred that other travertine platforms in New Mexico represent past degassing of CO₂ reservoirs. Hence, large-volume travertine deposits in New Mexico and Arizona provide important laboratories for continued studies of natural CO₂ sequestration and leakage, as well as tangible mantle-to surface system linkages.

ACKNOWLEDGEMENTS

The present work benefited from the input of Ryan Crow who provided valuable assistance to the model age calculations. U-series dating was performed at the radiogenic isotope laboratory at the University of New Mexico. We thank the staff of the New Mexico Bureau of Geology and Mineral Resources for making travertine cores from Mesa del Oro, Riley North

Mesa and Riley South Mesa available. We extend our thanks to Jim Lardner of New Mexico Travertine Inc. for access to the travertine quarries at Mesa Aparejo, and to different parties at Mesa del Oro: Bob Worsley, owner of NZ Legacy LLC, for access to his property and travertine quarries, Jim Harrison, manager of NZ Legacy LLC, for valuable information about the travertine deposit, and the rancher Mark Chavez for access to his land. We thank Andrea Brogi and an anonymous reviewer for their feedback and suggestions, which greatly improved the quality of the manuscript, and Drs. Tim Wawrzyniec and Francesco Mazzarini for helpful comments and editorial handling. This study was generously funded through Grants-In-Aid by the New Mexico Geological Society, scholarships by the Department of Earth and Planetary Sciences/University of New Mexico, Graduate Research Development Funds by the Graduate and Professional Students Association/University of New Mexico, and by National Science Foundation (NSF) EAR-0838575 (to Crossey).

REFERENCES

- Ake, J.P., and Sanford, A.R., 1988, New evidence for the existence and internal structure of a thin layer of magma at mid-crustal depths near Socorro, New Mexico: *Bulletin of the Seismological Society of America*, v. 78, no. 3, p. 1335–1359.
- Akers, J., 1964, *Geology and ground water in the central part of Apache County, Arizona: Geological Survey Water-Supply Paper 1771*, 116 p.
- Aldrich, M.J., 1986, Tectonics of the Jemez lineament in the Jemez Mountains and Rio Grande rift: *Journal of Geophysical Research*, v. 91, no. B2, p. 1753–1762.
- Aldrich, M.J., and Laughlin, A.W., 1984, A model for the tectonic development of the southeastern Colorado Plateau boundary: *Journal of Geophysical Research*, v. 89, no. B12, p. 10,207–10,218.
- Allis, R., Bergfeld, D., Moore, J., McClure, K., Chidsey, T., Heath, J., and Mcpherson, B., 2005, Implications of results from CO₂ flux surveys over known CO₂ systems for long-term monitoring, *in* *Fourth Annual Conference on Carbon Capture & Sequestration*, Alexandria, Virginia, p. 1–22.

- Asmerom, Y., Polyak, V.J., and Burns, S.J., 2010, Variable winter moisture in the southwestern United States linked to rapid glacial climate shifts: *Nature Geoscience*, v. 3, p. 114–117, doi: 10.1038/ngeo754.
- Austin, G.S., and Barker, J.M., 1990, Commercial travertine in New Mexico: *New Mexico Geology*, v. 12, no. 3, p. 49–58.
- Bachman, G.O., and Mehnert, H.H., 1978, New K-Ar dates and the late Pliocene to Holocene geomorphic history of the central Rio Grande region, New Mexico: *Geological Society of America Bulletin*, v. 89, no. 2, p. 283–292, doi: 10.1130/0016-7606(1978)89<283.
- Balch, R.S., Hartse, H.E., Sanford, A.R., and Lin, K. -w., 1997, A new map of the geographic extent of the Socorro mid-crustal magma body: *Bulletin of the Seismological Society of America*, v. 87, no. 1, p. 174–182.
- Baldrige, W.S., Perry, F.V., and Shafiqullah, M., 1987, Late Cenozoic volcanism of the southeastern Colorado Plateau: I. Volcanic geology of the Lucero area, New Mexico: *Geological Society of America Bulletin*, v. 99, p. 463–470.
- Baldwin, J.A., and Anderholm, S.K., 1992, Hydrogeology and ground-water chemistry of the San Andres-Glorieta aquifer in the Acoma embayment and eastern Zuni uplift, west-central New Mexico: U.S. Geological Survey Water-Resources Investigations Report 91-4033, 302 p.
- Ballentine, C.J., and Holland, G., 2008, What CO₂ well gases tell us about the origin of noble gases in the mantle and their relationship to the atmosphere: *Philosophical Transactions of The Royal Society A*, v. 366, p. 4183–4203, doi: 10.1098/rsta.2008.0150.
- Ballentine, C.J., Marty, B., Sherwood Lollar, B., and Cassidy, M., 2005, Neon isotopes constrain convection and volatile origin in the Earth's mantle: *Nature*, v. 433, p. 33–38, doi: 10.1038/nature03182.
- Ballentine, C.J., Schoell, M., Coleman, D., and Cain, B.A., 2001, 300-Myr-old magmatic CO₂ in natural gas reservoirs of the west Texas Permian basin: *Nature*, v. 409, p. 327–331, doi: 10.1038/35053046.
- Ballentine, C.J., and Sherwood Lollar, B., 2002, Regional groundwater focusing of nitrogen and noble gases into the Hugoton-Panhandle giant gas field, USA: *Geochimica et Cosmochimica Acta*, v. 66, no. 14, p. 2483–2497.
- Barker, J.M., 1983, Preliminary investigation of the origin of the Riley Travertine, Socorro County, New Mexico: *New Mexico Geological Society Guidebook, 34th Field Conference*, v. 34, p. 269–276.

- Barker, J.M., Austin, G.S., and Sivils, D.J., 1996, Travertine in New Mexico - Commercial deposits and otherwise: New Mexico Bureau of Mines and Mineral Resources Bulletin, v. 154, p. 73–92.
- Berglund, H.T., Sheehan, A.F., Murray, M.H., Roy, M., Lowry, A.R., Nerem, R.S., and Blume, F., 2012, Distributed deformation across the Rio Grande Rift, Great Plains, and Colorado Plateau: *Geology*, v. 40, no. 1, p. 23–26, doi: 10.1130/G32418.1.
- Broadhead, R.F., 2005, Helium in New Mexico — geologic distribution , resource demand , and exploration possibilities: *New Mexico Geology*, v. 27, no. 4, p. 93–101.
- Brogi, A., and Capezzuoli, E., 2009, Travertine deposition and faulting: the fault-related travertine fissure-ridge at Terme S. Giovanni, Rapolano Terme (Italy): *International Journal of Earth Sciences*, v. 98, p. 931–947, doi: 10.1007/s00531-007-0290-z.
- Brogi, A., Capezzuoli, E., Aqué, R., Branca, M., and Voltaggio, M., 2010, Studying travertines for neotectonics investigations: Middle–Late Pleistocene syn-tectonic travertine deposition at Serre di Rapolano (Northern Apennines, Italy): *International Journal of Earth Sciences*, v. 99, p. 1383–1398, doi: 10.1007/s00531-009-0456-y.
- Burnside, N.M., 2010, U-Th dating of travertine on the Colorado Plateau : Implications for the leakage of geologically stored CO₂ [Ph.D. thesis]: University of Glasgow, 290 p.
- Callender, J., and Zilinski, Jr, R., 1976, Kinematics of Tertiary and Quaternary deformation along the eastern edge of the Lucero uplift, central New Mexico, *in* Woodward, L.A. and Northrop, S.A. eds., *Tectonics and Mineral Resources of Southwestern North America*, New Mexico Geological Society, p. 53–61.
- Cather, S.M., 2004, Laramide orogeny in central and northern New Mexico and southern Colorado, *in* Mack, G.H. and Giles, K.A. eds., *The Geology of New Mexico*, New Mexico Geological Society Special Publication 11, p. 203–248.
- Cather, S.M., and Read, A.S., 2003, Preliminary Geologic Map of the Silver Creek 7.5-min quadrangle: New Mexico Bureau of Geology and Mineral Resources, scale 1:24 017, 1 sheet.
- Chafetz, H.S., and Folk, R.L., 1984, Travertines; depositional morphology and the bacterially constructed constituents: *Journal of Sedimentary Petrology*, v. 54, no. 1, p. 289–316.
- Chafetz, H.S., and Guidry, S.A., 2003, Deposition and diagenesis of Mammoth Hot Springs travertine , Yellowstone National Park , Wyoming , U . S . A . 1: *Canadian Journal of Earth Sciences*, v. 40, p. 1515–1529, doi: 10.1139/E03-051.
- Chamberlin, R.M., 2007, Evolution of the Jemez lineament: connecting the volcanic “dots” through late cenozoic time: *New Mexico Geological Society Guidebook*, 58th Field Conference,, p. 80–82.

- Chamberlin, R.M., 2004, Preliminary Map of the San Lorenzo Spring 7.5-minute Quadrangle: New Mexico Bureau of Geology and Mineral Resources, scale 1:24 000, 1 sheet.
- Cheng, H., Edwards, R., Hoff, J., Gallup, C., Richards, D., and Asmerom, Y., 2000, The half-lives of uranium-234 and thorium-230: *Chemical Geology*, v. 169, p. 17–33.
- Clark, I., and Fritz, P., 1997, *Environmental isotopes in hydrogeology*: Boca Raton, New York, Lewis Publishers, 328 p.
- Condit, C.D., and Connor, C.B., 1996, Recurrence rates of volcanism in basaltic volcanic fields: An example from the Springerville volcanic field, Arizona: *Geological Society of America Bulletin*, v. 108, no. 10, p. 1225–1241, doi: 10.1130/0016-7606(1996)108<1225.
- Cron, B., 2011, Geochemical characteristics and microbial diversity of CO₂-rich mound springs of the Tierra Amarilla anticline, New Mexico [M.S. thesis]: Albuquerque, University of New Mexico, 110 p.
- Crossey, L.J., Fischer, T.P., Patchett, P.J., Karlstrom, K.E., Hilton, D.R., Newell, D.L., Huntoon, P., Reynolds, A.C., and de Leeuw, G.A.M., 2006, Dissected hydrologic system at the Grand Canyon: Interaction between deeply derived fluids and plateau aquifer waters in modern springs and travertine: *Geology*, v. 34, no. 1, p. 25–28, doi: 10.1130/G22057.1.
- Crossey, L.J., Karlstrom, K.E., Newell, D.N., Kooser, A., and Tafoya, A., 2011, The La Madera travertines, Rio Ojo Caliente, northern New Mexico : Investigating the linked system of CO₂-rich springs and travertines as neotectonic and paleoclimate indicators, *in* *New Mexico Geological Society Guidebook, 62nd Field Conference, Geology of the Tusas Mountains - Ojo Caliente*, p. 121–136.
- Crossey, L.J., Karlstrom, K.E., Springer, A.E., Newell, D., Hilton, D.R., and Fischer, T., 2009, Degassing of mantle-derived CO₂ and He from springs in the southern Colorado Plateau region--Neotectonic connections and implications for groundwater systems: *Geological Society of America Bulletin*, v. 121, no. 7-8, p. 1034–1053, doi: 10.1130/B26394.1.
- Curewitz, D., and Karson, J.A., 1997, Structural settings of hydrothermal outflow: Fracture permeability maintained by fault propagation and interaction: *Journal of Volcanology and Geothermal Research*, v. 79, p. 149–168.
- Dockrill, B., and Shipton, Z.K., 2010, Structural controls on leakage from a natural CO₂ geologic storage site: Central Utah, U.S.A.: *Journal of Structural Geology*, v. 32, p. 1768–1782, doi: 10.1016/j.jsg.2010.01.007.
- Dunbar, N., 2005, Quaternary volcanism in New Mexico: *New Mexico Museum of Natural History and Science Bulletin*, v. 28, p. 95–106.

- Edwards, R., Chen, J., and Wasserburg, G., 1987, ^{238}U - ^{234}U - ^{230}Th - ^{232}Th systematics and the precise measurement of time over the past 500,000 years: *Earth and Planetary Science Letters*, v. 81, p. 175–192.
- Embid, E.H., 2009, U-Series dating, geochemistry, and geomorphic studies of travertines and springs of the Springerville Area, east-central Arizona, and tectonic implications [M.S. thesis]: Albuquerque, University of New Mexico, 103 p.
- Faccenna, C., Soligo, M., Billi, A., De Filippis, L., Funicello, R., Rossetti, C., and Tuccimei, P., 2008, Late Pleistocene depositional cycles of the Lapis Tiburtinus travertine (Tivoli, Central Italy): possible influence of climate and fault activity: *Global and Planetary Change*, v. 63, p. 299–308, doi: 10.1016/j.gloplacha.2008.06.006.
- Feth, J.H., and Barnes, I., 1979, Spring-deposited travertine in eleven western states: Geological Survey Water-Resources Investigations 79-85 Open-File Report.
- Fialko, Y., and Simons, M., 2001, Evidence for on-going inflation of the Socorro Magma Body, New Mexico, from Interferometric Synthetic Aperture Radar imaging: *Geophysical Research Letters*, v. 28, no. 18, p. 3549–3552, doi: 10.1029/2001GL013318.
- De Filippis, L., Faccenna, C., Billi, A., Anzalone, E., Brilli, M., Soligo, M., and Tuccimei, P., 2013, Plateau versus fissure ridge travertines from Quaternary geothermal springs of Italy and Turkey: Interactions and feedbacks between fluid discharge, paleoclimate, and tectonics: *Earth-Science Reviews*, v. 123, p. 35–52, doi: 10.1016/j.earscirev.2013.04.004.
- Forbes, J., and Stephens, D., 1994, Caves of the Mesa del Oro travertine, New Mexico, U.S.A.: Breakthroughs in Karst Geomicrobiology and Redox Geochemistry Special Publication, v. 1, p. 18–20.
- Ford, T.D., and Pedley, H.M., 1996, A review of tufa and travertine deposits of the world: *Earth-Science Reviews*, v. 41, p. 117–175.
- Fouke, B.W., Bonheyo, G.T., Sanzenbacher, B., and Frias-lopez, J., 2003, Partitioning of bacterial communities between travertine depositional facies at Mammoth Hot Springs, Yellowstone National Park, U.S.A.: *Canadian Journal of Earth Sciences*, v. 40, p. 1531–1548, doi: 10.1139/E03-067.
- Fouke, B.W., Farmer, J.D., Des Marais, D.J., Pratt, L., Sturchio, N.C., Burns, P.C., and Discipulo, M.K., 2000, Depositional facies and aqueous-solid geochemistry of travertine-depositing hot springs (Angel Terrace, Mammoth Hot Springs, Yellowstone National Park, U.S.A.): *Journal of Sedimentary Research*, v. 70, no. 3, p. 565–585.
- Gilfillan, S.M.V., Ballentine, C.J., Holland, G., Blagburn, D., Sherwood Lollar, B., Stevens, S., Schoell, M., and Cassidy, M., 2008, The noble gas geochemistry of natural CO_2 gas reservoirs from the Colorado Plateau and Rocky Mountain provinces, USA: *Geochimica et Cosmochimica Acta*, v. 72, no. 4, p. 1174–1198, doi: 10.1016/j.gca.2007.10.009.

- Gilfillan, S.M.V., Sherwood Lollar, B., Holland, G., Blagburn, D., Stevens, S., Schoell, M., Cassidy, M., Ding, Z., Zhou, Z., Lacrampe-Couloume, G., and Ballentine, C.J., 2009, Solubility trapping in formation water as dominant CO₂ sink in natural gas fields: *Nature*, v. 458, p. 614–618, doi: 10.1038/nature07852.
- Glover, C., and Robertson, A.H.F., 2003, Origin of tufa (cool-water carbonate) and related terraces in the Antalya area, SW Turkey: *Geological Journal*, v. 38, p. 329–358, doi: 10.1002/gj.959.
- Goff, F., McCormick, T., Gardner, J.N., Trujillo, P.E., Counce, D., Vidale, R., and Charles, R., 1983, Water geochemistry of the Lucero uplift, New Mexico: A geothermal investigation of low-temperature mineralized fluids: Los Alamos National Laboratory LA-9738-OBES, 26 p.
- Grauch, V.J.S., and Connell, S.D., 2013, New perspectives on the geometry of the Albuquerque Basin, Rio Grande rift, New Mexico: Insights from geophysical models of rift-fill thickness, *in* Hudson, M.R. and Grauch, V.J.S. (Tien) eds., *New Perspectives on Rio Grande Basins: From Tectonics to Groundwater*, The Geological Society of America Special Paper 494, p. 427–462.
- Hancock, P.L., Chalmers, R.M., Altunel, E., and Cakir, Z., 1999, Travertines: using travertines in active fault studies: *Journal of Structural Geology*, v. 21, p. 903–916.
- Hogan, J.F., Phillips, F.M., Mills, S.K., Hendrickx, J.M.H., Ruiz, J., Chesley, J.T., and Asmerom, Y., 2007, Geologic origins of salinization in a semi-arid river: The role of sedimentary basin brines: *Geology*, v. 35, no. 12, p. 1063–1066, doi: 10.1130/G23976A.1.
- Ingebritsen, S., Sanford, W., and Neuzil, C., 2008, *Groundwater in geologic processes*: Cambridge University Press, New York, 536 p.
- Jayko, A.S., 2009, The Mono Arch, eastern Sierra region, California: dynamic topography associated with upper-mantle upwelling?: *International Geology Review*, v. 51, no. 7-8, p. 702–722, doi: 10.1080/00206810902880271.
- Jicha, H., 1958, *Geology and mineral resources of Mesa del Oro Quadrangle, Socorro and Valencia Counties, New Mexico*: State Bureau of Mines and Mineral Resources Bulletin, v. 56, p. 1–67.
- Kampman, N., Burnside, N.M., Shipton, Z.K., Chapman, H.J., Nicholl, J. a., Ellam, R.M., and Bickle, M.J., 2012, Pulses of carbon dioxide emissions from intracrustal faults following climatic warming: *Nature Geoscience*, v. 5, p. 352–358, doi: 10.1038/ngeo1451.
- Karlstrom, K.E., Crossey, L.J., Hilton, D.R., and Barry, P.H., 2013, Mantle 3He and CO₂ degassing in carbonic and geothermal springs of Colorado and implications for neotectonics of the Rocky Mountains: *Geology*, v. 41, p. 495–498, doi: 10.1130/G34007.1.

- Karlstrom, K.E., Coblenz, D., Dueker, K., Ouimet, W., Kirby, E., Van Wijk, J., Schmandt, B., Kelley, S., Lazear, G., Crossey, L.J., Crow, R., Aslan, A., Darling, A., Aster, R., et al., 2012, Mantle-driven dynamic uplift of the Rocky Mountains and Colorado Plateau and its surface response: Toward a unified hypothesis: *Lithosphere*, v. 4, no. 1, p. 3–22, doi: 10.1130/L150.1.
- Karlstrom, K.E., Crow, R., Crossey, L.J., Coblenz, D., and Van Wijk, J.W., 2008, Model for tectonically driven incision of the younger than 6 Ma Grand Canyon: *Geology*, v. 36, no. 11, p. 835–838, doi: 10.1130/G25032A.1.
- Karlstrom, K.E., Whitmeyer, S.J., Dueker, K., Williams, M.L., Bowring, S.A., Levander, A.R., Humphreys, E.D., Keller, G.R., and CD-ROM, W.G., 2005, Synthesis of results from the CD-ROM Experiment: 4-D image of the lithosphere beneath the Rocky Mountains and implications for understanding the evolution of continental lithosphere, *in* Karlstrom, K.E. and Keller, G.R. eds., *The Rocky Mountain Region - An Evolving Lithosphere*, American Geophysical Union Geophysical Monograph, p. 421–441.
- Karlstrom, K.E., and Humphreys, E.D., 1998, Persistent influence of Proterozoic accretionary boundaries in the tectonic evolution of southwestern North America: Interaction of cratonic grain and mantle modification events: *Rocky Mountain Geology*, v. 33, no. 2, p. 161–179.
- Keller, G.R., and Baldrige, W.S., 1999, The Rio Grande rift A geological and geophysical overview: *Rocky Mountain Geology*, v. 34, no. 1, p. 121–130.
- Lewis, C., and Baldrige, W., 1994, Crustal extension in the Rio Grande rift, New Mexico: Half-grabens, accommodation zones, and shoulder uplifts in the Ladron Peak-Sierra Lucero area: *Geological Society of America Special Paper*, v. 291, p. 135–155.
- Linares, R., Rosell, J., Roqué, C., and Gutiérrez, F., 2010, Origin and evolution of tufa mounds related to artesian karstic springs in Isona area (Pyrenees, NE Spain): *Geodinamica Acta*, v. 23, no. 1-3, p. 129–150, doi: 10.3166/ga.23.129-150.
- Love, D.W., and Connell, S.D., 2005, Late Neogene drainage developments on the southeastern Colorado Plateau, New Mexico, *in* Lucas, S.G., Morgan, G.S., and Zeigler, K.E. eds., *New Mexico's Ice Ages*, New Mexico Museum of Natural History and Science Bulletin No. 28, p. 151–170.
- Ludwig, K.R., 2003, User's Manual for Isoplot 3.0: Berkeley Geochronology Center Special Publication No. 4, 70 p.
- Magnani, M.B., Miller, K.C., Levander, A., and Karlstrom, K., 2004, The Yavapai-Mazatzal boundary: A long-lived tectonic element in the lithosphere of southwestern North America: *Geological Society of America Bulletin*, v. 116, no. 7/8, p. 1–6, doi: 10.1130/B25414.1.

- McMillan, M.E., Heller, P.L., and Wing, S.L., 2006, History and causes of post-Laramide relief in the Rocky Mountain orogenic plateau: *Geological Society of America Bulletin*, v. 118, no. 3-4, p. 393–405, doi: 10.1130/B25712.1.
- Minissale, A., Kerrick, D.M., Magro, G., Murrell, M.T., Paladini, M., Rihs, S., Sturchio, N.C., Tassi, F., and Vaselli, O., 2002, Geochemistry of Quaternary travertines in the region north of Rome (Italy): structural, hydrologic and paleoclimatic implications: *Earth and Planetary Science Letters*, v. 203, p. 709–728.
- Minor, S.A., Hudson, M.R., Cain, J.S., and Thompson, R.A., 2013, Oblique transfer of extensional strain between basins of the middle Rio Grande rift, New Mexico: Fault kinematic and paleostress constraints, *in* Hudson, M.R. and Grauch, V.J.S. (Tien) eds., *New Perspectives on Rio Grande Basins: From Tectonics to Groundwater*, The Geological Society of America Special Paper 494, p. 345–382.
- Moore, J., Adams, M., Allis, R., Lutz, S., and Rauzi, S., 2005, Mineralogical and geochemical consequences of the long-term presence of CO₂ in natural reservoirs: An example from the Springerville–St. Johns Field, Arizona, and New Mexico, U.S.A.: *Chemical Geology*, v. 217, p. 365–385, doi: 10.1016/j.chemgeo.2004.12.019.
- Nereson, A., Stroud, J., Karlstrom, K., Heizler, M., and McIntosh, W., 2013, Dynamic topography of the western Great Plains: Geomorphic and ⁴⁰Ar/³⁹Ar evidence for mantle-driven uplift associated with the Jemez lineament of NE New Mexico and SE Colorado: *Geosphere* 10.1130/GES00837.1.
- Newell, D.L., Crossey, L.J., Karlstrom, K.E., Fischer, T.P., and Hilton, D.R., 2005, Continental-scale links between the mantle and groundwater systems of the western United States: Evidence from travertine springs and regional He isotope data: *GSA Today*, v. 15, no. 12, p. 4–10.
- NMBGMR, 2003, *Geologic Map of New Mexico*: New Mexico Bureau of Geology and Mineral Resources, scale 1:500 000, 2 sheets.
- Özkul, M., Kele, S., Gökgöz, A., Shen, C.-C., Jones, B., Baykara, M.O., Fórizs, I., Németh, T., Chang, Y.-W., and Alçiçek, M.C., 2013, Comparison of the Quaternary travertine sites in the Denizli extensional basin based on their depositional and geochemical data: *Sedimentary Geology*, v. 294, p. 179–204, doi: 10.1016/j.sedgeo.2013.05.018.
- Pearse, J., and Fialko, Y., 2010, Mechanics of active magmatic intraplate in the Rio Grande Rift near Socorro, New Mexico: *Journal of Geophysical Research*, v. 115, p. 1–16, doi: 10.1029/2009JB006592.
- Pentecost, A., 2005, *Travertine*: Springer Verlag Berlin Heidelberg, 445 p.
- Pigati, J.S., Miller, D.M., Bright, J.E., Mahan, S. a., Nekola, J.C., and Paces, J.B., 2011, Chronology, sedimentology, and microfauna of groundwater discharge deposits in the

- central Mojave Desert, Valley Wells, California: Geological Society of America Bulletin, v. 123, no. 11-12, p. 2224–2239, doi: 10.1130/B30357.1.
- Priewisch, A., Crossey, L.J., and Karlstrom, K.E., 2013, U-series ages and morphology of a large-volume travertine deposit at Mesa del Oro, NM: Implications for paleohydrology, paleoclimate, and neotectonic processes, *in* Kate Zeigler, J. Michael Timmons, S.T. and S.S. ed., Geology of the Route 66 region: Flagstaff to Grants, New Mexico Geological Society Fall Field Conference Guidebook 64, p. 229–237.
- Rauzi, S.L., 1999, Carbon Dioxide in the St. Johns - Springerville Area, Apache County, Arizona: Arizona Geological Survey, Open-File Report 99-2, 24 p.
- Rawling, G.C., 2005, Geology and hydrologic setting of springs and seeps on the Sevilleta National Wildlife Refuge: New Mexico Bureau of Geology and Mineral Resources, Open-File Report 495, 90 p.
- Reiter, M., and Chamberlin, R.M., 2011, Alternative perspectives of crustal and upper mantle phenomena along the Rio Grande rift: GSA Today, v. 21, no. 2, p. 4–9, doi: 10.1130/GSATG79AR.
- Reiter, M., Chamberlin, R.M., and Love, D.W., 2010, New data reflect on the thermal antiquity of the Socorro magma body locale, Rio Grande Rift, New Mexico: Lithosphere, v. 2, p. 447–453, doi: 10.1130/L115.1.
- Ricketts, J.W., Priewisch, A., Kolomaznik, M., and Karlstrom, K.E., 2012, Calcite-filled fractures in travertine used to constrain the timing and orientation of Quaternary extension along the western margin of the Rio Grande rift, central New Mexico: New Mexico Geological Society Spring Meeting, Program with Abstracts.
- Rinehart, E.J., and Sanford, A.R., 1981, Upper crustal structure of the Rio Grande rift near Socorro, New Mexico, from inversion of microearthquake S-wave reflections: Bulletin of the Seismological Society of America, v. 71, no. 2, p. 437–450.
- Russell, L.R., and Snelson, S., 1994, Structure and tectonics of the Albuquerque Basin segment of the Rio Grande rift: Insights from reflection seismic data: Geological Society of America Special Papers, v. 291, p. 83–112.
- Sanford, W., 2002, Recharge and groundwater models: an overview: Hydrogeology Journal, v. 10, p. 110–120, doi: 10.1007/s10040-001-0173-5.
- Schmandt, B., and Humphreys, E., 2010, Complex subduction and small-scale convection revealed by body-wave tomography of the western United States upper mantle: Earth and Planetary Science Letters, v. 297, p. 435–445, doi: 10.1016/j.epsl.2010.06.047.

- Seager, W., 2004, Laramide (Late Cretaceous-Eocene) tectonics of southwestern New Mexico, *in* Mack, G.H. and Giles, K.A. eds., *The Geology of New Mexico*, New Mexico Geological Society Special Publication 11, p. 183–202.
- Sherwood Lollar, B., Ballentine, C.J., and O’Nions, R.K., 1997, The fate of mantle-derived carbon in a continental sedimentary basin: Integration of C/He relationships and stable isotope signatures: *Geochimica et Cosmochimica Acta*, v. 61, no. 11, p. 2295–2307.
- Shipton, Z.K., Evans, J.P., Dockrill, B., Heath, J., Williams, A., Kirchner, D., and Kolesar, P.T., 2005, Natural leaking CO₂-charged systems as analogs for failed geologic storage reservoirs, *in* Thomas, D.C. and Benson, S.M. ed., *Carbon Dioxide Capture for Storage in Deep Geologic Formations*, Volume 2, Elsevier Ltd., p. 699–712.
- Sierralta, M., Kele, S., Melcher, F., Hambach, U., Reinders, J., van Geldern, R., and Frechen, M., 2010, Uranium-series dating of travertine from Süttö: implications for reconstruction of environmental change in Hungary: *Quaternary International*, v. 222, p. 178–193.
- Sturchio, N.C., Pierce, K.L., Murrell, M.T., and Sorey, M.L., 1994, Uranium-series ages of travertines and timing of the last glaciation in the northern Yellowstone area, Wyoming-Montana: *Quaternary Research*, v. 41, no. 3, p. 265–277.
- Szabo, B.J., 1990, Ages of travertine deposits in eastern Grand Canyon National Park, Arizona: *Quaternary Research*, v. 34, p. 24–32.
- Uysal, I.T., Feng, Y. -x., Zhao, J. -x., Isik, V., Nuriel, P., and Golding, S.D., 2009, Hydrothermal CO₂ degassing in seismically active zones during the late Quaternary: *Chemical Geology*, v. 265, p. 442–454, doi: 10.1016/j.chemgeo.2009.05.011.
- VanHart, D., 2001, Field Trip to the Tierra Amarilla anticline and its travertine springs, New Mexico: Albuquerque Geological Society, 33 p.
- West, M., Ni, J., Baldrige, W.S., Wilson, D., Aster, R., Gao, W., and Grand, S., 2004, Crust and upper mantle shear wave structure of the southwest United States: Implications for rifting and support for high elevation: *Journal of Geophysical Research*, v. 109, p. 1–16, doi: 10.1029/2003JB002575.
- Williams, A.J., Crossey, L.J., and Karlstrom, K.E., 2009, An integrated geochemical and structural study of the Sevilleta National Wildlife Refuge: geochemistry and salinity sources of waters spanning the Rio Grande rift, New Mexico: *Geological Society of America Abstracts with Programs*, v. 41, no. 7, p. 413.
- Williams, A.J., Crossey, L.J., Karlstrom, K.E., Newell, D., Person, M., and Woolsey, E., 2013, Hydrogeochemistry of the Middle Rio Grande aquifer system — Fluid mixing and salinization of the Rio Grande due to fault inputs: *Chemical Geology*, v. 351, p. 281–298, doi: 10.1016/j.chemgeo.2013.05.029.

- Wisniewski, P.A., Pazzaglia, F.J., The, S., and July, N., 2002, Epeirogenic Controls on Canadian River Incision and Landscape Evolution , Great Plains of Northeastern New Mexico
Epeirogenic Controls on Canadian River Incision and Landscape Evolution , Great Plains of Northeastern New Mexico: *The Journal of Geology*, v. 110, no. 4, p. 437–456.
- Zachos, J., Pagani, M., Sloan, L., Thomas, E., and Billups, K., 2001, Trends, rhythms, and aberrations in global climate 65 Ma to present: *Science*, v. 292, p. 686–693, doi: 10.1126/science.1059412.
- Zhu, C., Waddell, R.K., Star, I., and Ostrander, M., 1998, Responses of ground water in the Black Mesa basin, northeastern Arizona, to paleoclimatic changes during the late Pleistocene and Holocene: *Geology*, v. 26, no. 2, p. 127–130, doi: 10.1130/0091-7613(1998)026<0127:ROGWIT>2.3.CO;2.

CHAPTER 2

U-Series Ages and Morphology of a Quaternary large-volume Travertine Deposit at Mesa del Oro, NM: Implications for Paleohydrology, Paleoclimate, and neotectonic Processes

Priewisch, A.¹, Crossey, L.J.¹, and Karlstrom, K.E.¹

¹ *Dept. of Earth and Planetary Sciences, University of New Mexico, Albuquerque, NM 87131*

(Published in New Mexico Geological Society Guidebook, 64th Field Conference, Geology of Route 66 Region: Flagstaff to Grants, 2013, p. 119-237)

CHAPTER ABSTRACT

This paper describes a large-volume travertine deposit that formed at the northeastern end of Mesa del Oro, a basalt mesa located at the southwestern edge of the Colorado Plateau and along the Jemez lineament. The travertine deposit forms two topographically elevated platforms that cover an area of 27 m², are up to 63 m thick, and have a calculated volume of 0.7 m³. We report six new dates for the Mesa del Oro accumulation. U-series ages of the travertine deposit are 566 ± 68.5 ka, 360 ± 13.5 ka, 337 ± 8.0 ka, and 253 ± 5.4 ka, and these ages, combined with model ages of 590-760 ka, show that travertine formation occurred in two main intervals, 360-250 ka and 760-560 ka. The intervals overlap with episodes of basaltic volcanism in the area. The northern platform was deposited along a fissure ridge and an associated marsh as shown by both travertine morphology and facies. Large-volume travertine formation requires both high CO₂ influx and significant groundwater discharge. The high CO₂ influx is interpreted to be related to the episodic volcanic activity that produced over-pressuring of the CO₂/groundwater system with magmatic gasses. Intervals of high groundwater discharge are attributed to high head in a confined aquifer achieved through increased recharge and thus, episodes of travertine formation at Mesa del Oro are interpreted to record wet paleoclimate periods.

INTRODUCTION

Travertines are groundwater discharge deposits made of calcite or aragonite that precipitate from CO₂-rich groundwater. Travertine deposits are common throughout New Mexico (Fig. 2.1; Barker et al., 1996) and are generally well-preserved due to the resistance of carbonate to erosion in the arid climate. They predominantly occur along the Rio Grande rift flanks and on the Colorado Plateau along the Jemez lineament (Fig. 2.1). Here we describe a large-volume

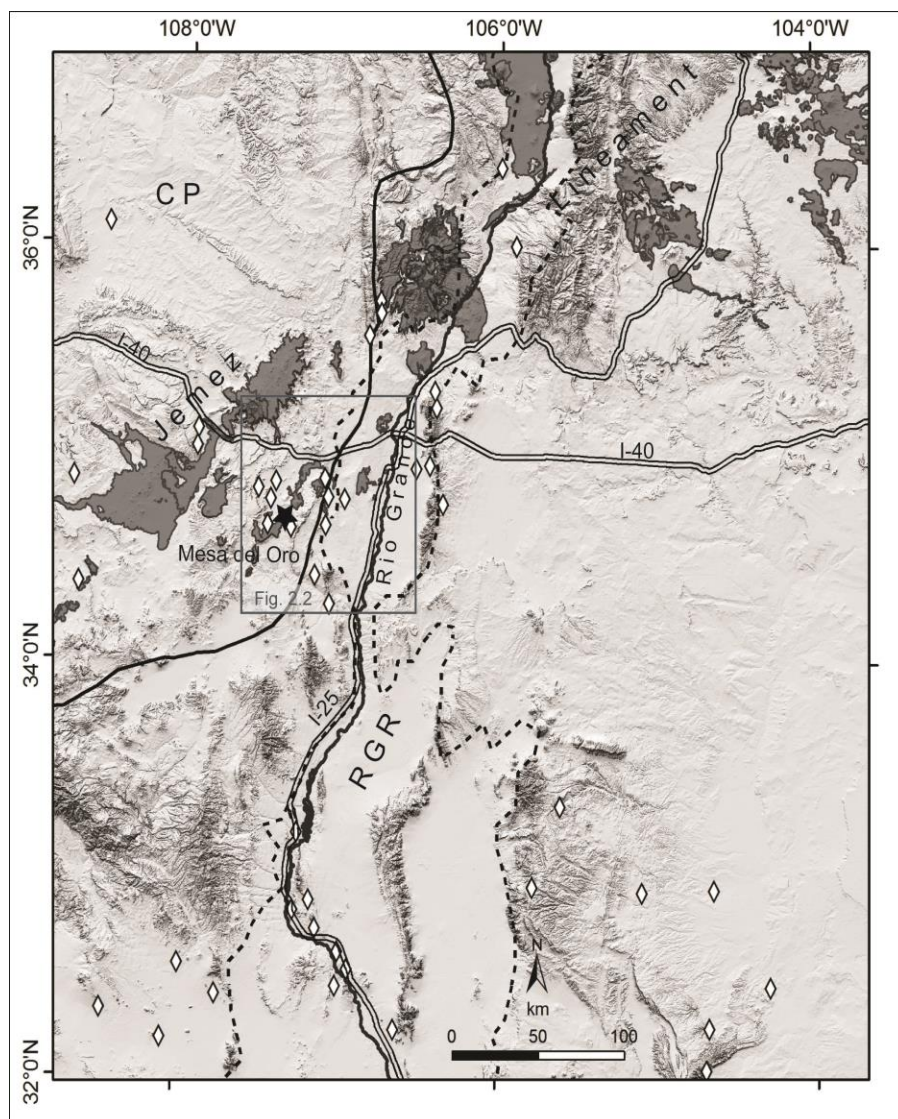


Figure 2.1. Shaded relief map of New Mexico showing locations of travertine accumulations (white diamonds; Barker et al., 1996), the large-volume travertine deposit at Mesa del Oro (black star; this study), late Cenozoic volcanics (dark grey areas outlined in black), and associated tectonic features such as the Rio Grande rift (RGR, dashed black line), Colorado Plateau (CP, solid black line), and Jemez lineament. The box indicates the area of interest.

travertine deposit at Mesa del Oro, a Tertiary basalt-capped mesa located near the southeastern boundary of the Colorado Plateau and along the Jemez lineament, about 30 km south of I-40 and to the west of the Lucero uplift (Fig. 2.2). The travertine deposit formed between two basalt flows, at the northeastern end of the Mesa del Oro basalts (Jicha, 1958) and south of a second basalt flow that flowed north from Volcano Hill vent (Fig. 2.2). The travertine occurs in two

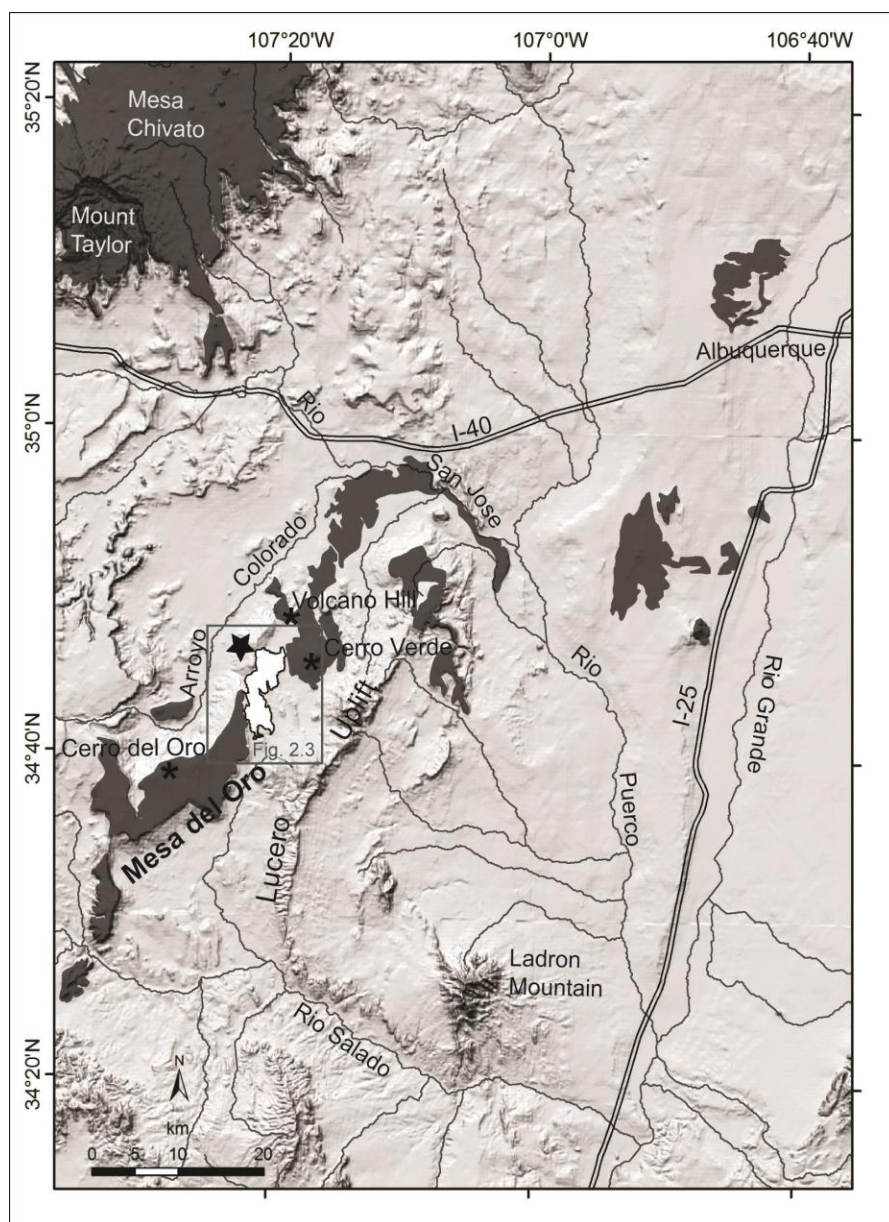


Figure 2.2. Shaded relief map showing the large-volume travertine deposit at Mesa del Oro (black star, outlined in black). Also shown are late Cenozoic volcanics (dark grey areas outlined in black), and volcanic vents (black asterisks). The box indicates the study area.

connected platforms, herein called northern and southern platforms (Fig. 2.3). The travertine overlies Triassic Chinle Formation and, at the northwestern edge, Cenozoic basalt (Fig. 2.3). The travertine at Mesa del Oro was mentioned and mapped by Wright (1946), and discussed in detail by Jicha (1958) who also mapped the southern platform. The northern platform has been quarried to a minor extent by NZ Legacy LLC and is well-known among cavers for its Pronoun Caves (Forbes and Stephens, 1994). The travertine-precipitating groundwater at Mesa del Oro, although no longer active, is inferred to have issued from springs along fault-related fissures which lead to the formation of a fissure ridge on the northern platform (Fig. 2.3; Chafetz and Folk, 1984; Pentecost, 2005; Brogi and Capezzuoli, 2009). Travertine can be dated with the precise U-series method and because the deposits are well-preserved in the landscape they provide a powerful tool for understanding paleohydrology, paleoclimate, and neotectonic processes (Glover and Robertson, 2003; Faccenna et al., 2008; Crossey et al., 2011; De Filippis et al., 2012; Kampman et al., 2012). In this paper, we report new results for travertine morphologies and facies at Mesa del Oro, six new travertine ages and associated volumes, and implications for paleohydrology, paleoclimate, and neotectonics.

BACKGROUND ON TRAVERTINE AND TRAVERTINE FORMATION

Travertines are fresh-water carbonates that precipitate at springs and along streams due to the degassing of CO₂ from groundwater that is supersaturated with respect to calcium carbonate: (Pentecost, 2005; Crossey et al., 2006):



Travertine deposits usually occur along faults that are conduits for CO₂-charged groundwater (Hancock et al., 1999), and the ascent of the groundwater along faults requires high hydraulic

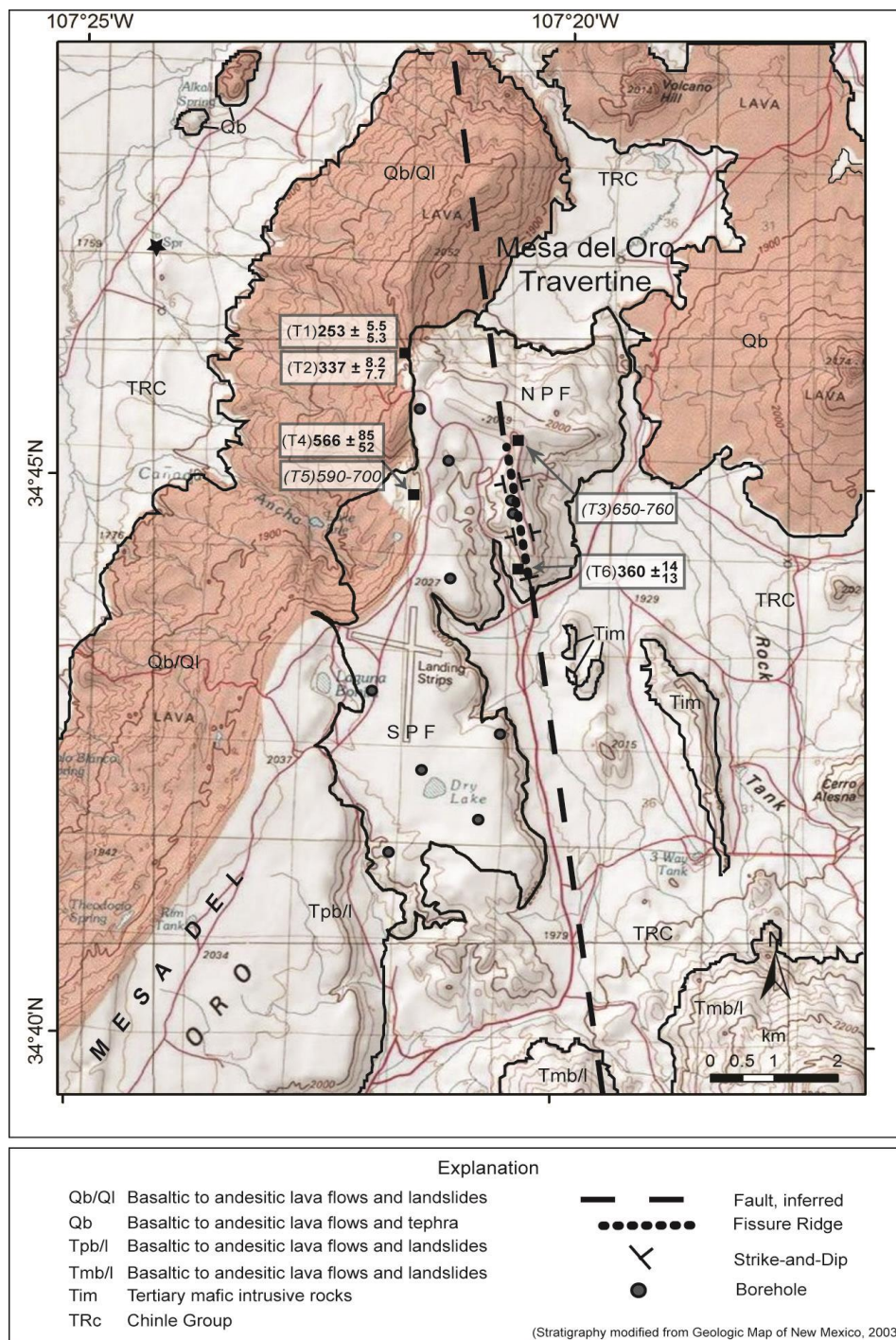


Figure 2.3. Topographic map showing the extent of the large-volume travertine deposit at Mesa del Oro (outlined in black), with its two platforms: northern platform (NPF) and southern platform (SPF). Also shown are ages of the travertine: ages in bold print are stratigraphic ages (ka), and ages in italics are model ages (ka). Numbered black squares are locations of measured sections (1-3), and a sampling location (4). The location of the modern travertine-precipitating Eddleman Spring is marked by a black star. Geographic locations of the samples can be found in Table 2.1. Stratigraphy is based on the Geologic Map of New Mexico (NMBGMR, 2003).

head in a confined aquifer (Crossey et al., 2011; Priewisch et al., 2013). Modern studies show that a significant component of the CO₂ in travertine-depositing springs is derived from deep geological sources (Crossey et al., 2009; Williams et al., 2009). CO₂ is considered to be the carrier gas of helium and helium isotopes provide a tracer of potential mantle contributions (Ballentine and Sherwood Lollar, 2002). The water chemistry of modern travertine-depositing springs shows complex mixing of shallow meteoric recharge and deeply-derived fluids (Newell et al., 2005; Crossey et al., 2006; Williams et al., 2009). Travertines can be dated with the precise U-series method (Uysal et al., 2007; Embid, 2009; Sierralta et al., 2010) because uranium, which is soluble in natural waters, becomes incorporated in the crystal lattice of calcite during travertine precipitation (Hillaire-Marcel, 2009). Travertine deposits are often associated with Cenozoic basaltic volcanism which indicates over-pressuring of the CO₂/groundwater system with magmatic gasses (Gilfillan et al., 2008).

METHODS

Mapping of the travertine platforms was conducted on RGIS digital orthophotos (1 m) and USGS 7.5' topographic maps in the field, using additional information from geologic maps compiled by Jicha (1958) and the New Mexico Bureau of Geology and Mineral Resources (NMBGMR, 2003). The travertine extent was digitized on digital orthophotos in ArcMap GIS in order to assess the volume of the deposit. The area was multiplied by an average thickness of the two platforms which was determined through field mapping and available borehole reports provided by the NMBGMR. Measured sections at the northern platform were sampled for U-series and petrographic analysis to assess travertine ages and facies, respectively. The samples were cut into slabs and micro-drilled to obtain powder from dense travertine layers for U-series analysis. Cut hand samples and slabs were used to analyze travertine facies macroscopically. The

powdered samples were dated at the Radiogenic Isotope Laboratory at the University of New Mexico with the U-series method described in Asmerom et al. (2010), which is a reliable dating method for measuring geologic age of about 500-600 ka (Edwards et al., 1987) because the ^{234}U - ^{230}Th system returns to secular equilibrium within analytical resolution after about 6-8 half-lives of the daughter isotope, ^{230}Th , which has a half-life of 75,700 years (Cheng et al., 2000). We calculated ^{234}U model ages for two samples that were out of U-series range (Table 2.1) by assuming the initial ^{234}U for these samples based on the initial ^{234}U of successfully dated samples (Priewisch et al., 2013).

Table 2.1: Locations, U-Series and Model Ages of Travertine Samples

Sample No.	Sample ID	Easting	Northing	U-Series Age	+ Error	- Error	Model Age*
		NAD 83		(ka)	(ka)	(ka)	(ka)
T1	AP10-MDO4a	284164	3849773	252,750	5,500	5,275	
T2	AP10-MDO13-b1	284132	3849805	337,163	8,241	7,728	
T3	AP10_MDO12C-a	285719	3848485				650-760
T4	AP10-MDO30	284181	3847946	565,700	84,917	52,105	
T5	AP10-MDO46A-b	284171	3847946				590-700
T6	AP10-MDO53B-a	285808	3846487	360,581	13,800	12,628	

*(Priewisch et al., 2013)

TRAVERTINE MORPHOLOGIES AND FACIES

The travertine of the northern platform was mapped in detail and dated. Its eastern part is a fissure ridge in terms of classic travertine morphology (Chafetz and Folk, 1984; Pentecost, 2005) that formed along an approximately NNW-SSE trending fault (Fig. 2.3). The fault is now concealed by travertine but we infer its trace from a fault mapped by Jicha (1958) to the south of the deposit. The central fissure is not well-preserved, but evidence for it is given by the bedding orientation of the travertine: along the central part of the fissure ridge the beds dip away from each other (Fig. 2.3). Fault-related fissure ridges like at Mesa del Oro form on tensional fissures

where travertine precipitates from spring orifices along a central fracture (Chafetz and Folk, 1984; Hancock et al., 1999; Pentecost, 2005; Brogi and Capezzuoli, 2009). The fissure ridge is cross-cut by horizontal and vertical feeder veins (Figs. 2.4 A and 2.5) that conveyed travertine-precipitating fluids to the surface (Brogi and Capezzuoli, 2009; De Filippis et al., 2012).

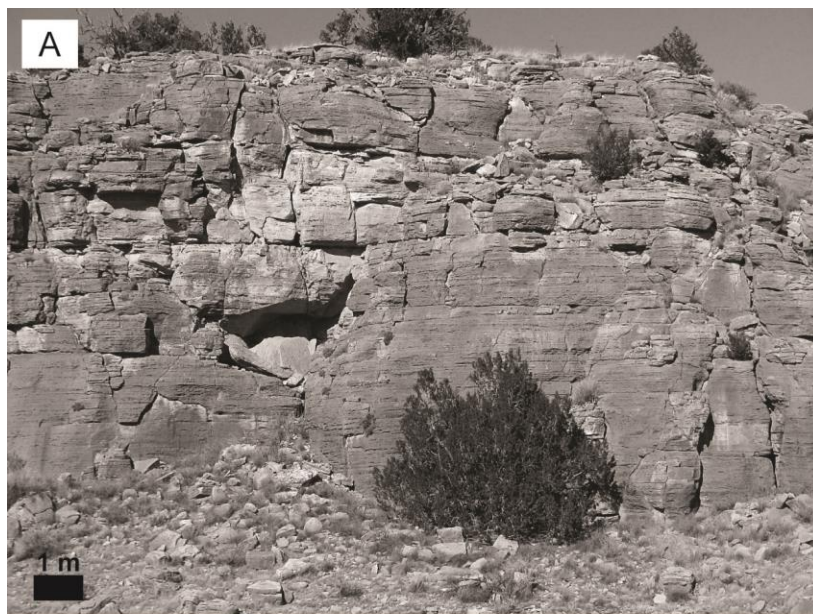


Figure 2.4. A) Fractured beds of horizontally bedded travertine at the southern end of the fissure ridge. B) E-W striking horizontal feeder vein (outlined in black) cutting across bedded travertine. The vein formed when travertine-precipitating groundwater was pushed into fractures in the existing travertine deposit during times of high hydraulic head. The vein is filled with sparry calcite.



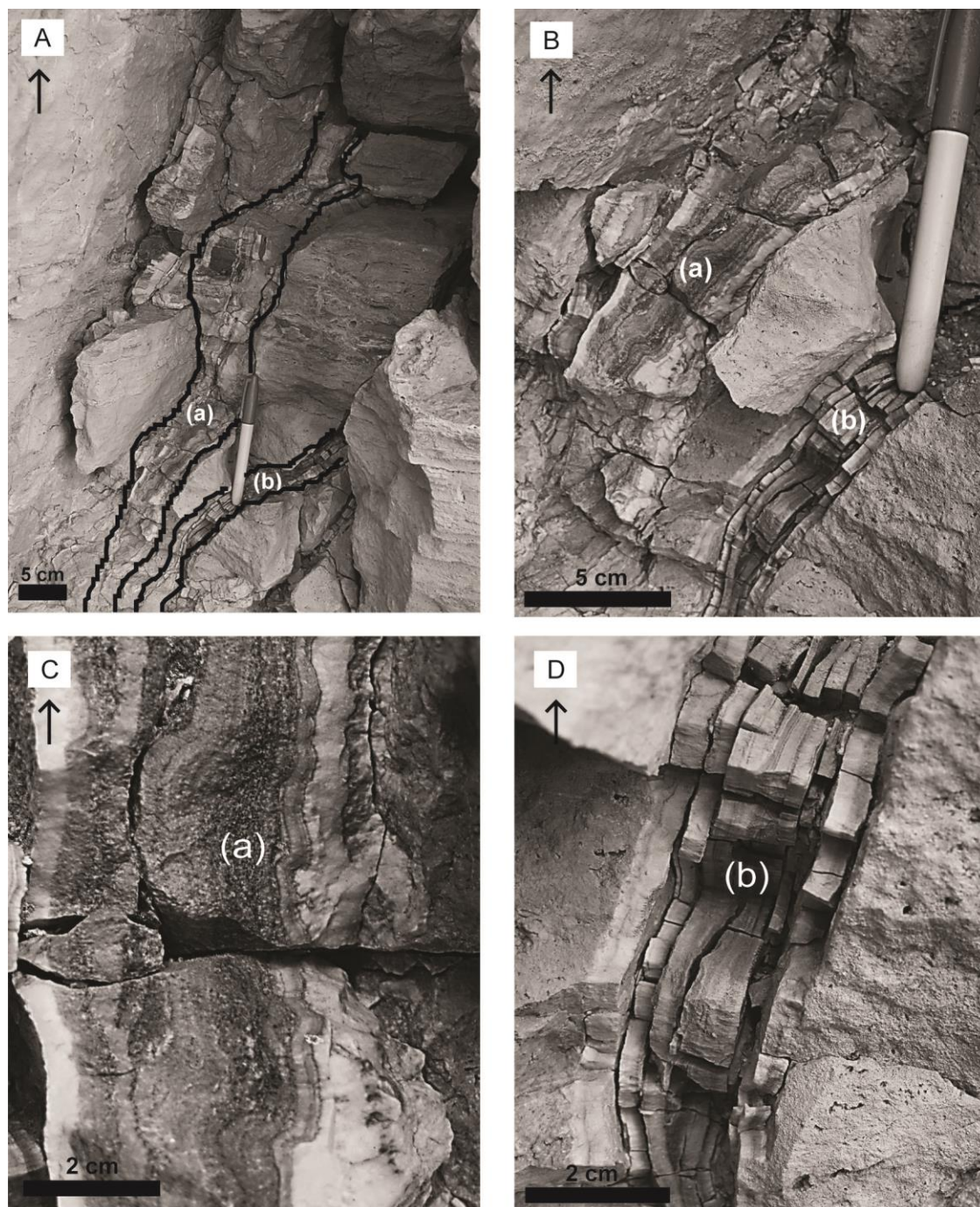


Figure 2.5. A) N-S striking vertical feeder veins (outlined in black) cutting across bedded travertine that is highly fractured. The veins formed when travertine-precipitating groundwater was pushed into fractures in the existing travertine deposit during times of high hydraulic head. B) Close-up view of the two central veins, (a) and (b). C) Close-up view of vein (a) showing intricate sparry calcite layers in different colors filling the vein. D) Close-up view of vein (b) showing parallel sparry calcite layers filling the vein. Black arrows in the photos are pointing upwards.

We identified two travertine facies for the northern platform at Mesa del Oro, which are described in the following. Our classifications are influenced by Chafetz and Folk (1984) and Alonso-Zarza and Tanner (2010) who give excellent overviews of travertine facies and morphologies. However, their facies classifications are based on modern, still active travertine systems which are very different from ancient travertine deposits like the one at Mesa del Oro. It is often difficult to interpret the depositional environment of an ancient deposit based only on travertine types shown in the rock record because the same travertine type may form in different environments. Therefore, we modified the existing facies classifications to describe our ancient deposit. The northern platform at Mesa del Oro is dominated by two travertine facies: a step-pool facies along the fissure ridge (Fig. 2.3: locations 3 and 4), and a palustrine facies to the northwest and to the west of the fissure ridge (Fig. 2.3: locations 1 and 2, respectively).

The fissure ridge is characterized by the step-pool facies that formed when water emanating from the central fissure flowed down the flanks of the growing fissure ridge. Figure 2.6 shows a stratigraphic column of the different travertine types that represent the step-pool facies: peloidal travertine and horizontally bedded travertine that form in pools behind travertine dams, travertine drapes (Fig. 2.6, A) that represent the overflow of travertine dams, and microterraces (Fig. 2.6, B) that form on steeply sloped dams and drapes (Fouke et al., 2000; Pentecost, 2005). An additional travertine type of the step-pool facies is stromatolitic travertine that forms from microbial mats growing in pools behind travertine dams (Fig. 2.7; Fouke et al., 2000; Pentecost, 2005). The step-pool facies is an important travertine facies for interpreting the carbonates as spring deposits, as opposed, for example, to lake carbonates.

The northwestern and western edge of the platform is characterized by a marsh-related or palustrine travertine facies that formed when water flowing off the fissure ridge collected on

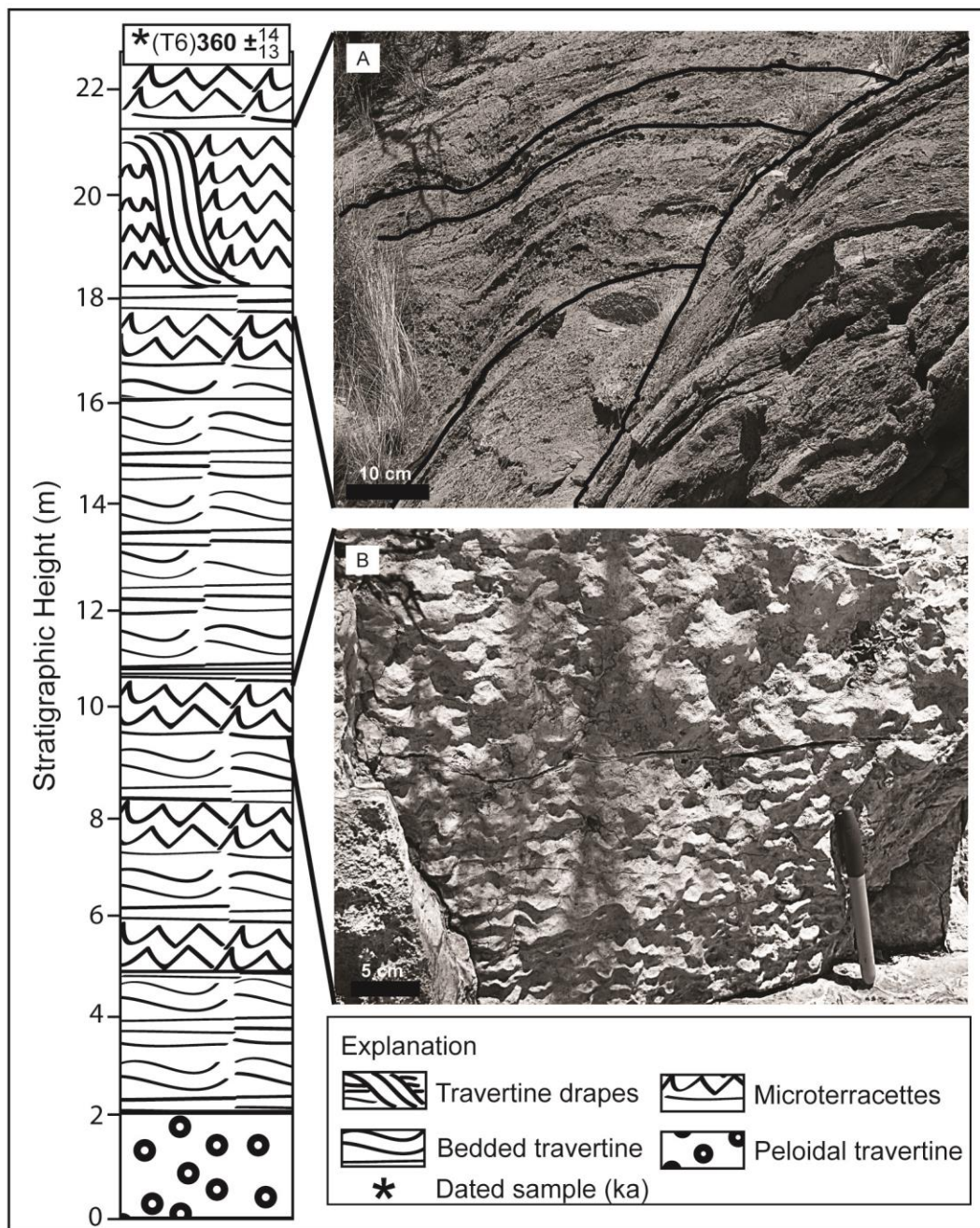


Figure 2.6. Stratigraphic column of the step-pool travertine facies from the west slope of the fissure ridge (see Fig. 2.3, location 3) showing travertine types that are indicative of this facies. A) Cross-sectional view of drapes that formed at large dams where the water flowed over the edge of one pool and down into the next pool. Some of the drapes are outlined in black. Flow direction of the water was down the slope of the fissure ridge to the west (left). B) Microterraces that formed on the surface of steeply sloping drape. Flow direction of the water was down the slope of the fissure ridge to the west (toward the viewer). Note that the orientation of the microterraces indicates the surface steepness (steeper toward the base of the outcrop).



Figure 2.7. Step-pool travertine facies at the northern end of the fissure ridge (see Fig. 2.3, location 4). A) E-W striking bedded travertine exposed in a quarry on top of the northern platform. B) Close-up view of travertine fabric formed by calcification of microbial mats that grew in the step-pools.



surrounding flats and in depressions where standing bodies of water promoted development of vegetated areas in wetlands (Guo and Riding, 1999; Glover and Robertson, 2003; Pentecost, 2005). Figure 2.8 shows a stratigraphic column of the different travertine types that represent the palustrine facies: bedded travertine (Fig. 2.8, A), peloidal travertine with phytoclasts (Fig. 2.8, B)

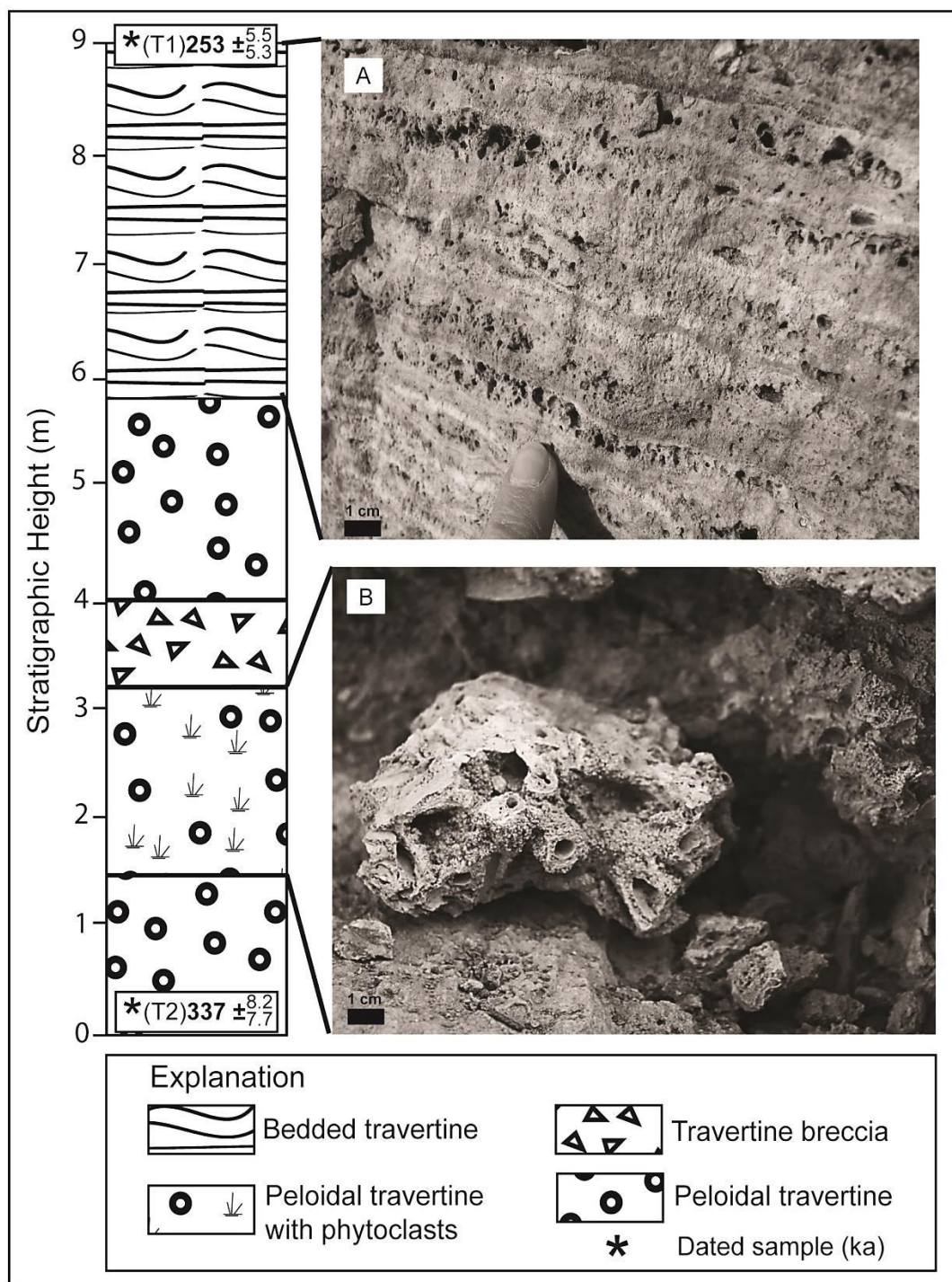


Figure 2.8. Stratigraphic column of the palustrine travertine facies to the northwest of the northern platform (see Fig. 2.3, location 2) showing travertine types that are indicative of this facies. A) Example of bedded travertine with alternating irregular layers of different colors and porosity. B) Peloidal travertine with phytoclasts: the micritic travertine contains calcite-encrusted stems and plant casts.

and peloidal travertine that form in shallow ponds in the marsh, and travertine breccia that form when travertine crusts break up during flood events and get deposited in nearby areas.

According to drilling reports provided by the New Mexico Bureau of Geology and Mineral Resources the travertine is thickest (up to 63 m) in the central part of the fissure ridge, while the thickness decreases (~8 m to 11m) to the northwest and to the west of the northern platform which was determined by field mapping. The drilling reports provided by the New Mexico Bureau of Geology and Mineral Resources also show that at the southern platform the travertine is thickest (up to 48 m) in the southern central part of the deposit where we infer the location of the primary spring vents.

TRAVERTINE VOLUMES AND AGES

The two travertine platforms at Mesa del Oro cover an area of 27 km² and have an estimated travertine volume of 0.7 km³. The calculated volume is a minimum volume because we do not know how much of the travertine has been eroded. New U-series ages are 566 ± 68.5 ka, 360 ± 13.5 ka, 337 ± 8.0 ka, and 253 ± 5.4 ka (Fig. 2.3; Table 2.1). We calculated model ages (Priewisch et al., 2013) for two samples that were out of U-series range (> 500 ka) and these model ages are slightly older, 590-700 ka and 650-760 ka (Table 2.1). Based on these results we infer that travertine formation at Mesa del Oro occurred in two intervals, from 360 ka to 250 ka and from ~560 ka to 760 ka. Two samples from the northwestern edge of the northern platform gave stratigraphic ages of 337 ka at the bottom of the section and 253 ka at the top (Figs. 2.3 and 2.8). Stratigraphic ages are in accordance with the principle of superposition. The two measured ages suggest travertine deposition took place over 84 ky, resulting in a long-term average deposition rate of 10 cm/ky which we interpret to be a maximum accumulation rate given the likelihood of unconformities in the section.

DISCUSSION

Travertine morphology and facies as well as the volume and ages of the travertine deposit have implications for understanding neotectonic processes, paleohydrology, and paleoclimate. The NNW-SSE trending fissure ridge at the northern platform (Fig. 2.3) likely formed due to the E-W extension of the Rio Grande rift and attests to repeated fault activity (Brogi et al., 2010; Ricketts et al., 2012) as shown by vertical and horizontal veins that cross-cut the deposit (Fig. 2.5). These veins suggest that CO₂-rich groundwater ascended along the fault and was precipitated in extensional veins. We infer that part of the CO₂ was derived from the mantle by analogy to the nearby active Eddleman Spring (Fig. 2.3), which may be similar to the springs responsible for depositing the travertine. The geochemistry of this spring is characterized by a high amount of CO₂ and the presence of primordial ³He that suggests the input of mantle volatiles (Newell et al., 2005). Volcanic activity that might have led to an over-pressuring of the CO₂/groundwater system with magmatic gasses (Baldrige et al., 1987; Gilfillan et al., 2008; Embid, 2009) is recorded by the Mesa del Oro basalt flows which were dated by Baldrige et al. (1987) between 3.4 Ma and 1.1 Ma. Younger flows to the northeast of Mesa del Oro have ages between 800 ka and 300 ka (Baldrige et al., 1987), and the two intervals of travertine formation from 360 ka to 250 ka and from ~560 ka to 760 ka (Fig. 2.3; Table 2.1) overlap this period of Quaternary basaltic volcanism.

Although there are no active springs on the travertine platforms, the existence of the Pronoun Caves, which are dissolution caves in the travertine, provide evidence for past groundwater activity (Forbes and Stephens, 1994). The feeder veins (Figs. 2.4 B and 2.5) cutting horizontally and vertically across the fissure ridge show that the hydraulic head was episodically high enough to push groundwater up and through the existing travertine deposit and we infer that groundwater

originating from a confined aquifer system had significant artesian head to ascend along faults and fractures at these times. Modern hydrologic studies have identified the Permian San Andres-Glorieta (SAG) aquifer and Pennsylvanian Madera limestone as the regional aquifers at Mesa del Oro (Goff et al., 1983; Baldwin and Anderholm, 1992; Rauzi, 1999; Rawling, 2005) and they also show groundwater mixing and complex flow paths because of two different recharge areas for these aquifers, the Lucero uplift to the east and the Zuni Mountains to the west (Baldwin and Anderholm, 1992). We assume that aquifers, recharge areas, and groundwater flow paths were very similar at the time of travertine formation, and that the recharge areas received enough precipitation during extended wet times to increase the hydraulic head of the aquifers and facilitate travertine precipitation at Mesa del Oro during both glacial and interglacial paleoclimate periods (Priewisch et al., 2013).

Paleohydrologic conditions, topography, and the amount of CO₂ degassing affected travertine precipitation and facies at Mesa del Oro. Although the fissure ridge itself is related to normal faulting (Brogi and Capezuoli, 2009; De Filippis et al., 2012), the flow rate of the water flowing out of the central fissure influenced its height and width (Hancock et al., 1999), and thus slope gradient. The step-pool facies requires a certain gradient in order to develop pools and drapes of different sizes and microterraces (Fouke et al., 2000; Pentecost, 2005). The peloidal and bedded travertine of the palustrine travertine facies to the northwest and west of the fissure ridge reflect the presence of stagnant bodies of water, such as ponds and lakes, and hence the availability of significant amounts of water that collected in the marsh. Windblown clastic material accumulated in these water bodies and led to the formation of marly sediment. The availability of water also led to the growth of abundant vegetation represented by travertine layers that contain plant casts and fibrous material.

Various authors (e. g. Glover and Robertson, 2003; Crossey et al., 2011; De Filippis et al., 2012; Kampman et al., 2012) have shown a connection between paleoclimate, aquifer recharge, and travertine formation and our own results confirm this connection at Mesa del Oro.

CONCLUSIONS

New ages show that large-volume travertine formation at Mesa del Oro occurred in two intervals, from 360 ka to 250 ka, and from ~560 ka to 760 ka. These intervals coincide with local basaltic volcanism between 300 ka and 800 ka which we infer led to high CO₂ influx to the groundwater system. Increased recharge during wet climate periods are interpreted to have caused high hydraulic head in a confined aquifer leading to artesian springs and facilitating travertine precipitation. The formation of a fissure ridge and associated marsh reflect the availability of significant amounts of water and hence, we conclude that travertine formation at Mesa del Oro represents extended wet times during paleoclimate periods.

ACKNOWLEDGEMENTS

We thank the staff of the New Mexico Bureau of Geology and Mineral Resources for providing travertine cores from Mesa del Oro. We extend our thanks to Bob Worsley, owner of NZ Legacy LLC, for access to his property and travertine quarries at Mesa del Oro, to Jim Harrison, manager of NZ Legacy LLC, for valuable information about the travertine deposit, to the rancher Mark Chavez for access to his land, and to Alexander Nereson for his invaluable support as a field assistant. We thank Bruce Allen and Peter Mozley for valuable edits which helped greatly to improve this paper. We also thank Stacy Timmons and Kate Ziegler for editorial handling and additional comments. This material is based upon work supported by the National Science Foundation under Grant no. NSF 0838575 and support was also provided by generous funding through Grants-In-Aid by the New Mexico Geological Society.

REFERENCES

- Asmerom, Y., Polyak, V.J., and Burns, S.J., 2010, Variable winter moisture in the southwestern United States linked to rapid glacial climate shifts: *Nature Geoscience*, v. 3, p. 114–117, doi: 10.1038/ngeo754.
- Baldrige, W.S., Perry, F.V., and Shafiqullah, M., 1987, Late Cenozoic volcanism of the southeastern Colorado Plateau: I. Volcanic geology of the Lucero area, New Mexico: *Geological Society of America Bulletin*, v. 99, p. 463–470.
- Baldwin, J.A., and Anderholm, S.K., 1992, Hydrogeology and ground-water chemistry of the San Andres-Glorieta aquifer in the Acoma embayment and eastern Zuni uplift, west-central New Mexico: U.S. Geological Survey Water-Resources Investigations Report 91-4033, 302 p.
- Ballentine, C.J., and Sherwood Lollar, B., 2002, Regional groundwater focusing of nitrogen and noble gases into the Hugoton-Panhandle giant gas field, USA: *Geochimica et Cosmochimica Acta*, v. 66, no. 14, p. 2483–2497.
- Barker, J.M., Austin, G.S., and Sivils, D.J., 1996, Travertine in New Mexico - Commercial deposits and otherwise: *New Mexico Bureau of Mines and Mineral Resources Bulletin*, v. 154, p. 73–92.
- Brogi, A., and Capezzuoli, E., 2009, Travertine deposition and faulting: the fault-related travertine fissure-ridge at Terme S. Giovanni, Rapolano Terme (Italy): *International Journal of Earth Sciences*, v. 98, p. 931–947, doi: 10.1007/s00531-007-0290-z.
- Brogi, A., Capezzuoli, E., Aqué, R., Branca, M., and Voltaggio, M., 2010, Studying travertines for neotectonics investigations: Middle–Late Pleistocene syn-tectonic travertine deposition at Serre di Rapolano (Northern Apennines, Italy): *International Journal of Earth Sciences*, v. 99, p. 1383–1398, doi: 10.1007/s00531-009-0456-y.
- Chafetz, H.S., and Folk, R.L., 1984, Travertines; depositional morphology and the bacterially constructed constituents: *Journal of Sedimentary Petrology*, v. 54, no. 1, p. 289–316.
- Cheng, H., Edwards, R., Hoff, J., Gallup, C., Richards, D., and Asmerom, Y., 2000, The half-lives of uranium-234 and thorium-230: *Chemical Geology*, v. 169, p. 17–33.
- Crossey, L.J., Fischer, T.P., Patchett, P.J., Karlstrom, K.E., Hilton, D.R., Newell, D.L., Huntoon, P., Reynolds, A.C., and De Leeuw, G.A.M., 2006, Dissected hydrologic system at the Grand Canyon: Interaction between deeply derived fluids and plateau aquifer waters in modern springs and travertine: *Geology*, v. 34, no. 1, p. 25–28, doi: 10.1130/G22057.1.

- Crossey, L.J., Karlstrom, K.E., Springer, A.E., Newell, D., Hilton, D.R., and Fischer, T., 2009, Degassing of mantle-derived CO₂ and He from springs in the southern Colorado Plateau region--Neotectonic connections and implications for groundwater systems: *Geological Society of America Bulletin*, v. 121, no. 7-8, p. 1034–1053, doi: 10.1130/B26394.1.
- Crossey, L.J., Karlstrom, K.E., Newell, D.N., Kooser, A., and Tafoya, A., 2011, The La Madera travertines, Rio Ojo Caliente, northern New Mexico : Investigating the linked system of CO₂-rich springs and travertines as neotectonic and paleoclimate indicators, *in* *New Mexico Geological Society Guidebook, 62nd Field Conference, Geology of the Tusas Mountains - Ojo Caliente*, p. 121–136.
- Edwards, R., Chen, J., and Wasserburg, G., 1987, ²³⁸U- ²³⁴U- ²³⁰Th- ²³²Th systematics and the precise measurement of time over the past 500,000 years: *Earth and Planetary Science Letters*, v. 81, p. 175–192.
- Embid, E.H., 2009, U-Series dating, geochemistry, and geomorphic studies of travertines and springs of the Springerville Area, east-central Arizona, and tectonic implications [M.S. thesis]: Albuquerque, University of New Mexico, 103 p.
- Faccenna, C., Soligo, M., Billi, A., De Filippis, L., Funicello, R., Rossetti, C., and Tuccimei, P., 2008, Late Pleistocene depositional cycles of the Lapis Tiburtinus travertine (Tivoli, Central Italy): possible influence of climate and fault activity: *Global and Planetary Change*, v. 63, p. 299–308, doi: 10.1016/j.gloplacha.2008.06.006.
- De Filippis, L., Faccenna, C., Billi, a., Anzalone, E., Brillì, M., Ozkul, M., Soligo, M., Tuccimei, P., and Villa, I.M., 2012, Growth of fissure ridge travertines from geothermal springs of Denizli Basin, western Turkey: *Geological Society of America Bulletin*, v. 124, no. 9-10, p. 1629–1645, doi: 10.1130/B30606.1.
- Forbes, J., and Stephens, D., 1994, Caves of the Mesa del Oro travertine, New Mexico, U.S.A.: Breakthroughs in Karst Geomicrobiology and Redox Geochemistry Special Publication, v. 1, p. 18–20.
- Fouke, B.W., Farmer, J.D., Des Marais, D.J., Pratt, L., Sturchio, N.C., Burns, P.C., and Discipulo, M.K., 2000, Depositional facies and aqueous-solid geochemistry of travertine-depositing hot springs (Angel Terrace, Mammoth Hot Springs, Yellowstone National Park, U.S.A.): *Journal of Sedimentary Research*, v. 70, no. 3, p. 565–585.

- Gilfillan, S.M.V., Ballentine, C.J., Holland, G., Blagburn, D., Sherwood Lollar, B., Stevens, S., Schoell, M., and Cassidy, M., 2008, The noble gas geochemistry of natural CO₂ gas reservoirs from the Colorado Plateau and Rocky Mountain provinces, USA: *Geochimica et Cosmochimica Acta*, v. 72, no. 4, p. 1174–1198, doi: 10.1016/j.gca.2007.10.009.
- Glover, C., and Robertson, A.H.F., 2003, Origin of tufa (cool-water carbonate) and related terraces in the Antalya area, SW Turkey: *Geological Journal*, v. 38, p. 329–358, doi: 10.1002/gj.959.
- Goff, F., McCormick, T., Gardner, J.N., Trujillo, P.E., Counce, D., Vidale, R., and Charles, R., 1983, Water geochemistry of the Lucero uplift, New Mexico: A geothermal investigation of low-temperature mineralized fluids: Los Alamos National Laboratory LA-9738-OBES, 26 p.
- Guo, L.I., and Riding, R., 1999, Rapid facies changes in Holocene fissure ridge hot spring travertines, Rapolano Terme, Italy: *Sedimentology*, v. 46, p. 1145–1158.
- Hancock, P.L., Chalmers, R.M., Altunel, E., and Cakir, Z., 1999, Travitronics: using travertines in active fault studies: *Journal of Structural Geology*, v. 21, p. 903–916.
- Jicha, H., 1958, Geology and mineral resources of Mesa del Oro Quadrangle, Socorro and Valencia Counties, New Mexico: State Bureau of Mines and Mineral Resources Bulletin, v. 56, p. 1–67.
- Kampman, N., Burnside, N.M., Shipton, Z.K., Chapman, H.J., Nicholl, J. a., Ellam, R.M., and Bickle, M.J., 2012, Pulses of carbon dioxide emissions from intracrustal faults following climatic warming: *Nature Geoscience*, v. 5, p. 352–358, doi: 10.1038/ngeo1451.
- Newell, D.L., Crossey, L.J., Karlstrom, K.E., Fischer, T.P., and Hilton, D.R., 2005, Continental-scale links between the mantle and groundwater systems of the western United States: Evidence from travertine springs and regional He isotope data: *GSA Today*, v. 15, no. 12, p. 4–10.
- NMBGMR, 2003, Geologic Map of New Mexico: New Mexico Bureau of Geology and Mineral Resources, scale 1:500 000, 2 sheets.
- Pentecost, A., 2005, *Travertine*: Springer Verlag Berlin Heidelberg, 445 p.
- Priewisch, A., Crossey, L.J., Karlstrom, K.E., Polyak, V.J., Asmerom, Y., Nereson, A., and Ricketts, J.W., 2013, U-series geochronology of large-volume travertine deposits of the southeastern Colorado Plateau: Evaluating episodicity, tectonic and paleohydrologic controls: New Mexico Geological Society Annual Spring Meeting, Program with Abstracts.

- Rauzi, S.L., 1999, Carbon Dioxide in the St. Johns - Springerville Area, Apache County, Arizona: Arizona Geological Survey, Open-File Report 99-2, 24 p.
- Rawling, G.C., 2005, Geology and hydrologic setting of springs and seeps on the Sevilleta National Wildlife Refuge: New Mexico Bureau of Geology and Mineral Resources, Open-File Report 495, 90 p.
- Ricketts, J.W., Priewisch, A., Kolomaznik, M., and Karlstrom, K.E., 2012, Calcite-filled fractures in travertine used to constrain the timing and orientation of Quaternary extension along the western margin of the Rio Grande rift, central New Mexico: New Mexico Geological Society Spring Meeting, Program with Abstracts.
- Williams, A.J., Crossey, L.J., and Karlstrom, K.E., 2009, An integrated geochemical and structural study of the Sevilleta National Wildlife Refuge: geochemistry and salinity sources of waters spanning the Rio Grande rift, New Mexico: Geological Society of America Abstracts with Programs, v. 41, no. 7, p. 413.
- Wright, H.E., 1946, Tertiary and Quaternary geology of the lower Rio Puerco area, New Mexico: Geological Society of America Bulletin, v. 57, no. 5, p. 383–456, doi: 10.1130/0016-7606(1946)57.

CHAPTER 3

Extensive CO₂ Leakage from extinct and modern CO₂ Reservoirs in New Mexico and Arizona: Evaluating the Role of Seal Bypass and large-volume Travertine Deposition with Implications for CO₂ Sequestration

Priewisch, A.¹, Crossey, L.J.¹, Karlstrom, K.E.¹, and Mozley, P.S.²

¹ *Department of Earth and Planetary Sciences, University of New Mexico, Albuquerque, NM*

² *Department of Earth and Environmental Science, New Mexico Tech, Socorro, NM*

(Submitted to International Journal of Greenhouse Gas Control: April 2014)

CHAPTER ABSTRACT

Quaternary large-volume travertine deposits in New Mexico and Arizona occur along the Rio Grande rift and on the southeastern Colorado Plateau. Travertines are natural analogues for CO₂ leakage along fault systems because they form due to the degassing of CO₂ from carbonic groundwater that migrates up fault systems. Travertine volumes can be used to infer integrated CO₂ leakage along faults, which includes: (1) CO₂ that becomes fixed in CaCO₃/travertine (tons of carbon converted into tons of carbonate), (2) the amount of CO₂ that degassed into the atmosphere (twice the amount of (1), based on reaction stoichiometry), (3) dissolved CO₂ that is carried away with the water discharging from a spring (based on modern spring discharge and dissolved carbon content), and (4) CO₂ that escapes through the soil (based on modern soil flux measurements). The total CO₂ leakage (1 and 2) calculated in this study is estimated as ~6 Gt (gigatons) whereas the integrated CO₂ leakage (1-4) is estimated as ~128 Gt. Better understanding of integrated CO₂ leakage along fault systems is needed to better constrain global estimates of natural CO₂ fluxes, and to help in risk assessment of CO₂ sequestration sites designed to effectively store anthropogenic CO₂ in the subsurface.

INTRODUCTION

Long-term storage of anthropogenic carbon dioxide (CO₂) in subsurface geologic formations (geologic CO₂ sequestration) is one way to reduce the concentration of CO₂ in the atmosphere (Benson and Cole, 2008; IPCC, 2013). The storage reservoir must have lateral and vertical seals to confine the injected CO₂, and a major concern in this context is CO₂ leakage along fault systems that allow CO₂ migration towards the surface (i.e. seal bypass; Shipton et al., 2004; Shipton et al., 2005; Bachu, 2008). Natural analogues for CO₂ leakage over geologic time scales like travertine deposits can improve understanding of variables controlling seal bypass, and help to quantify natural CO₂ leakage along fault systems. This study reports for the first time integrated amounts of CO₂ leakage based on travertine volumes, spring CO₂ flux, and diffuse CO₂ flux through the soil. An estimated integrated amount of 128 gigatons (Gt) CO₂ leaked along fault systems in New Mexico and Arizona. Integrated CO₂ leakage along faults has the potential to compromise storage sites and should be taken into account in characterizing potential CO₂ sequestration sites.

Suitable geological formations for CO₂ storage are depleted oil and gas reservoirs, deep saline formations, and coal seams (Holloway, 2001; Bachu, 2008; Benson and Cole, 2008) which must not only have the necessary storage capacity but also effective seals to confine the CO₂ for thousands of years. Effective geologic seals are rocks with very low permeabilities (e. g. shales and evaporites), which prevent vertical and lateral migration of fluids and natural gas (Downey, 1984; Davies and Handschy, 2003; Cartwright et al., 2007). However, one of the biggest concerns is that the injected CO₂ could leak back to the surface or into adjacent aquifers (Holloway, 2001; Bachu, 2008; Benson and Cole, 2008; Kharaka et al., 2010) when seals are bypassed by fault systems as described by Cartwright et al. (2007). Cartwright et al. (2007)

indicate that faults are the most common type of seal bypass system. Because of their heterogeneous nature, faults may seal in some areas and leak in others depending on the fault zone permeability architecture, and thus can act as a barrier, conduit, or a dynamic barrier-conduit system (Sibson et al., 1975; Caine et al., 1996; Caine and Forster, 1999; Goodwin et al., 1999; Aydin, 2000; Rawling et al., 2001).

For the assessment of safe storage sites it is crucial to understand CO₂ leakage along faults and seal bypass fluxes over geologic timescales since the stored CO₂ should be retained for thousands of years (Gale, 2004; Hepple and Benson, 2004). Natural analogues for CO₂ leakage such as travertine deposits allow evaluation of fluid flow and CO₂ migration along faults over tens to hundreds of thousands of years. U-series dating shows that travertine formation and hence CO₂ leakage occurs episodically at times of high hydraulic head due to increased recharge of aquifers and high CO₂ flux associated with volcanic and seismic activity (Uysal et al., 2009; Kampman et al., 2012; Priewisch et al., 2014). The volume of travertine deposits was used by some researchers (Dockrill, 2005; Burnside, 2010; Burnside et al., 2013) in order to estimate the amount of CO₂ that leaked over a given period of time along a faults and, constrained by U-series ages of the travertines, to calculate the CO₂ leakage rate or CO₂ flux. However, CO₂ leakage estimates based on travertine volumes alone do not represent all of the CO₂ that leaks to the surface. Significant amounts of CO₂ are also carried away in solution with discharging spring water (James et al., 1999; Crossey et al., 2009; Karlstrom et al., 2013) and escape through the soil (Allis et al., 2005; Lewicki et al., 2013; Han et al., 2013).

CO₂ springs and travertines are widespread on the Colorado Plateau and in the Rocky Mountain region (Crossey et al., 2009; Karlstrom et al., 2013) and numerous well-preserved travertine deposits are located on the southeastern Colorado Plateau in New Mexico and Arizona

(Fig. 3.1; Barker et al., 1996; Embid, 2009; Priewisch et al., 2014) This study focuses on several large-volume travertine deposits (Fig. 3.1) that are of particular interest because they attest to degassing of significant amounts of CO₂ over tens of thousands to hundreds of thousands of years.

The goals of this paper are 1) to calculate the amount of CO₂ that leaked along fault systems in the study areas in order to estimate the magnitude of CO₂ leakage, 2) to explore the role of the fault systems and seal bypass for these travertine occurrences, and 3) to explore the implications of CO₂ leakage along the studied fault systems in the risk assessment of potential CO₂ sequestration sites.

BACKGROUND ON TRAVERTINE FORMATION

This section gives an overview of the processes that lead to travertine formation and the origin of the CO₂; see Priewisch et al. (2014) for additional information .

Travertines are freshwater carbonates that form at springs and along streams due to the degassing of CO₂ from groundwater that is supersaturated with respect to calcium carbonate, according to the following reactions (Pentecost, 2005; Crossey et al., 2006, 2009):



The external CO₂ that makes the groundwater acidic enough to dissolve the limestone is magmatic in origin and likely derived from the mantle (Crossey et al., 2009; Karlstrom et al., 2013; Williams et al., 2013). He isotopes as tracers of potential mantle contributions which are carried by the CO₂ have been measured at various modern travertine-depositing springs and they support the mantle origin of the CO₂ (Ballentine and Sherwood Lollar, 2002; Newell et al., 2005; Crossey et al., 2009; Karlstrom et al., 2013; Williams et al., 2013). Modern groundwater of

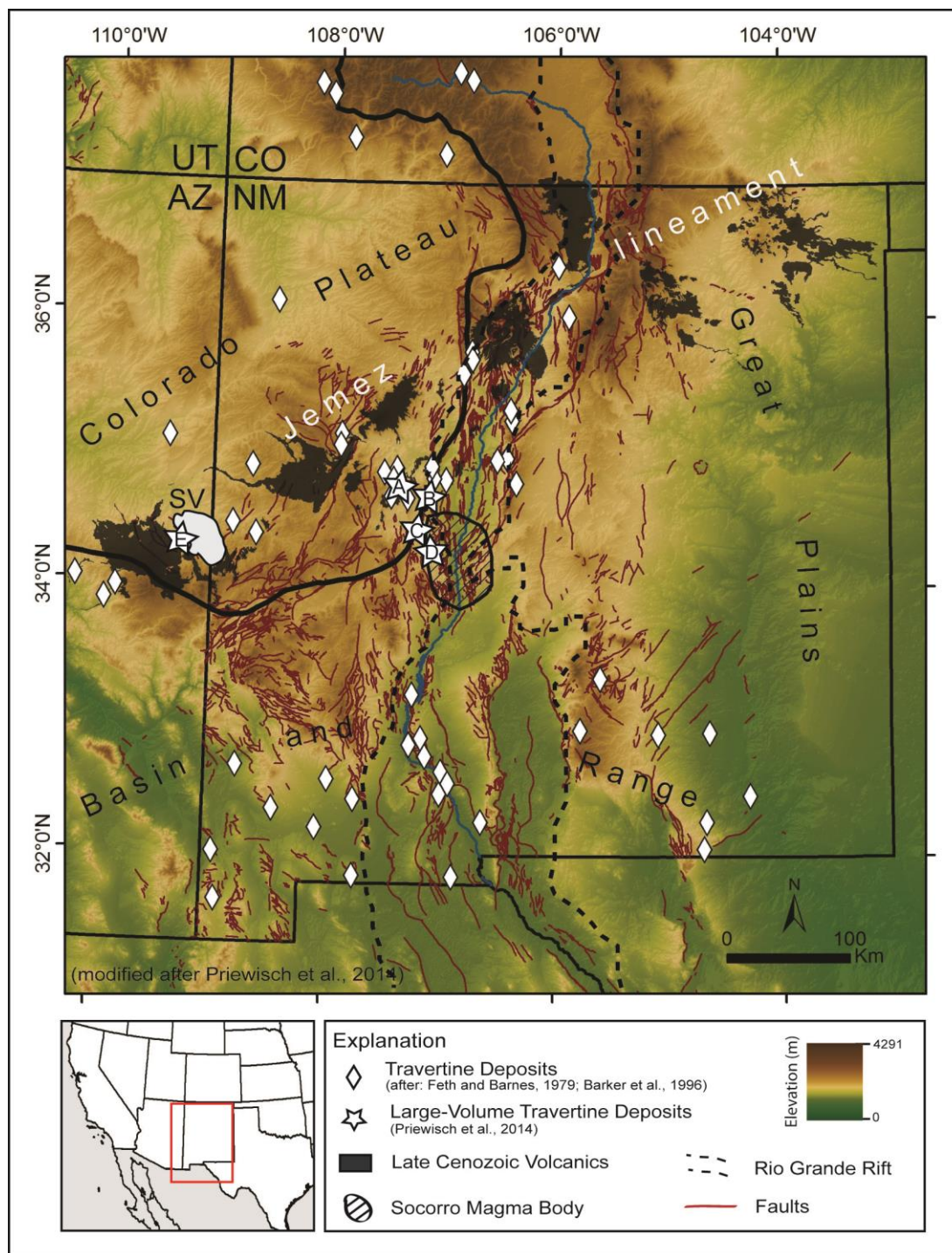


Figure 3.1. Map showing locations of travertine accumulations (Feth and Barnes, 1979; Barker et al., 1996), large-volume travertine deposits (Prewisch et al., 2014), the Rio Grande rift, and Jemez lineament. Also shown are the Colorado Plateau, Great Plains, and Basin and Range physiographic provinces. Large-volume travertine deposits New Mexico are Mesa del Oro (A), Mesa Aparejo (B), Riley North Mesa (C), and Riley South Mesa (D). The travertine deposits at Springerville in Arizona (E) are associated with an active CO₂ gas field (SV).

travertine-precipitating springs shows complex mixing of shallow meteoric water, deeply derived fluids, and groundwater with long residence times (Minissale et al., 2002; Newell et al., 2005; Crossey et al., 2006; Embid, 2009; Williams et al., 2013).

GEOLOGICAL SETTING OF THE STUDY AREAS

Large-volume travertine deposits in the study areas in New Mexico and Arizona are located along the Rio Grande rift, and the Jemez lineament, a prominent northeast–trending belt of Cenozoic volcanic fields located on the southwestern Colorado Plateau (Fig. 3.1; Aldrich, 1986; Dunbar, 2005; Chamberlin, 2007). The north-south–trending Rio Grande rift extends over 1000 km from Colorado to Mexico and it is bounded by complex fault systems (e.g. Keller and Baldrige, 1999; Cather, 2004; Seager, 2004; Minor et al., 2013). The large-volume travertine deposits form massive platforms of ranging from ~4 m to 25 m in thickness (Fig. 3.2). Travertine occurrences in New Mexico are interpreted to be extinct CO₂ reservoirs (Priewisch et al., 2014) whereas the deposits at Springerville, Arizona, are associated with a still active CO₂ field (Fig. 3.1; Embid, 2009). U-series dating of travertine samples show that the large-volume travertine deposits formed episodically at 700-500 ka, 300-250 ka, and 100-40 ka during times of high hydraulic head and regional volcanic activity that contributed to excess magmatic/mantle-derived CO₂ (Priewisch et al., 2014). For a more detailed description of the geologic setting of the study areas see Priewisch et al. (2014).

METHODS

Calculation of Travertine Volume

The calculation of the travertine volume as reported in Priewisch et al. (2014) is summarized in this section to provide a better understanding of the method. The extent of the travertine deposits was mapped based on U.S. Geological Survey 7.5' topographic maps and

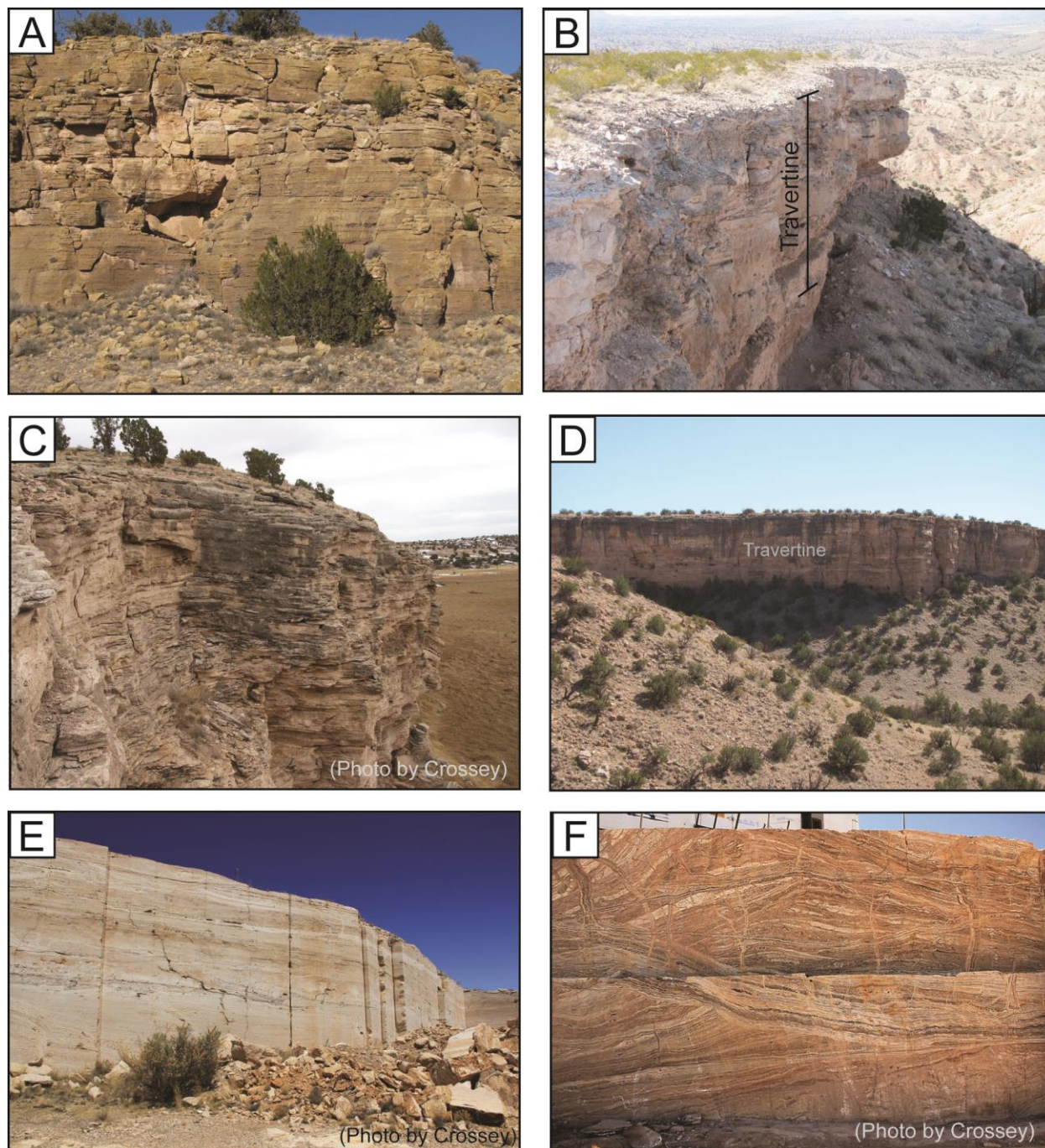


Figure 3.2. Field photos of travertine deposits: Mesa del Oro (A), Riley South Mesa (B), Springerville (C), Riley North Mesa (D), and Mesa Aparejo (E and F). The thickness of the travertine sections are ~15 m (A), ~8m (B), ~ 20 m (C), ~25 m (D), ~10 m (E), and ~ 4m (F). (E) and (F) are two different travertine quarries located at Mesa Aparejo, the latter (F) showing different generations of veins.

digital orthophotos (1m) from RGIS (New Mexico Resource Geographic Information System Program) in the field and digitally with ArcMap GIS (Geographic Information System) ©1995-2014 Esri (Environmental Systems Research Institute, Inc.). The area covered by travertine for each deposit was determined using digital orthophotos in ArcMap. The area was then multiplied by the average thickness of each deposit based on mapping results, borehole reports provided by the New Mexico Bureau of Geology and Mineral Resources, and published data (Moore et al., 2005; Embid, 2009) in order to calculate the travertine volume (Table 3.1; Fig. DR1).

Table 3.1: Total Amount of CO₂ and Total CO₂ Flux

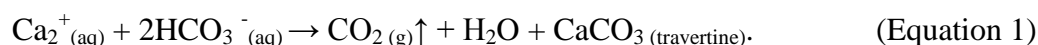
Location	Travertine Volume (km ³)	Fixed CO ₂ (Gt)	Degassed CO ₂ (Gt)	Total Amount of CO ₂ (Gt)	Age of Deposit* (yrs)	Total CO ₂ Flux (t/yr)
Mesa del Oro	0.7	0.85	0.85	1.71	312,950	5,462
Mesa Aparejo	0.2	0.24	0.24	0.49	455,819	1,071
Riley North Mesa	0.5	0.61	0.61	1.22	370,000	3,300
Riley South Mesa	0.2	0.24	0.24	0.49	149,450	3,268
Springerville	0.9	1.10	1.10	2.20	318,317	6,904

See Tables DR1 and DR2 for detailed calculations

*For detailed U-series and model ages see Priewisch et al. (2014)

Calculation of the Total Amount of CO₂

The total amount of CO₂ that leaked to the surface is part of the integrated CO₂ flux discussed below and it is determined based on the reaction



In order to estimate CO₂ leakage along a fault, the amount of CO₂ fixed in travertine is calculated using the stoichiometry and density of calcite (CaCO₃) such that 1 cm³ of calcite (travertine) equals 0.33g of carbon (C). 0.33g C/cm³_(CaCO₃) is then multiplied by the travertine volume which results in the total amount of carbon that is fixed in travertine. Using the atomic masses of C and CO₂, the total amount of carbon is converted into CO₂. The total amount of CO₂ is doubled

according to the stoichiometry of Equation 1, where 1 mole of CO₂ degasses into the atmosphere and 1 mole of CO₂ becomes fixed in travertine. The sum, the total amount of CO₂ leakage, is divided by the age of the travertine deposit to obtain the CO₂ flux in gigatons (Gt) per year (Table 3.1). The individual steps of the calculation are described in Item DR1 and shown in Tables DR1 and DR 2. The same calculations are used to determine the episodic amount of CO₂ leakage based on the volume of travertine that accumulated during individual episodes of travertine formation. Dividing the episodic amount of CO₂ leakage by the duration of an episode gives the episodic CO₂ flux (Table 3.2; Tables DR3-DR5).

Table 3.2: Episodic Amount of CO₂ and Episodic CO₂ Flux

Location	Travertine Volume			Episodic Amount of CO ₂		
	Episode A (km ³)	Episode B (km ³)	Episode C (km ³)	Episode A (Gt)	Episode B (Gt)	Episode C (Gt)
Mesa del Oro		0.2	0.4		0.5	0.9
Mesa Aparejo		0.09	0.09		0.2	0.2
Riley North Mesa			0.5			1.2
Riley South Mesa		0.1			0.5	
Springerville	0.3	0.6		0.6	1.6	

(continued)

Location	Episodic CO ₂ Flux		
	Episode A* (t/yr)	Episode B* (t/yr)	Episode C* (t/yr)
Mesa del Oro		3,333	4,500
Mesa Aparejo		1,333	1,000
Riley North Mesa			6,000
Riley South Mesa		3,333	
Springerville	10,000	10,667	

See Tables DR3-DR5 for detailed calculations

*Episode A: 100-40 ka; Episode B: 350-200 ka; Episode C: 700-500 ka (Priewisch et al., 2014)

Calculation of Spring CO₂ Flux

Crossey et al. (2009) and Karlstrom et al. (2013) use water chemistry to estimate CO₂ flux through springs: the dissolved inorganic carbon (DIC) of the groundwater is multiplied by

the discharge of the spring where DIC or alkalinity is a measure of the amount of inorganic CO₂ that is dissolved in the water. In this study, spring CO₂ flux is estimated based on alkalinity and discharge data from springs in the vicinity of the large-volume travertine deposits because most of the deposits, except for Springerville, lack active springs (Wright, 1946; Goff et al., 1983; Moore et al., 2005; Newell et al., 2005; Embid, 2009; Williams et al., 2013). The modern spring CO₂ fluxes are multiplied by both the age of the travertine deposits and the individual episodes of travertine formation to calculate spring CO₂ fluxes and episodic spring CO₂ fluxes (Table 3.3; Tables DR6 and DR7). Riley North Mesa and Riley South Mesa are not included because of a lack of discharge data for springs in these areas.

Table 3.3: Spring CO₂ Flux

Location	Spring Name	Modern Spring CO ₂ Flux (t/yr)	Modern Spring CO ₂ Flux (mol/yr)	Age of Deposit* (yrs)	Spring CO ₂ Flux (t)
Mesa del Oro	Crane Spring Eddleman Spring	2.0	9.0E+07	312,950	636,958
Mesa Aparejo	Unnamed Salt Spring/Salado Arroyo Spring Ojo Monte Largo	57.3	2.5E+09	455,819	26,138,011
Springerville	Salado Springs	334.8	1.5E+10	318,317	106,572,625

(continued)

Location	Spring Name	Episodic Spring CO ₂ Flux		
		Episode A** [t]	Episode B** (t)	Episode C** (t)
Mesa del Oro	Crane Spring Eddleman Spring		305,300	407,067
Mesa Aparejo	Unnamed Salt Spring/Salado Arroyo Spring Ojo Monte Largo		8,601,444	11,468,592
Springerville	Salado Springs	20,088,000	50,220,000	

See Tables DR6 and DR7 for detailed calculations

*For detailed U-series ages see Priewisch et al. (2014)

**Episode A: 100-40 ka; Episode B: 350-200 ka; Episode C: 700-500 ka (Priewisch et al., 2014)

Calculation of Diffuse CO₂ Flux

Diffuse CO₂ flux is CO₂ that escapes through the soil in the vicinity of faults. Diffuse CO₂ flux calculations for this study are based on CO₂ flux measurements along the Little Grand

Wash Fault in Utah. Because CO₂ fluxes cluster at 0-150 g/m²/day (Allis et al., 2005; Han et al., 2013), the mean CO₂ flux of 75 g/m²/day was used and converted into kg/m²/year (Table 3.4; Tables DR8 and DR9). In a separate step, areas of highest diffuse CO₂ flux were assigned to

Table 3.4: Diffuse CO₂ Flux

Location	Highest Diffuse CO ₂ Flux* (m ²)	Mean Diffuse CO ₂ Flux** (kg/m ² /day)	Mean Diffuse CO ₂ Flux** (t/year)	Age of Deposit*** (yrs)	Diffuse CO ₂ Flux (Gt)
Mesa del Oro	2,505,580	27.4	68,590	312,950	21.5
Mesa Aparejo	4,290,813	27.4	117,461	455,819	53.5
Riley North Mesa	2,214,549	27.4	60,623	370,000	22.4
Riley South Mesa	1,176,400	27.4	32,204	149,450	4.8
Springerville	2,214,568	27.4	60,624	318,317	19.3

(continued)

Location	Episodic Diffuse CO ₂ Flux		
	Episodic Soil CO ₂ Flux		
	Episode A [#] (Gt)	Episode B [#] (Gt)	Episode C [#] (Gt)
Mesa del Oro		10.3	13.7
Mesa Aparejo		17.6	23.5
Riley North Mesa			12.1
Riley South Mesa		4.8	
Springerville	3.6	9.1	

See Tables DR8 and DR9 for detailed calculations

*For detailed explanation see Fig. DR1

**Mean soil flux is based on a range of 0-150 g/m²/day from Allis et al. (2005) and Han et al. (2013)

***For detailed U-series and model ages see Priewisch et al. (2014)

[#]Episode A: 100-40 ka; Episode B: 350-200 ka; Episode C: 700-500 ka (Priewisch et al., 2014)

each large-volume travertine deposit (Table 3.4; Fig. DR1); the extent of these areas is based on CO₂ flux profiles along the Little Grand Wash Fault in Utah (Allis et al., 2005; Han et al., 2013). The areas of highest diffuse CO₂ flux were multiplied by the mean CO₂ flux in kg/m²/year to calculate the mean diffuse CO₂ flux in t/year which was then multiplied by both the age of the

travertine deposits and the individual episodes of travertine formation to obtain diffuse CO₂ flux and episodic diffuse CO₂ flux, respectively (Table 3.4; Tables DR8 and DR9).

Calculation of the Integrated Amount of CO₂ Leakage

The integrated amount of CO₂ leakage is the sum of the total amount of CO₂ leakage, spring CO₂ flux, and diffuse CO₂ flux calculated over the age of a travertine deposit and the episodic integrated amount of CO₂ leakage is calculated for the different episodes of travertine formation (Tables 3.5 and 3.6; Tables DR10 and DR11).

Table 3.5: Comparison of Total and Integrated Amount of CO₂ and CO₂ Flux

Location	Age of Deposit* (yrs)	Total Amount of CO ₂ (Gt)	Total CO ₂ Flux (t/yr)	Integrated Amount of CO ₂ (Gt)	Integrated CO ₂ Flux (t/yr)
Mesa del Oro	312,950	1.71	5,462	23.2	74,055
Mesa Aparejo	455,819	0.49	1,071	54.1	118,590
Riley North Mesa	370,000	1.22	3,300	23.7	63,923
Riley South Mesa	149,450	0.49	3,268	5.3	35,472
Springerville	318,317	2.20	6,904	21.6	67,863

See Table DR10 for detailed calculations

*For detailed U-series and model ages see Priewisch et al. (2014)

Table 3.6: Comparison of Episodic CO₂ Flux and Integrated Episodic CO₂ Flux

Location	Episodic CO ₂ Flux			Integrated Episodic CO ₂ Flux		
	Episode A* (t/yr)	Episode B* (t/yr)	Episode C* (t/yr)	Episode A* (Gt/yr)	Episode B* (Gt/yr)	Episode C* (Gt/yr)
Mesa del Oro		3,333	4,500		11.0	15.0
Mesa Aparejo		1,333	1,000		18.0	24.0
Riley North Mesa			6,000			13.0
Riley South Mesa		3,333			5.0	
Springerville	10,000	10,667		4.0	11.0	

See Table DR11 for detailed calculations

*Episode A: 100-40 ka; Episode B: 350-200 ka; Episode C: 700-500 ka (Priewisch et al., 2014)

RESULTS

Discussion of Assumptions for CO₂ Leakage Calculations

The assumptions that went into the CO₂ leakage calculations below are briefly discussed in this section.

The calculated amounts of CO₂ are based on the stoichiometry of the chemical reaction

$$\text{Ca}^{2+}_{(\text{aq})} + 2\text{HCO}_3^{-}_{(\text{aq})} \rightarrow \text{Ca}^{2+}_{(\text{aq})} + 2\text{H}^{+} + 2\text{CO}_3^{-}_{(\text{aq})} \rightarrow \text{CO}_2(\text{g})\uparrow + \text{H}_2\text{O} + \text{CaCO}_3(\text{travertine}).$$

One of the two carbonate ions is converted into CO_{2(g)} whereas the other carbonate ion is incorporated into calcite and hence stoichiometry leads to the assumption that half of the CO₂ degasses while the other half gets fixed in travertine. Spring discharge in the vicinity of the large-volume travertine deposits in New Mexico was used to calculate spring CO₂ flux assuming that ancient springs discharged water from the same aquifers as the modern springs. CO₂ flux measurements along the Little Grand Wash Fault were used to approximate diffuse CO₂ flux because the fault system is actively degassing CO₂ and, therefore, a modern analogue for CO₂ leakage through the soil. All of the calculated amounts of CO₂ leakage based on travertine are minima because it is not known how much of the travertine was eroded. Modern spring CO₂ fluxes are considered to be minima given that the current climatic interval is an interglacial characterized by warm and dry conditions; spring discharge was certainly larger when the large-volume travertine deposits accumulated. The amounts of diffuse CO₂ flux are also minima because it is not known how much CO₂ escaped through the soil when the large-volume travertine deposits formed and additionally, the calculated amounts are based on a mean value of modern measurements.

Calculated Amounts of CO₂ Leakage

The total amounts of CO₂ that leaked along the faults in the study areas range from 0.49 Gt to 2.2 Gt and if continuous travertine deposition over the entire age of the deposits is assumed total CO₂ fluxes vary between 1,071 t/yr and 6,904 t/yr (Table 3.1). Because travertine formation occurred episodically, the amount of CO₂ leakage for each individual episode was calculated as well as episodic CO₂ fluxes and values range from 0.2 Gt to 1.6 Gt and from 1,000 t/yr to 10,667 t/yr, respectively (Table 3.2). Modern spring CO₂ fluxes per year are 2t, 57.3 t, and 334.8 t for springs at Mesa del Oro, Mesa Aparejo, and Springerville, respectively (Table 3.3; Goff et al., 1983; Moore et al., 2005; Newell et al., 2005). Averaged CO₂ fluxes over the entire age of the deposits range from ~637,000 t to ~107 million tons (Mt) and episodic spring CO₂ fluxes vary between ~305,000 t and ~50 Mt (Table 3.3). Defined areas of highest diffuse CO₂ flux on the large-volume travertine deposits range from ~1 km² to ~4 km² and mean diffuse CO₂ fluxes vary between ~32 t/yr and ~117 t/yr (Table 3.4). Averaged diffuse CO₂ fluxes over the entire age of the deposit vary from 4.8 Gt to 53.5 Gt, and episodic diffuse CO₂ fluxes range from ~5 Gt and ~24 Gt (Table 3.4). Integrated amounts of CO₂ leakage vary between 5.3 Gt and 54.1 Gt and integrated CO₂ fluxes range from 35,472 t/yr to 118,590 t/yr whereas integrated episodic CO₂ fluxes vary between 4 Gt and 24 Gt (Tables 3.5 and 3.6).

DISCUSSION

Importance of Seal Bypass

This section attempts to evaluate regional seals of the Colorado Plateau and Rio Grande rift, the complex hydrologic system of the region, and the importance of seal bypass that led to CO₂ leakage in the study areas.

The main regional seals are shales of the Triassic Chinle Formation with thicknesses ranging from 236 m to 533 m on the Colorado Plateau and of 450 m in the Rio Grande rift which commonly confine the Permian San Andres-Glorieta aquifer, the main aquifer on the Colorado Plateau (Figs. 3.3, 3.4, and 3.5; Jicha, 1958; Akers, 1964; Baldwin and Anderholm, 1992; Baldwin and Rankin, 1995; Rauzi, 1999; Connell, 2008). Another important confined aquifer is the Pennsylvanian Madera Formation, called Madera Limestone hereafter (Figs. 3.3, 3.4, and 3.5). The complex hydrologic system of the Colorado Plateau and Rio Grande rift is the driver for travertine deposition and CO₂ leakage, as shown in the schematic cross-section in Figure 3.5: the two main aquifers are recharged in the Zuni Mountains to the west and in the Lucero Uplift to the east which leads to groundwater mixing in the San Andres-Glorieta aquifer; because of high hydraulic head in the confined aquifers the groundwater flows up faults where it mixes with deeply-derived CO₂; upward migration of CO₂-charged groundwater leads to CO₂ leakage and travertine deposition at the surface due to the degassing of CO₂ (e.g. at Mesa del Oro and Mesa Aparejo); groundwater locally flows from the Colorado Plateau into the Rio Grande rift although the main recharge area is in the Manzano Mountains to the east. The fault zones in the study areas mainly developed in crystalline and well-lithified sedimentary rocks (Figs. 3.6 and 3.7; Jicha, 1958; Lewis and Baldrige, 1994; Barker et al., 1996; Cather and Read, 2003; Embid, 2009, and references therein) where groundwater flow and CO₂ migration mainly occurred along the highly fractured damage zones whereas the less permeable fault cores acted as barriers to cross-fault flow (Caine et al., 1996; Caine and Forster, 1999; Goodwin et al., 1999; Faulkner et al., 2010). On the Colorado Plateau, the fault systems bypassed shales of the Triassic Chinle Formation at Springerville and at Mesa del Oro which are directly overlain by large-volume travertine deposits (Fig. 3.6). At Springerville, shales of the Permian Supai Formation were also

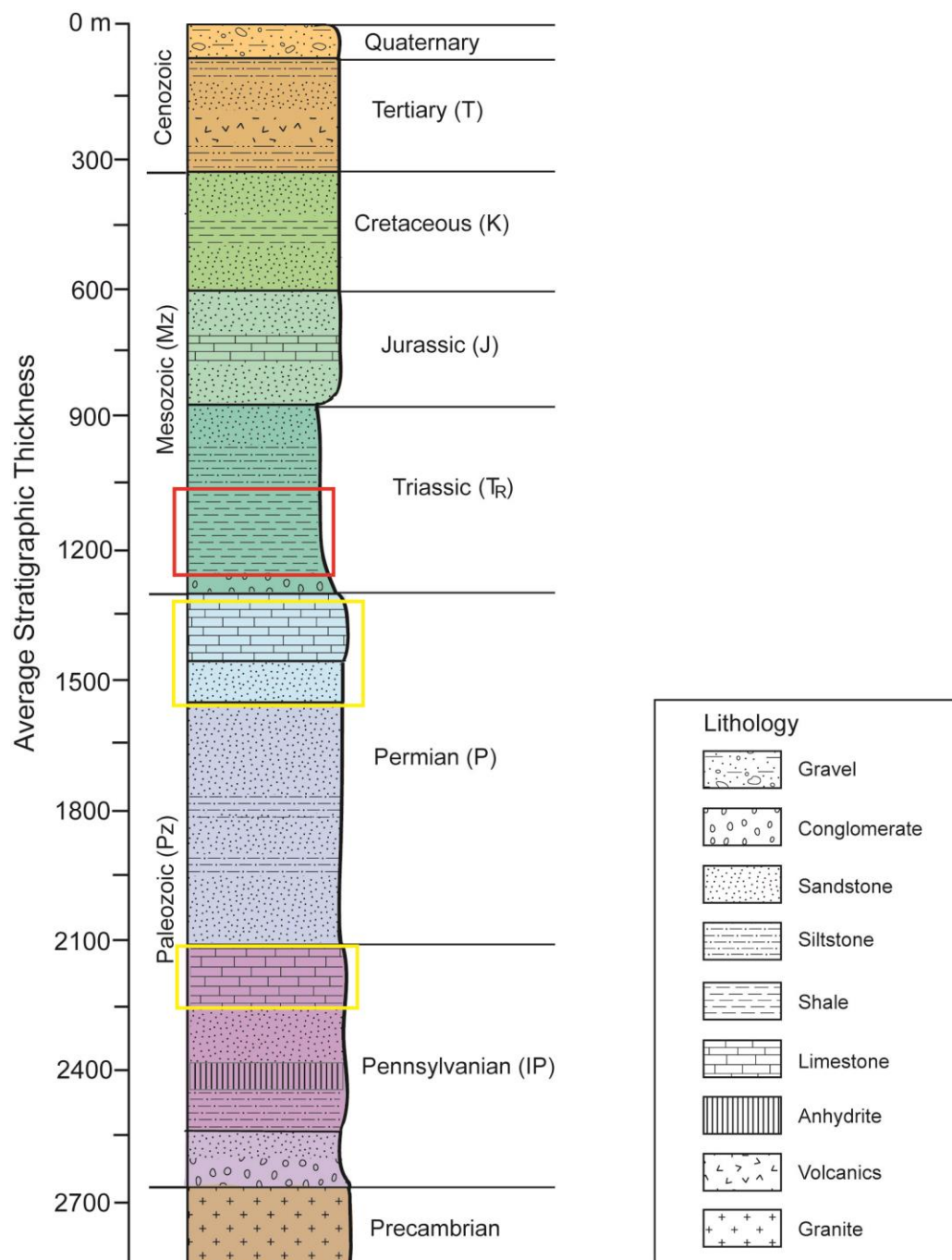


Figure 3.3. Schematic stratigraphic column of the Colorado Plateau. Geologic eras (Paleozoic, Mesozoic, Cenozoic) and periods (Precambrian through Quaternary) and their abbreviations are shown as well as lithologies. The lithologies represent examples of the most important rock types of the individual geologic periods and are not to scale. Thicknesses and lithologies are compiled after Akers (1964), Jicha (1958), Baldwin and Anderholm (1992), Baldwin and Rankin (1995), and Rauzi (1999). Red box outlines regional seal, yellow boxes outline regional aquifers.

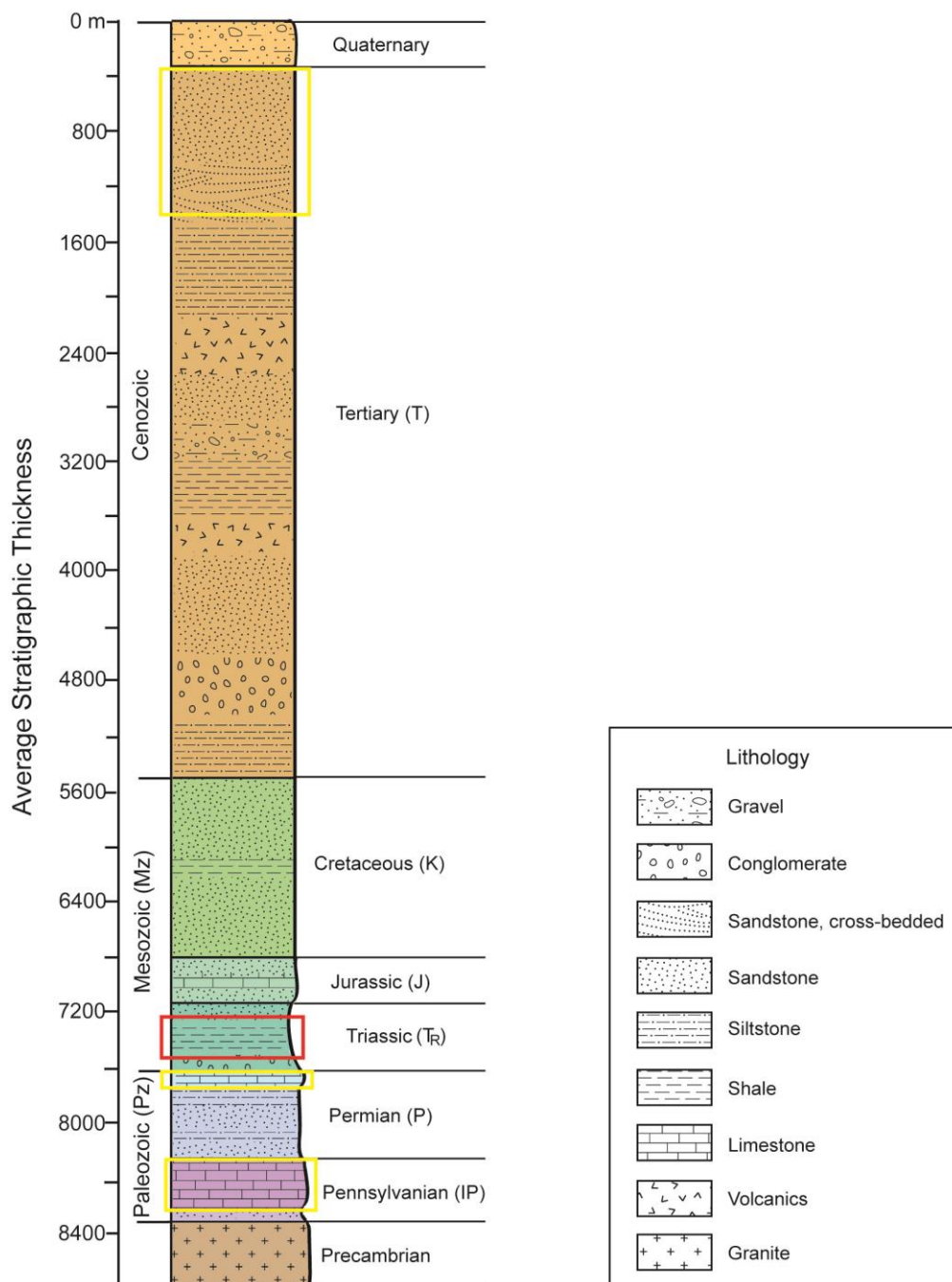


Figure 3.4. Schematic stratigraphic column of the Rio Grande rift. Geologic eras (Paleozoic, Mesozoic, Cenozoic) and periods (Precambrian through Quaternary) and their abbreviations are shown as well as lithologies. The lithologies of the different formations represent examples of the most important rock types of the individual periods and are not to scale. Thicknesses and lithologies are compiled after Connell (2008). Red box outlines regional seal, yellow boxes outline regional aquifers.

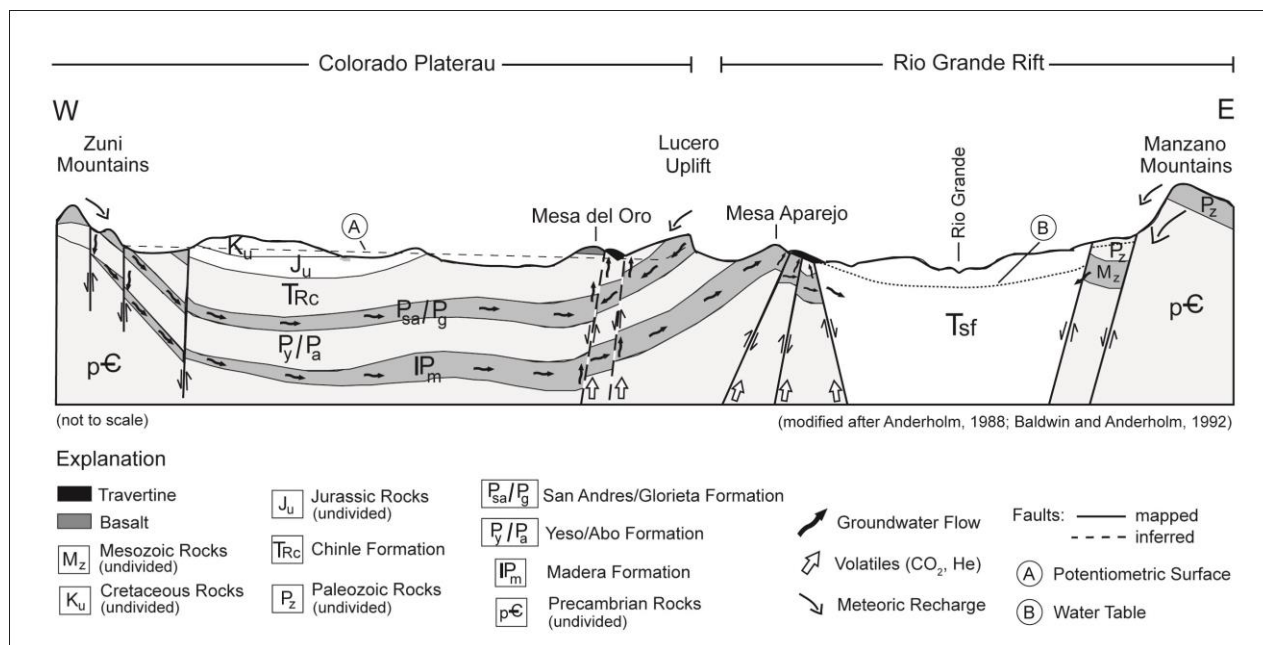


Figure 3.5. Schematic hydrologic cross-section across the Colorado Plateau and the Rio Grande rift. Recharge areas, main aquifers, and groundwater flow are shown and migration of groundwater and volatiles along faults. Travertine deposits formed above faults. See text for more detailed description. Abbreviations of geologic periods and eras are explained in Figs. 3.3 and 3.4; circled A = potentiometric surface of the San Andres-Glorieta aquifer; circled B = water table in the Rio Grande rift.

bypassed (Fig. 3.6 A). In the study areas along the Rio Grande rift, at Mesa Aparejo and Riley North Mesa, the fault systems did not bypass regional seals but cut through Madera Limestone, the regional aquifer, which is directly overlain by large-volume travertine deposits (Fig. 3.7). Seal bypass may play a role at Riley North where an inferred fault system cuts through shales of the Permian Yeso Formation (Fig. 3.7 B). Riley South Mesa is not included because this area has not been mapped in detail. A conceptual model of CO₂ leakage along a fault is shown in Figure 3.8: the highly fractured damage zone is permeable enough to allow groundwater flow and CO₂ migration along the fault while the fault core is impermeable and prevents groundwater flow across the fault zone; fractures and smaller faults extend into the host rock adjacent to the damage zone; when CO₂-charged groundwater reaches the surface, some of the CO₂ degasses

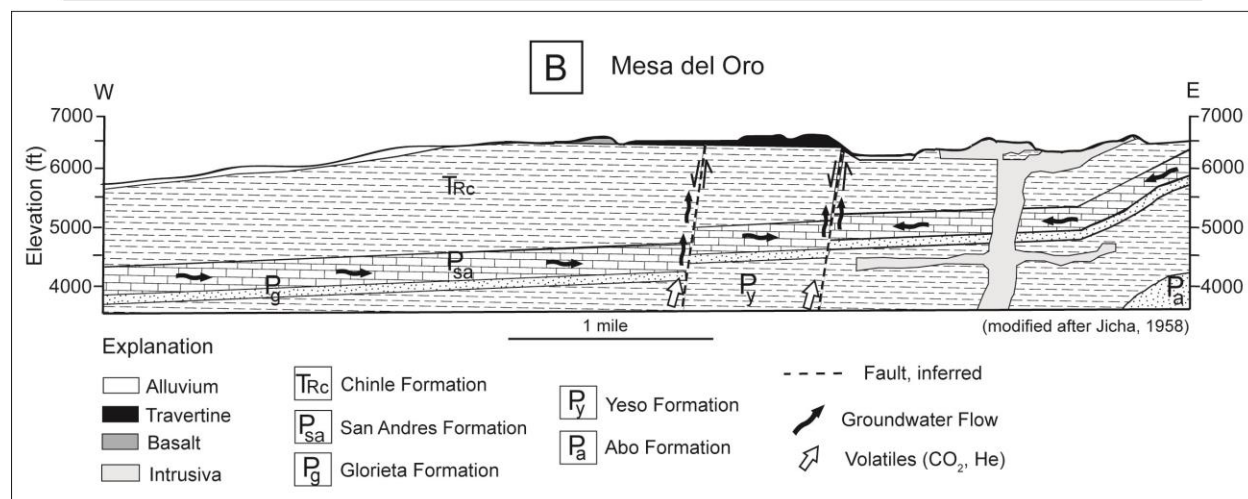
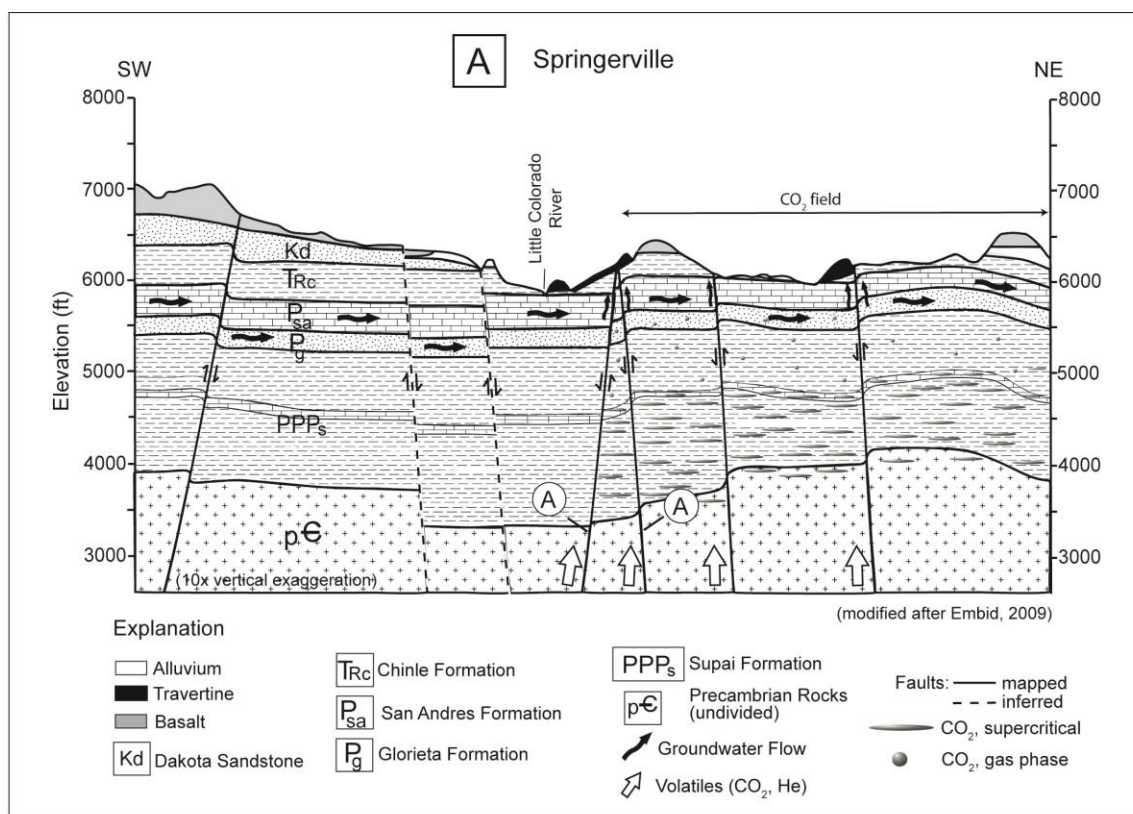


Figure 3.6. Cross-sections of study areas on the Colorado Plateau. A) Springerville (modified after Embid, 2009): groundwater flow in main aquifer (San Andres-Glorieta aquifer) is shown and migration of groundwater and volatiles along faults. Travertine deposits that formed above faults are associated with a modern CO₂ field, represented by supercritical CO₂ below 5000 ft and CO₂ in the gas phase above 5000 ft. Abbreviations of geologic periods are explained in Figs. 3.3 and 3.4; circled A = Coyote Wash Fault system. B) Mesa del Oro (modified after Jicha, 1958): groundwater flow in main aquifer (San Andres-Glorieta aquifer) and migration of groundwater and volatiles along faults are shown and travertine deposits that formed above faults. Groundwater flow is from west to east and east to west because of two different recharge areas. Abbreviations of geologic periods are explained in Figs. 3.3 and 3.4.

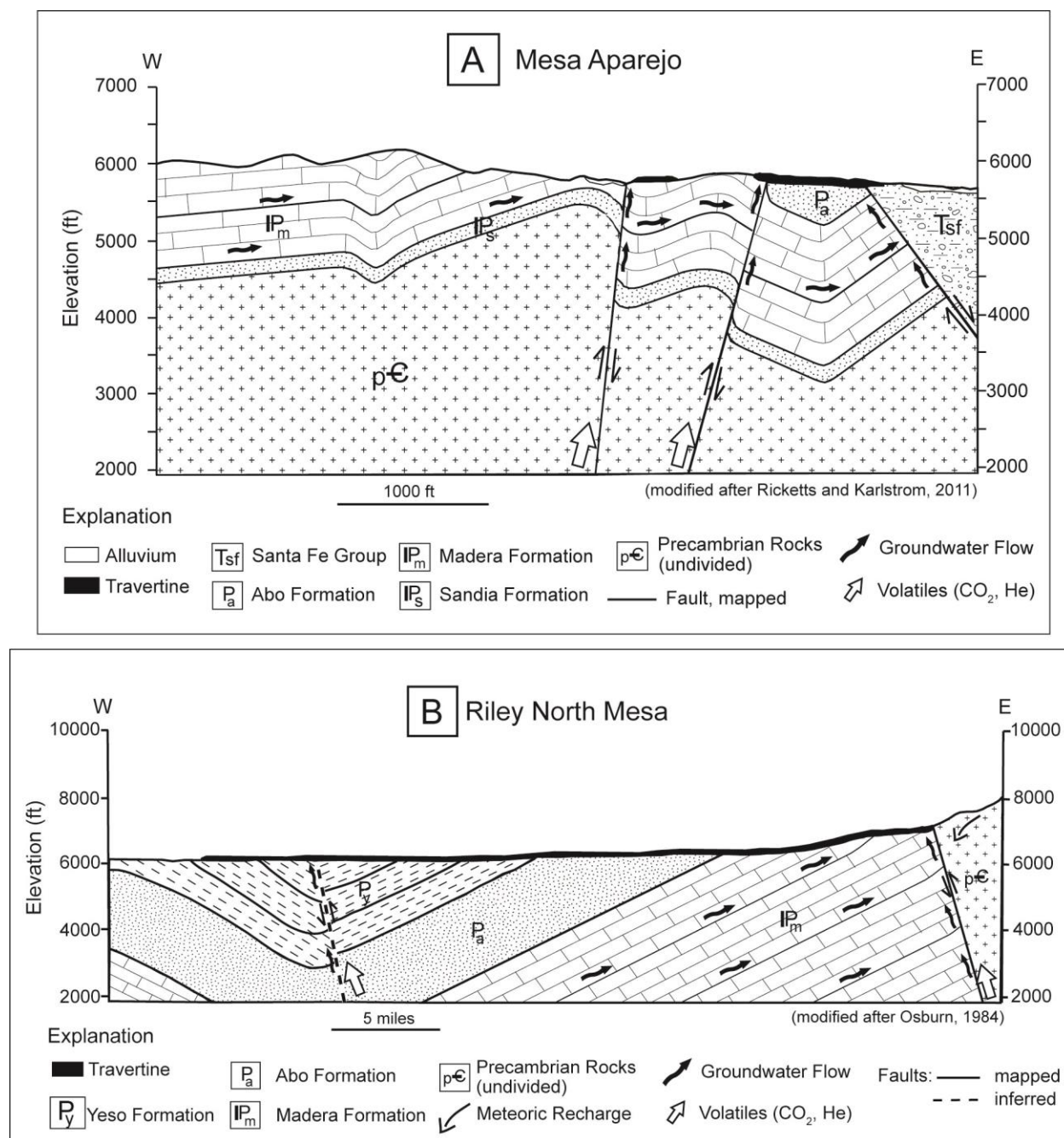


Figure 3.7. Cross-sections of study areas along the Rio Grande rift. A) Mesa Aparejo (modified after Ricketts and Karlstrom, 2011): groundwater flow in main aquifer (Madera Limestone) and migration of groundwater and volatiles along faults are shown and travertine deposits that formed above faults. Abbreviations of geologic periods are explained in Figs. 3.3 and 3.4. B) Riley North Mesa (modified after Osburn, 1984): groundwater flow in main aquifer (Madera Limestone) and migration of groundwater and volatiles along faults are shown and travertine deposits that formed above faults. Groundwater flow is mainly from west to east; however, meteoric recharge also occurs to the east due to a local recharge area. Abbreviations of geologic periods are explained in Figs. 3.3 and 3.4.

into the atmosphere while some of the CO₂ becomes fixed in travertine (total amount of CO₂). CO₂ also remains in solution and is carried away with the water (spring CO₂ flux), and migrates along fractures and smaller faults in the host rock to escape through the soil (diffuse CO₂ flux). Episodic travertine deposition as constrained by U-series dating and the presence of different generations of vein systems in travertine deposits (Fig. 3.2 F) attest to repeated reactivation of fault systems as well as episodic influx of CO₂ and episodic high hydraulic head in the aquifers (Kampman et al., 2012; Priewisch et al., 2014; Ricketts et al., 2014); consequently, seal bypass occurs episodically. An interesting aspect is that even though seals are bypassed, CO₂ sequestration is happening through the precipitation of travertine. In the following section, the magnitude of CO₂ leakage due to seal bypass will be discussed.

Wider Significance of Integrated CO₂ Leakage and Implications for CO₂ Sequestration

This section attempts to evaluate the amounts of past CO₂ leakage from modern and extinct CO₂ reservoirs, and implications for CO₂ sequestration projects.

Travertine volumes can be used to calculate CO₂ leakage (Table 3.1; Burnside et al., 2013) but the calculated amounts represent only a part of the leaked CO₂. CO₂ leakage based on travertine volumes does not take into account CO₂ leakage through springs and the soil both constituting a significant amount of leaked CO₂ that has to be included into the calculations. Crossey et al. (2009) and Karlstrom et al. (2013) show in their studies of springs in Arizona and Colorado that considerable amounts of CO₂ remain dissolved in the water and are carried away, ranging from 3×10^8 mol/yr to 1×10^9 mol/yr. High CO₂ fluxes are also reported from springs in Oregon with amounts ranging from 7.9×10^7 mol/yr to 3.5×10^8 mol/yr (James et al., 1999), and from thermal springs in Italy where amounts are as high as 6.5×10^{10} mol/yr (Chiodini et al., 2000). Modern spring CO₂ fluxes which were used in this study to estimate past spring CO₂

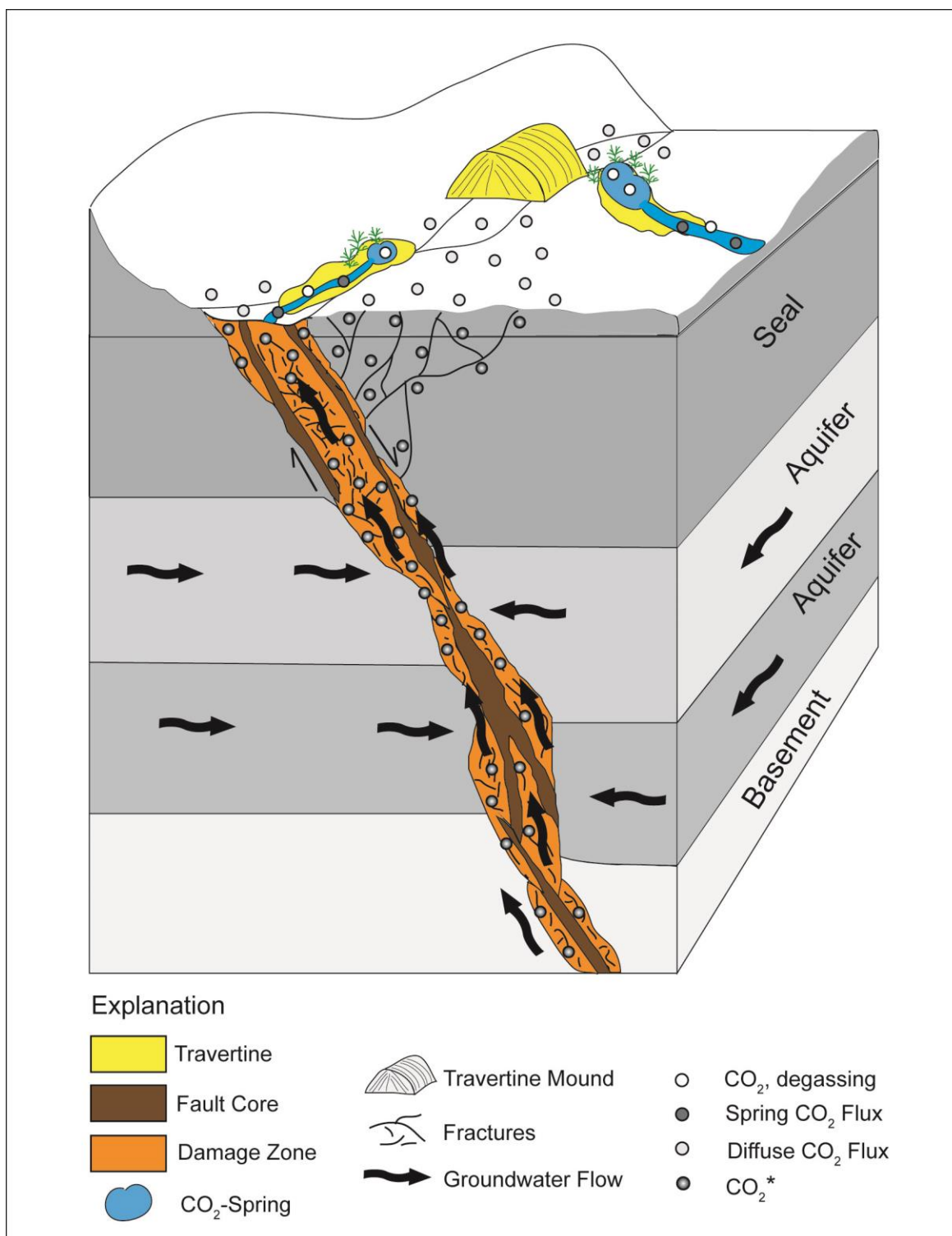


Figure 3.8. Conceptual model of CO₂ leakage along a fault system and seal bypass. Fault architectural elements, e. g. fault core and damage zone, are shown and different manifestations of CO₂ leakage: CO₂ degassing from groundwater into the atmosphere, CO₂ fixed in travertine, spring CO₂ flux, and diffuse CO₂ flux. See text for explanation. CO₂* represents both CO₂ dissolved in groundwater and CO₂ in the gas phase.

fluxes are equally high with amounts varying between 9×10^7 mol/yr and 1×10^{10} mol/yr (Table 3.3). Degassing of CO₂ through the soil also contributes to considerable CO₂ leakage. CO₂ flux surveys along the Little Grand Wash Fault in Utah carried out by Allis et al. (2005) and Han et al. (2013) show CO₂ fluxes from 25 to > 700 g/m²/day and 0-1600 g/m²/day, respectively, and Lewicki et al. (2013) report CO₂ fluxes from 1 to 52,178 g/m²/day from Soda Springs in Idaho.

Integrated CO₂ leakage accounts for all of the different manifestations of CO₂ leakage along faults and is, therefore, a better estimate of CO₂ leakage. A comparison between the total amounts of CO₂ and the integrated amounts of CO₂, which range from ~0.5 Gt to 2.2 Gt and 5 Gt to 54 Gt, respectively, shows that the integrated amount of leaked CO₂ is about 10 to 20 times higher than the amount based on travertine volume alone (Table 3.5). Because travertine formation and, consequently, CO₂ leakage occurred episodically, the amounts of total and integrated episodic CO₂ leakage were also calculated: they vary between 1,000 t to 10,667 t and 4 Gt to 24 Gt (Table 3.6), respectively, showing an even more dramatic increase by many orders of magnitude which emphasize the significance of integrated CO₂ leakage.

For comparison, Burnside et al. (2013) estimate that a total of 14.4 Mt CO₂ over 114 ka and 10.7 Mt CO₂ over 413 ka leaked along the Little Grand Wash Fault and the Salt Wash Graben in Utah, respectively. Their calculations are solely based on travertine volumes which amount to 107,510 m³ along the Little Grand Wash Fault and to 79,809 m³ along the Salt Wash Graben and are much smaller than the volumes of the travertine deposits in New Mexico and Arizona (Table 3.1). Because of the smaller travertine volumes and because neither spring CO₂ flux nor diffuse CO₂ flux were taken into account, the calculated CO₂ leakage along the two fault systems in Utah is much smaller than integrated CO₂ leakage calculated in this study (Fig. 3.9).

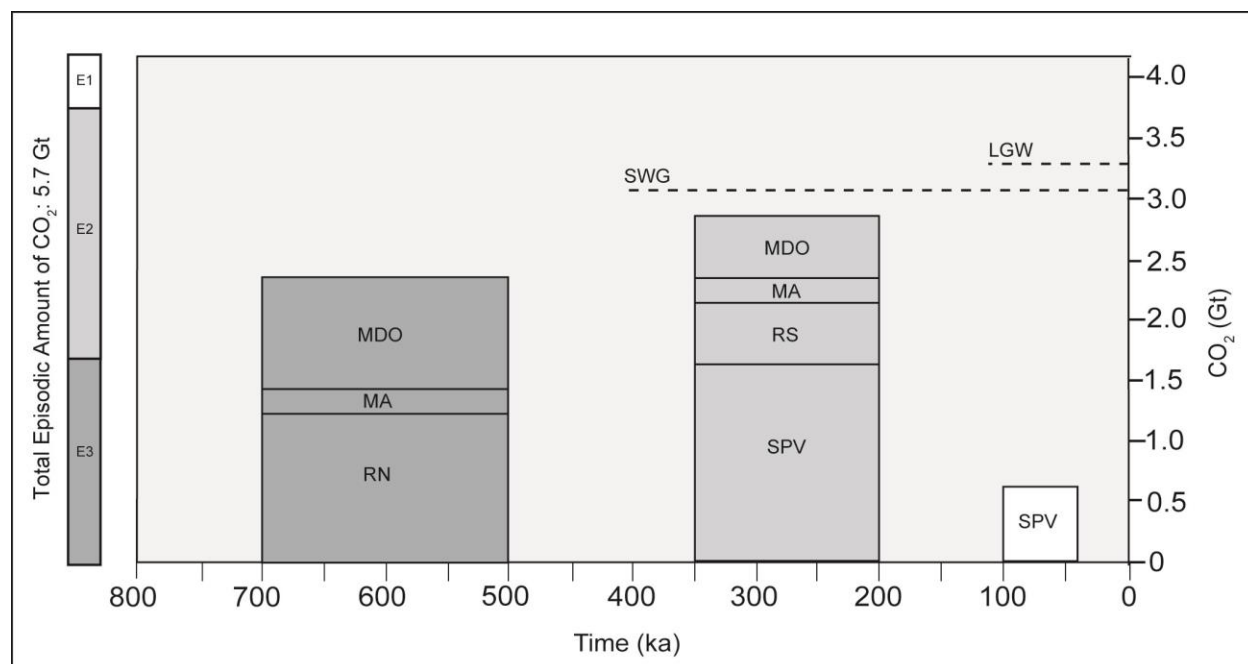


Figure 3.9. Diagram showing episodic CO₂ leakage for the study areas in New Mexico and Arizona: Mesa del Oro (MDO), Mesa Aparejo (MA), Riley North Mesa (RN), Riley South Mesa (RS), and Springerville (SPV). Episodes of travertine formation are color-coded and labeled: E1 = episode 1 (100-40 ka), E2 = episode 2 (350-200 ka), E3 = episode 3 (700-500 ka). Episodic amounts of CO₂ from New Mexico and Arizona are represented by the scale bar: individual volumes add up to 5.7 Gt (Table 2). For comparison, calculated amounts of CO₂ leakage from Utah (dashed lines) according to Burnside et al. (2013) are shown: 14.4 Mt (= 0.014 Gt) CO₂ leaked over 114 ka along the Little Grand Wash Fault (LGW), and 10.7 Mt (= 0.01 Gt) CO₂ leaked over 413 ka along the Salt Wash Graben (SWG).

Furthermore, Burnside et al. (2013) assume that the calculated 14.4 Mt and 10.7 Mt of CO₂ represent only 1% of leaked CO₂ that became fixed in travertine (= efficiency of CO₂ leakage) while 99% degassed into the atmosphere or were retained in solution. Considering the large amounts of travertine that precipitated in New Mexico and Arizona, a 1% efficiency of CO₂ leakage appears to be very small while an estimate of 50% efficiency assumed for the calculations in this study can be considered relatively large. Therefore, it might be more realistic to assume values between 5% and 10% total efficiency of CO₂ leakage and these amounts range from 12.2 Gt to 54.9 Gt and from 2.4 Gt to 11 Gt, respectively, for the total efficiency of CO₂

leakage which corresponds to the calculations by Burnside et al. (2013). The integrated efficiency of CO₂ leakage for 5% and 10% gives values that range from 265.1 Gt to 2702.8 Gt and from 53 Gt to 540.6 Gt (Table 3.7).

Table 3.7: Efficiency of CO₂ Leakage

Location	Age of Deposit* (yrs)	Efficiency of Leaked CO ₂ (Total**)			
		50% Fixed CO ₂ (Gt)	10% Fixed CO ₂ (Gt)	5% Fixed CO ₂ (Gt)	1% Fixed CO ₂ (Gt)
Mesa del Oro	312,950	1.71	8.5	42.7	85.5
Mesa Aparejo	455,819	0.49	2.4	12.2	24.4
Riley North Mesa	370,000	1.22	6.1	30.5	61.1
Riley South Mesa	149,450	0.49	2.4	12.2	24.4
Springerville	318,317	2.20	11.0	54.9	109.9

(continued)

Location	Efficiency of Leaked CO ₂ (Integrated***)			
	50% Fixed CO ₂	10% Fixed	5% Fixed	1% Fixed
Mesa del Oro	46.4	231.8	1158.8	2317.5
Mesa Aparejo	108.1	540.6	2702.8	5405.5
Riley North Mesa	47.3	236.5	1182.6	2365.2
Riley South Mesa	10.6	53.0	265.1	530.1
Springerville	43.2	216.0	1080.1	2160.2

See Table DR12 for detailed calculations

*For detailed U-series and model ages see Priewisch et al. (2014)

**based on total amount of CO₂

***based on integrated amount of CO₂

An integrated approach to quantifying integrated CO₂ leakage is extremely important in assessing long-term storage of CO₂ in geologic media. Globally, depleted oil and gas reservoirs, deep saline formations, and unminable coal seams are estimated to have storage capacities of 675-900 Gt CO₂, 1000 Gt CO₂, and 3-200 Gt CO₂, respectively (IPCC, 2005). It is interesting to compare these storage capacities to integrated episodic CO₂ fluxes and integrated efficiencies of CO₂ leakage between 5% and 10% (Tables 3.6 and 3.7). For example, 1000 Gt CO₂ stored globally in deep saline formations could theoretically leak back to the surface along fault systems

over a period of ~42 years assuming an episodic CO₂ flux of 24 Gt/yr (Table 3.6) and most results of the integrated efficiencies of CO₂ leakage between 5% and 10% exceed global storage capacities (Table 3.7). Integrated CO₂ leakage also has the potential to compromise efforts to reduce CO₂ emissions as suggested by Pacala and Socolow (2004). They introduce a model to reduce CO₂ emissions until 2055 based on 7 stabilization wedges where each wedge is an activity that saves ~3 Gt CO₂/yr of emissions, CO₂ sequestration being one of them. It is noteworthy that all of the integrated episodic CO₂ fluxes and efficiencies of CO₂ leakage calculated in this study are larger than 3 Gt CO₂.

CONCLUSIONS

The accumulation of large-volume travertine deposits on the Colorado Plateau and along the Rio Grande rift attest to extensive CO₂ leakage from ancient CO₂ reservoirs. Travertine volumes are used to calculate total CO₂ leakage which comprises CO₂ fixed in travertine and CO₂ that degassed into the atmosphere. However, a more realistic estimate is integrated CO₂ leakage because the calculation includes spring CO₂ flux and diffuse CO₂ flux in addition to total CO₂ flux. Episodic integrated CO₂ leakage takes into account that travertine formation and hence CO₂ leakage occurred episodically. Total CO₂ leakage ranges from ~0.5 Gt to 2.2 Gt whereas integrated total CO₂ leakage varies between 5 Gt to 54 Gt which is about 10 to 20 times higher than the amount based on travertine volume alone. Total and integrated episodic CO₂ leakage were calculated with 1,000 t to 10,667 t and 4 Gt to 24 Gt, respectively, showing a dramatic increase by many orders of magnitude which emphasizes the significance of integrated CO₂ leakage. CO₂ leakage occurred along fault systems which served as conduits for groundwater and deeply-derived CO₂. Some faults bypassed regional shale seals on the Colorado Plateau and in the Rio Grande rift. Fault systems have been responsible for very large amounts of CO₂ leakage,

and not only as a one-time-event but repeatedly over geologic time scales. In order to assess the risk of CO₂ leakage it is crucial to meticulously evaluate fault systems in or close to potential CO₂ sequestration sites because episodic integrated CO₂ leakage has the potential to compromise global storage capacities and attempts to reduce CO₂ emissions.

ACKNOWLEDGEMENTS

Funding for this research was provided by the Association of American Petroleum Geologists Grants-In-Aid, by the New Mexico Geological Society Grants-In-Aid, and by National Science Foundation (NSF) EAR-0838575 (to Crossey).

REFERENCES

- Akers, J., 1964, Geology and ground water in the central part of Apache County, Arizona: Geological Survey Water-Supply Paper 1771, 116 p.
- Aldrich, M.J., 1986, Tectonics of the Jemez lineament in the Jemez Mountains and Rio Grande rift: *Journal of Geophysical Research*, v. 91, no. B2, p. 1753–1762.
- Allis, R., Bergfeld, D., Moore, J., McClure, K., Chidsey, T., Heath, J., and Mcpherson, B., 2005, Implications of results from CO₂ flux surveys over known CO₂ systems for long-term monitoring, *in* Fourth Annual Conference on Carbon Capture & Sequestration, Alexandria, Virginia, p. 1–22.
- Aydin, A., 2000, Fractures, faults, and hydrocarbon entrapment, migration and flow: *Marine and Petroleum Geology*, v. 17, p. 797–814.
- Bachu, S., 2008, CO₂ storage in geological media: Role, means, status and barriers to deployment: *Progress in Energy and Combustion Science*, v. 34, p. 254–273, doi: 10.1016/j.pecs.2007.10.001.
- Baldwin, J.A., and Anderholm, S.K., 1992, Hydrogeology and ground-water chemistry of the San Andres-Glorieta aquifer in the Acoma embayment and eastern Zuni uplift, west-central New Mexico: U.S. Geological Survey Water-Resources Investigations Report 91-4033, 302 p.
- Baldwin, J.A., and Rankin, D.R., 1995, Hydrogeology of Cibola County, New Mexico: U.S. Geological Survey Water-Resources Investigations Report 94-4178, 122 p.

- Ballentine, C.J., and Sherwood Lollar, B., 2002, Regional groundwater focusing of nitrogen and noble gases into the Hugoton-Panhandle giant gas field, USA: *Geochimica et Cosmochimica Acta*, v. 66, no. 14, p. 2483–2497.
- Barker, J.M., Austin, G.S., and Sivils, D.J., 1996, Travertine in New Mexico - Commercial deposits and otherwise: *New Mexico Bureau of Mines and Mineral Resources Bulletin*, v. 154, p. 73–92.
- Benson, S.M., and Cole, D.R., 2008, CO₂ Sequestration in Deep Sedimentary Formations: *Elements*, v. 4, p. 325–331, doi: 10.2113/gselements.4.5.325.
- Burnside, N.M., 2010, U-Th dating of travertine on the Colorado Plateau : Implications for the leakage of geologically stored CO₂ [Ph.D. thesis]: Glasgow, University of Glasgow, 290 p.
- Burnside, N.M., Shipton, Z.K., Dockrill, B., and Ellam, R.M., 2013, Man-made versus natural CO₂ leakage: A 400 k.y. history of an analogue for engineered geological storage of CO₂: *Geology*, v. 41, no. 4, p. 471–474, doi: 10.1130/G33738.1.
- Caine, J.S., Evans, J.P., and Forster, C.B., 1996, Fault zone architecture and permeability structure: *Geology*, v. 24, p. 1025–1028, doi: 10.1130/0091-7613(1996)024<1025.
- Caine, J.S., and Forster, C.B., 1999, Fault zone architecture and fluid flow: Insights from field data and numerical modeling, *in* Haneberg, W.C., Mozley, P.S., Moore, J.C., and Goodwin, L.B. eds., *Faults and Subsurface Fluid Flow in the Shallow Crust*, Geophysical Monograph 113, p. 101–127.
- Cartwright, J., Huuse, M., and Aplin, A., 2007, Seal bypass systems: *AAPG Bulletin*, v. 91, no. 8, p. 1141–1166, doi: 10.1306/04090705181.
- Cather, S.M., 2004, Laramide orogeny in central and northern New Mexico and southern Colorado, *in* Mack, G.H. and Giles, K.A. eds., *The Geology of New Mexico*, New Mexico Geological Society Special Publication 11, p. 203–248.
- Cather, S.M., and Read, A.S., 2003, Preliminary Geologic Map of the Silver Creek 7.5-min quadrangle: *New Mexico Bureau of Geology and Mineral Resources*, scale 1:24 017, 1 sheet.
- Chamberlin, R.M., 2007, Evolution of the Jemez lineament: connecting the volcanic “dots” through late cenozoic time: *New Mexico Geological Society Guidebook*, 58th Field Conference, p. 80–82.
- Chiodini, G., Frondini, F., Cardellini, C., Parello, F., and Peruzzi, L., 2000, Rate of diffuse carbon dioxide Earth degassing estimated from carbon balance of regional aquifers: The case of central Apennine, Italy: *Journal of Geophysical Research*, v. 105, no. B4, p. 8423–8434.

- Connell, S.D., 2008, Geologic map of the Albuquerque-Rio Rancho metropolitan area and vicinity, Bernalillo and Sandoval Counties, New Mexico: New Mexico Bureau of Geology and Mineral Resources, scale 1:50,000.
- Crossey, L.J., Fischer, T.P., Patchett, P.J., Karlstrom, K.E., Hilton, D.R., Newell, D.L., Huntoon, P., Reynolds, A.C., and de Leeuw, G.A.M., 2006, Dissected hydrologic system at the Grand Canyon: Interaction between deeply derived fluids and plateau aquifer waters in modern springs and travertine: *Geology*, v. 34, no. 1, p. 25–28, doi: 10.1130/G22057.1.
- Crossey, L.J., Karlstrom, K.E., Springer, A.E., Newell, D., Hilton, D.R., and Fischer, T., 2009, Degassing of mantle-derived CO₂ and He from springs in the southern Colorado Plateau region-Neotectonic connections and implications for groundwater systems: *Geological Society of America Bulletin*, v. 121, no. 7-8, p. 1034–1053, doi: 10.1130/B26394.1.
- Davies, R.K., and Handschy, J.W., 2003, Introduction to AAPG Bulletin thematic issue on fault seals: *AAPG Bulletin*, v. 87, no. 3, p. 377–380, doi: 10.1306/00000001136.
- Dockrill, B., 2005, Understanding leakage from a fault-sealed CO₂ reservoir in east-central Utah: a natural analogue applicable to CO₂ storage [Ph.D. thesis]: Dublin, University of Dublin, 165 p.
- Downey, M.W., 1984, Evaluating seals for hydrocarbon accumulations: *The American Association of Petroleum Geologists*, v. 68, no. 11, p. 1752–1763.
- Dunbar, N., 2005, Quaternary volcanism in New Mexico: *New Mexico Museum of Natural History and Science Bulletin*, v. 28, p. 95–106.
- Embid, E.H., 2009, U-Series dating, geochemistry, and geomorphic studies of travertines and springs of the Springerville Area, east-central Arizona, and tectonic implications [M.S. thesis]: Albuquerque, University of New Mexico, 103 p.
- Faulkner, D.R., Jackson, C. a. L., Lunn, R.J., Schlische, R.W., Shipton, Z.K., Wibberley, C. a. J., and Withjack, M.O., 2010, A review of recent developments concerning the structure, mechanics and fluid flow properties of fault zones: *Journal of Structural Geology*, v. 32, p. 1557–1575, doi: 10.1016/j.jsg.2010.06.009.
- Feth, J.H., and Barnes, I., 1979, Spring-deposited travertine in eleven western states: *Geological Survey Water-Resources Investigations 79-85 Open-File Report*.
- Gale, J., 2004, Why do we need to consider geological storage of CO₂?, *in* Baines, S.J. and Worden, R.H. eds., *Geological Storage of Carbon Dioxide*, Geological Society, London, Special Publication 233, p. 7–15.
- Goff, F., McCormick, T., Gardner, J.N., Trujillo, P.E., Counce, D., Vidale, R., and Charles, R., 1983, Water geochemistry of the Lucero uplift, New Mexico: A geothermal investigation of

- low-temperature mineralized fluids: Los Alamos National Laboratory LA-9738-OBES, 26 p.
- Goodwin, L.B., Mozley, P.S., Moore, J.C., and Haneberg, W.C., 1999, Introduction, *in* Haneberg, W.C., Mozley, P.S., Moore, J.C., and Goodwin, L.B. eds., *Faults and Subsurface Fluid Flow in the Shallow Crust*, Geophysical Monograph 113, p. 1–4.
- Han, W.S., Lu, M., McPherson, B.J., Keating, E.H., Moore, J., Park, E., Watson, Z.T., and Jung, N.-H., 2013, Characteristics of CO₂-driven cold-water geyser, Crystal Geyser in Utah: experimental observation and mechanism analyses: *Geofluids*, v. 13, p. 283–297.
- Hepple, R.P., and Benson, S.M., 2004, Geologic storage of carbon dioxide as a climate change mitigation strategy: performance requirements and the implications of surface seepage: *Environmental Geology*, v. 47, no. 4, p. 576–585, doi: 10.1007/s00254-004-1181-2.
- Holloway, S., 2001, Storage of fossil fuel-derived carbon dioxide beneath the surface of the Earth: *Annual Review of Energy and the Environment*, v. 26, p. 145–166.
- IPCC, 2013, *Climate Change 2013: The Physical Science Basis. Contribution of Working Group I to the Fifth Assessment Report of the Intergovernmental Panel on Climate Change* (T. F. Stocker, D. Qin, G.-K. Plattner, M. Tignor, S. K. Allen, J. Boschung, A. Nauels, Y. Xia, V. Bex, & P. M. Midgley, Eds.): Cambridge University Press, Cambridge, United Kingdom and New York, NY, USA, 1535 p.
- IPCC, 2005, *IPCC Special Report on Carbon Dioxide Capture and Storage*. Prepared by Working Group III of the Intergovernmental Panel on Climate Change (B. Metz, O. Davidson, H. de Coninck, M. Loos, & L. Meyer, Eds.): Cambridge University Press, Cambridge, United Kingdom and New York, NY, USA, 442 p.
- James, E.R., Manga, M., and Rose, T.P., 1999, CO₂ degassing in the Oregon Cascades: *Geology*, v. 27, p. 823–826, doi: 10.1130/0091-7613(1999)027<0823.
- Jicha, H., 1958, *Geology and mineral resources of Mesa del Oro Quadrangle, Socorro and Valencia Counties, New Mexico*: State Bureau of Mines and Mineral Resources Bulletin, v. 56, p. 1–67.
- Kampman, N., Burnside, N.M., Shipton, Z.K., Chapman, H.J., Nicholl, J. a., Ellam, R.M., and Bickle, M.J., 2012, Pulses of carbon dioxide emissions from intracrustal faults following climatic warming: *Nature Geoscience*, v. 5, no. 5, p. 352–358, doi: 10.1038/ngeo1451.
- Karlstrom, K.E., Crossey, L.J., Hilton, D.R., and Barry, P.H., 2013, Mantle 3He and CO₂ degassing in carbonic and geothermal springs of Colorado and implications for neotectonics of the Rocky Mountains: *Geology*, v. 41, p. 495–498, doi: 10.1130/G34007.1.
- Keller, G.R., and Baldrige, W.S., 1999, The Rio Grande rift A geological and geophysical overview: *Rocky Mountain Geology*, v. 34, no. 1, p. 121–130.

- Kharaka, Y.K., Thordsen, J.J., Kakouros, E., Ambats, G., Herkelrath, W.N., Beers, S.R., Birkholzer, J.T., Apps, J.A., Spycher, N.F., Zheng, L., Trautz, R.C., Rauch, H.W., and Gullickson, K.S., 2010, Changes in the chemistry of shallow groundwater related to the 2008 injection of CO₂ at the ZERT field site, Bozeman, Montana: *Environmental Earth Sciences*, v. 60, p. 273–284, doi: 10.1007/s12665-009-0401-1.
- Lewicki, J.L., Hilley, G.E., Dobeck, L., Mcling, T.L., Kennedy, B.M., Bill, M., and Marino, B.D. V, 2013, Geologic CO₂ input into groundwater and the atmosphere, Soda Springs, ID, USA: *Chemical Geology*, v. 339, p. 61–70, doi: 10.1016/j.chemgeo.2012.06.013.
- Lewis, C., and Baldrige, W., 1994, Crustal extension in the Rio Grande rift, New Mexico: Half-grabens, accommodation zones, and shoulder uplifts in the Ladron Peak-Sierra Lucero area: *Geological Society of America Special Paper*, v. 291, p. 135–155.
- Minissale, A., Kerrick, D.M., Magro, G., Murrell, M.T., Paladini, M., Rihs, S., Sturchio, N.C., Tassi, F., and Vaselli, O., 2002, Geochemistry of Quaternary travertines in the region north of Rome (Italy): structural, hydrologic and paleoclimatic implications: *Earth and Planetary Science Letters*, v. 203, p. 709–728.
- Minor, S.A., Hudson, M.R., Cain, J.S., and Thompson, R.A., 2013, Oblique transfer of extensional strain between basins of the middle Rio Grande rift, New Mexico: Fault kinematic and paleostress constraints, *in* Hudson, M.R. and Grauch, V.J.S. (Tien) eds., *New Perspectives on Rio Grande Basins: From Tectonics to Groundwater*, The Geological Society of America Special Paper 494, p. 345–382.
- Moore, J., Adams, M., Allis, R., Lutz, S., and Rauzi, S., 2005, Mineralogical and geochemical consequences of the long-term presence of CO₂ in natural reservoirs: An example from the Springerville–St. Johns Field, Arizona, and New Mexico, U.S.A.: *Chemical Geology*, v. 217, p. 365–385, doi: 10.1016/j.chemgeo.2004.12.019.
- Newell, D.L., Crossey, L.J., Karlstrom, K.E., Fischer, T.P., and Hilton, D.R., 2005, Continental-scale links between the mantle and groundwater systems of the western United States: Evidence from travertine springs and regional He isotope data: *GSA Today*, v. 15, no. 12, p. 4–10.
- Osburn, G.R., 1984, *Geology of Socorro County: New Mexico Bureau of Geology and Mineral Resources*, Open-File Report 238, 13 p.
- Pacala, S., and Socolow, R., 2004, Stabilization wedges: solving the climate problem for the next 50 years with current technologies.: *Science*, v. 305, p. 968–972, doi: 10.1126/science.1100103.
- Pentecost, A., 2005, *Travertine: Springer Verlag Berlin Heidelberg*, 445 p.
- Priewisch, A., Crossey, L.J., Karlstrom, K.E., Polyak, V.J., Asmerom, Y., Nereson, A., and Ricketts, J.W., 2014, U-series geochronology of large-volume Quaternary travertine

- deposits of the southeastern Colorado Plateau: Evaluating episodicity and tectonic and paleohydrologic controls: *Geosphere*, v. 10, no. 2, doi: 10.1130/GES00946.1.
- Rauzi, S.L., 1999, Carbon Dioxide in the St. Johns - Springerville Area, Apache County, Arizona: Arizona Geological Survey, Open-File Report 99-2, 24 p.
- Rawling, G.C., Goodwin, L.B., and Wilson, J.L., 2001, Internal architecture , permeability structure , and hydrologic significance of contrasting fault-zone types: *Geology*, v. 29, p. 43–46, doi: 10.1130/0091-7613(2001)029<0043.
- Ricketts, J.W., and Karlstrom, K.E., 2011, Geologic Map of the Western Boundary of the Rio Grande rift - South Garcia SE and Mesas Mojinas Quadrangles, central New Mexico: New Mexico Bureau of Geology and Mineral Resources, scale 1:12 000, 1 sheet.
- Ricketts, J.W., Karlstrom, K.E., Priewisch, A., Crossey, L.J., Polyak, V.J., and Asmerom, Y., 2014, Quaternary extension in the Rio Grande rift at elevated strain rates recorded in travertine deposits, central New Mexico: *Lithosphere*, v. 6, no. 1, p. 3–16, doi: 10.1130/L278.1.
- Seager, W., 2004, Laramide (Late Cretaceous-Eocene) tectonics of southwestern New Mexico, *in* Mack, G.H. and Giles, K.A. eds., *The Geology of New Mexico*, New Mexico Geological Society Special Publication 11, p. 183–202.
- Shipton, Z.K., Evans, J.P., Dockrill, B., Heath, J., Williams, A., Kirchner, D., and Kolesar, P.T., 2005, Natural leaking CO₂-charged systems as analogs for failed geologic storage reservoirs, *in* Thomas, D.C. and Benson, S.M. ed., *Carbon Dioxide Capture for Storage in Deep Geologic Formations*, Volume 2, Elsevier Ltd., p. 699–712.
- Shipton, Z.K., Evans, J.P., Kirchner, D., Kolesar, P.T., Williams, A.P., and Heath, J., 2004, Analysis of CO₂ leakage through “low-permeability” faults from natural reservoirs in the Colorado Plateau, east-central Utah, *in* Baines, S.J. and Worden, R.H. eds., *Geological Storage of Carbon Dioxide*, Geological Society London Special Publication 233, p. 43–58.
- Sibson, R.H., Moore, J.M., and Rankin, A.H., 1975, Seismic pumping-a hydrothermal fluid transport mechanism: *Journal of the Geological Society*, v. 131, p. 653–659, doi: 10.1144/gsjgs.131.6.0653.
- Uysal, I.T., Feng, Y. -x., Zhao, J. -x., Isik, V., Nuriel, P., and Golding, S.D., 2009, Hydrothermal CO₂ degassing in seismically active zones during the late Quaternary: *Chemical Geology*, v. 265, p. 442–454, doi: 10.1016/j.chemgeo.2009.05.011.
- Williams, A.J., Crossey, L.J., Karlstrom, K.E., Newell, D., Person, M., and Woolsey, E., 2013, Hydrogeochemistry of the Middle Rio Grande aquifer system — Fluid mixing and salinization of the Rio Grande due to fault inputs: *Chemical Geology*, v. 351, p. 281–298, doi: 10.1016/j.chemgeo.2013.05.029.

Wright, H.E., 1946, Tertiary and Quaternary geology of the lower Rio Puerco area, New Mexico: Geological Society of America Bulletin, v. 57, no. 5, p. 383–456, doi: 10.1130/0016-7606(1946)57.

CHAPTER 4

Geochemical Analysis of Quaternary Travertine Deposits on the southeastern Colorado Plateau: Evaluation of Travertine Facies for Paleohydrology and Paleoenvironment Studies

CHAPTER ABSTRACT

Quaternary large-volume travertine deposits in New Mexico and Arizona occur along the margins of the Rio Grande rift and on the southwestern Colorado Plateau. Three travertine depositional facies are identified based on sedimentary textures and petrologic features: step-pool facies, paludal facies, and vein facies. U-series dating shows that large volumes (2.5 km³) of travertine accumulated episodically at times also associated with increased volcanism, and times where other climate proxies indicate a likelihood of increased recharge leading to high hydraulic head in confined aquifer systems. Paleohydrology controls depositional environments of the travertines and thus travertine facies such as step-pool, paludal, and vein facies. We apply geochemical tracers including stable isotopes and trace elements to compare travertine locations as well as facies. Stable oxygen and carbon isotope analyses overlap substantially exhibiting $\delta^{18}\text{O}_c$ values that range between -14‰ and -3.8‰, and $\delta^{13}\text{C}$ values that range from -4.9‰ to 9.8‰. The range of $\delta^{18}\text{O}_c$ values is interpreted to reflect groundwater mixing and mixing of groundwater with meteoric water, whereas high $\delta^{13}\text{C}$ values are predominantly controlled by the CO₂ degassing rate. Results of minor and trace element analyses show similar trends throughout the region but distinct differences between facies. The vein facies exhibits high concentrations of minor and trace elements such as Mg, Na, Ni, and Sr, whereas the step-pool facies has the highest concentrations in Al, B, Fe, and Si. Very low Ca/Mg ratios indicate high discharge and

short residence times of groundwater during wet times which is also reflected by very low concentrations of rare earth elements (REE). Modeling of past groundwater temperatures allows an evaluation of the hydrologic conditions at the time of travertine formation. If the travertine facies can be unambiguously distinguished in the rock record, stable isotope and trace element results of analyzed samples can be used for paleoenvironmental interpretation.

INTRODUCTION

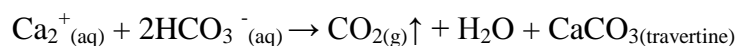
Travertines are groundwater discharge deposits that occur at many localities in the United States (Feth and Barnes, 1979; Ford and Pedley, 1996) and they are exceptional diagnostic tools for paleoenvironmental studies. Composed dominantly of the mineral calcite, travertines are datable with the precise U-series method, and their isotopic and elemental compositions provide a rich geochemical record that can be used to model paleohydrology and paleoclimate (Minissale et al., 2002a; Smith et al., 2004; Andrews, 2006; Anzalone et al., 2007; Faccenna et al., 2008; Crossey et al., 2011; Kampman et al., 2012; Özkul et al., 2014). Stable oxygen isotopes of travertines can be used to evaluate the hydrologic conditions at the time of travertine deposition, i.e. water temperature and water composition, and terrestrial temperatures and precipitation patterns, whereas stable carbon isotopes elucidate the origin of the CO₂ involved in travertine formation and CO₂ degassing rates. (Andrews et al., 2000; Kele et al., 2008, 2011; Demeny et al., 2010; Özkul et al., 2014). Travertine formation is characterized by dynamic processes which result in both a variety of depositional environments and travertine facies (Chafetz and Folk, 1984; Pedley, 1990, 2009; Pentecost and Viles, 1994; Guo and Riding, 1998, 1999; Glover and Robertson, 2003; Pentecost, 2005; Jones and Renaut, 2010; Özkul et al., 2014). Various researchers used stable oxygen isotopes of fossil and modern travertines to calculate water temperatures and their results show that the depositional travertine facies have a strong impact on

the stable isotopic composition which needs to be carefully addressed when fossil travertines are used for high-resolution paleoclimate reconstructions (Anzalone et al., 2007; Kele et al., 2011; Yan et al., 2012; Sun et al., 2014; Wang et al., 2014). Trace element analysis of travertines can be used to determine water temperatures, aquifer processes, and the origin of the water and allow elucidating groundwater flow paths and climate change (Ihlenfeld et al., 2003; Garnett et al., 2004; Uysal et al., 2007; Kele et al., 2011; Kampman et al., 2012).

In this study multiple geochemical tracers are used to 1) characterize different travertine facies, 2) model past water temperatures and water compositions, and 3) evaluate the use of fossil travertines for paleohydrology and paleoclimate studies.

TRAVERTINE AND TRAVERTINE FORMATION

In this study, the term “travertine” is used for chemically-precipitated continental limestone that forms at springs and in streams (Ford and Pedley, 1996; Pentecost, 2005). The fresh-water carbonate deposits form due to the degassing of CO₂ from groundwater that is supersaturated with respect to calcium carbonate according to the following reactions (Pentecost, 2005; Crossey et al., 2006, 2009):



Travertine accumulations represent places of persistent and significant mantle CO₂ degassing in high discharge spring systems along faults that serve as conduits for deep-circulating waters and CO₂ and modern travertine-depositing springs indicate that part of the CO₂ is derived from the mantle, according to carbon isotope and ³He/⁴He ratios (Hancock et al., 1999; (Minissale et al., 2002b, 2005; Ballentine and Sherwood Lollar, 2002; Newell et al., 2005; Crossey et al., 2006, 2009; Embid, 2009; Karlstrom et al., 2013; Williams et al., 2013). The

spring waters represent mixtures of hydrologic flow systems, including meteoric recharge, groundwater with long residence times, and deeply-derived fluids (Newell et al., 2005; Crossey et al., 2006, 2009; Embid, 2009; Williams et al., 2013). U-series ages of travertine samples show that large volume of travertine accumulated episodically at 700-500 ka, 300-250 ka, and 100-40 ka when hydraulic head was high and when regional volcanic activity contributed excess magmatic/mantle-derived CO₂ to the system (Priewisch et al., 2014). For a more detailed description of travertine formation in the region see Priewisch et al. (2014).

Geologic setting of the study areas

This section gives an overview of the geologic setting of the study areas; see Priewisch et al. (2014) for additional information.

Large-volume travertine deposits (0.2-0.9 km³) in New Mexico and Arizona are located along the Rio Grande rift and the Jemez lineament (Fig. 4.1). The Rio Grande rift is a series of north-south-trending sedimentary basins which extend over 1000 km from Colorado to Mexico and it is bounded by complex fault systems (e.g. Keller and Baldrige, 1999; Cather, 2004; Seager, 2004; Minor et al., 2013). The Jemez lineament is a prominent northeast-trending belt of Cenozoic volcanic fields that cut across the southwestern Colorado Plateau (Aldrich, 1986; Dunbar, 2005; Chamberlin, 2007). The study areas in New Mexico and Arizona host large travertine platforms that range from ~4 m to 25 m in thickness which are interpreted to be both extinct and still active CO₂ reservoirs, respectively (Embid, 2009; Priewisch et al., 2014).

METHODS

Facies Analysis

Travertine samples were collected at representative exposures throughout the study areas and the field sampling was complemented by detailed mapping of the travertine deposits and

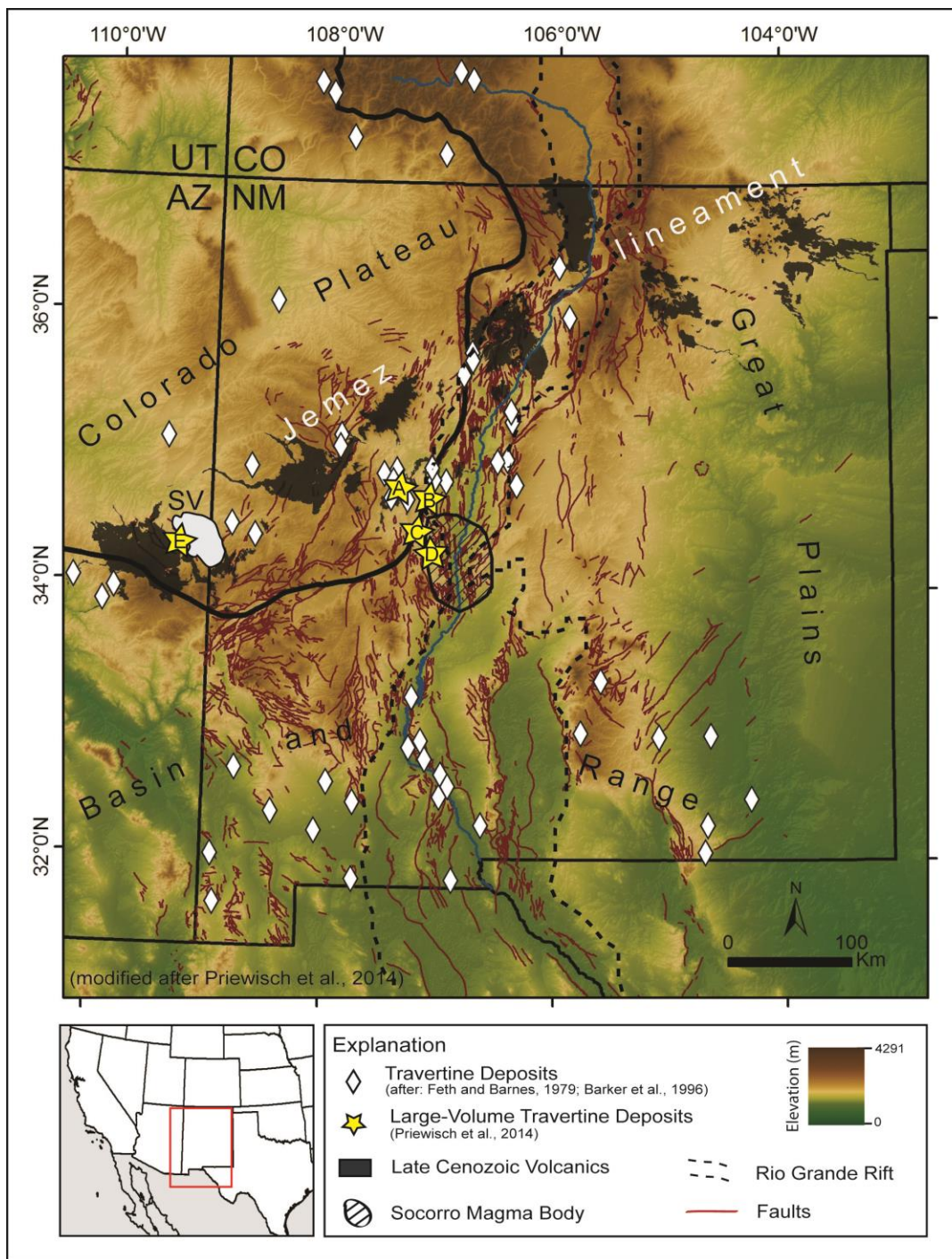


Figure 4.1. Map showing locations of travertine accumulations (Feth and Barnes, 1979; Barker et al., 1996), large-volume travertine deposits (Prewisch et al., 2014), the Rio Grande rift, and Jemez lineament. Also shown are the three physiographic provinces Colorado Plateau, Great Plains, and Basin and Range. Study areas in New Mexico are Mesa del Oro (A), Mesa Aparejo (B), Riley North Mesa (C), and Riley South Mesa (D). The study area in Arizona is Springerville (E), where the travertine deposits are associated with and active CO₂-gas field (SV).

compilation of stratigraphic travertine sections (Priewisch et al., 2014). Hand specimens were cut into slabs and petrographic analysis was used to evaluate different travertine facies and depositional environments.

Stable Isotope Analysis

Powdered samples were drilled from sparry and micritic calcite layers in travertine slabs. Between 0.5 mg and 1 mg of travertine powder were loaded in 12 mL borosilicate containers and flushed with helium and reacted with phosphoric acid at 50°C for 24 hours. The evolved CO₂ was measured with a continuous flow Finnigan Mat Delta Plus Isotope Ratio Mass Spectrometer coupled to a Gasbench device. Results are reported in per mil (‰) using the delta notation versus PDB. Reproducibility is better than 0.15‰ for both δ¹³C and δ¹⁸O based on repeated measurements of a laboratory standard (Carrara Marble). The standard is calibrated versus NBS 19, for which the δ¹³C is 1.95‰ and δ¹⁸O is 2.2‰. The samples were measured in the Center for Stable Isotopes, College of Arts & Sciences, University of New Mexico using the method described by Spötl and Vennemann (2003).

Trace Element Analysis

Minor and trace elements of the carbonate fraction of the travertine samples were analyzed, including rare earth elements (REE). Between 0.1 g and 0.3 g of powdered sample were digested in 1 ml 50% nitric acid and fluxed for one hour at 95°C. The solution was filtered into 25 ml glass flasks and brought to volume with 18 MΩ water. This sample preparation was chosen in order to avoid leaching of non-carbonate detrital material that might have been present in the travertine. Six ml of the solution were used to measure selected minor and trace elements using a Perkin-Elmer Optima 5300DV ICP-OES (Inductively Coupled Plasma Optical Emission Spectrometer). Elements below the detection limit were measured again using a Perkin-Elmer

Nexion 300D (Inductively Coupled Plasma Mass Spectrometer). In order to analyze REE, 0.5 g of sample powder was digested in 3 ml ultrapure (70%) nitric acid and 1.5 ml concentrated (48%) hydrofluoric acid and fluxed for 3 hours at 95°C. The solution was filtered into plastic tubes and brought to a volume of 10 ml with 18 M Ω water. The aliquots were analyzed using a Perkin-Elmer Nexion 300D (Inductively Coupled Plasma Mass Spectrometer). The samples were measured in the Analytical Chemistry Laboratory, Department of Earth and Planetary Sciences, University of New Mexico.

RESULTS

Travertine Facies and their Depositional Environment

Based on field relationships and petrographic analysis of approximately 200 travertine samples, three different travertine facies were identified: a step-pool facies, paludal facies, and vein facies. In the following, the characteristic lithologies and features for each facies are summarized, whereas a detailed facies description of individual samples can be found in Table DR1.

The step-pool facies (Fig. 4.2A) consists of dams and pools which may vary in size from several meters to centimeters or millimeters; dams and pools on the centimeter and millimeter scale are called microterraces and cover the face of steep dams (Figs. 4.2B and 4.2C; Fouke et al., 2000, 2003). Dams which vary in size from tens of centimeter to meters lead to drapes in the rock record (Fig. 4.2D). The travertine lithology of the step-pool facies (Fig. 4.3) largely depends on the depositional environment, i.e. pool or dam, and generally consists of either dense or layered micrite in various colors, e. g. white, yellow, grey, beige, brown, or red; the layers can be horizontal, wavy, irregular, or convoluted. The micritic layers may contain peloids, pisoids, shrubs, travertine clasts and lithoclasts, phytoclast travertine, travertine rafts, and calcified

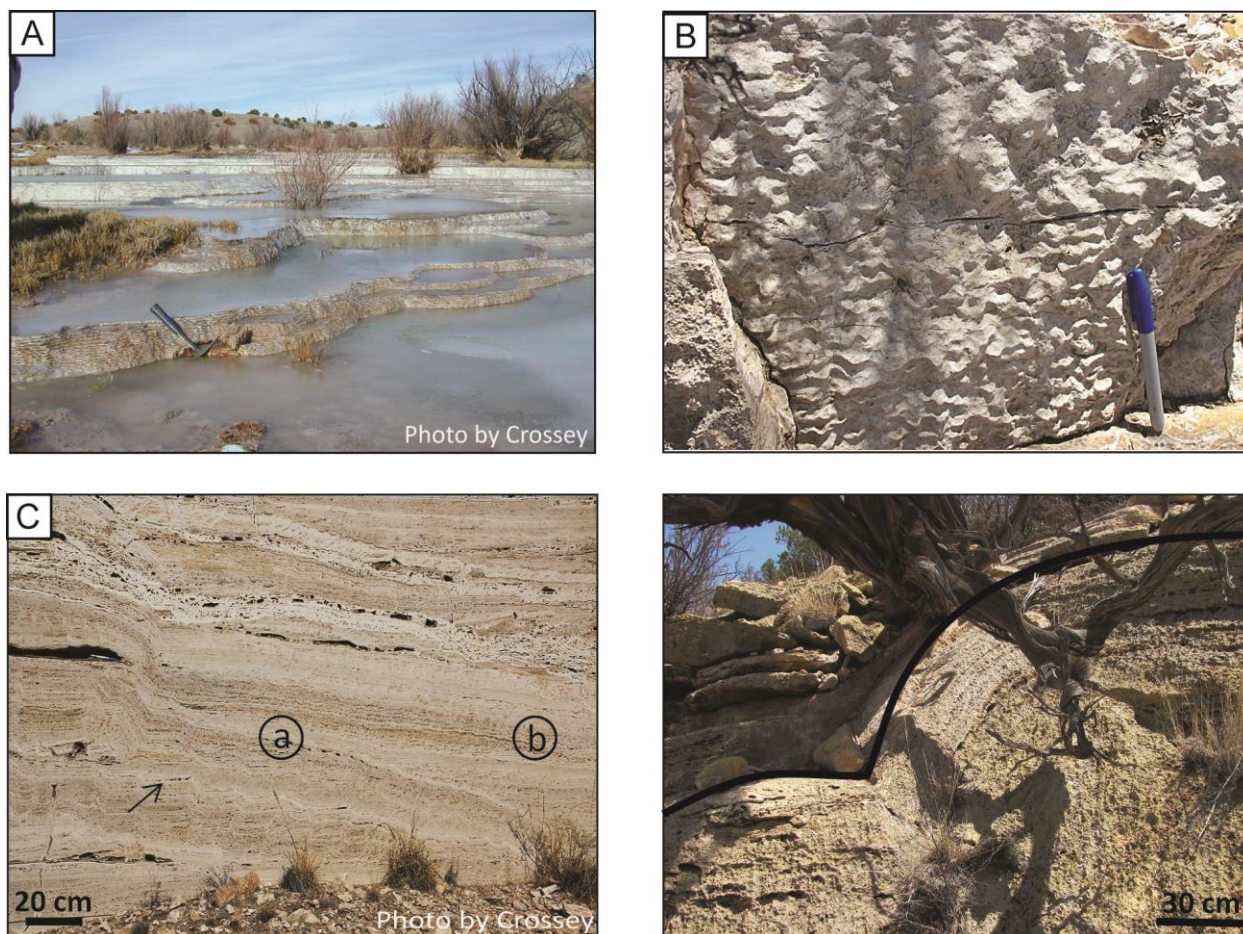


Figure 4.2. Photos of the step-pool facies. A) Step-pools in Comanche Arroyo, NM; note microterraces along the dams of individual pools and vegetation in the pools (hammer for scale). B) Microterraces at Mesa del Oro, NM; flow direction was from top to bottom of the photo (pen for scale = 13.5 cm). C) Drape (a) and microterraces (black arrow) in a quarry at Mesa Aparejo, NM; horizontal layers (b) represent pool. D) Drape at Mesa del Oro (outlined in black).

bubbles. Peloids are round micritic particles of less than a millimeter to a few millimeters in size, pisoids are concentric grains that are usually several millimeters to a few centimeters large, and shrubs are feathery or bush-like precipitates of either micrite or spar (Guo and Riding, 1998; Pentecost, 2005). Travertine clasts and lithoclasts are a few millimeters to centimeters in size, the latter being clastic material such as sand grains or small pebbles. Phytoclast travertine consists of encrusted parts of vegetation and plant casts (Figs. 4.3, 4.4A, and 4.4B). Travertine rafts are thin, delicate crystalline layers and calcified bubbles are gas bubbles that get coated by rapidly

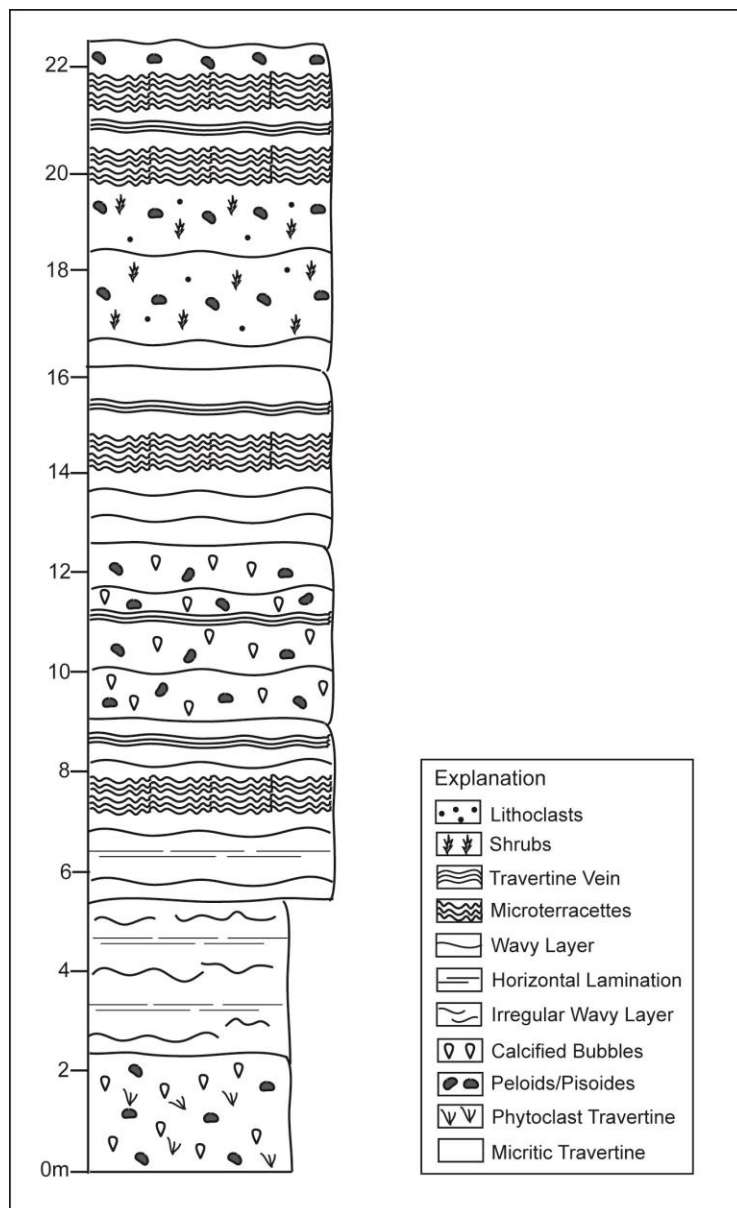


Figure 4.3. Schematic stratigraphic column of the step-pool facies. Lithology is based on a stratigraphic travertine section at Mesa del Oro (not drawn to scale). Textures of the step-pool facies are explained in the text.

precipitating calcium carbonate (Fig. 4.3; Chafetz and Folk, 1984; Guo and Riding, 1998). The step-pool facies forms on gently or steeply sloping surfaces of fissure ridges or spring mounds, and along streams as a succession of dams which are separated by pools (Fig. 4.2A). The water eventually flows over the rim of a dam into the next pool. The observed horizontal layering is mostly the result of travertine precipitation in quiet or deeper parts of a pool, whereas wavy, irregular, or convoluted layers are likely caused by turbulent flow within the pool and over the

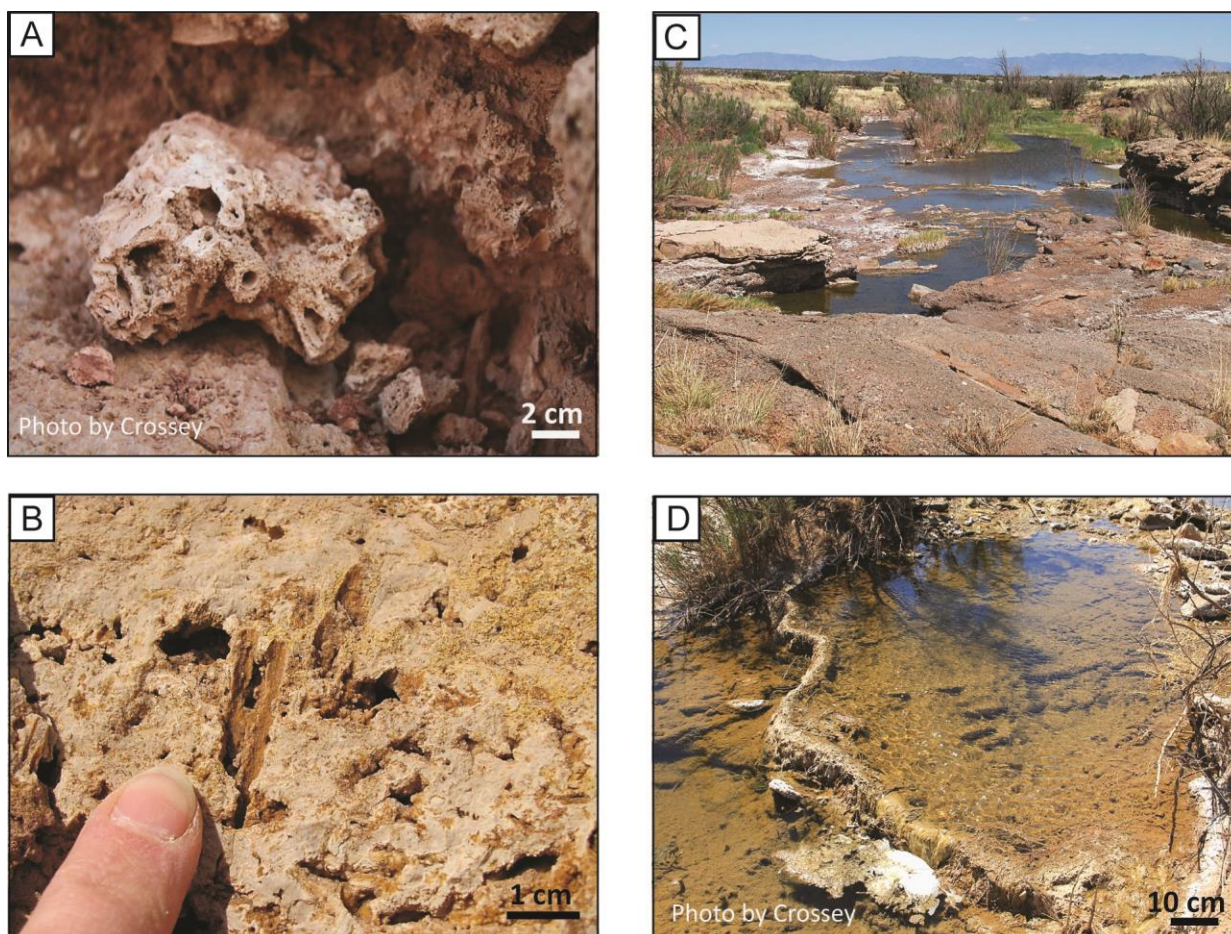


Figure 4.4. Photos of the paludal facies. A) Phytoclast travertine consisting of encrusted stems at an outcrop at Mesa del Oro, NM. B) Plant casts in travertine at an outcrop at Mesa del Oro, NM. C) Stream flowing through a marsh in Salado Arroyo, Mesa Aparejo, NM; note step-pools and vegetation. D) Close-up view of a step-pool along Salado Arroyo, NM.

dam (Guo and Riding, 1998). Areas between pools can be vegetated and lead to the formation of phytoclast travertine (Figs. 4.4A and 4.4B). Pools may become dry when discharge decreases which may lead to the formation of travertine crusts that may be reworked and broken up into travertine clasts. Lithoclasts may be blown or washed into pools and peloids, pisoids, and shrubs form at the bottom of pools (Chafetz and Folk, 1984; Guo and Riding, 1994; Pentecost, 2005).

The paludal facies forms in a marsh environment with step-pools, ponds, and vegetated areas (Fig. 4.4C and 4.4D). The travertine lithology (Fig. 4.5) predominantly consists of micrite in various colors, e.g. beige, red, and brown, which is often porous and either massive or layered;

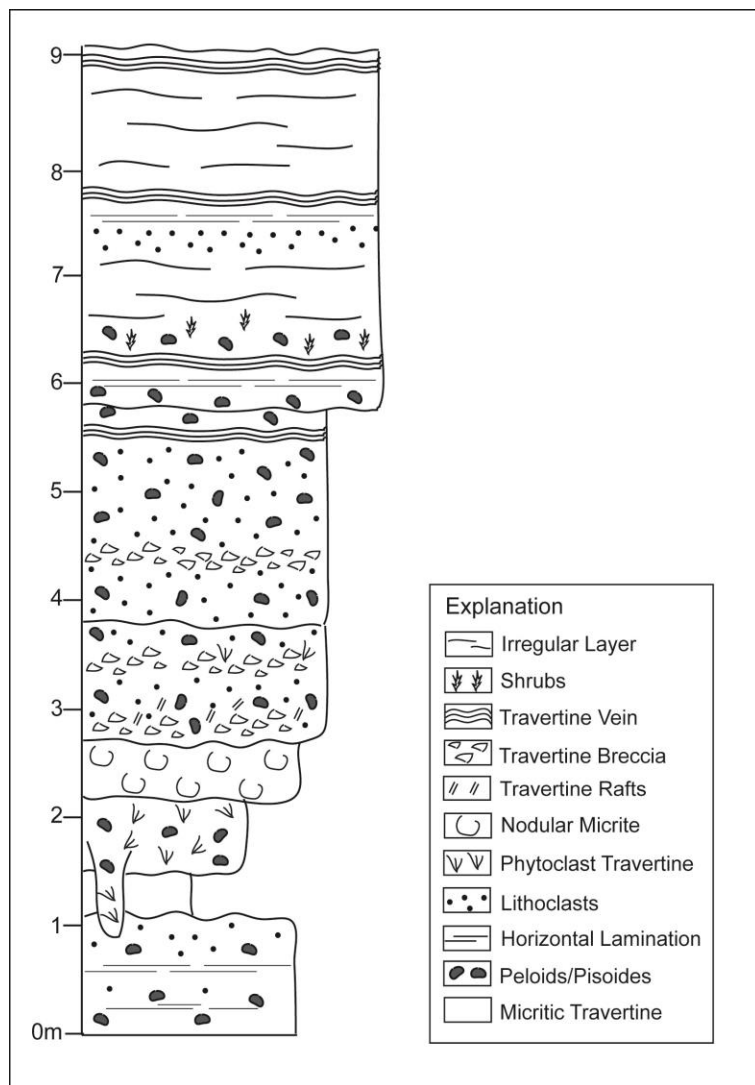


Figure 4.5. Schematic stratigraphic column of the paludal facies. Lithology is based on a stratigraphic travertine section at Mesa del Oro (not drawn to scale). Textures of the paludal facies are explained in the text.

layers can be horizontal, wavy, or irregular and the micrite nodular or concentric. The micritic layers may contain peloids, pisoids, travertine clasts and lithoclasts, and phytoclast travertine (Figs. 4.4A, 4.4B, and 4.5), components which have already been described for the step-pool facies. The paludal facies also contains carbonate mud and silt layers (Fig. 4.5). The paludal facies represents a marsh or lake margin environments either at the foot of or at a distance from a fissure ridge or spring mound which is characterized by ephemeral ponds and lakes, and variable vegetated areas (Figs. 4.4C and 4.4D; Glover and Robertson, 2003; Pentecost, 2005; Alonso-Zara and Wright, 2010). The travertine lithology of the paludal facies varies according to wet

and dry conditions in the marsh. Ponds and lakes may form during times of high discharge when the water table is high, whereas pools and dams may form in streams that flow through the marsh and these environments will exhibit the same sedimentologic and textural characteristics as the step-pool facies. Paludal deposits may contain a considerable amount of fine-grained clastic material that is blown into the marsh by wind or carried with the streams that flow through or into the marsh. Carbonate mud and silt may form during dry conditions, representing influx of detritus from the action of wind and flowing water (runoff) from surrounding areas as well as incipient weathering of travertine.

The vein facies consists of travertine filling horizontal and vertical fractures that vary in size from a few millimeters to several tens of centimeters and cut across both older travertine and older veins (Figs. 4.6A and 4.6B). The travertine lithology predominantly consists of spar in different colors, e.g. white, grey, yellow, red, and brown, and white micrite (Figs. 4.6C and 4.6D). Individual calcite crystals are up to a centimeter in size (Fig. 4.6C). Both spar and micrite veins are internally layered; individual layers can range in size from 1 mm to a centimeter and they can be horizontal, wavy, irregular, or convoluted (Figs. 4.6C and 4.6D). The vein facies formed in subsurface fractures inside an existing travertine deposit and fracturing was likely induced by elevated fluid pressure of the CO₂-charged groundwater that flowed through the fractures (Sibson, 2000; Ricketts et al., 2014). Vertical veins represent the feeder system that conveyed the groundwater from depth to the surface, whereas horizontal veins represent fluid flow parallel to bedding (Uysal et al., 2007; De Filippis et al., 2012, 2013a, 2013b; Gratier et al., 2012).

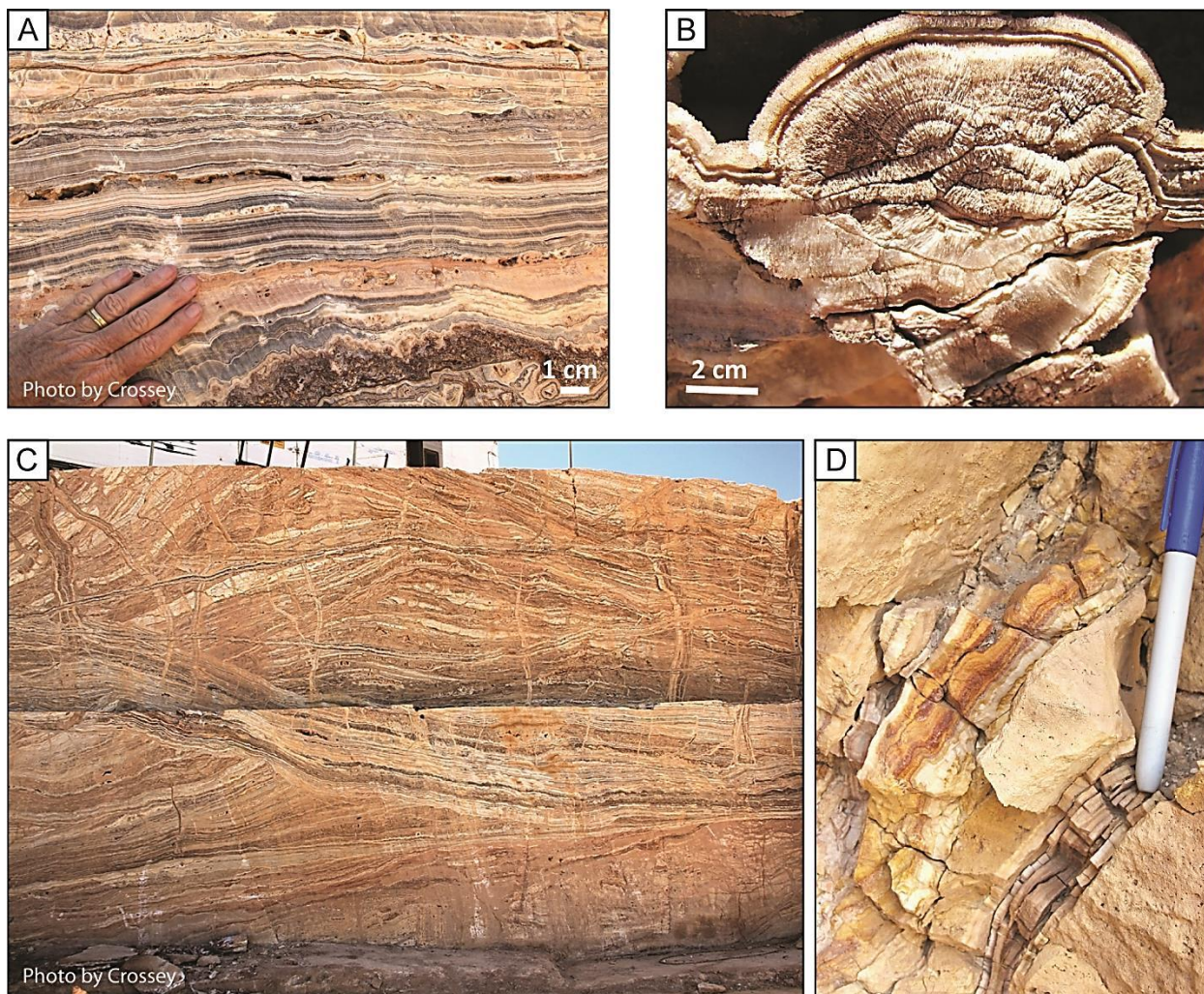


Figure 4.6. Photos of the vein facies. A) Horizontal wavy and convoluted veins in a quarry at Mesa Aparejo, NM. B) Different generations of horizontal and vertical veins in a quarry at Mesa Aparejo, NM; quarry wall is 4 m high. C) Vein with botryoidal-shaped radial calcite at Red Hill, Mesa Aparejo, NM. D) Vertical veins at Mesa del Oro; veins consist of layers with different colors (pen for scale = 13.5 cm).

Stable Isotope Analysis

Stable oxygen and carbon isotopes of 325 travertine samples from New Mexico and Arizona were analyzed (Table DR2). Results overlap substantially and exhibit a wide range of $\delta^{13}\text{C}$ and $\delta^{18}\text{O}$ values, varying between -5‰ and + 10‰, and -3.5‰ and -14‰, respectively (Fig. 4.7). Even though stable isotope values overlap, there is a characteristic range of $\delta^{13}\text{C}$ and $\delta^{18}\text{O}$ values for each travertine facies. For the step-pool facies, the majority of $\delta^{13}\text{C}$ values vary

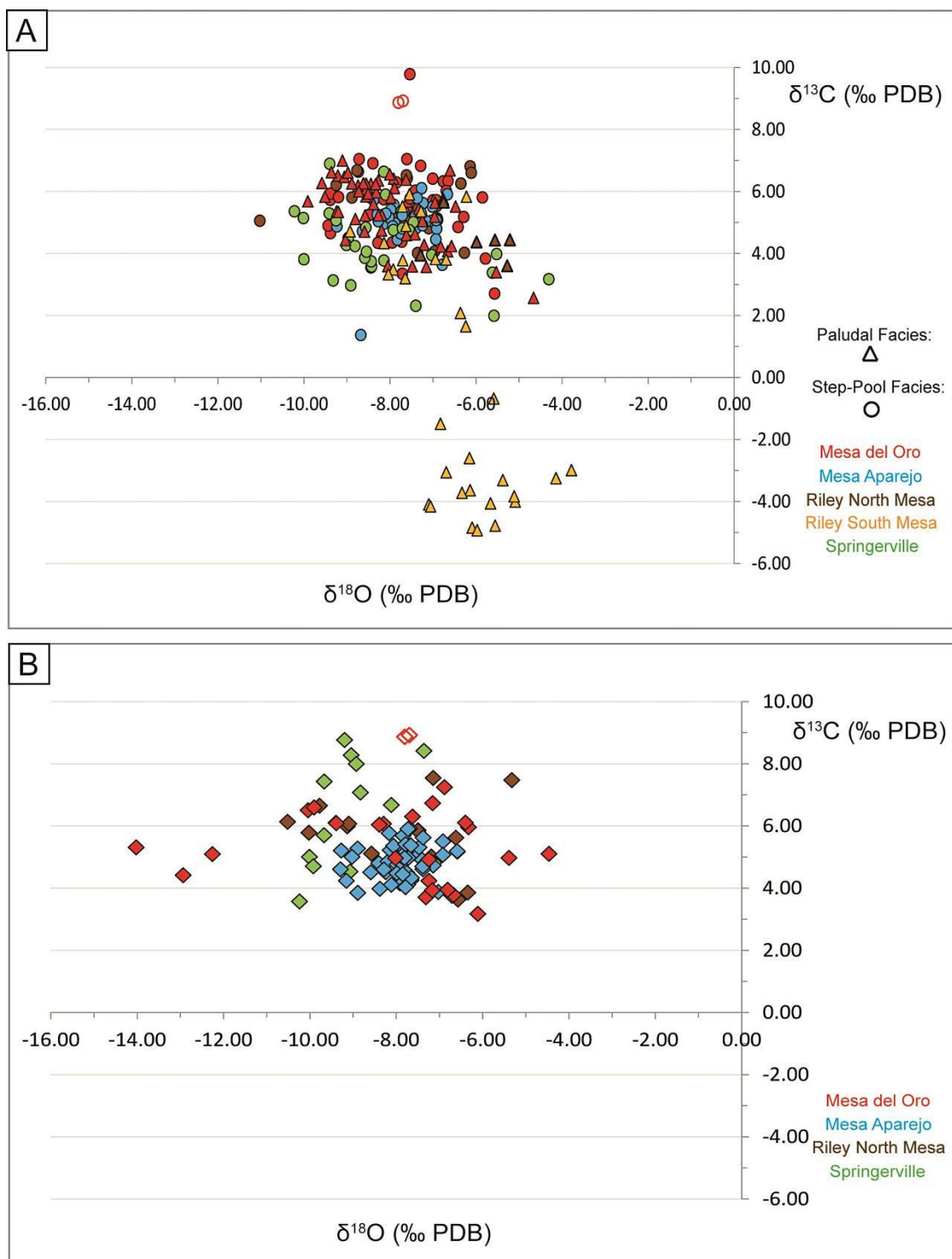


Figure 4.7. Stable isotope results of different travertine facies and different study areas. (A) Stable isotope results of the vein facies. (B) Stable isotope results of the step-pool and paludal facies. Study areas are color-coded, open circles and diamonds are explained in the text.

between +1.5‰ and +7.5‰, only one sample has a $\delta^{13}\text{C}$ value of +10‰, and $\delta^{18}\text{O}$ values range from -11‰ to -4.5‰ (Fig. 4.7A). The paludal facies shows two distinctive sample groups: $\delta^{13}\text{C}$ values of the first group vary between +2‰ and +6‰, and $\delta^{18}\text{O}$ values between -9‰ and -4.5‰; $\delta^{13}\text{C}$ values of the second group vary between -5‰ and -0.5‰, and $\delta^{18}\text{O}$ values between \sim -7‰ and -4‰ (Fig. 4.7A). $\delta^{13}\text{C}$ values of the vein facies vary between +3‰ and +9‰, whereas $\delta^{18}\text{O}$ values range from -14‰ to -4.5‰ (Fig. 4.7B). However, the spread of stable isotope values differs considerably among study areas: Samples from Mesa Aparajo have the smallest variations, with $\delta^{13}\text{C}$ values ranging from +4‰ to 6‰ and $\delta^{18}\text{O}$ values from -9‰ to -7‰, whereas samples from Mesa del Oro show the widest spread which is, at the same time, the general range of the vein facies: $\delta^{13}\text{C}$ values vary between +3‰ and +9‰, and $\delta^{18}\text{O}$ values between -4.5‰ and -14‰; $\delta^{13}\text{C}$ values of samples from Riley North Mesa range from +3.5‰ to +9‰, and $\delta^{18}\text{O}$ values from -10.5‰ and -5.5‰; samples from Springerville have $\delta^{13}\text{C}$ values varying between +3.5‰ and +9‰, and $\delta^{18}\text{O}$ values between -10.5‰ and -7‰.

Major, Minor and Trace Elements of Travertine Samples

In a pilot study, a subset of 24 travertine samples were analyzed for minor and trace elements, including rare earth elements (REE) (Tables 4.1 and 4.2). Mg concentrations are variable and can be as low as 77 ppm and as high as 5960 ppm (Table 4.1). Trace element analyses show similar trends throughout the region and for different travertine facies (Fig. 4.8; Table 4.1). Some trace elements have relatively high concentrations (>1000 ppm), e.g. Mg, Na, and Sr, and some are characteristically lower (>400 ppm) such as Al, B, and Fe. The vein facies shows the largest variability in trace element concentrations (Fig. 4.8A), whereas the trace element distribution of the step-pool facies seems to be more homogenous (Fig. 4.8B). REE in general have very low concentrations or are below detection limit (Fig. 4.9; Table 4.2). The vein

Table 4.1: Concentrations and Ratios of Major, Minor, and Trace Elements

Sample ID	Facies	Ca		Mg	K	Na	Al	As	B	Ba	Be	Cd	Co	Cr	Cu
		(weight%)	ppm	ppm	ppm	ppm	ppm	ppm	ppm	ppm	ppm	ppm	ppm	ppm	ppm
EE07-61	Vein	39	391,667	3809	267	1547	442	1.6	606	15	3.9	0.2	2.5	1.1	0.6
EE09-5A	Step-Pool	38	379,703	2068	253	1100	608	4.2	564	18	4.3	0.2	3.2	1.1	3.0
AP10-MDO4a	Vein	35	351,235	1904	135	117	168	2.6	111	228	0.0	0.0	0.0	0.0	6.2
AP10-MDO11B-b	Vein	40	397,816	1243	232	927	526	0.9	532	4.6	1.8	0.2	2.6	1.0	13
AP10-MDO21	Vein	40	402,451	1002	203	913	455	49	547	15	1.0	0.3	2.7	3.6	7.9
AP10-MDO24	Vein	40	397,330	1305	175	825	415	1.1	495	3.9	0.1	0.1	2.7	1.4	0.0
AP10-MDO53B-a	Vein	39	385,096	937	105	63	85	3.7	105	11	0.0	0.0	0.0	0.0	6.5
AP11-MDO66a	Vein	40	400,000	1033	183	785	402	1.1	471	43	1.1	0.2	2.5	0.8	0.0
AP11-MDO71a	Vein	40	400,000	77	196	1319	631	2.0	487	20	2.8	0.4	2.3	0.9	4.3
AP12-RN20	Step-Pool	41	411,520	1078	299	861	744	0.2	479	6.6	0.4	0.1	2.9	1.6	5.0
AP12-RN23a	Step-Pool	40	403,960	1694	303	1309	497	0.7	613	12	16	0.1	3.4	1.0	7.5
KLC11-SH2b	Vein	38	377,184	5960	353	3713	455	8.8	557	17	70	0.1	2.6	0.9	1.8
KLC11-SH10b	Step-Pool	41	406,971	3274	264	1380	542	2.2	464	15	9.2	0.9	2.7	1.0	6.8
LC02-BQTC-b	Step-Pool	41	410,817	2220	217	1118	495	3.8	494	9.8	21	0.3	4.4	1.2	0.0
KLC11-TC2	Step-Pool	40	403,365	1943	225	1213	506	1.6	474	5.8	16	0.1	2.6	2.3	0.6
KLC11-VG1a	Vein	40	399,038	3632	183	974	413	8.1	469	12	17	0.1	2.6	2.4	11
KLC11-VG4a	Vein	39	387,010	2050	249	948	591	73	478	7.8	47	0.1	2.8	1.5	0.8

Table 4.1: Concentrations and Ratios of Major, Minor, and Trace Elements (cont.)

Sample ID	Facies	Fe	Li	Mn	Mo	Ni	Pb	Se	Si	Sr	V	Zn	Mg/Ca	Sr/Ca
		ppm	ppm	ppm	molar	molar								
EE07-61	Vein	3.2	8.2	3.3	0.6	53	1.8	0.7	207	905	0.2	16	0.0160	0.0011
EE09-5A	Step-Pool	474	11	77	0.6	59	4.5	1.7	329	476	1.0	38	0.0090	0.0006
AP10-MDO4a	Vein	12	19	19	0.0	156	29	3.1	233	924	0.0	3.1	0.0089	0.0012
AP10-MDO11B-b	Vein	81	6.3	55	0.6	307	0.0	0.3	373	619	0.2	10	0.0052	0.0007
AP10-MDO21	Vein	51	6.3	8.1	0.6	53	3.3	2.3	211	553	2.4	27	0.0041	0.0006
AP10-MDO24	Vein	24	6.2	12	0.5	53	0.3	2.4	180	1473	0.2	13	0.0054	0.0017
AP10-MDO53B-a	Vein	68	11	47	0.0	652	4.2	3.5	24	1114	0.0	0.0	0.0040	0.0013
AP11-MDO66a	Vein	8.6	6.6	33	0.6	52	9.6	3.0	224	512	0.1	3.1	0.0043	0.0006
AP11-MDO71a	Vein	44	7.4	7.0	0.5	50	0.7	2.1	377	5655	0.7	24	0.0003	0.0065
AP12-RN20	Step-Pool	391	7.7	33	0.6	58	1.1	2.4	744	341	0.6	28	0.0043	0.0004
AP12-RN23a	Step-Pool	176	6.3	40	0.6	61	1.8	4.3	267	1021	0.4	77	0.0069	0.0012
KLC11-SH2b	Vein	19	24	165	0.5	54	0.0	1.7	263	692	0.4	20	0.0261	0.0008
KLC11-SH10b	Step-Pool	88	8.5	7.5	0.6	57	2.9	1.8	289	1045	0.4	43	0.0133	0.0012
LC02-BQTC-b	Step-Pool	83	9.1	27	0.4	55	1.2	2.8	254	804	0.5	48	0.0089	0.0009
KLC11-TC2	Step-Pool	152	8.4	53	0.8	55	1.5	2.7	297	675	0.4	17	0.0079	0.0008
KLC11-VG1a	Vein	19	9.5	10	0.4	54	30	1.6	144	241	0.7	18	0.0150	0.0003
KLC11-VG4a	Vein	457	7.8	58	0.8	52	0.6	1.9	389	775	0.4	55	0.0087	0.0009

(green = samples were measured using an ICP-OES, red = samples were measured using an ICP-MS)

Method detection limit for ICP-OES (in ppm): Ca, Mg, Na, Al = 0.2; K = 0.5; B = 0.04; Fe = 0.06; Si = 0.1; Sr = 0.008

Method detection limit for ICP-MS (in ppb): 0.01

Table 4.2: Concentration of Rare Earth Elements

Sample ID	Facies	La	Ce	Pr	Nd	Sm	Eu	Gd	Tb	Dy	Ho	Er	Tm	Yb	Lu
		ppm													
EE07-61	Vein	1.0	0.1	0.2	0.1	0.1	0.1	0.4	0.4	0.0	0.0	0.0	0.0	0.0	0.0
EE09-5A	Step-Pool	0.9	0.2	0.3	0.1	0.1	0.1	0.4	0.3	0.0	0.0	0.0	0.1	0.0	0.1
AP10-MDO11B-b	Vein	1.3	0.4	0.4	0.2	0.1	0.1	0.5	0.5	0.0	0.0	0.0	0.0	0.0	0.1
AP10-MDO21	Vein	0.9	0.3	0.3	0.2	0.1	0.1	0.3	0.3	0.0	0.0	0.0	0.0	0.0	0.1
AP10-MDO24	Vein	0.8	0.2	0.2	0.1	0.0	0.0	0.3	0.3	0.0	0.0	0.0	0.0	0.0	0.0
AP10-MDO41	Step-Pool	4.3	3.4	2.8	2.5	1.4	1.0	1.7	0.8	0.4	0.3	0.3	0.3	0.3	0.8
AP10-MDO53B-a	Vein	1.1	0.2	0.3	0.1	0.1	0.0	0.4	0.4	0.0	0.0	0.0	0.0	0.0	0.1
AP11-MDO66a	Vein	1.2	0.2	0.3	0.1	0.2	0.3	0.4	0.4	0.0	0.0	0.0	0.0	0.0	0.1
AP11-MDO71a	Vein	1.9	0.5	0.5	0.3	0.2	0.3	0.8	0.8	0.2	0.3	0.4	0.4	0.3	0.6
JR10-9	Step-Pool	5.5	4.4	3.5	3.2	1.6	1.0	2.2	1.2	0.6	0.5	0.4	0.5	0.4	1.1
AP12-RN20	Step-Pool	1.9	1.5	1.1	1.0	0.5	0.4	0.8	0.4	0.2	0.2	0.1	0.2	0.1	0.4
AP12-RN23a	Step-Pool	0.8	0.2	0.2	0.1	0.1	0.1	0.3	0.3	0.0	0.0	0.0	0.0	0.0	0.1
KLC11-SH2b	Vein	1.9	0.3	0.4	0.1	0.0	0.1	0.7	0.8	0.0	0.0	0.0	0.0	0.0	0.0
KLC11-SH10b	Step-Pool	2.1	0.5	0.9	0.6	0.4	0.3	0.7	0.6	0.2	0.1	0.1	0.1	0.1	0.3
LC02-BQTC-b	Step-Pool	1.2	0.4	0.4	0.2	0.1	0.1	0.4	0.4	0.0	0.0	0.0	0.0	0.0	0.1
KLC11-TC2	Step-Pool	1.2	0.6	0.5	0.4	0.2	0.1	0.5	0.4	0.1	0.0	0.0	0.1	0.0	0.1
KLC11-VG1a	Vein	2.0	0.3	0.4	0.1	0.0	0.0	0.7	0.8	0.0	0.0	0.0	0.0	0.0	0.0
KLC11-VG4a	Vein	1.3	0.4	0.4	0.2	0.1	0.1	0.5	0.5	0.0	0.0	0.0	0.0	0.0	0.1
AP12-RS1A	Paludal	16	12	9.7	8.4	4.6	3.2	5.7	2.9	1.5	1.3	1.2	1.2	1.0	2.8
LC03-RS7	Step-Pool	6.7	6.2	4.8	4.4	2.8	2.1	3.0	1.7	1.0	0.8	0.7	0.8	0.6	1.7

Method detection limit for ICP-MS (in ppb): 0.01

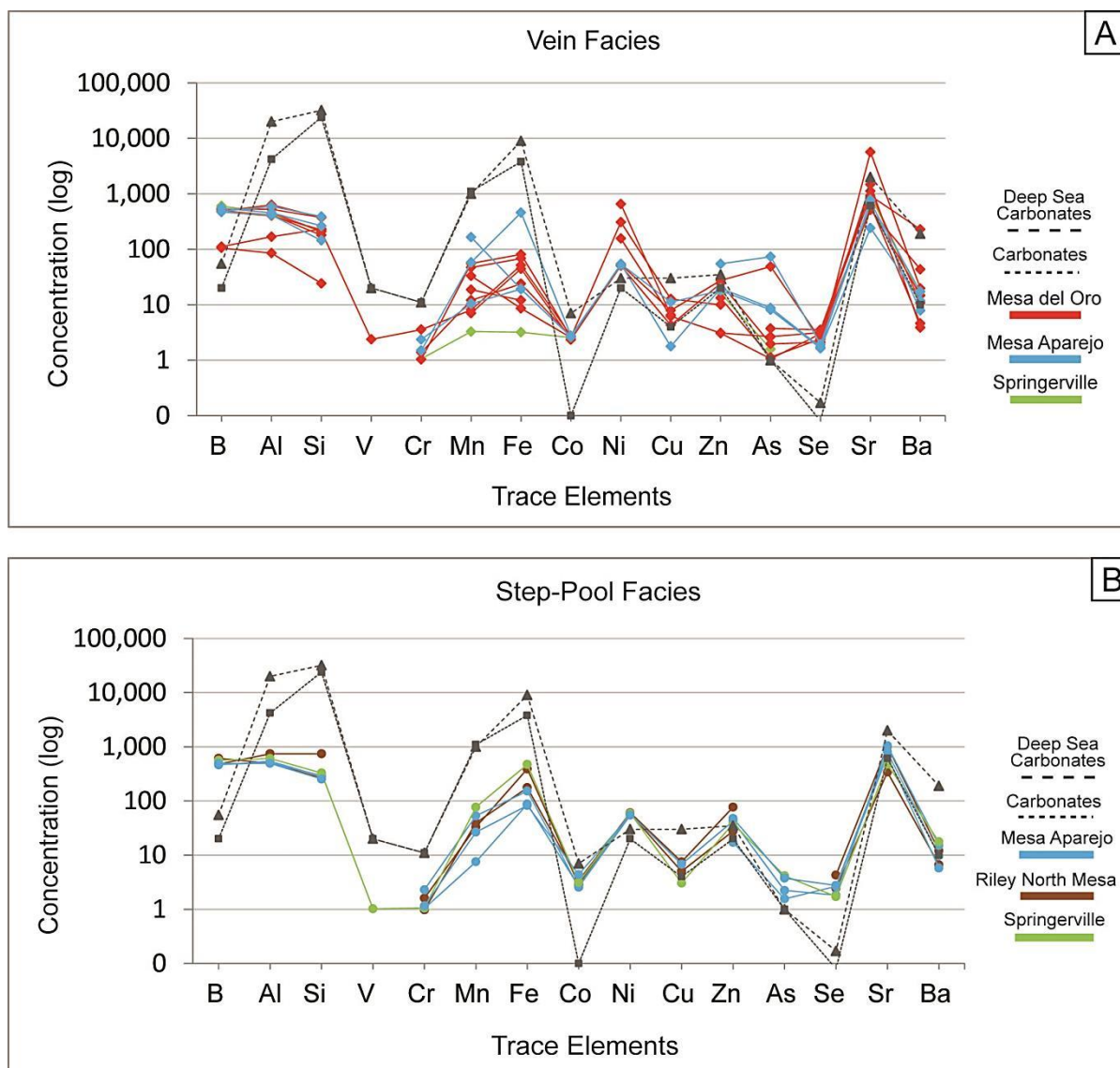


Figure 4.8. Trace element concentrations of different travertine facies and different study areas. (A) Trace element concentrations of the step-pool facies, (B) Trace element concentrations of the vein facies. The average chemical compositions of marine carbonates and deep sea carbonates are shown for comparison (Veizer, 1990). Trace elements are ordered from left to right according to their relative atomic mass.

facies (Fig. 4.9A) exhibits lower REE concentrations than the step-pool and paludal facies (Fig. 4.9B), and the paludal facies has the highest REE concentrations (Fig. 4.9B). The light REE are enriched over the heavy REE (Fig. 4.9).

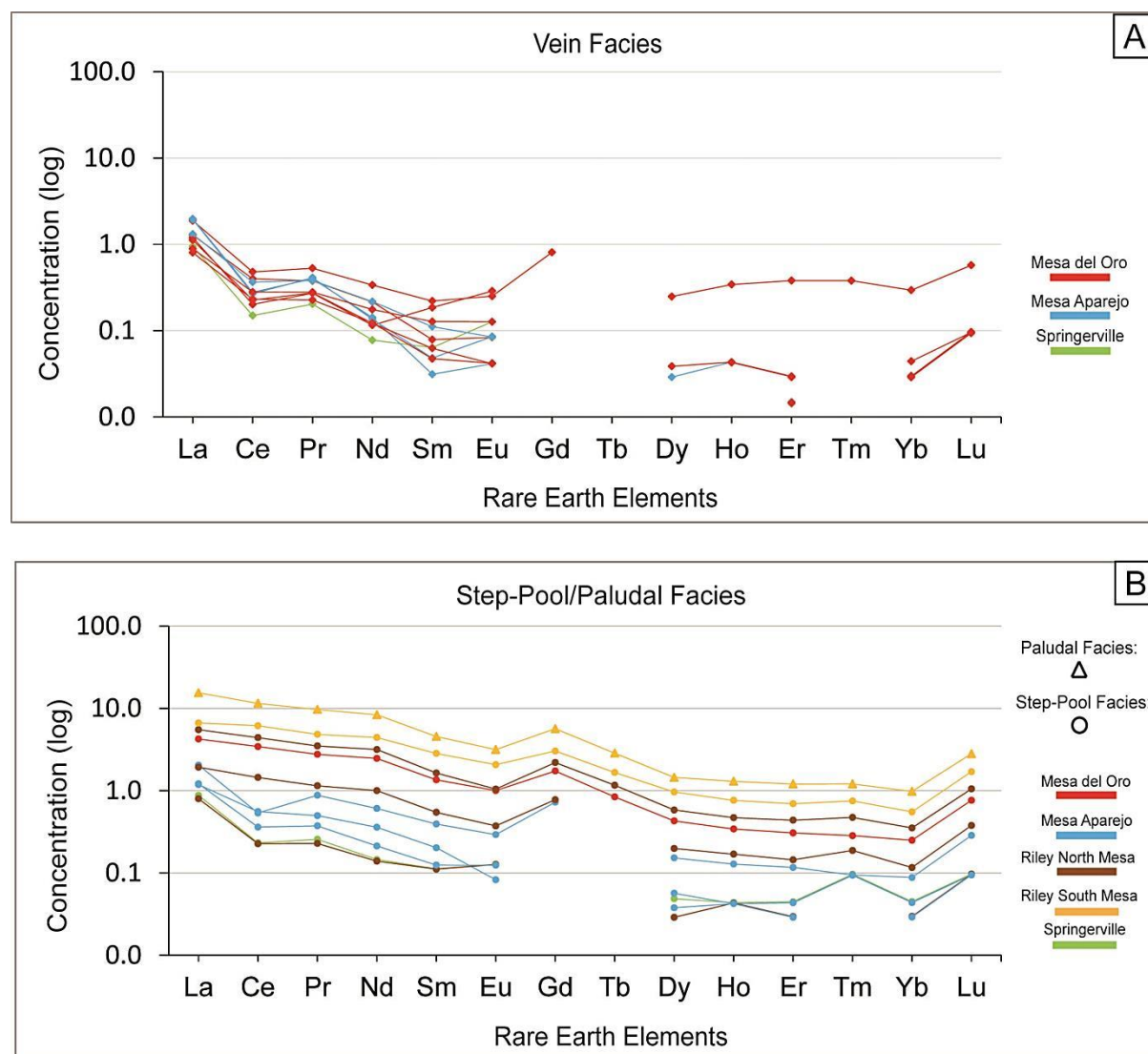


Figure 4.9. Rare earth element concentrations of different travertine facies and different study areas. (A) Rare earth element concentrations of the step-pool and paludal facies. (B) Rare earth element concentrations of the vein facies. Rare earth element concentrations are chondrite-normalized.

DISCUSSION

This section evaluates the relationship between travertine facies, geochemical composition of travertines, and the impact of past water temperatures and compositions.

Interpretation of the Stable Isotopic Composition of Travertines According to Facies

The observed overlapping stable isotope results of the step-pool and paludal facies are interpreted to reflect similar depositional environments, such as pools, dams, and vegetated areas which are characteristic for both facies (Figs. 4.2A, 4.4C and 4.4D). Stable isotope results of the vein facies that overlap with stable isotope results of the step-pool facies suggest that the composition and temperature of the water these two facies precipitated from may have been very similar (Fig. 4.7).

Oxygen Isotopes of Travertines

Controls on the oxygen isotopic composition of travertines, including composition and temperature of the groundwater source fluids, have been studied by various authors (e. g. Turi, 1986; Minissale et al., 2002b; Minissale, 2004; Newell et al., 2005; Crossey et al., 2006; Kele et al., 2011; Yan et al., 2012; Williams et al., 2013; Özkul et al., 2014; Sun et al., 2014; Wang et al., 2014). The $\delta^{18}\text{O}_c$ values are controlled by temperature and oxygen isotopic composition of the source water that precipitates the travertines. These conditions are in turn affected by 1) mixing of deeply-derived and shallow groundwater, 2) water-rock interactions along groundwater flow paths, 3) mixing of groundwater with meteoric water, and 4) evaporation (Fig. 4.7). Mixing of groundwater and surface water may lead to overall lower $\delta^{18}\text{O}$ values of the water ($\delta^{18}\text{O}_w$) and the travertine ($\delta^{18}\text{O}_c$); higher water temperature also result in lower $\delta^{18}\text{O}_w$ and $\delta^{18}\text{O}_c$ values, whereas lower water temperature leads to higher $\delta^{18}\text{O}_w$ and $\delta^{18}\text{O}_c$ values; evaporation and high travertine deposition rates result in higher $\delta^{18}\text{O}_c$ values (Gonfiantini et al., 1968; Turi, 1986; Pentecost, 2005; Kele et al., 2011; Yan et al., 2012; Özkul et al., 2014; Sun et al., 2014; Wang et al., 2014).

The observed wide range of $\delta^{18}\text{O}_c$ values of the step-pool, paludal, and vein facies suggest that groundwater mixing, mixing of groundwater and meteoric water, and changes in water temperature played an important role during travertine precipitation (Fig. 4.7). The vein facies precipitated from groundwater flowing through subsurface fractures where mixing of deeply-derived and shallow groundwater likely played an important role. The step-pool and paludal facies formed above the surface which suggests that mixing of groundwater with meteoric water and evaporation were likely controls of the oxygen isotopic composition. Both facies were probably also influenced by variations in water temperature, e. g. due to changing seasons as well as longer term changes in climate.

Carbon Isotopes of Travertines

The carbon isotopic composition of travertines is primarily controlled by the CO_2 degassing rate which depends on 1) partial pressure of CO_2 , 2) water temperature, and 3) flow velocity (Groves and Howard, 1994; Howard and Groves, 1995; Hoffer-French and Herman, 1989; Qian et al., 2005; Hammer et al., 2007; Kele et al., 2011). Turbulent and laminar flow in fractures is likely important for the vein facies because flow conditions impact CO_2 degassing rates which increase towards the surface where decreasing pressure leads to strong CO_2 degassing (Groves and Howard, 1994; Howard and Groves, 1995; Hoffer-French and Herman, 1989; Qian et al., 2005; Hammer et al., 2007). Strong and turbulent degassing of CO_2 causes kinetic fractionation and isotopic disequilibrium, because the light carbon isotope ^{12}C will preferentially escape which leads to an enrichment in the heavy carbon isotope ^{13}C and hence higher $\delta^{13}\text{C}$ values (Turi, 1986; Kele et al., 2011). Water temperature impacts the CO_2 degassing rate in that higher water temperatures increase CO_2 escape (e. g. Wang et al., 2014) and probably affected all three facies. CO_2 degassing is strongest from fast flowing water, e. g. at dams, which

leads to higher $\delta^{13}\text{C}$ values, whereas degassing rates are much lower from pools and ponds because the pCO_2 of the water has time to equilibrate with atmospheric pCO_2 which results in lower $\delta^{13}\text{C}$ values (Fig. 4.7A; Fuller et al., 2011; Kele et al., 2011; Yan et al., 2012; Wang et al., 2014). Another control on the carbon isotopic composition of travertines, particularly of the step-pool and paludal facies, is vegetation and microbiological activity. Both plants and microorganisms preferentially use the light carbon isotope, ^{12}C , for photosynthesis and cell metabolic reactions, respectively, which lead to an enrichment in ^{13}C and hence higher $\delta^{13}\text{C}$ values (Turi, 1986; Pentecost, 2005; Kele et al., 2011). However, the decomposition of plant material in well-vegetated areas releases the light carbon isotope, ^{12}C , which results in lower $\delta^{13}\text{C}$ values (Talbot, 1990; Leng and Marshall, 2004; Pentecost, 2005). Most samples of the paludal facies from Riley South Mesa exhibit markedly low $\delta^{13}\text{C}$ values from -5‰ to -0.5‰ (Fig. 4.7A). These samples might have formed in stagnant shallow pools in vegetated areas where the CO_2 of the water had time to equilibrate with atmospheric CO_2 . Atmospheric CO_2 exhibits a range of $\delta^{13}\text{C}$ values from -6‰ to -9‰ (Sharp, 2007) but the $\delta^{13}\text{C}$ values of the travertine samples are clearly higher (Fig. 4.7A) which suggests that both photosynthesis of plants and metabolic processes of microorganism in the pools led to the observed higher $\delta^{13}\text{C}$ values (Fig. 4.7A). In combination with the $\delta^{18}\text{O}_\text{c}$ values these samples comes closest to an open-lake environment as described by Talbot (1990).

It can be difficult to unambiguously identify travertine facies and geochemical analyses can help distinguishing between facies. In Figure 4.7A, two open circles represent samples that were originally interpreted and plotted as step-pool facies. Because of their high $\delta^{13}\text{C}$ values the samples were reexamined and could be identified and plotted as vein facies, represented by two

open diamonds in Figure 4.7B. The high $\delta^{13}\text{C}$ value of $\sim 10\text{‰}$ of another step-pool sample in Figure 4.7A suggests that it also belongs to the vein facies but the hand sample is ambiguous.

Geochemical Analysis of Minor and Trace Elements According to Facies (excluding Rare Earth Elements)

The carbonate fraction of travertine samples was analyzed for trace element composition in order to evaluate whether trace elements have the potential to characterize travertines and can be used as a tracer (e.g., to distinguish mixing process, source fluids, etc.), similar to stable oxygen and carbon isotopes.

Trace element concentrations of the step-pool and vein facies overlap to a certain extent (Fig. 4.8), however, the vein facies exhibits larger variations in most trace element concentrations (Fig. 4.8A; Table 4.1). Concentrations of Ni, As, Sr, and Ba are significantly higher in the vein facies than in the step-pool facies (Fig. 4.8; Table 4.1). Although absolute amounts are very different, travertines exhibit similar trends in trace element composition as marine carbonates (Fig. 4.8), most notably a typical enrichment in Mn and Sr and it is inferred that these similar trends are caused by the affinity of calcite and aragonite for certain elements (Veizer, 1990; Bricker and Jones, 1995). The chemical composition of the travertine source water is mainly controlled by water-rock interactions, pH and redox conditions, and water temperature (e.g. Bricker and Jones, 1995).

The mobility of trace elements is mostly controlled by pH and redox conditions; e.g. As, Cr, Se go into solution at a neutral to alkaline pH, whereas acidification in general increases the mobility of trace elements (Hong et al., 1995). If conditions change from reducing to oxidizing, the mobility of Zn and Cu, for example, increases while the mobility of Mn and Fe decreases (Hong et al., 1995). Trace elements may precipitate due to a sudden increase in pH, e.g. when

travertine precipitates from CO₂-charged water, or when reducing groundwater mixes with oxidizing groundwater (Allard, 1995).

Shales can contain considerable amounts of B and might be a possible source for the high concentrations of B observed in both the step-pool and vein facies (Fig. 4.8; Table 4.1; 1984; Bricker and Jones, 1995); Pennsylvanian, Permian, and Triassic shales are a prevalent rock type in the study areas Mesa del Oro, Mesa Aparejo, Riley North Mesa, and Springerville (Jicha, 1958; Osburn, 1984; Bricker and Jones, 1995; Embid, 2009; Ricketts and Karlstrom, 2011). Granitic basement rocks may also be a source of boron since the element is contained in feldspars, quartz, and biotite (Bricker and Jones, 1995). Al and Si occur in most rock types in a variety of minerals (e. g. feldspar, plagioclase, quartz, muscovite, biotite, and pyroxene) but certain conditions are required in order to mobilize these elements: Si mobility is controlled by temperature, whereas Al mobility depends on pH and complexation (Drever, 2002). Si can precipitate together with travertine from hydrothermal water (Pentecost, 2005 and references therein). Both Al and Si concentrations are higher in the step-pool facies than in the vein facies (Fig. 4.8). V and Cr occur in higher concentrations in the step-pool and vein facies, respectively, and shales may be the source for the latter whereas vanadium might originate from minerals of igneous rocks (Fig. 4.8; Table 4.1; Allard, 1995; Bricker and Jones, 1995). Colloidal species (microinclusions) may be the source of high Mn concentrations most notably in the vein facies, as well as Cu and Zn (Fig. 4.8; Table 4.1; Veizer, 1990; Allard, 1995; Bricker and Jones, 1995). Higher concentrations of Co and Ni in the step-pool and vein facies, respectively, may originate from igneous rocks, especially mafic igneous rocks, and shales, in the case of Ni (Fig. 4.8; Table 4.1; Allard, 1995; Bricker and Jones, 1995). As and Se occur in higher concentrations in the vein and step-pool facies, respectively, and possible sources might be shales and also sandstones for

Se which are a common rock type in the study areas Mesa del Oro, Mesa Aparejo, Riley North Mesa, and Springerville (Fig. 4.8; Table 4.1; Jicha, 1958; Osburn, 1984; Allard, 1995; Bricker and Jones, 1995; Embid, 2009; Ricketts and Karlstrom, 2011). Sr concentrations are very high, particularly in the vein facies (Fig. 4.8; Table 4.1) and likely reflect an input of deeply-derived fluids (Crossey et al., 2006, 2009). Similar to Mn, Sr is a common trace element in carbonate rocks and the Pennsylvanian and Permian limestone aquifers maybe a possible source of elevated Sr concentrations (Bricker and Jones, 1995). Elevated concentrations of Ba, particularly for the vein facies, might be associated with igneous rocks and shales (Fig. 4.8; Table 4.1; Bricker and Jones, 1995). The presence of aragonite versus calcite also influences trace element concentrations because aragonite preferentially incorporates Sr, Na, and Ba, whereas calcite tends to incorporate Mg, Fe, Mn, Zn, Cu, and Cd (Reeder, 1990; Speer, 1990; Veizer, 1990). Travertines usually contain both aragonite and calcite and especially veins can consist of aragonite only (Guo and Riding, 1992; Fouke et al., 2000; Shipton et al., 2004; Kele et al., 2011; Gratier et al., 2012; Burnside et al., 2013; Özkul et al., 2014). Although the calcite and aragonite content of the travertines of this study was not determined it is likely that both minerals may be or may have been present. Variations in trace element concentrations between the vein and step-pool facies become clearer when the deviation of the mean of each element is plotted, as shown in Figure 4.10: the step-pool facies exhibits only small changes for the trace elements of individual samples (Fig. 4.10A), whereas the samples of the vein samples show significant variations (Fig. 4.10B).

Trace element concentrations in travertines appear to be variable. Geochemical analyses of travertines from Turkey by Özkul et al. (2014) show trace element concentrations similar to

the travertines in this study (Table 4.1) for Mn and Sr but significantly higher trace element concentrations of Si and Fe. Kele et al. (2011) also analyzed travertines from Turkey and

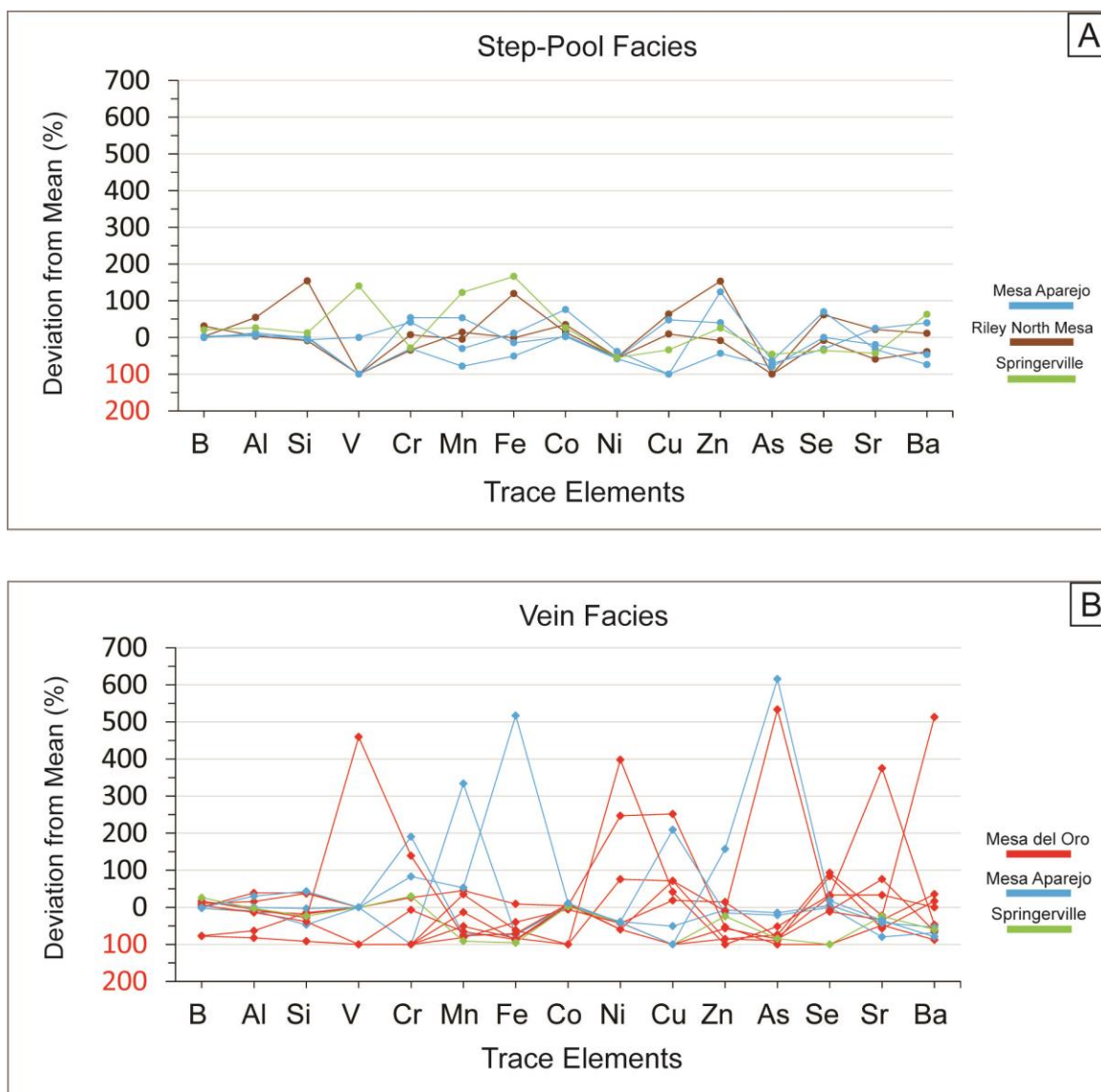


Figure 4.10. Deviations from the mean for trace elements of different travertine facies and different study areas. (A) Deviations from the mean of the step-pool facies. (B) Deviations from the mean of the vein facies. Deviations are explained in the text; study areas are color-coded. Trace elements are ordered from left to right according to their relative atomic mass.

obtained trace element concentration comparable to the travertines in this study (Table 4.1) for

Ba, Cu, and Sr, whereas As, B, Co, Ni, and Zn concentrations are significantly lower.

Relationships between selected major, minor and trace elements are shown in Figure

4.11: Ca correlates neither with Mg (Fig. 4.11A), Ba (Fig. 4.11B), nor Sr (Fig. 4.11C); Sr/Ca and Mg/Ca ratios do not co-vary either (Fig. 4.11D). Ratios of Mg/Ca and Sr/Ca represent water-rock

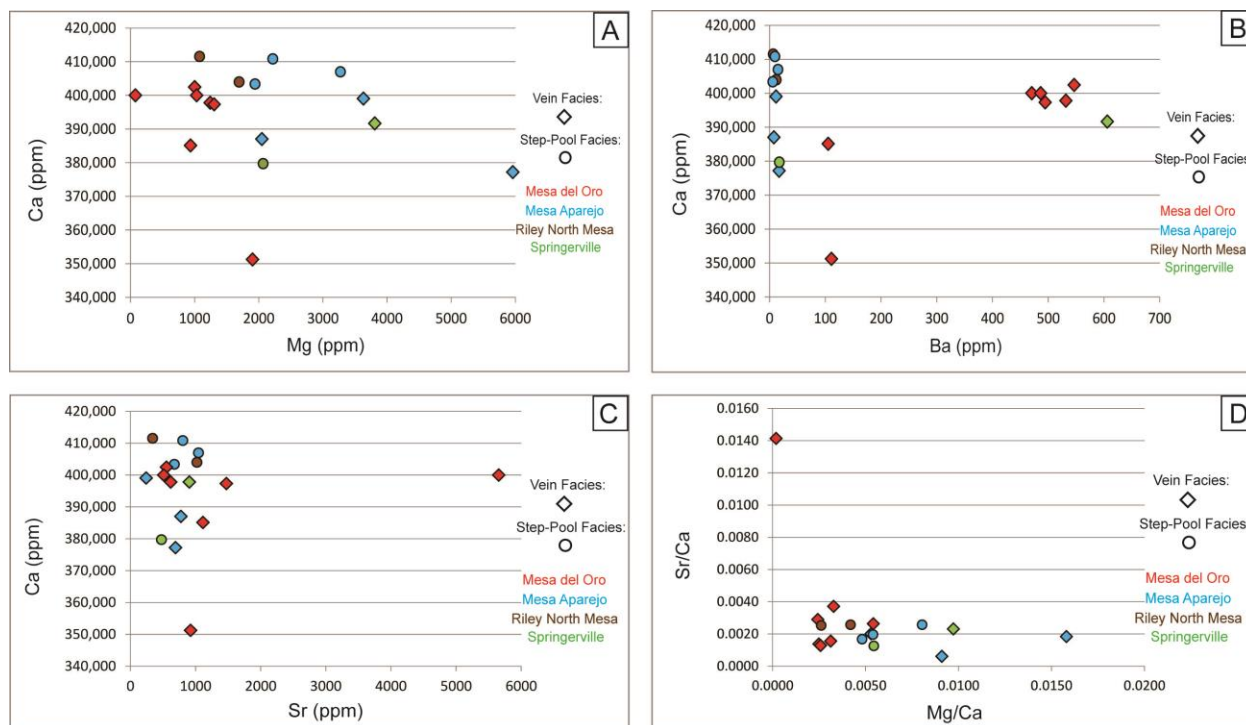


Figure 4.11. Trace element correlations of different travertine facies and different study areas. (A) Correlation of Mg and Ca. (B) Correlation of Ba and Ca. (C) Correlation of Sr and Ca. (D) Correlation of Mg/Ca and Sr/Ca. Study areas are color-coded.

interactions and elucidate residence time of groundwater in the aquifer (Veizer, 1983; Garnett et al., 2004). Figure 4.12 shows relationships between element ratios and stable isotopes of the travertines: Mg/Ca and Sr/Ca ratios neither correlate with $\delta^{18}\text{O}$ (Fig. 4.12A and 4.12B) nor $\delta^{13}\text{C}$ (Fig. 4.12C and 4.12D) which means that these ratios are neither temperature-dependent nor controlled by aquifer processes, respectively (Garnett et al., 2004). Mg/Ca ratios are very small (Table 4.1) and imply high discharge and short residence times of the groundwater during wet times (Garnett et al., 2004) which is consistent with results by Priewisch et al. (2014) who show

that large-volume travertine deposits accumulated during wet times when hydraulic head was high enough for CO₂-charged groundwater to ascend along faults.

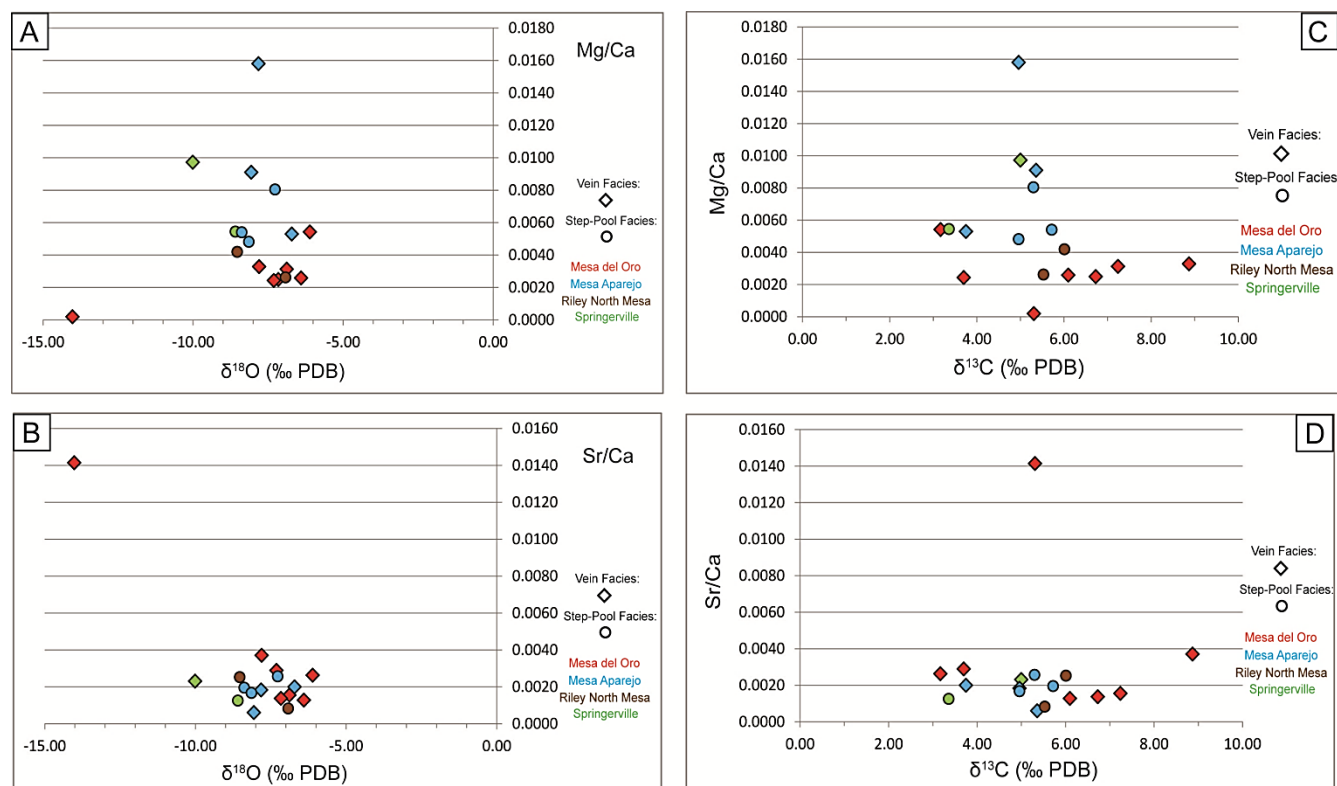


Figure 4.12. Correlation of trace element ratios and stable isotopes of different travertine facies and different study areas. (A) Plot showing the correlation of Mg/Ca and δ¹⁸O. (B) Plot showing the correlation of Sr/Ca and δ¹³C. (C) Plot showing the correlation of Mg/Ca and δ¹³C. (D) Plot showing the correlation of Sr/Ca and δ¹³C. Study areas are color-coded.

Rare Earth Element Concentrations According to Facies

Rare Earth Elements (REE) concentrations of the vein and step-pool facies are generally low; however, the vein facies exhibits the lowest concentration (Fig. 4.9A; Table 4.2), whereas a sample of the paludal facies has the highest REE concentrations (Fig. 4.9B; Table 4.2). REE concentrations are usually low in natural waters and seawater, the latter leading to low REE concentrations (<10ppm) in carbonate rocks (McLennan, 1989; Gosselin et al., 1992). These conditions might account for the low REE concentrations of the vein facies since the main

aquifers are carbonate rocks and travertines precipitate from groundwater. REE are considered to be tracers of groundwater-rock interactions and groundwater flow (Johannesson and Zhou, 1997) and low REE concentrations of the vein and step-pool facies might also reflect short residence time of the groundwater due to high discharge during times of travertine formation. Uysal et al. (2007) and Kele et al. (2011) analyzed REE of travertines from Turkey and also measured low concentrations. A common trend is that the travertines show an enrichment in LREE over HREE (Fig. 4.9; Table 4.2). The samples had to be diluted considerably in order to analyze for REE because of the high Ca concentrations and this could be a reason for the very low concentrations (in several cases below detection limit). Further work is needed to characterize the mineralogy of the deposits as well as refine the extraction techniques to yield improved detection limits.

Modeling Past Water Temperatures and Water Compositions

Measured travertine oxygen isotopic compositions depend both on source water isotopic composition and temperature – neither of which is known. Three different isotopic fractionation equations were used to model past water compositions and temperatures based on observed travertine isotopic values: fractionation equations by Kim and O'Neil (1997), Coplen (2007), and Demeny et al. (2010). The system was examined by (a) inputting a suite of source water isotopic compositions and outputting temperature for observed travertine isotopic compositions, as well as (b) by evaluating the equilibrium source water compositions associated with observed travertine composition at specific temperatures. For (a), water temperatures were modeled assuming a range of input source water $\delta^{18}\text{O}_w$ values from -4‰ to -14‰ which was constrained by the statistical analysis of measured $\delta^{18}\text{O}_c$ values of the travertines (Fig. 4.13; Table 4.3; Table DR3). For (b), water compositions ($\delta^{18}\text{O}_w$) were modeled assuming water temperature ranging

from 10°C to 50°C based on temperatures measured at regional modern springs (Table 4.4; Table DR4). The largest differences in water temperatures are observed between the fractionation equations by Kim and O'Neil (1997) and Coplen (2007) and modeled water temperatures can

Table 4.3: Statistical analysis of $\delta^{18}\text{O}_c$ values of travertine samples

Statistical Parameter	Step-Pool Facies					Vein Facies				Paludal Facies	
	MDO	MA	RN	RS	SPV	MDO	MA	RN	SPV	MDO	RS
Mean	-7.93	-7.64	-7.29	-7.40	-8.15	-8.10	-7.87	-8.05	-9.01	-6.24	-6.27
Standard Error	0.10	0.09	0.25	0.27	0.27	0.47	0.09	0.40	0.27	0.69	0.24
Median	-7.98	-7.68	-7.29	-7.67	-8.44	-7.47	-7.80	-7.50	-9.07	-6.34	-6.24
Mode	-8.27	n.a.	n.a.	n.a.	n.a.	n.a.	n.a.	n.a.	n.a.	n.a.	n.a.
Standard Deviation	0.97	0.59	1.32	0.75	1.43	2.32	0.64	1.56	0.97	1.39	1.16
Sample Variance	0.94	0.35	1.75	0.56	2.06	5.38	0.41	2.43	0.95	1.92	1.34
Kurtosis	-0.57	-0.02	1.05	-0.31	0.88	1.20	0.32	-1.15	-0.07	-3.67	0.54
Skewness	0.19	-0.53	-0.77	1.12	1.04	-1.19	-0.28	0.00	0.84	0.23	0.03
Range	4.34	2.57	5.81	1.92	5.91	9.56	2.71	5.19	3.11	2.96	5.14
Minimum	-9.91	-9.23	-11.02	-8.14	-10.22	-14.02	-9.29	-10.52	-10.24	-7.63	-8.93
Maximum	-5.57	-6.67	-5.21	-6.22	-4.31	-4.46	-6.59	-5.32	-7.13	-4.66	-3.78
Count	91	40	27	8	29	24	50	15	13	4	24

MDO = Mesa del Oro, MA = Mesa Aparejo, RN = Riley North Mesa, RS = Riley South Mesa, SPV = Springerville
 $\delta^{18}\text{O}_c$ is the $\delta^{18}\text{O}$ value of the calcite/travertine.

Table 4.4: Location and hydrogeochemical parameters of modern springs

Spring	Northing/Easting		Latitude/Longitude		Travertine Deposit	Water Temp.* (°C)	$\delta^{18}\text{O}_w$ ** (SMOW)	Reference
Eddleman Spring	3851924	280038	34.7858	-107.392	Mesa del Oro	15.0 17.1	-14.05	Goff et al., 1983; Newell, 2007
Crane Spring	3836007	280779	34.6426	-107.392	Mesa del Oro	19.0	-14.2	Wright, 1946; Goff et al., 1983
Arroyo Salado Spring***	3841513	305562	34.6972	-107.123	Mesa Aparejo	19.2	-10.8	Goff et al., 1983 (***Unnamed Salt Spring)
Rio Salado Box Spring	3800467	307261	34.3276	-107.095	Riley North Mesa Riley South Mesa	21.3	-7.6, -8.4, -8.6 -8.9, -9.2	Williams et al., 2013
Salado Springs	3811280	647200	34.4325	-109.398	Springerville	18.1 20.0	-10.46	Bills and Hjalmarson, 1990; Embid, 2009

*Water Temp. = Water Temperature

** = $\delta^{18}\text{O}$ of the water, in ‰

SMOW = Standard Mean Ocean Water

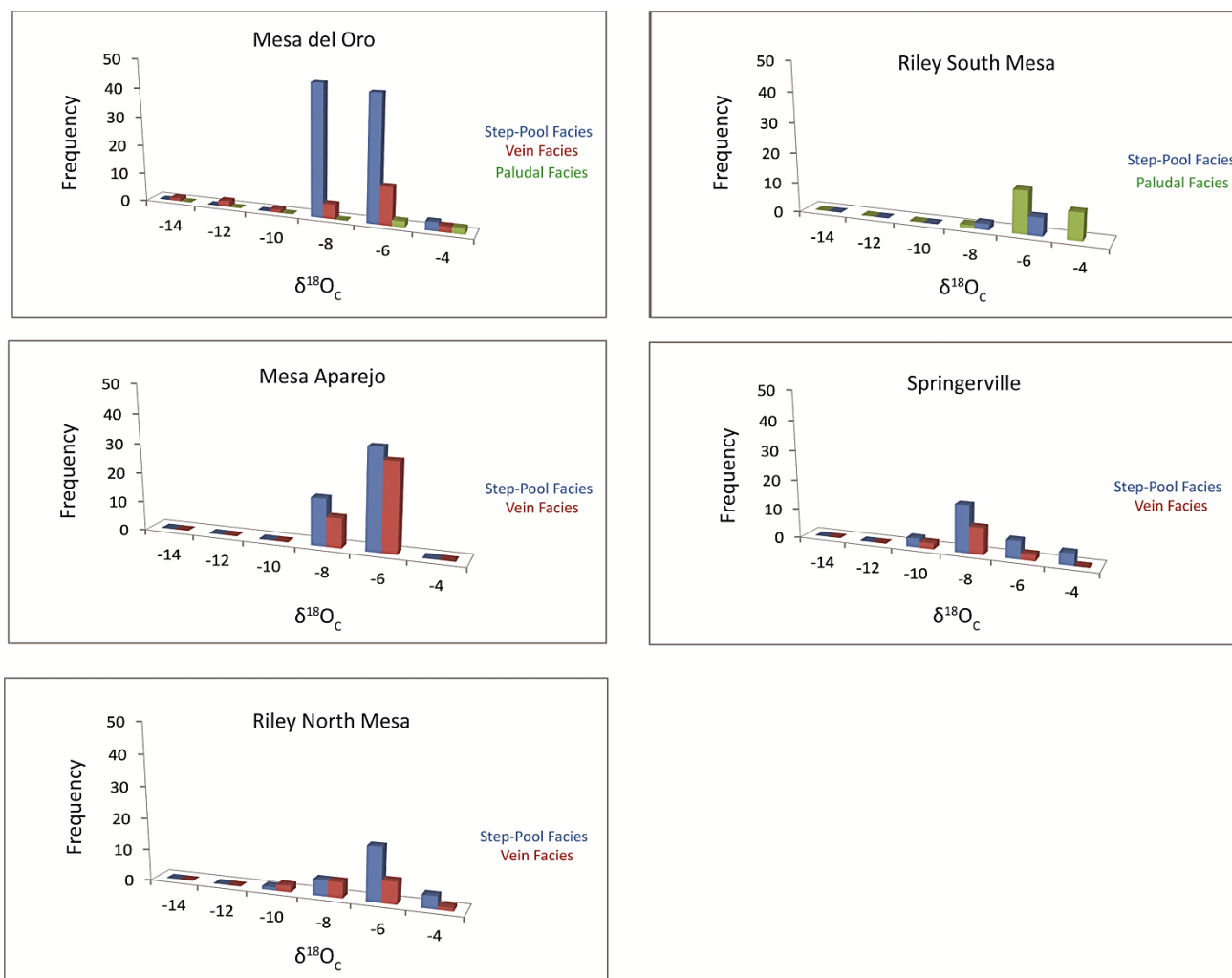


Figure 4.13. Statistical analysis of measured $\delta^{18}O_c$ values of the travertines according to facies. The histograms show how often certain $\delta^{18}O_c$ values occur in each study area (frequency).

differ as much as $13.8^{\circ}C$ (Table 4.5; Table DR5). Özkul et al. (2014) calculated water temperatures for travertines in Turkey based on six different fractionation equations and obtained temperature differences of $12^{\circ}C$ to $14^{\circ}C$ between different equations. The largest differences in water compositions occur between the fractionation equations by Demeny et al. (2010) and Kim and O'Neil (1997) where $\delta^{18}O_w$ values differ by 2.65‰ (Table 4.6; Table DR6). Kim and O'Neil (1997) and Coplen (2007) assume thermodynamic equilibrium of oxygen isotope fractionation

Table 4.5: Differences in water temperatures between fractionation equations

Study Areas	Step-Pool Facies			Vein Facies			Paludal Facies		
	Fractionation Equations								
	(1)-(3)	(2)-(1)	(3)-(2)	(1)-(3)	(2)-(1)	(3)-(2)	(1)-(3)	(2)-(1)	(3)-(2)
	Temperature (°C)								
Mesa del Oro	8.3	2.6	10.9	10.4	3.4	13.8	7.4	2.3	9.6
Mesa Aparejo	8.0	2.5	10.5	8.0	2.5	10.6	n.d.	n.d.	n.d.
Riley North Mesa	8.8	2.8	11.6	8.6	2.7	11.3	n.d.	n.d.	n.d.
Riley South Mesa	7.6	2.3	9.9	n.d.	n.d.	n.d.	7.9	2.5	10.3
Springerville	7.4	2.7	11.1	8.5	2.7	11.1	n.d.	n.d.	n.d.

(1) Demeny et al. (2010), (2) Coplen (2007), (3) Kim and O'Neil (1997)

Table 4.6: Differences in water compositions between fractionation equations

Study Areas	Step-Pool Facies			Vein Facies			Paludal Facies		
	Fractionation Equations								
	(1)-(3)	(2)-(1)	(3)-(2)	(1)-(3)	(2)-(1)	(3)-(2)	(1)-(3)	(2)-(1)	(3)-(2)
	$\delta^{18}\text{O}_w$ (‰, SMOW)								
Mesa del Oro	2.65	1.06	1.57	2.65	1.07	1.59	2.65	1.07	1.59
Mesa Aparejo	2.65	1.07	1.58	2.65	1.07	1.58	n.d.	n.d.	n.d.
Riley North Mesa	2.65	1.07	1.58	2.65	1.07	1.58	n.d.	n.d.	n.d.
Riley South Mesa	2.65	1.07	1.58	n.d.	n.d.	n.d.	2.65	1.07	1.59
Springerville	2.65	1.07	1.59	2.65	1.06	1.58	n.d.	n.d.	n.d.

(1) Demeny et al. (2010), (2) Coplen (2007), (3) Kim and O'Neil (1997)

$\delta^{18}\text{O}_w$ is the $\delta^{18}\text{O}_w$ value of the past groundwater; SMOW = Standard Mean Ocean Water

between calcite and water, whereas Demeny et al. (2010) account for travertine formation under isotopic fractionation disequilibrium which represents travertine formation more adequately (e. g. Gonfiantini et al., 1968; Andrews, 2006; Kele et al., 2011). Tafoya (2012) compared different isotope fractionation equations in her study of travertines, including active systems, from Soda Dam, New Mexico, and found that the results based on Demeny et al. (2010) were closest to modern measured calcite/water/temperature relationships.

Using the fractionation equation of Demeny et al. (2010) the range of assumed $\delta^{18}\text{O}_w$ values was slightly increased from +1‰ to -14‰ to calculate water temperatures (Table DR7). Mesa del Oro exhibits the largest variations in water temperatures (Table 4.7; Table DR7). The vein facies shows the highest temperatures and largest range of $\delta^{18}\text{O}_w$ values, whereas the

Table 4.7: Minimum and maximum temperatures at $\delta^{18}\text{O}_w$ values between -8‰ and -4‰

Study Areas	Step-Pool Facies		Vein Facies		Paludal Facies	
	$\delta^{18}\text{O}_w$ (‰, SMOW)					
	-8	-6	-8	-6	-6	-4
Temperature (°C)						
min	max	min	max	min	max	
Mesa del Oro	29.5	40.3	52.8	65.4	17.9	28.0
Mesa Aparejo	26.0	36.6	26.3	36.9	n.d.	n.d.
Springerville	31.1	53.9	31.2	54.0	n.d.	n.d.
Riley North Mesa	35.4	46.7	32.7	43.8	n.d.	n.d.
Riley South Mesa	20.5	30.7	n.d.	n.d.	34.9	46.1

$\delta^{18}\text{O}_w$ is the $\delta^{18}\text{O}$ value of the travertine; SMOW = Standard Mean Ocean Water

paludal facies shows the lowest temperatures and smallest range of $\delta^{18}\text{O}_w$ values (Table 4.7; Tables DR7 to DR10). Based on the statistical analysis of the $\delta^{18}\text{O}_c$ values, most of the samples belonging to the step-pool and vein facies vary between -6‰ and -8‰ and assuming $\delta^{18}\text{O}_w$ values of the same range leads to water temperatures between 29.5°C and 40.3°C and 52.8°C and 65.4°C, respectively (Fig. 4.13; Table 4.7; Table DR9). The few samples of the paludal facies exhibit $\delta^{18}\text{O}_c$ values between -4‰ and -6‰ and $\delta^{18}\text{O}_w$ values of this range result in water temperatures between 17.9°C and 28.0°C (Fig. 4.13; Table 4.7; Table DR9). These results suggest that groundwater with relatively high temperatures discharged at the surface and gradually cooled along the flow path with increasing distance from the spring orifice. All of the samples from Mesa Aparejo exhibit $\delta^{18}\text{O}_c$ values between -6‰ and -8‰ for the step-pool and vein facies and corresponding $\delta^{18}\text{O}_w$ values lead to water temperatures of 26.0°C and 36.6°C and 26.3°C and 36.9°C, respectively (Fig. 4.13; Table 4.7; Table DR9). The temperature range is almost identical and suggests that the temperature of the discharging groundwater did not change significantly along the flow path. Almost identical temperatures for the step-pool and vein facies can also be observed at Springerville. The majority of samples exhibit $\delta^{18}\text{O}_c$ values between -6‰ and -8‰ (Fig. 4.13) and assuming $\delta^{18}\text{O}_w$ values of -6‰ and -8‰ leads to water temperatures between 31.1°C and 53.9°C and 31.2°C and 54.0°C for the step-pool and vein facies,

respectively (Table 4.7; Table DR9). The majority of samples belonging to the step-pool and vein facies from Riley North Mesa exhibit $\delta^{18}\text{O}_c$ values between -6‰ and -8‰ and $\delta^{18}\text{O}_w$ values of the same range lead to temperatures between 35.4°C and 46.7°C and 32.7°C and 43.8°C, respectively (Fig. 4.13; Table 4.7; Table DR9). Water temperatures for the step-pool facies are slightly higher than temperatures for the vein facies which suggests that the temperature of the discharging groundwater might have increased due to relatively high air temperatures. The latter could be interpreted as seasonal variations or climatic changes. A similar situation can be observed for the step-pool and paludal facies at Riley South Mesa, where temperatures for the paludal facies are slightly higher than for step-pool facies. $\delta^{18}\text{O}_c$ values of samples belonging to the step-pool facies vary between -6‰ and -8‰ and assuming the same range of $\delta^{18}\text{O}_w$ values results in temperatures between 20.5°C and 30.7°C (Fig. 4.13; Table 4.7; Table DR9). For the paludal facies $\delta^{18}\text{O}_c$ values of most of the samples range from -4‰ to -6‰ and $\delta^{18}\text{O}_w$ values of the same range lead to temperatures between 34.9°C and 46.1°C (Fig. 4.13; Table 4.7; Table DR9). The higher inferred water temperatures of the paludal facies might be due to standing bodies of water in a marsh environment where the water might be quite warm, especially during the summer – but these temperatures are unreasonably high. In all study areas, assumed $\delta^{18}\text{O}_w$ values of -14‰ to -10‰ result in negative water temperatures or temperatures that seem too low for the three facies, except for the vein facies at Mesa del Oro and Springerville (Table DR9), whereas assumed $\delta^{18}\text{O}_w$ values of 0‰ and +1‰ lead to temperatures that seem unrealistically high for most facies (Table DR9).

Modeled temperatures and $\delta^{18}\text{O}_w$ values (Tables DR9 and DR10) were plotted in Figure 4.14: the different curves represent possible combinations of assumed water temperatures and resulting water compositions for a given travertine composition, expressed as $\delta^{18}\text{O}_c$ value; the

selected travertine compositions are the minimum and maximum $\delta^{18}\text{O}_c$ values of all study areas combined, 16‰ (SMOW) and 27‰ (SMOW), respectively, as well as the mean values calculated for each study area, 22-24‰ (SMOW). Springerville has a mean $\delta^{18}\text{O}_c$ value of 22‰, whereas Mesa del Oro, Mesa Aparejo, and Riley North Mesa have the same mean $\delta^{18}\text{O}_c$ value of 23‰ and Riley South Mesa has a mean $\delta^{18}\text{O}_c$ value of 24‰ (Fig. 4.14). The plot clearly shows the range of $\delta^{18}\text{O}_w$ values where water temperatures are negative and thus $\delta^{18}\text{O}_w$ values which are unlikely (Fig. 4.14). Low $\delta^{18}\text{O}_w$ values in general result in low temperatures and high $\delta^{18}\text{O}_w$ values in high temperatures, at a given travertine composition (Fig. 4.14). For comparison, temperatures and $\delta^{18}\text{O}_w$ values of the modern springs in the study areas (Table 4.4) were also plotted in Figure 4.14 and most of them lie outside the possible combinations of modeled water temperatures and water compositions which implies that the modern water compositions must be different from past water compositions. The temperature calculations imply that past water temperatures might have been higher than modern spring temperatures. Moreover, Figure 4.14 allows evaluating the differences in water temperatures and $\delta^{18}\text{O}_w$ values between the fractionation equations of Kim and O'Neil (1997), Coplen (2007), and Demeny et al. (2010): the maximum temperature differences of 13.8°C, for example, leads to a difference of 2.5‰ and the maximum difference in $\delta^{18}\text{O}_w$ of 2.65‰ results in a temperature difference of 15°C (Tables 4.5 and 4.6; Tables DR5 and DR6).

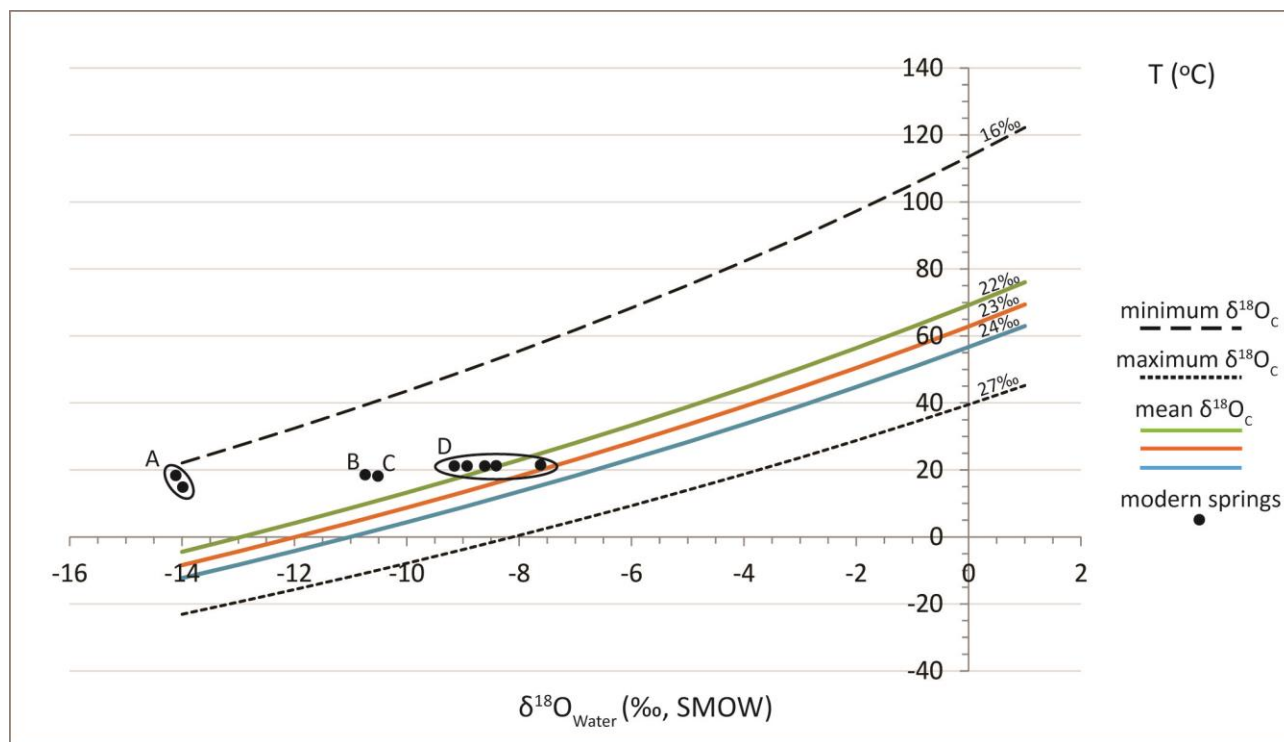


Figure 4.14. Traditional plot of water temperature versus $\delta^{18}\text{O}_w$. See text for explanation. Also plotted are modern spring temperatures and $\delta^{18}\text{O}_w$ values of Eddleman Spring and Crane Spring at Mesa del Oro (A), Arroyo Salado Spring at Mesa Aparejo (B), Salado Springs at Springerville (C), and Rio Salado Box Spring near Riley North Mesa and Riley South Mesa (D). Spring data is from Table 4; $\delta^{18}\text{O}_w$ is the $\delta^{18}\text{O}$ value of the past groundwater.

CONCLUSIONS

While more work is needed to characterize carbonate mineralogy, as well as improve extraction methods to improve detection limits for the trace elements, the results of this study show that geochemical tracers such as stable oxygen and carbon isotopes as well as trace elements can be used to characterize travertine facies. Stable isotope results overlap between facies but show trends that are characteristic for the step-pool, paludal and vein facies. From the stable oxygen isotope data can be inferred that the vein facies, which exhibits the largest spread of $\delta^{18}\text{O}_w$ values of the travertines, was primarily controlled by mixing of deep and shallow groundwaters at depth, whereas the step-pool and paludal facies were influenced by mixing of groundwater with surface water and precipitation since they form at the surface. Stable carbon

isotope results reflect the importance of CO₂ degassing rates which are highest for the vein facies and also significant for the step-pool and paludal facies although the latter are also controlled by microbiologic activity and vegetation. Trace element concentrations also vary according to facies. The vein facies exhibits the largest variability in trace element concentrations and some of the highest concentrations for certain elements. Small Mg/Ca ratios and low REE concentrations reflect low water-rock interactions in the aquifer due to high discharge and short groundwater residence time. The results of the trace element analyses are consistent with the accumulation of large volumes of travertine during wet times and high hydraulic head in the aquifer. Modeling of past water temperatures suggests that both water temperature and water composition controlled the oxygen isotopic composition of the travertines. A comparison of different isotope fractionation equations shows that temperature may vary by more than 10°C. Fossil travertines can be used for paleohydrologic and paleoclimate studies but travertine facies have to be evaluated and sampled with care in order to obtain reliable results from stable isotope and trace element analyses. Modeling past water temperatures requires choosing a fractionation equation that best represents isotope fractionation in travertines in order to infer paleoenvironmental conditions.

ACKNOWLEDGEMENTS

I thank my committee members, Laura Crossey, Karl Karlstrom, Yemane Asmerom, and Peter Mozley for helpful input. I thank Jim Lardner of New Mexico Travertine, Inc., for access to the travertine quarries at Mesa Aparejo, and different parties at Mesa del Oro: Bob Worsley, owner of NZ Legacy LLC, for access to his property and travertine quarries; Jim Harrison, manager of NZ Legacy LLC, for valuable information about the travertine deposit; and rancher Mark Chavez for access to his land. I extend thanks to Dave Love from the New Mexico Bureau

of Geology and Mineral Resources for his expertise during field work at Riley South, to Patrick Naranjo, Tom Kipling, Corentin Le Guillou, Jason Ricketts, and Nadine Warneke for invaluable field assistance, and to Rebecca Wacker for preparing hundreds of travertine samples for stable isotope analysis. Funding for this study was provided by National Science Foundation (NSF) EAR-0838575 (to Crossey), American Association of Petroleum Geologists Grants-In-Aid, New Mexico Geological Society grants-in-aid, and Graduate and Professional Student Association of the University of New Mexico.

REFERENCES

- Aldrich, M.J., 1986, Tectonics of the Jemez lineament in the Jemez Mountains and Rio Grande rift: *Journal of Geophysical Research*, v. 91, no. B2, p. 1753–1762.
- Allard, B., 1995, Groundwater, *in* Brit Salbu and Eiliv Steinnes ed., *Trace Elements in Natural Waters*, p. 151–176.
- Alonso-Zara, A.M., and Wright, V.P., 2010, Palustrine Carbonates, *in* Alonso-Zara, A.M. and Tanner, L.H. eds., *Carbonates in Continental Settings, Developments in Sedimentology 61*, p. 103–131.
- Andrews, J.E., 2006, Palaeoclimatic records from stable isotopes in riverine tufas: synthesis and review: *Earth-Science Reviews*, v. 75, p. 85–104, doi: 10.1016/j.earscirev.2005.08.002.
- Andrews, J.E., Pedley, M., and Dennis, P.F., 2000, Palaeoenvironmental records in Holocene Spanish tufas: a stable isotope approach in search of reliable climatic archives: *Sedimentology*, v. 47, p. 961–978, doi: 10.1046/j.1365-3091.2000.00333.x.
- Anzalone, E., Ferreri, V., Sprovieri, M., and D'Argenio, B., 2007, Travertines as hydrologic archives: the case of the Pontecagnano deposits (southern Italy): *Advances in Water Resources*, v. 30, p. 2159–2175, doi: 10.1016/j.advwatres.2006.09.008.
- Ballentine, C.J., and Sherwood Lollar, B., 2002, Regional groundwater focusing of nitrogen and noble gases into the Hugoton-Panhandle giant gas field, USA: *Geochimica et Cosmochimica Acta*, v. 66, no. 14, p. 2483–2497.
- Barker, J.M., Austin, G.S., and Sivils, D.J., 1996, Travertine in New Mexico - Commercial deposits and otherwise: *New Mexico Bureau of Mines and Mineral Resources Bulletin*, v. 154, p. 73–92.

- Bricker, O.W., and Jones, B.F., 1995, Main factors affecting the composition of natural waters, *in* Salbu, B. and Steinnes, E. eds., *Trace Elements in Natural Waters*, p. 1–20.
- Burnside, N.M., Shipton, Z.K., Dockrill, B., and Ellam, R.M., 2013, Man-made versus natural CO₂ leakage: A 400 k.y. history of an analogue for engineered geological storage of CO₂: *Geology*, v. 41, no. 4, p. 471–474, doi: 10.1130/G33738.1.
- Cather, S.M., 2004, Laramide orogeny in central and northern New Mexico and southern Colorado, *in* Mack, G.H. and Giles, K.A. eds., *The Geology of New Mexico*, New Mexico Geological Society Special Publication 11, p. 203–248.
- Chafetz, H.S., and Folk, R.L., 1984, Travertines; depositional morphology and the bacterially constructed constituents: *Journal of Sedimentary Petrology*, v. 54, no. 1, p. 289–316.
- Chamberlin, R.M., 2007, Evolution of the Jemez lineament: connecting the volcanic “dots” through late cenozoic time: *New Mexico Geological Society Guidebook*, 58th Field Conference, p. 80–82.
- Coplen, T.B., 2007, Calibration of the calcite–water oxygen-isotope geothermometer at Devils Hole, Nevada, a natural laboratory: *Geochimica et Cosmochimica Acta*, v. 71, p. 3948–3957, doi: 10.1016/j.gca.2007.05.028.
- Crossey, L.J., Fischer, T.P., Patchett, P.J., Karlstrom, K.E., Hilton, D.R., Newell, D.L., Huntoon, P., Reynolds, A.C., and de Leeuw, G.A.M., 2006, Dissected hydrologic system at the Grand Canyon: Interaction between deeply derived fluids and plateau aquifer waters in modern springs and travertine: *Geology*, v. 34, no. 1, p. 25–28, doi: 10.1130/G22057.1.
- Crossey, L.J., Karlstrom, K.E., Newell, D.N., Kooser, A., and Tafoya, A., 2011, The La Madera travertines, Rio Ojo Caliente, northern New Mexico : Investigating the linked system of CO₂-rich springs and travertines as neotectonic and paleoclimate indicators, *in* *New Mexico Geological Society Guidebook*, 62nd Field Conference, *Geology of the Tusas Mountains - Ojo Caliente*, p. 121–136.
- Crossey, L.J., Karlstrom, K.E., Springer, A.E., Newell, D., Hilton, D.R., and Fischer, T., 2009, Degassing of mantle-derived CO₂ and He from springs in the southern Colorado Plateau region--Neotectonic connections and implications for groundwater systems: *Geological Society of America Bulletin*, v. 121, no. 7-8, p. 1034–1053, doi: 10.1130/B26394.1.
- Demeny, A., Kele, S., and Siklosy, Z., 2010, Empirical equations for the temperature dependence of calcite-water oxygen isotope fractionation from 10 to 70 C: *Rapid Communications in Mass Spectrometry*, v. 24, p. 3521–3526, doi: 10.1002/rcm.
- Drever, J.I., 2002, *The geochemistry of natural waters: Upper Saddle River, NJ*, Prentice Hall.
- Dunbar, N., 2005, Quaternary volcanism in New Mexico: *New Mexico Museum of Natural History and Science Bulletin*, v. 28, p. 95–106.

- Embid, E.H., 2009, U-Series dating, geochemistry, and geomorphic studies of travertines and springs of the Springerville Area, east-central Arizona, and tectonic implications [M.S. thesis]: Albuquerque, University of New Mexico, 103 p.
- Faccenna, C., Soligo, M., Billi, A., De Filippis, L., Funicello, R., Rossetti, C., and Tuccimei, P., 2008, Late Pleistocene depositional cycles of the Lapis Tiburtinus travertine (Tivoli, Central Italy): possible influence of climate and fault activity: *Global and Planetary Change*, v. 63, p. 299–308, doi: 10.1016/j.gloplacha.2008.06.006.
- Feth, J.H., and Barnes, I., 1979, Spring-deposited travertine in eleven western states: Geological Survey Water-Resources Investigations 79-85 Open-File Report.
- De Filippis, L., Anzalone, E., Billi, A., Faccenna, C., Poncia, P.P., and Sella, P., 2013, The origin and growth of a recently-active fissure ridge travertine over a seismic fault, Tivoli, Italy: *Geomorphology*, v. 195, p. 13–26, doi: 10.1016/j.geomorph.2013.04.019.
- De Filippis, L., Faccenna, C., Billi, A., Anzalone, E., Brilli, M., Ozkul, M., Soligo, M., Tuccimei, P., and Villa, I.M., 2012, Growth of fissure ridge travertines from geothermal springs of Denizli Basin, western Turkey: *Geological Society of America Bulletin*, v. 124, no. 9-10, p. 1629–1645, doi: 10.1130/B30606.1.
- De Filippis, L., Faccenna, C., Billi, A., Anzalone, E., Brilli, M., Soligo, M., and Tuccimei, P., 2013, Plateau versus fissure ridge travertines from Quaternary geothermal springs of Italy and Turkey: Interactions and feedbacks between fluid discharge, paleoclimate, and tectonics: *Earth-Science Reviews*, v. 123, p. 35–52, doi: 10.1016/j.earscirev.2013.04.004.
- Ford, T.D., and Pedley, H.M., 1996, A review of tufa and travertine deposits of the world: *Earth-Science Reviews*, v. 41, p. 117–175.
- Fouke, B.W., Bonheyo, G.T., Sanzenbacher, B., and Frias-lopez, J., 2003, Partitioning of bacterial communities between travertine depositional facies at Mammoth Hot Springs, Yellowstone National Park, U.S.A.: *Canadian Journal of Earth Sciences*, v. 40, p. 1531–1548, doi: 10.1139/E03-067.
- Fouke, B.W., Farmer, J.D., Des Marais, D.J., Pratt, L., Sturchio, N.C., Burns, P.C., and Discipulo, M.K., 2000, Depositional facies and aqueous-solid geochemistry of travertine-depositing hot springs (Angel Terrace, Mammoth Hot Springs, Yellowstone National Park, U.S.A.): *Journal of Sedimentary Research*, v. 70, no. 3, p. 565–585.
- Fuller, B.M., Sklar, L.S., Compson, Z.G., Adams, K.J., Marks, J.C., and Wilcox, A.C., 2011, Ecogeomorphic feedbacks in regrowth of travertine step-pool morphology after dam decommissioning, Fossil Creek, Arizona: *Geomorphology*, v. 126, p. 314–332, doi: 10.1016/j.geomorph.2010.05.010.

- Garnett, E.R., Andrews, J.E., Preece, R.C., and Dennis, P.F., 2004, Climatic change recorded by stable isotopes and trace elements in a British Holocene tufa: *Journal of Quaternary Science*, v. 19, no. 3, p. 251–262, doi: 10.1002/jqs.842.
- Glover, C., and Robertson, A.H.F., 2003, Origin of tufa (cool-water carbonate) and related terraces in the Antalya area, SW Turkey: *Geological Journal*, v. 38, p. 329–358, doi: 10.1002/gj.959.
- Gonfiantini, R., Panichi, C., and Tongiorgi, E., 1968, Isotopic disequilibrium in travertine deposition: *Earth and Planetary Science Letters*, v. 5, p. 55–58.
- Gosselin, D.C., Smith, M.R., Lepel, E.A., and Laul, J.C., 1992, Rare earth elements in chloride-rich groundwater, Palo Duro Basin, Texas, USA: *Geochimica et Cosmochimica Acta*, v. 56, p. 1495–1505.
- Gratier, J.-P., Frery, E., Deschamps, P., Royne, A., Renard, F., Dysthe, D., Ellouz-Zimmerman, N., and Hamelin, B., 2012, How travertine veins grow from top to bottom and lift the rocks above them: The effect of crystallization force: *Geology*, p. 1–4, doi: 10.1130/G33286.1.
- Groves, G., and Howard, A.D., 1994, Early development of karst systems: 1. Preferential flow path enlargement under laminar flow: v. 30, no. 10, p. 2837–2846.
- Guo, L., and Riding, R., 1992, Aragonite laminae in hot water travertine crusts, Rapolano Terme, Italy: *Sedimentary Geology*, v. 39, p. 1067–1079.
- Guo, L., and Riding, R., 1998, Hot-spring travertine facies and sequences, Late Pleistocene, Rapolano Terme, Italy: *Sedimentology*, v. 45, p. 163–180.
- Guo, L., and Riding, R., 1994, Origin and diagenesis of Quaternary travertine shrub fabrics, Rapolano Terme, central Italy: *Sedimentology*, v. 41, p. 499–520.
- Guo, L.I., and Riding, R., 1999, Rapid facies changes in Holocene fissure ridge hot spring travertines, Rapolano Terme, Italy: *Sedimentology*, v. 46, p. 1145–1158.
- Hammer, O., Dysthe, D., and Jamtveit, B., 2007, The dynamics of travertine dams: *Earth and Planetary Science Letters*, v. 256, p. 258–263, doi: 10.1016/j.epsl.2007.01.033.
- Hancock, P.L., Chalmers, R.M., Altunel, E., and Cakir, Z., 1999, Travitronics: using travertines in active fault studies: *Journal of Structural Geology*, v. 21, p. 903–916.
- Hoffer-French, K.J., and Herman, J.S., 1989, Evaluation of hydrological and biological influences on CO₂ fluxes from a karst system: *Journal of Hydrology*, v. 108, p. 189–212.
- Hong, J., Calmano, W., and Forstner, U., 1995, Interstitial waters, *in* Salbu, B. and Steinnes, E. eds., *Trace Elements in Natural Waters*, p. 117–150.

- Howard, A.D., and Groves, C.G., 1995, Early development of karst systems: 2. Turbulent flow: v. 31, no. 1, p. 19–26.
- Ihlenfeld, C., Norman, M.D., Gagan, M.K., Drysdale, R.N., Maas, R., and Webb, J., 2003, Climatic significance of seasonal trace element and stable isotope variations in a modern freshwater tufa: *Geochimica et Cosmochimica Acta*, v. 67, no. 13, p. 2341–2357, doi: 10.1016/S0016-7037(00)01344-3.
- Jicha, H., 1958, Geology and mineral resources of Mesa del Oro Quadrangle, Socorro and Valencia Counties, New Mexico: State Bureau of Mines and Mineral Resources Bulletin, v. 56, p. 1–67.
- Johannesson, K.H., and Zhou, X., 1997, Geochemistry of the rare earth elements in natural terrestrial waters: A review of what is currently known: *Chinese Journal of Geochemistry*, v. 16, no. 1, p. 20–42, doi: 10.1007/BF02843369.
- Jones, B., and Renaut, R.W., 2010, Calcareous spring deposits in continental settings, *in* Alonso-Zara, A.M. and Tanner, L.H. eds., *Carbonates in Continental Settings, Developments in Sedimentology* 61, p. 177–224.
- Kampman, N., Burnside, N.M., Shipton, Z.K., Chapman, H.J., Nicholl, J. a., Ellam, R.M., and Bickle, M.J., 2012, Pulses of carbon dioxide emissions from intracrustal faults following climatic warming: *Nature Geoscience*, v. 5, no. 5, p. 352–358, doi: 10.1038/ngeo1451.
- Karlstrom, K.E., Crossey, L.J., Hilton, D.R., and Barry, P.H., 2013, Mantle ³He and CO₂ degassing in carbonic and geothermal springs of Colorado and implications for neotectonics of the Rocky Mountains: *Geology*, v. 41, p. 495–498, doi: 10.1130/G34007.1.
- Kele, S., Demény, A., Siklósy, Z., Németh, T., Tóth, M., and Kovács, M.B., 2008, Chemical and stable isotope composition of recent hot-water travertines and associated thermal waters, from Egerszalók, Hungary: Depositional facies and non-equilibrium fractionation: *Sedimentary Geology*, v. 211, p. 53–72, doi: 10.1016/j.sedgeo.2008.08.004.
- Kele, S., Özkul, M., Fórizs, I., Gökgöz, A., Baykara, M.O., Alçiçek, M.C., and Németh, T., 2011, Stable isotope geochemical study of Pamukkale travertines: new evidences of low-temperature non-equilibrium calcite-water fractionation: *Sedimentary Geology*, v. 238, p. 191–212, doi: 10.1016/j.sedgeo.2011.04.015.
- Keller, G.R., and Baldrige, W.S., 1999, The Rio Grande rift A geological and geophysical overview: *Rocky Mountain Geology*, v. 34, no. 1, p. 121–130.
- Kim, S.-T., and O’Neil, J.R., 1997, Equilibrium and nonequilibrium oxygen isotope effects in synthetic carbonates: *Geochimica et Cosmochimica Acta*, v. 61, no. 16, p. 3461–3475, doi: 10.1016/S0016-7037(97)00169-5.

- Leng, M.J., and Marshall, J.D., 2004, Palaeoclimate interpretation of stable isotope data from lake sediment archives: *Quaternary Science Reviews*, v. 23, p. 811–831, doi: 10.1016/j.quascirev.2003.06.012.
- McLennan, S.M., 1989, Rare earth elements in sedimentary rocks: influence of provenance and sedimentary processes, *in* Lipin, B.R. and McKay, G.A. eds., *Geochemistry and Mineralogy of Rare Earth Elements*, *Reviews in Mineralogy* 21, p. 169–200.
- Minissale, A., 2004, Origin, transport and discharge of CO₂ in central Italy: *Earth-Science Reviews*, v. 66, p. 89–141, doi: 10.1016/j.earscirev.2003.09.001.
- Minissale, A., Kerrick, D.M., Magro, G., Murrell, M.T., Paladini, M., Rihs, S., Sturchio, N.C., Tassi, F., and Vaselli, O., 2002, Geochemistry of Quaternary travertines in the region north of Rome (Italy): structural, hydrologic and paleoclimatic implications: *Earth and Planetary Science Letters*, v. 203, p. 709–728.
- Minissale, A., Paladini, M., and Sturchio, N.C., 2005, Travertine of central Italy: relation between genesis, tectonics and paleoclimate: *Proceedings of the 1st International Symposium on Travertine*, p. 106–115.
- Minissale, A., Vaselli, O., Tassi, F., Magro, G., and Grechi, G.P., 2002, Fluid mixing in carbonate aquifers near Rapolano (central Italy): chemical and isotopic constraints: *Applied Geochemistry*, v. 17, p. 1329–1342.
- Minor, S.A., Hudson, M.R., Cain, J.S., and Thompson, R.A., 2013, Oblique transfer of extensional strain between basins of the middle Rio Grande rift, New Mexico: Fault kinematic and paleostress constraints, *in* Hudson, M.R. and Grauch, V.J.S. (Tien) eds., *New Perspectives on Rio Grande Basins: From Tectonics to Groundwater*, *The Geological Society of America Special Paper* 494, p. 345–382.
- Newell, D.L., Crossey, L.J., Karlstrom, K.E., Fischer, T.P., and Hilton, D.R., 2005, Continental-scale links between the mantle and groundwater systems of the western United States: Evidence from travertine springs and regional He isotope data: *GSA Today*, v. 15, no. 12, p. 4–10.
- Osburn, G.R., 1984, *Geology of Socorro County: New Mexico Bureau of Geology and Mineral Resources*, Open-File Report 238, 13 p.
- Özkul, M., Gökgöz, A., Kele, S., Baykara, M.O., Shen, C.-C., Chang, Y.-W., Kaya, A., Hançer, M., Aratman, Ci., Akin, T., and Örü, Z., 2014, Sedimentological and geochemical characteristics of a fluvial travertine: A case from the eastern Mediterranean region (E. Capezzuoli, Ed.): *Sedimentology*, v. 61, no. 1, p. 291–318, doi: 10.1111/sed.12095.
- Pedley, H.M., 1990, Classification and environmental models of cool freshwater tufas: *Sedimentary Geology*, v. 68, p. 143–154.

- Pedley, M., 2009, Tufas and travertines of the Mediterranean region: a testing ground for freshwater carbonate concepts and developments: *Sedimentology*, v. 56, p. 221–246, doi: 10.1111/j.1365-3091.2008.01012.x.
- Pentecost, A., 2005, *Travertine*: Springer Verlag Berlin Heidelberg, 445 p.
- Pentecost, A., and Viles, H., 1994, A review and reassessment of travertine classification: *Geographie physique et Quaternaire*, v. 48, no. 3, p. 305–314.
- Priewisch, A., Crossey, L.J., Karlstrom, K.E., Polyak, V.J., Asmerom, Y., Nereson, A., and Ricketts, J.W., 2014, U-series geochronology of large-volume Quaternary travertine deposits of the southeastern Colorado Plateau: Evaluating episodicity and tectonic and paleohydrologic controls: *Geosphere*, v. 10, no. 2, doi: 10.1130/GES00946.1.
- Qian, J., Zhan, H., Zhao, W., and Sun, F., 2005, Experimental study of turbulent unconfined groundwater flow in a single fracture: *Journal of Hydrology*, v. 311, p. 134–142, doi: 10.1016/j.jhydrol.2005.01.013.
- Reeder, R.J., 1990, Crystal chemistry of the rhombohedral carbonates, *in* Reeder, R.J. ed., *Carbonates: Mineralogy and Chemistry*, *Reviews in Mineralogy* 11, p. 1–47.
- Ricketts, J.W., and Karlstrom, K.E., 2011, Geologic Map of the Western Boundary of the Rio Grande rift - South Garcia SE and Mesas Mojinas Quadrangles, central New Mexico: New Mexico Bureau of Geology and Mineral Resources, scale 1:12 000, 1 sheet.
- Ricketts, J.W., Karlstrom, K.E., Priewisch, A., Crossey, L.J., Polyak, V.J., and Asmerom, Y., 2014, Quaternary extension in the Rio Grande rift at elevated strain rates recorded in travertine deposits, central New Mexico: *Lithosphere*, v. 6, no. 1, p. 3–16, doi: 10.1130/L278.1.
- Seager, W., 2004, Laramide (Late Cretaceous–Eocene) tectonics of southwestern New Mexico, *in* Mack, G.H. and Giles, K.A. eds., *The Geology of New Mexico*, New Mexico Geological Society Special Publication 11, p. 183–202.
- Sharp, Z., 2007, *Stable Isotope Geochemistry*: Pearson Prentice Hall, Upper Saddle River, NJ.
- Shipton, Z.K., Evans, J.P., Kirschner, D., Kolesar, P.T., Williams, A.P., and Heath, J., 2004, Analysis of CO₂ leakage through “low-permeability” faults from natural reservoirs in the Colorado Plateau, east-central Utah, *in* Baines, S.J. and Worden, R.H. eds., *Geological Storage of Carbon Dioxide*, Geological Society London Special Publication 233, p. 43–58.
- Sibson, R.H., 2000, Fluid involvement in normal faulting: *Journal of Geodynamics*, v. 29, p. 469–499, doi: 10.1016/S0264-3707(99)00042-3.
- Smith, J.R., Giegengack, R., and Schwarcz, H.P., 2004, Constraints on Pleistocene pluvial climates through stable-isotope analysis of fossil-spring tufas and associated gastropods,

- Kharga Oasis, Egypt: Palaeogeography, Palaeoclimatology, Palaeoecology, v. 206, p. 157–175, doi: 10.1016/j.palaeo.2004.01.021.
- Speer, J.A., 1990, Crystal chemistry and phase relations of orthorhombic carbonates, *in* Reeder, R.J. ed., Carbonates: Mineralogy and Chemistry, Reviews in Mineralogy 11, p. 145–190.
- Spötl, C., and Vennemann, T.W., 2003, Continuous-flow isotope ratio mass spectrometric analysis of carbonate minerals: Rapid Communications in Mass Spectrometry, v. 17, no. 9, p. 1004–1006.
- Sun, H., Liu, Z., and Yan, H., 2014, Oxygen isotope fractionation in travertine-depositing pools at Baishuitai, Yunnan, SW China: Effects of deposition rates: *Geochimica et Cosmochimica Acta*, v. 133, p. 340–350, doi: 10.1016/j.gca.2014.03.006.
- Tafoya, A.J., 2012, Uranium-series geochronology and stable isotope analysis of travertine from Soda Dam, New Mexico: A Quaternary record of episodic spring discharge and river incision in the Jemez Mountains hydrothermal system [M.S. thesis]: University of New Mexico, Albuquerque, 104 p.
- Talbot, M.R., 1990, A review of the palaeohydrological interpretation of carbon and oxygen isotopic ratios in primary lacustrine carbonates: *Chemical Geology*, v. 80, p. 261–279.
- Turi, B., 1986, Stable isotope geochemistry of travertines, *in* Fritz, B.P. and Fontes, J.C. eds., *Environmental Isotope Geochemistry*, Elsevier, Amsterdam, p. 207–235.
- Uysal, I.T., Feng, Y., Zhao, J. -x., Altunel, E., Weatherley, D., Karabacak, V., Cengiz, O., Golding, S.D., Lawrence, M.G., and Collerson, K.D., 2007, U-series dating and geochemical tracing of late Quaternary travertine in co-seismic fissures: *Earth and Planetary Science Letters*, v. 257, p. 450–462, doi: 10.1016/j.epsl.2007.03.004.
- Veizer, J.A.N., 1983, Chemical diagenesis of carbonates: theory and application of trace element technique, *in* Arthur, M.A. and Al., E. eds., *Stable Isotopes in Sedimentary Geology*, SEPM Short Course Notes 10, p. Ch. 3.
- Veizer, J., 1990, Trace elements and isotopes in sedimentary carbonates, *in* Reeder, R.J. ed., *Carbonates: Mineralogy and Chemistry*, Reviews in Mineralogy 11, p. 265–299.
- Wang, H., Yan, H., and Liu, Z., 2014, Contrasts in variations of the carbon and oxygen isotopic composition of travertines formed in pools and a ramp stream at Huanglong Ravine, China: Implications for paleoclimatic interpretations: *Geochimica et Cosmochimica Acta*, v. 125, p. 34–48, doi: 10.1016/j.gca.2013.10.001.
- Williams, A.J., Crossey, L.J., Karlstrom, K.E., Newell, D., Person, M., and Woolsey, E., 2013, Hydrogeochemistry of the Middle Rio Grande aquifer system — Fluid mixing and salinization of the Rio Grande due to fault inputs: *Chemical Geology*, v. 351, p. 281–298, doi: 10.1016/j.chemgeo.2013.05.029.

Yan, H., Sun, H., and Liu, Z., 2012, Equilibrium vs. kinetic fractionation of oxygen isotopes in two low-temperature travertine-depositing systems with differing hydrodynamic conditions at Baishuitai, Yunnan, SW China: *Geochimica et Cosmochimica Acta*, v. 95, p. 63–78, doi: 10.1016/j.gca.2012.07.024.